

**MORPHODYNAMICS AND SEDIMENTOLOGY OF THE
MALINDI-FUNDISA COASTAL AREA ASSOCIATED WITH
THE HEAVY MINERAL DEPOSITION**

BY

JOSEPH ODHIAMBO Z. ABUODHA

THIS THESIS HAS BEEN ACCEPTED FOR
THE DEGREE OF M.Sc. (1989)
AND A COPY MAY BE PLACED IN THE
UNIVERSITY LIBRARY.

A thesis submitted in partial fulfilment for the degree of Master
of Science in the University of Nairobi

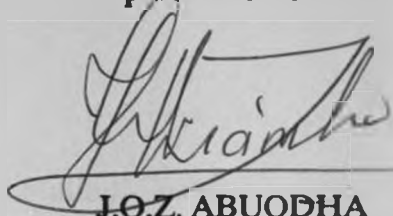
**MORPHODYNAMICS AND SEDIMENTOLOGY OF THE
MALINDI-FUNDISA COASTAL AREA ASSOCIATED WITH
THE HEAVY MINERAL DEPOSITION**

BY

JOSEPH ODHIAMBO Z. ABUODHA

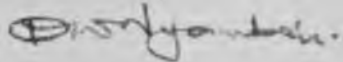
A thesis submitted in partial fulfilment for the degree of Master
of Science in the University of Nairobi

This thesis is my original work and has not been presented for a degree in any other University

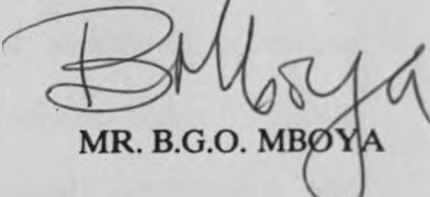


J.O.Z. ABUODHA

This thesis has been submitted for examination with our knowledge as University Supervisors.



PROF. I.O. NYAMBOK



MR. B.G.O. MBOYA

Abstract

The short-term morphodynamic states of the Malindi-Fundisa coasts varying in morphological, tidal, grain size and mineralogical characteristics have been examined as a basis for describing the different environments of sediment deposition taking place at present. Further examination of coastal geomorphology, sediment characteristics and process elements has shown that the Fundisa coast is transgressional; Mambui-Sabaki is depositonally emergent and the Silversands Beach is erosional. In addition the coast is further characterized by the degree of protection, namely those areas bordered by fringing reefs subrecent beach barriers are protected and the rest are exposed.

A casual study of fluctuation in density or abundance of certain organisms dwelling within the shallow marine ecosystem makes it possible to determine the cross effect of fauna-floral contribution and morphodynamic distribution. The organism- sediment relationship become more evident when the morphodynamic state of the beach and nearshore environment is taken into consideration.

The present investigation also provides information on the localities of heavy mineral deposition along the Malindi-Fundisa coast. Geochemical and petrographical parameters of surface sediments have been examined to delineate the heavy mineral-rich (consisting essentially of ilmenite, haematite, magnetite, zircon and rutile) regions. The results demonstrate a

well defined correlation between the heavy mineral concentrations and the corresponding morphodynamic processes.

Acknowledgements

I gratefully acknowledge the help obtained from all my friends and colleagues during the preparation of this thesis. In particular, I extend my thanks to Dr.M.P.Tole and Dr.J.S.Ogola for their help in formulating the proposal at the initial stages. I am glad to have this opportunity of acknowledging the help and guidance that Prof.I.O.Nyambok has given me both as my supervisor and as Chairman of the Geology Department. My second supervisor, Mr.B.G.O.Mboya provided very helpful critical reviews of this work, which I also acknowledge.

Interest in the study commenced during a regional training course in Marine Geology held at Malindi in September 1986 under the joint sponsorship of the University of Nairobi, IFAO (Free University of Brussels-V.U.B.) and UNESCO. I am particularly thankful to Prof. Dr.Paepe, Prof.Dr.Wartel and Dr. Henriet of V.U.B., Prof.I.O.Nyambok and Dr.S.J.Gaciri for the discussions.

I wish to express my appreciation to a number of persons who made significant contributions to the improvement of this thesis. Information on the continental shelf sediments was supplied by Dr. E.O. Odada. Help with the identification and discussion of marine flora and fauna was provided by Prof. F. Blasco, Miss J. Wakhungu and Miss. J. Mutere. The regional Centre for Services in Remote Sensing, Surveying and Mapping (R.C.S.R.S.S.M.) and the Survey of Kenya were very helpful in providing remote sensing data and aerial photographs. Additional information was

incorporated into this project while I was participating in the course on Monitoring and Management of Coastal Environments using SPOT Satellite Data that was organized by R.C.S.R.S.S.M. during February-March, 1988.

The author is indebted to DAAD for their financial assistance and a grant which permitted a study visit to the Federal Republic of Germany to undertake geochemical analyses of the samples used in this work. I am deeply indebted to Prof. Dr. E. Klitzsch and Dr. rer. nat. G. Matheis for their assistance in organizing my attachment to the Special Research Project at the Technical University of Berlin, along with Dr. O. Hankel, to whom I am also grateful. Prof. Dr. J. Schroeder, Prof. Dr. K.-H. Jacob and Prof. Dr. G. German made many helpful and important suggestions and criticisms of this work to which I express my gratitude.

The Kenya Marine and Fisheries Research Institute provided numerous assistance during the final stages of thesis publication. I thank the Director of K.M.F.R.I., Mr. S.O. Allela for his kind support, and also Mrs. Sussan Okello for her typing skill and patience. I must also thank everyone who gave me material and moral support throughout the exercise, and above all, my wife, Pamela Abuodha, for help with sample preparation and statistical analyses.

J.O.Z. Abuodha

University of Nairobi

September, 1989

Table of Contents

Abstract	i
Acknowledgements	iii
LIST OF FIGURES	x
LIST OF TABLES	xii
LIST OF PLATES	xiii
LIST OF MAPS AND SATELLITE IMAGERY (In Pocket)	xxviii
APPENDICES	xxix
1. INTRODUCTION	1
1.1 Location and description of the field area	1
1.2 Major geomorphological features of the coastal belt of Kenya	2
1.2.1 The Coastal Plain	6
1.2.2 The Foot Plateau	6
1.2.3 The Coastal Range	6
1.2.4 The Nyika	7
1.3 General Description of the eastern Africa continental shelf	7
1.4 Climate	9
1.5 Major oceanographical factors operating off the Kenyan coast	11
1.6 Previous Work	12

1.7	Theories behind the research project	15
1.8.	Objectives of this study	20
2.	METHODOLOGY	22
2.1.	Field Methods	22
2.1.1.	Mobility	22
2.1.1.1.	Locomotion.	22
2.1.1.2	Position Fixing.	22
2.1.2	Data Collection and Measured Parameters	22
2.1.3	Facies Analysis	23
2.1.4	Beach Stage Model Parameters	24
2.1.4.1.	Measurement of process elements	25
2.1.4.2.	Measurement of response elements	26
2.2	Laboratory Methods	27
2.2.1	Grain size distribution analysis	27
2.2.2.	Roundness and sphericity analysis	28
2.2.3	Mineralogical studies	29
2.2.4	Geochemical analyses	29
2.2.5.	Coastal classification: Cartography and Morphometrical Analyses	30
2.2.6	Analysis of Data	31
2.2.7	Presentation of Results	31
3.	MALINDI - FUNDISA SEACOAST CLASSIFICATION .	32
4.	RESULTS	42

4.1.	Morphology	42
4.1.1.	Silversands Beach	42
4.1.2.	Gilani Beach	45
4.1.3.	Sabaki Beach and Delta, and Mambui Beach	50
4.1.4.	Sheshale Bay, Maridadi Bay and Casuarina Bay	62
4.1.5.	Ngomeni Beach	66
4.1.6.	Simiti Island	69
4.1.7.	Robinson Island and Giryama Village Island	75
4.1.8.	Ras Kiswakini Island	75
4.1.9.	Tamamba Island and Kanagoni Island	82
4.2.	Processes	85
4.2.1.	Silversands Beach	85
4.2.2.	Gilani Beach	88
4.2.3.	Sabaki Beach and Delta, and Mambui Beach	89
4.2.4.	Sheshale Bay, Maridadi Bay and Casuarina Bay	93
4.2.5.	Ngomeni Beach	95
4.2.6.	Fundisa Barrier Islands	95
4.3.	Materials	98
4.3.1.	Silversands Beach	98
4.3.2.	Gilani Beach	110
4.3.3.	Sabaki Beach and Mambui Beach	110
4.3.4.	Sheshale Bay, Maridadi Bay and Casurina Bay	114
4.3.5.	Ngomeni Beach	114

4.3.6	Simiti Island	117
4.3.7	Robinson Island and Giriyama Village Island	119
4.3.8.	Ras Kiswakini Island	120
4.3.9.	Tamamba Island and Kanagoni Island	121
4.4	Structures	126
4.4.1.	Silversands Beach	126
4.4.2	Gilani Beach	128
4.4.3.	Sabaki Beach and Delta, and Mambrui Beach	130
4.4.4	Sheshale Bay, Maridadi Bay and Casuarina Bay	139
4.4.5	Ngomeni Beach	141
4.4.6	Simiti Island	142
4.4.7	Robinson Island and Giriyama Village Island.	147
4.4.8	Ras Kiswakini Island	149
4.4.9	Tamamba island and Kanagoni island	154
4.5.	Fauna and Flora	160
4.5.1	Silversands Beach	160
4.5.2	Gilani Beach	162
4.5.3.	Sabaki Beach and Mambrui Beach	162
4.5.4	Sheshale Bay Maridadi Bay and Casuarina Bay	163
4.5.5.	Ngomeni Beach	164
4.5.6.	Simiti Island	165
4.5.7.	Robinson Island and Giriyama Village Island	166
4.5.8.	Ras Kiswakini Island	167

4.5.9.	Tamamba Island and Kanagoni Island	167
5.	DISCUSSION AND CONCLUSIONS	169
5.1	MALINDI - FUNDISA NEAR-SHORE ENVIRONMENTS	169
5.1.1.	Coastal processes on the Malindi-Fundisa Coast	169
5.1.2	Malindi-Fundisa Beaches	173
5.1.2.1	Beach Sediments	173
5.1.2.2	Beach Morphology	181
5.1.3	The Coastal Sand Dunes of Sabaki-Mambrui Area	186
5.1.4.	Barrier Systems	190
5.1.5.	Tidal Flats	193
5.2	SUBTIDAL ENVIRONMENTS	198
5.2.1	Malindi-Fundisa shallow-water Carbonates	198
5.2.1.1.	Reefs	198
5.2.1.2	The reef-flats	200
5.2.1.3.	The reef front	201
5.2.1.4.	Lagoon	202
5.2.1.5.	The role of plants in the formation of shallow-water carbonates	204
5.2.2.	The shelf Environment of Malindi-Fundisa area	204
5.3.	Heavy Mineral Beach Sand Deposits	208
6.	REFERENCES	218

LIST OF FIGURES

Figure

1. Map of Kenya showing location of study area 3
2. Geomorphological and drainage map of the Malindi area 4
3. Generalized geological map of the Kenya coast 5
4. Coastal features of Silversands area at Leopard Point 46
5. Coastal features of the Silversands area at Driftwood club. 46
6. Shore profiles of Silversands Beach. 46
7. Shore profiles of Gilani Beach. 51
8. Plan and section views of the Sabaki Delta and its
distributary mouth bars. 53
9. Shore profiles of Sabaki and Mambui Beaches at
dunefield. 54
10. Shore profiles of Sheshale Bay ,Maridadi Bay and
Casuarina Bay 65
11. Shore features at Ngomeni Beach 66
12. Shore profiles of Robinson Island and Giryama
village Island Beaches 74
13. Shore features of Ras Kiswakini Island 77
14. Shore features of Tamamba and Kanagoni Island 84
15. A rose diagram for orientation of long axes of 100
pebbles at South Mambui. 113

16. A rose diagram for orientation of long axes of 225 gastropod shells at Ngomeni Beach. 113
17. Zonation of structure across Gilani Beach. 132
18. Correlation of sorting and mean diameter for the beach samples from Malindi-Fundisa area. 178
19. Plot of skewness Vs. sorting of sand samples from Malindi-Fundisa area. 179
20. Plot of heavy minerals Vs. Sorting determinations of sand samples from beaches in Malindi-Fundisa area. 180
21. Correlation of beach gradient and wave period for observations made in Malindi-Fundisa area. 183
22. Correlation of the mean diameter of beach sand and beach gradient for beaches in Malindi-Fundisa area. 184
23. Changes in particle roundness in beach and dune environments. 188
24. Bathymetric profile of Malindi, Sabaki and Ngomeni continental shelf areas. 205
25. Location of heavy mineral deposits north of Malindi. 209

LIST OF TABLES

Table

1.	Annual long term average rainfall up to 1988 at Lamu, Malindi, Mombasa and Shimoni. (Courtesy of Meteorological department, Dagoretti).	10
2.	Tidal condition during neap and spring tides at 4 stations along the Kenya coast.	12
3.	Coastal terraces of Southern Kenya: Previous workers.	5
4.	Beach-face shape dimension parameters for beaches in Malindi-Fundisa area.	43
5.	Wave conditions averaged over all traverses along the Malindi-Fundisa coast.	86
6.	Grain count analyses of beach sand constituents in the Malindi-Fundisa area.	100
7.	Heavy mineral content, sieve size distribution, roundness and sphericity.	105
8.	Orientation of long axes of 100 pebbles at South Mambrui Beach.	12
9.	Positions of pelecypod valves on the sediment surface at Ngomeni Beach.	116
10.	Orientation of long axes of gastropod shells at Ngomeni Beach.	116

11. Chemical analyses of coastal sediments from
 Malindi Fundisa area. 210

LIST OF PLATES

PLATE

1. Shore features at Silversands Beach. Note steeply sloping shore and boulders derived from the fringing reef. 46
2. Beach, upper sandy platform, cliffs and stacks at Silversands Beach. Note parallel bedding of Pleistocene eolian deposits towards the top of cliffs. 46
3. Coastal erosion at the Silversands Beach; showing a house precariously built with no sea walls at the edge of a rapidly retreating eolian cliff. 47
4. Concrete slabs placed in front of the monumental Vasco da Gama Pillar for protection against wave erosion. 47
5. Uneven surface of a gently sloping coral platform, with parts completely uncovered, parts with shallow water, large and small pools and channels. This is during low tide. 48

6. Interdistributary tidal flat exposed during low-tide showing bifurcating symmetrical wave ripples, characteristic mottling and bioturbation . 48
7. Sabaki Delta. A shifting rivermouth sand bar and the two main distributaries on either side. 55
8. Reef siltation. Covering of fringing reef by beach sand at the Mambrui beach. 55
9. Beach runnel with erosional megaripples. To the left is a beach ridge (longshore bar). The view is parallel to the shoreline. 56
10. A broad berm with many plant debris leading to vegetated frontal dunes (note stabilizing effect of vegetation). The tree is *Cyperus*. 56
11. Barchan dunes. Vegetation is *Ipomea pes carpes*. Note wind sand ripples on a wind blown sandy surface. 57
12. A gently sloping beach showing foredune ridge and deflation of upper beach surface. 57
13. Seaward view from the innermost dune ridge. Vegetation is present on all ridges, but does not prevent migration of dunes. 58
14. Longitudinal dune ridge. Vegetation is present on the adjacent dune ridge landwards. 58

15. Transverse second dune ridge showing wind sand ripple marks on the surface and vegetated third dune ridge. 59
16. Landward view from second dune ridge across sebkha. Note dark level bottom of sebkha. 59
17. Seaward view of the third dune ridge from the first dune ridge across second dune ridge. Vegetation is present on both the second and third dune ridges. 60
18. View of crescent-shaped beach located in a bight at Sheshale Bay. Note gentle slope of the foreshore. 60
19. General view of Maridadi Bay. 63
20. The tombolo at Ras Ngomeni. 64
21. Geomorphic forms of beach surface. Wave-cut cliff on foredune at Casuarina Bay. 64
22. Landward view of Ngomeni Beach across the Pleistocene rocky reef platform. Note vegetated Pleistocene dunes in the background. 68
23. General view of the Simiti Island foreshore showing how marine transgression has caused recession of mangrove zone and leaving behind peat. 68
24. General view of Simiti Island foreslope showing sandy surface protected by thin algal mats, and shallow erosional depressions with ripples. 70

25. Seaward view of typical, longshore trough and longshore bar at the northern lobate end of Simiti Island. 70
26. View of shore features looking northward along Robinson Island beach . Note heavy mineral concentrations and many shells on active berm zone. 71
27. Northern Robinson Island beach showing small wave- cut cliff on foredune ridge. Note the Ghost Crab, a crustacea Ocypode. 71
28. View of tidal channel across tidal delta. Note lingoid-shaped small-current ripples, current marks, many shells and heavy mineral concentrations on the surface. The direction of flow is from right to left. Southern Robinson Island. 72
29. A lagoon behind Robinson Island. In the left margin of the photograph are sluice gates leading to salt extraction ponds. 72
30. A lagoon behind the Giryama Village Island. Note lagoonward sandy beach surface protected by thin algal mats. 73

31. Southern Kiswakini Island beach showing foredune ridge with vegetation, heavy minerals and seaweed flotsam near base. 73
32. A near vertical scarp, cut into the foredune by large waves, contribution of dune material to beach and heavy minerals. 78
33. Relict foredune partially stabilized by mangrove roots: *Avicennia marina*. Note backwash marks and swash marks. About 1 km north of Mto Marereni tidal inlet. 78
34. Foredune ridge showing vegetation and heavy mineral pavement at base. Note erosional rill marks on beach close to the Kiswakini reef flat. 79
35. A sandy ridge exposed during low water level. Material is derived from foredune ridge via beach showing shallow erosional depressions. This indicates barrier growth seaward. Southern Kiswakini Island. 79
36. Sand ridge indicative of seaward growth of barrier island. About 1 km north of Mto Marereni tidal inlet. 80

37. General view of shore features found at about 2km North of Mto Marereni tidal inlet - a typical coast of recent submergence. Rocky Pleistocene reef platform exposed during low-tide water level. 80
38. A typical coast of recent submergence shown by destruction of seaward facing mangrove zone. About 2km north of Mto Marereni tidal flat. 81
39. Crest of submerged dune barely visible during low tide, a typical coast of recent submergence. Southern Kiswakini Island. • 81
40. Tamamba Island beach showing foredune ridge in the background and beach runnel with lingoid-shaped small-current ripples in the lower portion of the photograph. The flow is from left to right. About 1km south of Mto Tamamba tidal inlet. 83
41. Seaward view across the Mto Tamamba tidal delta and channel. Note that barrier bar sediments are clean sands and is muddier toward the subtidal ponds. 83
42. Small breakers of the spilling type, beach 1 km south of Sabaki river mouth. Note sea-weeds transported onto the beach. 91

43. Spilling breakers; Even though waves are refracted upon entering shallow water so that the crests are more nearly parallel to the coast, the process is rarely complete, and most waves approach the shore obliquely. Beach 1km south of Mambrui. 91
44. Surging breakers. Note well-rounded pebbles on the lower foreshore-transported northward from Sabaki river mouth by longshore currents and then pushed toward the shore by waves. About 1km north of Sabaki delta. 92
45. Plunging breakers against the beach of Robinson Island. Heights reach upto 1.5m. 92
46. Eolian sand from barrier island migrating into lagoon. Northern Giryama Village Island. 97
47. Waves breaking on the crest of submerged dunes, which is also partly exposed during low-tide. About 1 km south of Mto Tamamba tidal inlet. 97
48. Heavy minerals and many shell confined to the active berm zone, shore of northern Simiti Island. 122
49. Trench showing laminated beach ridge sediments. Dark portions are rich in heavy minerals. Note various levels of erosional truncation. About 1 km north of Mto Marereni tidal inlet. 122

50. Beach sediments showing transitional forms between current marks and rill marks, and heavy mineral concentrations on surface. About 1km north of the reef platform. 123
51. Barrier bar sediments at Mto Tamamba tidal delta. Current marks and heavy mineral concentrations on the surface. Note a tidal channel connecting the sea (right) to the lagoon. 123
52. Trench showing laminated storm berm sediments: dark layers are heavy mineral concentrations. Note various levels of erosional truncation. Tamamba Island. 125
53. Straight, partly bifurcating symmetrical wave ripples in coarse to very coarse sand. Also flat-topped and rilled to the right. Wave propagation was from bottom. Silversands Beach. 125
54. Asymmetrical undulatory current-related ripples in coarse to very coarse sand. Current travelled from right. Silversands Beach. 127
55. Swash marks, debris left at the highest point reached by waves. The sand shows bubble sand structure which was produced from the entrapment of air bubbles in the beach sand. 127

56. Backwash marks on a fine-sand beach at Gilani Beach made by projecting plant debris, which deflect the backwash of the waves. 129
57. Typical current ripples produced in beach runnel along the lower foreshore by longshore currents. Wavelength approximately 20cm. Gilani Beach. 129
58. Surface markings produced by foam blown across a beach sediment surface. Elongated bubble impressions arranged in rows are formed. Gilani Beach. 131
59. Water-level marks on a shifting sand bar (left). They are produced as a result of a discontinuously falling water level. The distributary (right) running seaward. Sabaki Delta. 131
60. Comb-shaped rill marks on a sharp, steep edge of shifting rivermouth sand bar. The flow is toward northern distributary (left). Sabaki Delta. 134
61. Rill marks with accumulation tongues. Sediment eroded during rill formation is deposited at the end of the rill system in the form of tongues a few centimetres thick. The flow is toward the lower left. Sabaki Delta. 134

62. Backwash ripples with a typical 40-cm wavelength on a fine sandy beach due to runoff of retreating waves. Sabaki Beach. 135
63. Trench showing laminated beach sediments; dark layers are heavy mineral concentrations and light layers are mainly quartz. Mambrui Beach. 135
64. Sedimentary biostructures are abundant on these beaches, among them the radial feeding tracks and the vertical burrows of the *Dotilla fenestrata*, a crab. Scale is 1m long. 137
65. Slip or avalanche face on leeward side of dune. Avalanche are set in motion when the slope of the slip face exceeds 34°. With each avalanche the dune advances a few centimetres. Mambrui Beach. 137
66. Truncation of dunes by deflation. Level of truncation is determined by the position of the groundwater table. Note shell pavement at the base of leeward slope of dune. Mambrui Beach. 138
67. Flat topped asymmetrical wave-formed ripples in medium to coarse sand (spade 1m long). They are formed in runnel in the landward side of fringing reef. Sheshale Bay. 138

68. Lunate megaripples observed on sediments of the northern part of Ngomeni bay barrier. Heavy mineral concentrations are found on crests. 143
69. Asymmetrical wave-related ripples in medium to coarse sand (spade 1m long). Waves propagated from left. Simiti Island. 143
70. Pattern of wave ripples produced by two equally strong wave directions. Simiti Island. 144
71. Pattern of wave ripples produced by two simultaneously working wave directions of unequal strength. In the lower margin of the photograph are lingoid-shaped small current related ripples. The direction of flow is from left to right. Ngomeni Bay barrier. 144
72. Trench in small wave-cut cliff on berm showing irregularly alternating light and dark layers ; the dark ones are rich in heavy minerals and light ones are indicative of disconformity. Simiti Island. 145
73. Current marks and heavy mineral concentrations on surface sediments. Tidal inlet, Simiti Island. 145

74. Transverse ripples, crests are slightly undulatory, partly bifurcating. They originate under the combined action of waves and currents. Ripple crests run perpendicular to the current. Tidal inlet, Simiti Island. 146
75. Longitudinal ripples, crests are straight, showing no bifurcation. They originate under the combined action of waves and currents. Ripple crests run parallel to the current. The direction of wave propagation is at right angles to it. Tidal inlet, Simiti Island. 146
76. Straight crested wave-generated ripples in medium to coarse sand (spade 1m long). Wave propagation was from top. Ripple marks are crossed by small erosional channels. View from Robinson Island beach facing southern tidal inlet. 148
77. Ripple train showing transitional forms between lingoid and rhomboid megaripples. Flow is from left to right. Tidal delta, southern Robinson Island. 148

78. Cut in foredune showing nearly parallel bedding in the upper left portion of the photograph and large-scale cross-bedding in the upper-right of photograph. Note heavy minerals, swash marks and root horizons. About 1 km north of Mto Marereni tidal inlet. 150
79. Swash marks showing linear arrangement of shell material. Spacing is about 40-50cm. Ras Kiswakini Island beach. 150
80. Swash zone showing approximately 90% of the bivalves arranged with convexity downward. Note branching, bifurcating and meandering rill marks. The flow is toward the right. About 1/2km south of the Mto Tamamba tidal delta. 151
81. Straight-crested megaripples. Ripple troughs are still partly filled with water. On the lee face of the megaripples water-level marks are present. Megaripples are covered with small ripples, which were generated after megaripples ceased to migrate. Flow is toward the observer. Note current marks and heavy mineral concentrations on surface. Tamamba tidal delta. 151

82. Lunate megaripples. Flow is from left to right.
Foreshore, about 1km south of Tamamba tidal delta. 152
83. Eolian sand from Kanagoni barrier Island migrating
into lagoon. Small rill marks towards the lagoon
are formed during emergence of the surface. 152
84. Branching rill marks. Small rills meet together to
form a broad main channel. Bifurcation is in an
up-current direction. The flow is toward the sea.
Kanagoni Island. 155
85. Current marks and heavy mineral concentrations on
surface in the lower portion of the photograph and
line of breakers in the background indicating
seaward extension of the barrier Island. About
100m north of Mto Tamamba tidal inlet. 155
86. Symmetrical wave-related ripples in fine sand (spade
1m long). They are straight crested and partly
bifurcating. Waves propagated from bottom.
Intertidal zone, Mto Tamamba inlet. 156
87. Lingoid-shaped small-current ripples. The flow is
from battom to top. Metre rule as scale. Mto
Tamamba tidal inlet. 156

88. Current crescent - obstacle mark produced in association with a treestump 1m in height. The flow is away from the observer. Kanagoni Island intertidal zone. 157
89. Isolated wave ripples originated on a sandy bottom covered with a thin layer of sand differing in grain size characteristics. Tamamba intertidal flat. 157
90. Undulatory megacurrent ripples. Crests are continuous but projected forward into tongue-like extensions. On the lee face of the megaripples water-level marks are present. Flow is toward the observer (Metre rule as scale). Mto Tamamba tidal channel. 158
91. Straight-crested megaripples. They are partly made up of dark heavy minerals. Megaripples are covered with small ripples, which were generated after megaripples ceased to migrate. Flow is from right to left. Tamamba intertidal flat. 158
92. Flat-topped, straight-crested wave-related ripples in coarse sand (spade 1m long). They are symmetrical and partly bifurcating. Barren zone, Kanagoni Island. 159
93. Trail left by echinoid crawling along the beach. 159

LIST OF MAPS AND SATELLITE IMAGERY (In Pocket)

Map

1. Locality map of the study area showing profile and sampling locations.
2. Geomorphological map of the Malindi-Fundisa area showing terraces of the Coastal zone.
3. Bathymetric map, from Malindi to Kanagoni.

Imagery

1. SPOT Satellite imagery of Malindi-Sabaki-Mambrui area in 1987 reveals fringing reefs (South), the influx of sediment laden water from Sabaki River forming a swirling mass of sediment at the Sabaki delta, and the dune system. (Image courtesy of Regional Center for Services in Remote Sensing, Surveying and Mapping).
2. SPOT Satellite imagery of northern Mambrui to Ngomeni in 1987 showing the bays large scale circulation, the silted reef (south), subrecent barrier beaches, tombolo, spit, barrier systems and salt pans. (Image courtesy of Regional Center for Services in Remote Sensing, Surveying and Mapping).
- 3.

3.SPOT Satellite imagery (1987) of Fundisa barrier islands lagoons, tidal inlets and deltas, tidal flats and salt pans. Dark brown is the spectral response to vegetation , white is the barrier beach. (Image courtesy of Regional Center for Services in Remote Sensing, Surveying and Mapping).

APPENDICES

APPENDIX I

Cumulative grain-size distribution curves for coastal sediments in the Malindi-Fundisa area. 228

APPENDIX II

Source data for petrology, chemistry, and texture of modern beach sand, malindi-Fundisa area. 256

1. INTRODUCTION

Research into the beaches and shore processes is essential if we are to monitor coastal morphodynamics and describe the modern environments of deposition, and obtain information enabling us to elucidate sediment transport and accumulation. This last factor is particularly significant from an economic standpoint with respect to heavy mineral distribution and concentration, hence providing valuable information for use during prospecting, exploration, evaluation and mining of heavy minerals and carbonate sand deposits. The results of such studies constitute a basis of future protection, management and development of the coastal environment.

This study is mainly concerned with short-term changes of the beach-face within the intertidal zone, reef, tidal flats, lagoons, barrier islands, and the associated microenvironments. These environments experience varying degrees of exposure and the subsequent local morphology, sediment grain size and mineralogy show correspondence to the near-shore dynamics.

1.1 Location and description of the field area

The area investigated during this study is the coastal strip of approximately 70km stretching from Malindi to Fundisa, bounded geographically by the 2° 48'S and 3° 12'S latitudes and extending eastwards from longitude 40° 8'E to the Indian Ocean. It embraces the northern portion of the Kilifi District and extends 2km northwards beyond the

southern margin of the Tana River District, in the Coast Province, Kenya (Fig.1).

The occurrence of heavy minerals along the Kenya coast has been recognised for many years around Malindi (Thompson, 1956; Schroeder, 1974; Halse, 1980). Beach placers are formed as a result of the concentration of valuable minerals in depositions of the detritus developing during the disintegration and deposition of the materials of rocks and minerals.

1.2 Major geomorphological features of the coastal belt of Kenya

The coastal belt of Kenya may be divided into four physiographic units which are more or less parallel zones or plains, each slightly dissected by denudation, and rise in steps one above the other toward the interior (Fig.2). This subdivision is largely controlled by the local geology (Fig.3). In the Tana River District, however, the division does not apply as the coastal plain occupies the entire coastal belt. The coastal geomorphology of the present area is markedly influenced by the only two permanent rivers: the Tana and Sabaki rivers entering the Indian Ocean.

A brief description of the four major physiographic units starting from the coast to the hinterland is given below.

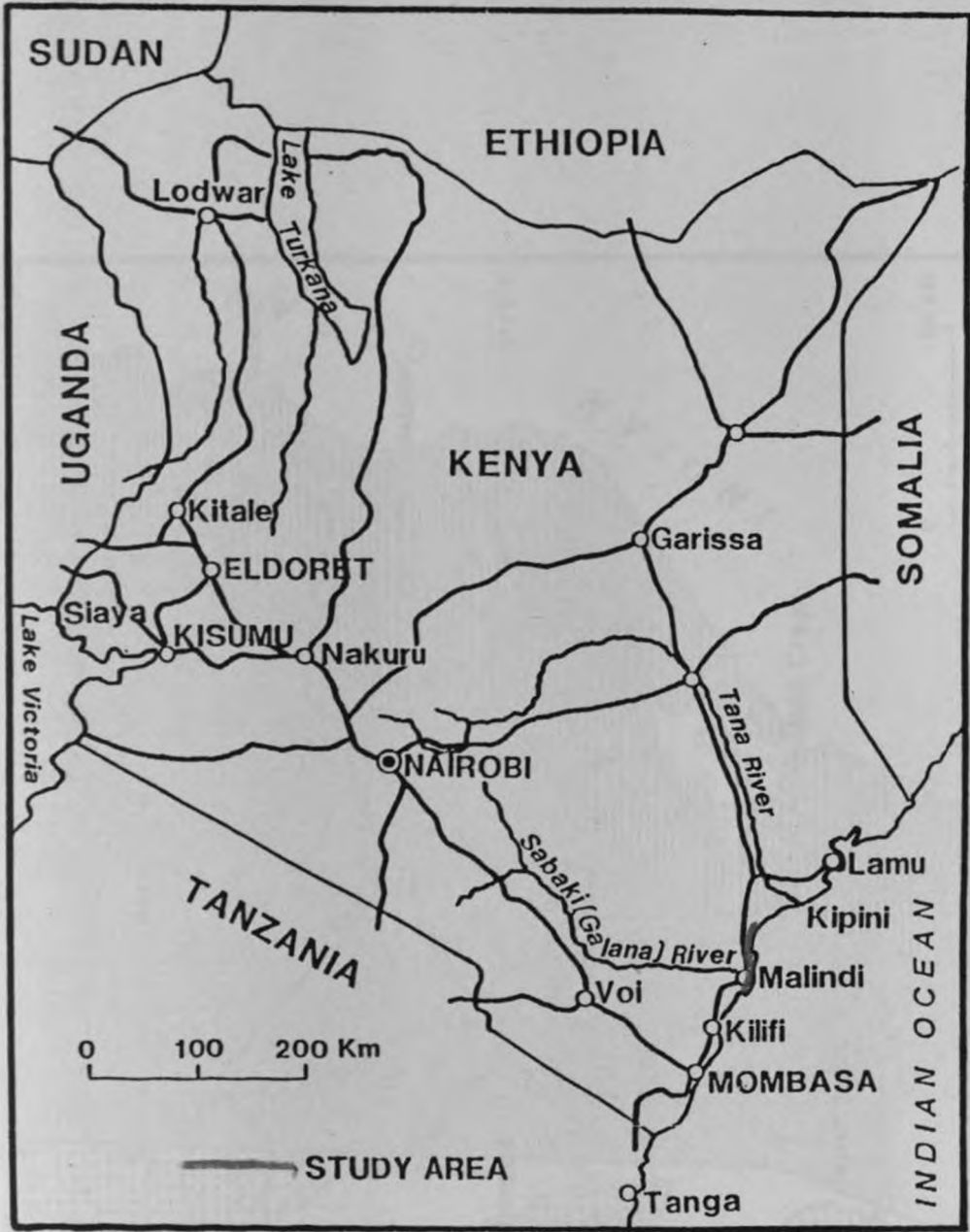


Fig.1. Map of Kenya showing location of study area.

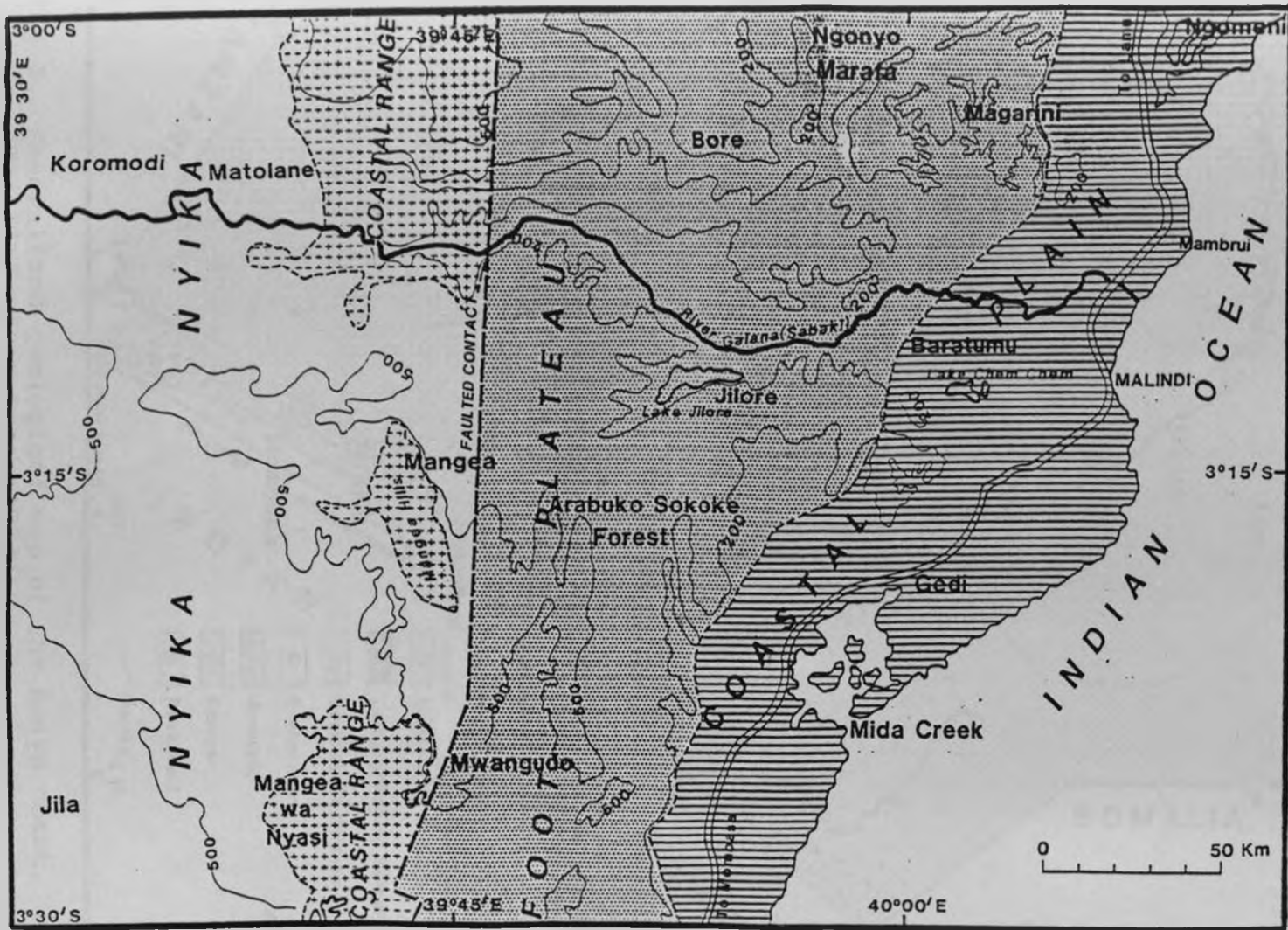


Fig.2. Geomorphological and drainage map of the Malindi area. (Modified after Thompson, 1956).

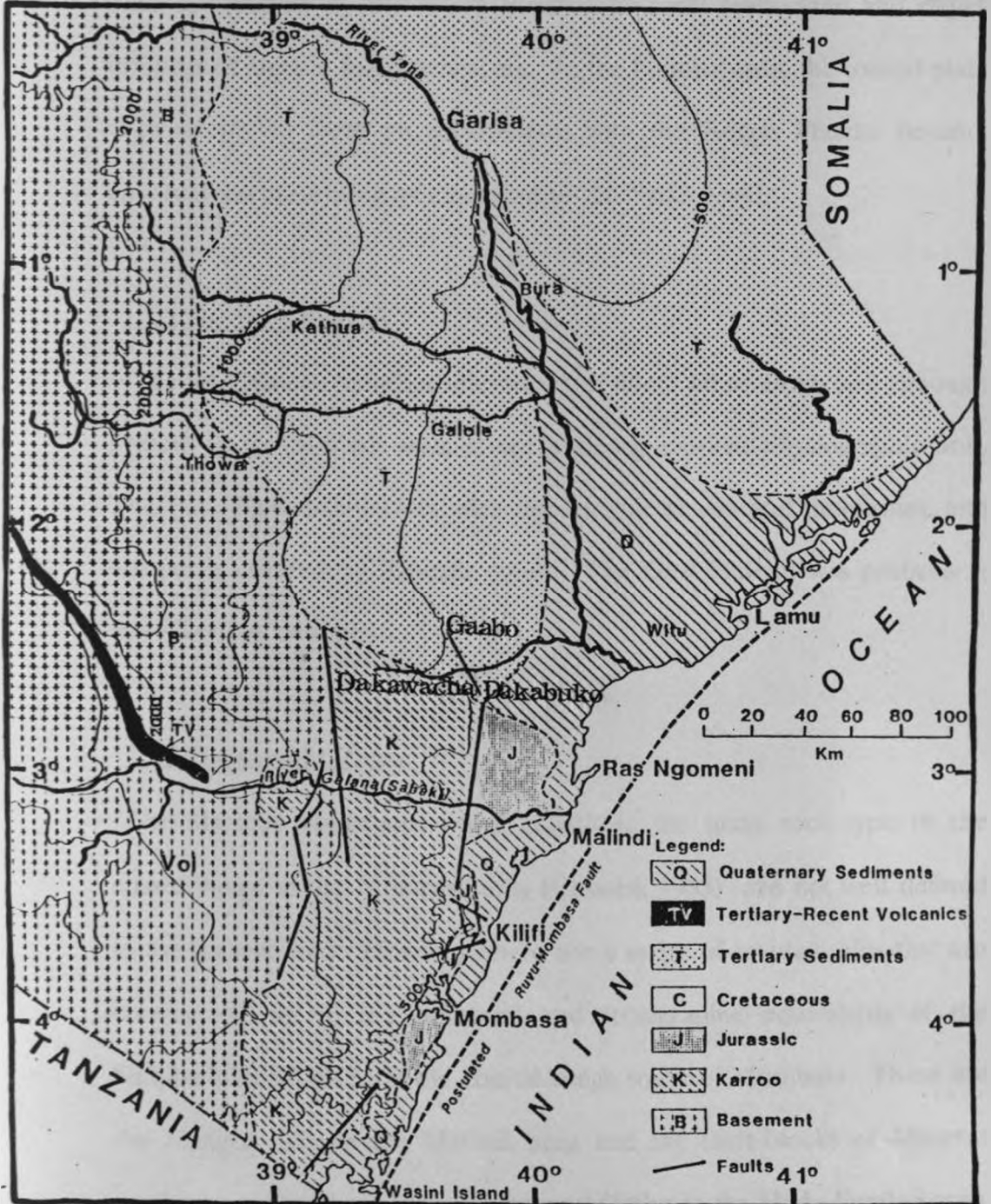


Fig.3. Generalized geological map of the Kenya coast.
(Modified after Ojany, 1984)

1.2.1 The Coastal Plain

The width of the coastal plain varies between 4km in the south and 16km in the north and generally is under 45m in altitude. The coastal plain is occupied by the raised Pleistocene coral reefs, sand and clayey infillings of lagoon, fossil dunes, etc. In the Fundisa area, the coastal plain rises steeply to form an escarpment, with the Rogge Plateau beyond, apparently representing an extension of the Nyika bevel.

1.2.2 The Foot Plateau

The foot plateau stands at elevations of about 60 to 140m and although present in the Malindi area, is not a clearly marked physiographic unit. The Foot Plateau coincides with the Jurassic shales and limestones, and are partly covered by Pliocene sands. The Foot Plateau was probably a late - Tertiary peneplain.

1.2.3 The Coastal Range

The Mazeras sandstones which constitute the main rock type of the coastal range in the Mombasa area (Caswell, 1953) are not well defined in the present area. However, there are a series of residual hills that are considered to be the structural and stratigraphic equivalents of the Shimba hills, which form the coastal range south of Mombasa. These are the Mangea hills in the Malindi area and the fault-blocks of Mazeras sandstone at Dakabuko, Dakawacha and Gaabo in the Hadu-Fundisa area.

The hills generally rise to an altitude of 180-300m above sea level and sometimes reaching 520m. The Mazeras Sandstones are of Triassic (Upper Karroo) age.

1.2.4 The Nyika

The Nyika is the area west of the contact between the Jurassic and Triassic rocks. Thus the Nyika bevels both the Triassic and Mariakani Sandstones. Caswell (1953) considers the Nyika to be the remnants of a peneplaned surface of mid-Pliocene age. The average altitude of the Nyika surface west of the Malindi area is about 150m.

1.3 General Description of the eastern Africa continental shelf

The East African coast is an Afro-trailing type (Inman and Nordstrom, 1971), but the Gulf of Aden at the north is a neo-trailing-edge type because of the more recent splitting of Africa from Arabia. The shelf on the east coast of Africa is narrow and poorly surveyed. In places there appears to be no shelf along the straight coast, the indentations are accompanied by a widening of the shelf, but narrow zones occur off the reefs and islands. The shelf widens south of the Zambezi River to 130km off Beira at 20° S latitude. Most of the shelf is shallow with marginal depths around 55m. A narrow stretch follows, and then the shelf again widens to about 130km between 25° and 26°S latitude but here the increase is related largely to a marginal plateau with depths of the outer

portion about 380 and 550m. The shelf is narrow again to the south except for a bulge north of Natal, where an unusually even bench terminates at 90m.

The continental slope off eastern Africa is not well sounded but appears to be mostly less than 3° with the steeper areas off Somali Republic and a portion of South Africa, south of Durban. Very gentle slopes are found off Kenya and Tanzania. The slope base is rarely deeper than 3000m.

The sediments on the East African continental shelf have been little studied. A few samples taken along the shore off Somalia and Kenya consist of calcareous sands (Schott and von Stackelberg, 1965; Muller, 1966). Shells and coral sand are indicated on the charts further south. In the present area of study, the continental shelf ranges from 3 to 25km wide with the seaward limit marked by a drop in depth of more than 1000m. Its geochronology involves flexure and subsidence of about 5000-6000m since Triassic times.

The shelf deposits consist of reefs and carbonate sand and mud whose distribution is largely unknown. An interesting geomorphological characteristic of the shelf in the Malindi Fundisa area is the terraces at about -8m, -33m and -44m which probably correspond to the benches on the sea-floor during the various stages of sea-level drop.

1.4 Climate

The coastal belt of Kenya experiences an equatorial monsoon climate with south-east trades prevailing from April to October and a north-east monsoon from November to March (Climatological Statistics for Kenya, 1984). The Malindi area has a humid climate with average rainfall of 90.2mm/year. There are two rainy seasons. Rainfall maxima occur in May and October, with over half the annual precipitation falling between April and June, during the south-east monsoon. Although Malindi has an average of 145 rainy days per year, the precipitation is usually concentrated in storms and showers. There is no real dry season due to the effect of the Indian Ocean, but the potential evaporation averages about 200mm per year and is nearly twice the mean annual precipitation. The amount of rainfall increases from north to south (Table 1, Climatological Statistics for Kenya, 1984).

Monthly variations in air temperatures are small. The hottest months are usually February or March which have average temperatures of 28.5° C and 28.8° C, whilst the coldest months are usually July and August with average temperatures of 24.7° C. Diurnal temperature variations are usually within the range of 7°C - 9°C, although the maximum and minimum temperatures recorded at Malindi are 35.6°C and 18.9°C. The relative humidity is nearly always above 70%.

The winds depend on monsoonal air currents. The strongest winds are produced by the south west trades. These generate large waves and swells.

Table 1: Annual long term average rainfall upto 1988. Courtesy of the Meteorological Department at

Dagoretti.

Name of Station	Jan.	Feb.	March.	April	May	June	July	Aug.	Sept.	Oct.	Nov.	Dec.	No. of Years	Av. annual Rainfall (m.)
Lamu Meteorological Station	5.6	3.0	25.9	129.4	343.4	163.6	75.2	40.7	38.4	40.4	35.6	27.3	78	77.2
Malindi Meteorological Station	7.8	10.2	44.1	167.1	325.3	150.5	94.7	63.7	45.6	71.2	69.4	32.3	25	90.2
Mombasa Old Observatory	24.9	16.2	58.8	200.6	316.5	113.0	85.4	66.7	66.2	90.6	96.6	55.5	96	99.3
Shimoni Fisheries Station	24.3	8.8	74.8	213.9	304.3	133.5	114.4	45.3	39.4	55.2	93.1	61.0	13	97.3

Cloudy and overcast skies are often associated with the south west trades, but clear skies, light winds and smooth calm seas usually accompany the north-east monsoon. Stormy winds above 7 Beaufort force are rare (about 1%). The coastal zone is subjected to tropical storms which are particularly prevalent during the south-west monsoon in the months of April to October. The north-easterly winds are generally 2-3 Beaufort force.

1.5 Major oceanographical factors operating off the Kenyan coast

From the south as far as Ras Biongwe ($2^{\circ} 25'S$ latitude) the East African coastal current flows northward during the whole year. North of Ras Biongwe the current goes northward only during the south-west monsoon, April to October/November. At the time of the north-east monsoon, November to March, the Somali Current prevails against it and sets southward (Johnson et al., 1982).

The south-west monsoon range to the Horn of Africa, flows at a depth of 110-130m and has a speed of 3- 7km/hour. During the north-east monsoon which ranges to Lamu/Malindi area and flows at a depth of 55-90m, the speed is 1.6-3.0km/hour.

The tides are semi-diurnal, with two maxima and two minima within a lunar day (24h 50min). The stream of rising tide sets northwards and that of falling tide southwards. Tidal variation increases from north to south (Table 2).

Table 2: Tidal condition during neap and spring tides at 4 stations along the Kenya coast.

Name of station	Mean High Water		Mean Low Water	
	Springs	Neaps	Springs	Neaps
Lamu harbour	2.7	1.9	0.5	1.3
Malindi	3.4	2.4	0.5	1.4
Mombasa	3.4	2.4	0.3	1.3
Wasini Island	3.6	2.5	0.3	1.4

Admiralty chart 6271, 1980 and 6272, 1970.

During April-October the dominant direction of waves breaking upon the beach area is from south-east. The deep-water wave height of more than 60% of them at break point is over 1m. During November-March the dominant direction is from north-east and 55% of the waves attain wave height below 1m. The mean monthly sea temperature is minimum at 24° C in August and maximum at 29°C in April. The sea water salinity varies from 34.5‰ minima during north-east monsoon to a maximum of 35.4‰ for the rest of the year.

1.6 Previous Work

Past investigations of heavy minerals centred on the Sabaki River mouth, Malindi and the Ungama (Formosa) Bay areas. The results of the investigations (Pulfrey, 1942) showed that although widespread, the deposits are of low grade in comparison to workable occurrences elsewhere in the world. The first mineralogical examination was made by

Pulfrey (1942) on the Gedi Silversand deposits. He reported that only the dune sands found 4km north of Malindi may be of economic value. He estimated the dune sands to contain about 28% of ilmenite. He noted that hornblende and garnet are also prolific, and concluded that search could probably not reveal higher concentrations of ilmenite. Further, rutile and zircon constitute a low percentage whilst monazite is rare. Ryan (1953), then holding an Exclusive Prospecting Licence for an area of approximately 0.8km of the Silversands beach south of Malindi, noted the cemented black sand but did not carry out any further prospecting.

Extensive prospecting operations and laboratory tests were carried out by Mc Guinness in 1953 (Thompson, 1956; Williams, 1962). The majority of samples were taken from banka drill holes sunk to an average depth of 3m along lines at approximately 1.6km interval. No regular close grid sampling was undertaken and sampling ceased at water saturation levels. The average ilmenite content was found to be less than 2% which on experimental concentration yielded about 40% TiO_2 , necessitating further treatment to increase the TiO_2 content to the minimum of 50% normally required to render the concentrate economical for exploitation. McGuinness had reported that upto 6% of the iron in the ilmenite can be successfully removed and also suggested that the vanadium can be extracted separately as an important by-product which would then offset the additional concentration costs.

Beinge (1957) examined sands in the Malindi-Fundisa area. His report indicated that the black sands in this area consist essentially of magnetite and ilmenite in approximately equal proportions and concludes that there is no other mineral of economic value. Thompson (1956) and Williams (1962) separately conducted geological reconnaissance surveys along the coast of the same area. Their investigations showed that the richer heavy mineral concentrations along the northern coast of the Malindi region consists principally of titaniferous iron sands (ilmenite, haematite, magnetite) with subordinate zircon, rutile and garnet. They further observed that minerals with high TiO_2 - content in beach sands from Ras Ngomeni are inhomogeneous. The composition of individual sand grains are affected by a complex intergrowth of ilmenite, haematite, and other titanium iron ore minerals.

In the 1950's and 1960's the British Standard Portland Cement Company Ltd. sporadically mined the Ngomeni beach sands as a source of iron for use in the manufacture of sulphate resistant cement. The most recent exploration of the Formosa Bay heavy mineral beach sand deposits was conducted by Halse (1980) in the area between the Tana and Sabaki river mouths. He divided the reserves into three categories of proved, probable and possible cases.

Schroeder (1974) carried out a brief review of basic sedimentological information during which he dwelt on the general aspects of specific near-shore sedimentary environments encountered in the Malindi area.

Schroeder and Jacob (1976) also carried out in-situ resin impregnation of cores and profiles in coastal sediments as an aid to the study of composition, fabric, and sedimentary structures of unconsolidated or poorly consolidated sediment in vertical sequence.

Nzioka (1981) presented oceanographic data on seasonal patterns of surface currents, waves, wind direction/force and cloud cover along the Kenya coast. Also informative on shelf dynamics and the extent to which ocean currents influence the coastal geomorphology is the work of Johnson et al. (1982). They used the transient monsoon current system of the northwestern Indian Ocean to investigate the dynamics of rapid western boundary currents as part of the Indian Ocean Experiment (INDEX). The study focussed on the southern boundary of the annually reversing Somali Current where interaction with the East Africa Coastal Current is an important feature. They suggested that the location of the southern boundary and the rapid switching action of the currents may, in part, be topographically controlled.

1.7 Theories behind the research project

There are various processes responsible for deposition of beach sands and the geological distribution can also be correspondingly varied. The fragmental rock material which reaches the coastal region via the mainland drainage system and the parent rock on the shelf and coast e.g. coral reefs and relict submarine features can be worked over by waves,

surfs and currents (jigging action). This often leads to hydraulic sorting and deposition of heavy minerals. Longshore and tidal currents can concentrate heavy minerals in the offshore zone by winnowing out the lighter materials and spreading the heavy minerals along the coast. Storm waves and breakers rework the placer deposits in very short time. Factors generally considered conducive for the formation of placer deposits (Schroeder, 1974) are:

- (a) Stable coastal area with neither erosion nor excessive deposition,
- (b) Energy of breaking waves exceeding the energy of the surf waves,
- (c) Presence of a narrow beach.

However, this view to some extent contradicts a little bit studies in North America and Dar-es-Salaam where concentrations of heavy minerals occurred when two conditions were fulfilled (1) High wave energy and (2) low sand supply. Here, the concentration process is related to erosion (Fay, personal Communication).

Sutherland (1982) has presented a sediment transport model which attempts to describe the systematic variation in size and quality of minerals that result from transport by marine processes. Alongshore transport can be followed for several hundred kilometers with a systematic reduction in grain size accompanying such transport. The mineral size and form distribution is progressively modified with increasing travel distance. However, this model must be used with caution as the systematic variation is frequently limited and sometimes obliterated altogether since various

parameters are involved in sediment distribution. The composition of beach sand concentrates is highly variable in both lateral and vertical directions (Smirnov, 1976).

It is therefore of both geological and economic interest to find out if there is any systematic variation along the direction of transport in size distribution and mineralogical content. This kind of sedimentologic approach is very relevant to the economic assessment of heavy mineral deposit. The relevance of the present study is due to the fact that the rivers are the means of introduction of the heavy minerals to the coastal zone, after which alongshore wave action transports, sorts and concentrates the minerals in such a direction as the dominant transport along the coast.

The sedimentary environment is characterized by a complex set of physical, chemical, and biological conditions under which the sediment accumulate. It is a spatial unit in which these conditions are sufficiently constant to form a characteristic deposit. The sedimentary facies result from various processes and factors effective in the sedimentary environments. Consequently spatial or temporal changes of the environment are reflected by corresponding changes in sedimentary facies. This forms the basis of the facies concept attributed to Walther (1894). Since a limited number of basic types of environments exist, the facies concept is a useful tool which can be used to construct horizontal and vertical facies pattern or a three- dimensional facies model.

Sediment textural analyses for the East Weddel sea- Antarctica samples from cores has been done by Bright and Anderson (1982) who observed variations in sediment character that they suggested would reflect the mechanics of transport dominantly by one or a combination of the following: littoral drift, wind currents and tidal currents. To provide a basis for documenting the various findings, it is necessary to present a three-dimensional beach model applicable to open sandy coastal environments. Short (1979) has suggested a model that consists of several beach stages incorporating erosional and accretionary sequences of beach-surfzone morphodynamic conditions. Each stage is associated with a particular level of breaker wave power. Beach-surfzone morphological shape is produced by dynamics associated with incident and resonant oscillation frequencies interacting with the beach gradient and sediment coupled with pre-existing morphologies. This combination of beach-surfzone morphology and wave-current dynamics is here called beach morphodynamics. Davis (1978) considered in depth the relationship between sediment parameters and beach morphology, and Cousminer and Puffer (1982) found that textural changes among the beach sediments correspond to the environment of deposition. Here, the depositional environment is the beach, where the energy conditions might vary.

Sakalowsky (1975) estimated the energy affecting the beach configuration from measurement of beach processes and response

elements. Beach and surfzone gradient ($\tan\beta$) in conjunction with incident waves determine the surf scaling parameters (n) and therefore the degree to which the beach is reflective or dissipative. Whereas the breaker wave power provides the energy to move a beach through various beach stages, the beach gradient and sediments determine the horizontal and lateral scales of morphodynamics

Sasaki and Horikawa (1975) also use $\tan\beta$ as a major parameter in defining the domains of nearshore circulation, edge wave, instability and infragravity. The seaward backwash is generally weaker than the shoreward movement of water from collapsing waves because of percolation and frictional drag on the swash. Sediment is thus moved up the beach slope until an equilibrium is established. Maximum percolation occurs on the most permeable coarse sand beaches and these usually have the highest slopes. Assuming that gravity opposes the net shoreward drift of sediment, Inman and Bagnold (1963) obtained the following relationship for local beach slope $\tan\beta$.

$$\tan\beta = \tan\theta \frac{1 - c}{1 + c}$$

where θ is the coefficient of internal friction, c is the asymmetry term for offshore versus onshore wave energy.

The influence of tides on the beach model increases with range. At high-tide, the steeper face is incorporated into $\tan\beta$ and more reflective conditions. The size and scale of beach morphologies is inversely related

to beach gradient, width, sediment volume and surfzone and spacing of the shore normal and shore parallel morphologies.

The distinction between beach and tidal flat has never been satisfactorily defined, but generally beaches occur as narrow intertidal to supratidal features dominated by wave action in which the sediment coarsens landward. In direct contrast, tidal flats are wide areas dominated by to and fro tidal motions in which the sediment fines landward. Tidal flats occur on open, macrotidal coasts or as part of back-barrier complexes on mesotidal coasts.

Coastal dunes develop where there is a sufficient supply of sand, mainly from the shoreface, and where a dominant strong wind is present in the onshore direction. According to Gripp (1968), coastal dunes develop on stable, and especially on prograding shores. The coastal dunes often occupy a broad zone along the coast (Cooper, 1967).

1.8. Objectives of this study

The Malindi-Fundisa area provides an excellent opportunity to study sedimentological aspects of varied and contrasting modern nearshore environments. The area has been chosen because it offers an opportunity to study the complex interaction of process and response elements on marine and related environments. One of the reasons why the study became necessary is that sedimentological knowledge of heavy mineral sand deposits of the area was scant. Therefore the objectives were to:

1. Design or formulate and recommend the necessary action plan for the protection, management and development of the marine and coastal environment of the Malindi-Fundisa region.
2. Elucidate the geomorphology and chronology and hence classify the present shape and position of the coast in relation to the process of emergence and submergence, of accumulation and erosion. Recognize specific geomorphological processes in the formation of coast.
3. Describe the sedimentology of the near-shore and shelf environments. This is intended to provide a better understanding of the geological circumstances and genesis of the deposits and to assess the economic potential of the valuable placer minerals on the beach, berm and frontal dune deposits.
4. Establish the provenance, transportation and accumulation of the beach and dune sediments from facies distribution.
5. Relate the process to response elements and hence present a beach-surfzone morphodynamic model through a comprehensive integration of the dynamics, beach morphology and sedimentology.

2.METHODOLOGY

2.1. Field Methods

2.1.1. Mobility

2.1.1.1. Locomotion.

Intertidal and supratidal areas were visited by foot. An occasional hired boat or canoe provided transport over subtidal and submerged areas. Investigations of the sea bottom were made by skin diving operations from the boat or canoe.

2.1.1.2 Position Fixing.

Positions were fixed by compass bearings, horizontal sextant angles, trigonometry and map or aerial photograph interpretation. Distances were measured with a plastic tape, pacing, estimation or calculation, depending upon the terrain, accessibility, working conditions and the accuracy required. Heights were measured by leveling with an Abney level or calculated with the aid of a clinometer. Depths were measured by hand lining.

2.1.2 Data Collection and Measured Parameters.

Sampling. 110 unlithified sediment samples were collected at 75 sampling locations (map 1). The beach was sampled parallel and perpendicular to the strand line. Beach-sediment samples were collected with a cylindrical plastic corer along grid lines at intervals of about 1/2 km

at various levels of the beach including the mid-tide level (Appendix II). Individual serial samples were recovered from particular areas such as berm zones, frontal and high dunes as well as spot samples of tidal flats, channels and bars. All samples were then packed in plastic bags and numbered. These were then transported to the University of Nairobi. On arrival at Nairobi the unlithified sediments were washed and dried.

The main problems encountered when sampling were inaccurate position fixing and plotting, or the collection of samples which were not typical for the environments or units sampled. However, errors in position fixing are not considered to be of great significance because absolute positions of sampling are not critical to the interpretation of the results. The relative position of adjacent or neighbouring sampling sites and stations, together with the nature of the surrounding environments, rocks or sediments are, however, of critical importance. Further, reduction of 1:50,000 scale working topo-sheets to a much smaller scale greatly reduces the errors in position fixing.

2.1.3 Facies Analysis

Sedimentary structures and geometry were largely, if not exclusively determined in the field together with information concerning the biogenic material as well as the preliminary data on lithology. Tools for collecting such data were measuring tape, rod, or line, compass, clinometer and hand lens. Reference slides for visual comparison of particle size were used.

With the aid of hand lens samples were compared en masse with the reference slides containing grains of 2mm (-1.0), 1mm (0.0), 0.5mm (1.0), 0.25mm (2.0) and 0.125mm (3.0Ø), and assigned each sample to appropriate size classes.

Basic information and terminology on the ecology of the near-shore environments was provided by Prof. Francois Blasco.

2.1.4 Beach State Model Parameters

With the intention to present a beach model in the final analysis, it was necessary to measure both the process and response elements. This was supplemented by aerial photograph interpretation, SPOT satellite data and detailed ground truth survey to enhance and confirm the validity of cartographic and morphometric analysis of the envisaged model. Daily field observations included deepwater and breaker wave height and period, wave direction, wind direction and velocity, and beach state. The beach state observations were recorded on a beach state map which represents the morphodynamic conditions existing between the upper swash limit and the outer breaker zone at low tide. The conditions observed include the position and scale of all beach (cusps, berms, scarps, megacusps, and other beach markings and structures) and surfzone (primarily bars and channels) that relate to breaker wave height and direction, and surfzone current direction and relative velocity.

2.1.4.1. Measurement of process elements

The process elements were recorded daily in the field at intervals of 4 hours for 12 hours of the day on the assumption that the processes in the next half of the tidal cycle are consistent and similar to those measured earlier on. Field traverse logistics were planned on day-to-day basis in accordance with the tidal tables by the Kenya Ports Authority for East African Ports. The author's measurements established the difference in tidal height for the two maxima and two minima within a lunar day as only slight.

Significant wave height H_s , that is, the average height of the highest one-third of the waves was measured during a period of 10 minutes. Estimates of height was made at the break point of the waves, that is, the instant before they break - by comparing the wave with a structure of known height and measuring with a meter stick. Wave period was recorded with a stop watch. Wave length being a function of wave period was determined through the empirical formula for deep-water wave length, where deep-water is defined as greater than half the wave length: $L = 1.56T^2$, where L is the length in metres and T is the period in seconds. Wave steepness was determined by the ratio of wave height to wave length. Longshore current was determined by measuring the horizontal distance that fluorescein dye moved within the breaker zone during a period of 60 seconds. During the survey trips, special current observations were made by means of a free drifting buoy (15 cm) attached to a weight

by one metre rope, for partial submersion in order to avoid the influence of the wind.

Wind direction, wind velocity, atmospheric pressure, temperature and precipitation were recorded with instruments of the Meteorological Department located at Malindi Airport adjacent to the study area. The author also referred to the already published tables at the Meteorological Department in the Ministry of Transport and Communications, Dagoretti Corner, Nairobi.

Tide level was recorded as the vertical distance of the high-tide line above mean sea level. This was done only at Malindi town using a scaled meter rod whitewashed with lime upto a mark beyond a probable high tide level. The rod was then placed in a cylinder with locking facilities attached to the Malindi Jetty.

2.1.4.2. Measurement of response elements.

The response elements were measured at low-tide along two profile lines 1/2km . The process elements were observed and recorded at least 24 hours prior to the response measurements (Krumbein, 1961), in order for the beach-face to adjust to those energy elements at work. Beach width is the area between the high-tide and low-tide levels. Beach height represents the elevations or vertical distance of the beach above mean sea level along the beach-face between the dune-base line and the water line

and is expressed as a tangent for the elevation differences between points of height across the beach-face.

2.2 Laboratory Methods

2.2.1 Grain size distribution analysis

Grain size analysis was accomplished using a mechanical shaker with a nest of 10 sieves of upward- increasing apertures. The grains became separated into their respective grades. Size values for the sands were obtained using sieves of -1.0,-0.5,0.0,0.5,1.0,1.5,2.25,3.0,3.5 and 4.0Ø mesh size and pan, sieve brush and balance. The weight percent of the total sample retained in each of the sieves measures the frequency in the sample of the grains ranging in size between the apertures of that sieve and the next coarsest.

Grain size data were subjected to statistical analysis after Folk and Ward (1957) to give a series of parameters descriptive of sediments. These include graphical median, mean, sorting, skewness and kurtosis and which are given by the formulae;

$$\begin{aligned}
 \text{Median} &= \text{Ø}50 \\
 \text{Mean } M_z &= \frac{\text{Ø}16 + \text{Ø}50 + \text{Ø}84}{3} \\
 \text{Sorting } s &= \frac{\text{Ø}84 - \text{Ø}16}{4} + \frac{\text{Ø}95 - \text{Ø}5}{6.6} \\
 \text{Skewness } s_k &= \frac{\text{Ø}16 + \text{Ø}84 - 2\text{Ø}50}{2(\text{Ø}84 - \text{Ø}16)} + \frac{\text{Ø}5 + \text{Ø}95 - 2\text{Ø}50}{2(\text{Ø}95 - \text{Ø}5)}
 \end{aligned}$$

$$\text{Kurtosis } K_g = \frac{\phi_{95} - \phi_5}{2.44(\phi_{75} - \phi_{25})}$$

Wentworth (1922) metric scale have been used for particle size measurement and the Krumbein (1938) phi (ϕ) scale ($\phi = -\log_2 d$, where d is the diameter of the particle in millimetres) adoption of this to simplify both plotting of the distribution of particle size and subsequent statistical analysis. The size distribution analysis is a useful technique in the understanding of processes of transport and deposition of sediments.

2.2.2. Roundness and sphericity analysis

Shape and form of sediment were given using the principal indices namely roundness and sphericity. Both roundness and sphericity of grains were determined by comparing 100 grains from each specimen with the Powers (1953) visual comparison charts, and from the results mean roundness and sphericity for each specimen were estimated.

Percentage of total sample in each roundness and sphericity class was calculated, then multiplied by the class midpoint and total values obtained. From these summed values, mean roundness and sphericity values were obtained. These principal grain form parameters have helped in the description of sedimentary materials and evaluate the present day processes in the marine environment.

2.2.3 Mineralogical studies

All samples were split and assayed for their mineral content, having sieved the sand fraction into standard sizes. Each fraction had been weighed during grainsize analysis, and a cut was taken from each sieve and spread over a gridded tray. Then 100 or more grains were classified and any bias was minimized by choosing the grains nearest grid intersections. The cut was made by spreading the sample over a large tray and small scoop samples taken from various parts of the tray. The counting of the grains was accomplished by using a Point Counter of the type with eight keys that was operated by the touch method without removing eyes from the field of view of the binocular microscope. When 100 grains had been counted, the percents of constituents in each size were multiplied by the weight percent for the respective grade sizes; thus, the percent of each constituent in the whole sample was calculated.

2.2.4 Geochemical analyses

The amount of carbonates in the samples was determined using acid-soluble content analysis with dilute (1:9) hydrochloric acid.

Air-dried sediments were ground to a fine powder, dilution carried out with wax and pellets made of approximately 5.00g. Silicon, titanium, calcium, iron and zirconium in the sediment samples were determined by X-ray fluorescence analysis, using a sequential X-ray spectrometer system PW1404. Element weight percents were derived by computer plotting

average element counts on standard curves which had been prepared with synthetic samples. 1g of powdered samples were attacked with aquaregia solution (1:3 mixture of concentrated nitric and hydrochloric acids) and placed on heated sand bath. The resulting salts were dissolved in distilled water and made up to 50 ml solution. Manganese concentrations were determined with a Perkin-Elmer P49400 Series Automatic Multi-Element Atomic Absorption Spectrometer, with intelligent flame optimisation and high-energy, beam-profile matched background correction. Vanadium and chromium concentrations were determined by the Perkin-Elmer ICP/6500 System-a computerized sequential inductively coupled emission spectrometer.

2.2.5. Coastal classification: Cartography and Morphometrical Analyses

Classification of the coast was based on a study of large-scale navigational charts, topographical maps, wave ray diagram, aerial photographs and airborne multispectral SPOT satellite data. This involved recognition of specific geomorphological or geological processes in the formation of coast according to Shepard's (1978) classification. Emphasis was placed on coastal remote sensing techniques as a basis of understanding these essentially dynamic environments such as dunes, barrier systems, suspended sediment patterns, wave spectra, sea state and the distribution of coastal ecosystems (mangrove, salt-marshes, coral reefs, etc) were

obtained from aerial photographs and multispectral data. Photographs provided additional support on ground controls data.

2.2.6 Analysis of Data

The results obtained from field and laboratory analyses are presented as cumulative frequency curves, scatter diagrams, line graphs and rose diagrams. Statistical analysis methods were then used for both descriptive and inferential purposes on the measured parameters. This involved graphical measures for median, mean, skewness, sorting and kurtosis. Numerical measures were also useful in this case. In specific instances, bivariate analysis was applied to test the degree of relationship between variables; as an aid to classification in order to define depositional environments and to study the processes and factors effective in the environments. An attempt was made to isolate significant energy components affecting beach morphology in the Malindi - Fundisa area. SPOT Satellite data was processed on computer by image stretching, dynamic contrast enhancement and classification.

2.2.7 Presentation of Results

The observations, results, interpretations and discussions are presented in the subsequent chapters and the tables, figures, plates and maps of this thesis. It is intended that these results satisfy the objectives outlined in section 1.7.

3. MALINDI - FUNDISA SEACOAST CLASSIFICATION

Analyses of geological and structural maps, topo sheets, aerial photographs and satellite images of the coast of the Malindi-Fundisa area show a great contrast in the configuration of the shoreline. Coasts, in Malindi-Fundisa and elsewhere, owe their present shape and position to the processes of emergence and submergence, of accumulation and erosion. They have been classified in terms of these processes by Valentin (1954) and Bloom (1965). Geomorphologically, Kenya's shoreline exhibits evidence of emergence, submergence and compound type coasts (Johnson, 1919). Another classification is based on land-sea morphological relations (Ottman, 1962). Here, the different relations between the profile of the coast and of the adjacent sea floor are used as a basis. The Ottman concept of classification will place the Malindi-Fundisa shoreline in its type-E consisting of coastal plains that continue beyond the shoreline as gentle slopes. This group includes deltas, barrier and lagoon margins, dune coasts, and low coasts inside coral reefs. Based on plate tectonics (Inman and Nordstrom, 1971), Kenya's coast is classified as an Afro-trailing edge coast having a prominence of plateaus alternating with plains and have relatively narrow continental shelves. It also has a low level of volcanic and seismic activity. However, these classifications may require considerable interpretation, besides there are many ways in which various materials react to various processes. Thus a more directly applicable classification was proposed by Shepard (1978). In his classification the

coasts are distinguished by specific geomorphological or geological processes (Map 2) which formed them. In terms of Shepard (1978) classification the Malindi- Fundisa coastline is dominated by the effects of marine action and (to a less extent), of a coastline whose form, is primarily due to non-marine agents.

Malindi marks the boundary between the southern and northern section of the Kenya coast which differ considerably. Along the Kenyan Coastal Belt and Plains, from Shimoni northwards into Lamu archipelago, there are marine features that show conclusively that this is an emergent coastline. The occurrence of weathered Kambe Limestone Formation considerable distance from the present shoreline provides such evidence as these rocks indicate the extent of emergent land.

In the southern section, the coastal plain is 3-6km wide and attains elevation of upto 50m; its landward boundary is marked by the rise of the foot plateau, whose elevations ranges from 60-130m (Fig.2). The coastal plain is composed of Pleistocene coral reef rock, infilling in reef lagoons and channels, and of coastal dunes. These rocks form the cliff which is the major coastal feature from Vasco da Gama point southwards. The cliff is up to 30m high; at a short stretch north of Kilifi it is directly exposed to wave erosion. For most of its extension, however, it is paralleled and protected by a coral-algal fringing reef with a platform of upto 2km width. At some portions of the coast, beaches accumulate behind the fringing reef at the foot of the cliff-Pocket beaches accumulate around Malindi for

example the Silversands Beach. An interruption of the fringing reef occurs north of Malindi due to outflow of fresh water from Sabaki (Galana) River, whose valley is deeply incised in the coral limestone.

The Kenyan coast is a low coastal plain broadening northwards, attaining widths of more than 50km, where rivers Tana and Sabaki (Galana) have deposited considerable amounts of fine sediments. In the Malindi area, features like sand dunes and tombolos become very prominent. Among features considered to indicate a shoreline of emergence is the higher land uplift or arching in the Malindi area, and the dunes.

Ras Ngomeni, a peninsula north of the outlet of the Sabaki River, consists of a small remnant of Pleistocene coral limestone in the north joined to the mainland by sandy deposits forming well developed dune ridges on the seaward side. The genesis of this characteristic feature can be traced back to the maximal phase of the Flandrian transgression when sea-level stood about 2 to 3m above present-day mean sea-level and the shoreline was further inland (Map 2). Then a submarine bar developed between the mainland and the island of Ras Ngomeni, which reached a position above sea-level when it fell to its present position. In the sheltered bay behind the new elevated bar, sediments accumulated and a vast mangrove swamp developed. After some time the inner part of the bay silted up by abnormally high waters to above mean sea-level and natural salt-pans originated in this manner. This suitable situation led to the construction of the Fundisa saltworks.

Normally, there are one or two dune ridges running along the shore, but adjacent to the Sheshale, Maridadi and Casuarina bays. There are as many as 6 ridges, five of them grouped together, and the outermost sixth is discontinuous and definitely separated from the others and with a different alignment. As expected the material of the dune ridges consists of medium and fine sand and their material is better sorted than that of beach ridges.

The foreshore in areas south of Ras Ngomeni consists generally of a series of low lying berms on which eolian processes are dominant. The berms are seldom more than 2 to 3 metres above the marine high tide water table. They are succeeded inland by dune system of upto 50m in height. The frontal dune formation forms part of the dynamics of coastal processes. Beach ridges are both of modern and subrecent origin. More often than not the subrecent formations show undercutting by a combination of marine processes. The modern beach ridges are either not covered by vegetation or have a "top-dressing" of pumice, probably originating from the 1883 Krakatoa eruption. The beach material consists of white, medium to coarse sand derived from weathered coral limestone as well as dark fine to medium grained heavy minerals, distributed aerially in all proportions depending on the active marine processes and the proximity of coral reefs.

The Malindi-Fundisa coast is dominated by the accumulation of terrigenous material brought in by the Sabaki in the south and the Tana in

the north (Fig.25). They are therefore the only rivers contributing to the deposition of heavy minerals in this area. Especially during the high-water periods enormous quantities of sediment are carried into the ocean, which influence the development of the coast considerably. Further, it would appear that while considerable volumes of sediments are transported by the Tana in times of flood, only the finer fraction reach the sea, due to a drop in velocity in the delta region. Conversely the Sabaki retains its flood velocity and load carrying capacity to its mouth north of Malindi, where wave, longshore and coastal currents, and wind action then distribute and concentrate materials in relation to their specific gravities.

It is worth noting that the Sabaki (Galana) River does not reach the sea in any floodplain at all. This is a relatively youthful stream whose upper course is conditioned by the Mozambique Belt metamorphic rocks, the Yatta Lava Plateau, and then cuts through the Mazeras and Mariakani sandstones. The river has incised a narrow valley, through the Pleistocene coral reef before reaching the sea. North of Ras Ngomeni begins the extensive Tana River Plains. It is therefore probable that the greater proportion of the heavy mineral deposits have their origin in the Sabaki rather than the Tana River systems.

The Malindi-Fundisa area is therefore a zone of greatest sedimentation on the Kenya coast. This part of the coastline is relatively youthful and is predominantly being shaped by deposits emanating primarily from the land. There is ample evidence of being reworked by coastal processes in

which these terrigenous sediments interfere with coral reef development. On the other hand, the presence of off-shore reef is a major factor impeding and disrupting the regular deposition of heavy mineral concentrations in this area of the Kenya coast. A great deal of carbonate sediments making up some beaches is derived from coral reefs. This is particularly so where the shoreline is bordered by fringing reefs. These in many areas form an off-shore barrier (for example south of Ras Ngomeni with a protected beach behind barrier reef), preventing the inshore transport of sand and their heavy mineral content. The heavy siltation is coupled with fairly extensive mangrove colonization of the tidal area. Examples of these are mainly found in areas to the north of Ras Ngomeni all the way to Mto Tamamba. Thirdly, wide beaches are formed with arrays of dune ridges behind them, or, in more protected areas, barrier islands notably at Silversands Beach and Ras Ngomeni respectively.

A three knot current runs from south to north in the area. This is reduced inshore, but in combination with the dominant southerly monsoon is the major factor in heavy mineral distribution north of the Sabaki mouth. Wind action has affected additional concentration in the dune systems in this area by the selective removal and redeposition of the lighter fraction in a northerly direction.

In areas north of Ras Ngomeni different conditions prevail. In these areas Pleistocene marine transgressions have largely destroyed the older

dune systems and the area today consists of lagoonal flats subject to spring tide flooding, tidal channels, mangrove swamps and low elevation shoreline sand bars or barrier islands constituting the active beach. Mangroves grow in swampy or lagoon areas behind dunes and barrier islands. A typical setting of this nature is found around the Robinson Island.

In general it can be stated that the area investigated falls within what can be termed "recent" coastal deposits. Further inland, to the west of the area, relicts of the lower to middle Pleistocene dune sands occur in an environment of low lying lagoonal sand and clay flats.

The landscape to the south of the Sabaki River is characterized in the main, by a series (staircase-like) of marine platforms and terraces which extends from the summit of the Pleistocene coral reef/crag right down to the present beach (and even lower to the present fairly extensive platform below the high water mark). Preliminary studies by Ase (1978,1981) show that 6 levels of terraces are present in the area (Table 3). Some of these levels are obviously composed of elements formed at different dates which makes the grouping uncertain. The levels gives an indication of higher land uplift in the northern part, e.g. Malindi area, compared to the area south of Kilifi, and even the Mombasa area. This is also supported by the fact that features like creeks are more common in the Mombasa- Kilifi areas than in the Malindi area, whereas dunes are more common in the latter, and especially north of Malindi. The dunes are generally

AUTHOR	Werth (1952)	(Caswell, 1953)	Thompson (1950)	Hori (1970)	Toya et al (1973)	Ase (1978)	Read (1981)	AGE 1000's
STUDY AREA	Tanzania and Kenya	Mombasa area	Malindi area	Southern Kenya	Southern Kenya	Mombasa area	Mombasa-Mtwapa area	-
TERRACE NAME AND ELEVATION ABOVE DATUM	75m Terrace	-	-	Matuga surface 90-140m	Marafa surface 80-120m	-	-	-
	50m Terrace	-	-	Changanwe Terrace 45-70m	Changanwe Terrace 45-70m	-	-	-
	25m Terrace	37m Terrace	37m Terrace	Upper Mombasa Terrace 15-37m	Ganda Terrace 20-37m	VIII: 20m	Ganda? Terrace 20m + ?	763
					Kilifi Terrace 15-18m		VII: 17m VI: 15m V: 13.5m	Nyali Terrace (subsurface) 3-7m Kilifi Terrace 15-18m
9m Terrace	7.6 Terrace		Lower Mombasa Terrace 10m	Malindi Terrace 7-10m	IV: 12m III: (9m) II: 7m	Malindi Terrace 7-10m	125	
2.5m Terrace			Shelly Beach Terrace 5m	Shelly Beach Terrace 4.5m	L: 5m	Shelly Beach Terrace 4-5m	0-10	

UNDERLYING DEPOSITS ARE RECENT/HOLOCENE

considered features of a shoreline of emergence. However, there are some indications of a rather recent age (below about 3000 years) for the lower levels which are occasionally covered by reddish soil derived from the underlying rock. They must be considerably older, maybe of late Pleistocene or early Holocene age. Africa is normally considered the most stable continent in the world. It is therefore probable that the raised terraces of the Kenyan area that have been studied by a number of authors (e.g. Werth, 1952; Caswell, 1953; Thompsom, 1956; Hori, 1971; Ase, 1978; and Andrew, 1981) could for rather good reasons be considered eustatic rather than isostatic or tectonic e.g. the reason for their position above present sea level would rather be a dropping sea level than a rise of land. However, the fact that some of the younger terraces are of late Pleistocene or Holocene age and nevertheless are found between 10-20m above Datum contradicts the idea of pure eustatic origin. According to current research (Fairbridge, 1961; Morner, 1976) sea level has not reached such high altitudes during the last 20,000 years. The grouping to as many as 8 levels is not unanimous but indicates a complicated interrelationship between eustatic and isostatic or tectonic movement. It is important to note that sea level changes is a rather controversial matter

and might even be subject to regional variations due to instability of the geoid configuration.

4. RESULTS

4.1. Morphology

4.1.1. Silversands Beach

A fringing reef extends from the Vasco da Gama Pillar to the Leopard Point in a continuous ribbon profile more or less paralleling the coastline. Their profile is often prism or wedge shaped, but sometimes merely consist of a veneer encrusting the substrate. The morphology of the inner portion of this area is determined by the reefs but toward the sea the influence gradually diminishes. They are patch or fringe reefs which combine to a perforated barrier. The seaward rim usually is a steep slope formed by corals, it is irregularly indented and individual reef structures of several metre's size rise from it or in front of it. The crest of the slope is exposed at low tide. The distance of the reef edge varies from place to place but for most part it lies 100-300m offshore. Most of the reef is composed of dead coral, whereas live coral is found on the outer edge and at places in the intertidal zone which are rarely or never uncovered by the sea.

The coral platform as a whole shows a gentle slope from shore to reef edge, but the surface is very uneven, with parts completely uncovered, parts with shallow water, larger and smaller pools, and channels. The

Table 4. Beach-face shape dimension parameters for beaches in Malindi-Fundi area

Location	Beach-face slope	Beach-face gradient ($\tan\beta$) ⁻¹	Beach-face dip direction	Beach width (m)	Beach height (m)
2	3.0	19.081	95 ⁰	36	1.8
4	7.0	8.144	111 ⁰	50	6.1
5	10.0	5.671	110 ⁰	48	8.3
10	4.0	14.301	44 ⁰	112	7.8
11	2.5	22.904	53 ⁰	115	5.2
12	2.5	22.904	101 ⁰	128	5.6
13	2.0	28.636	103 ⁰	125	4.4
14	2.0	28.636	120 ⁰	207	10.8
15	3.5	16.350	125 ⁰	223	13.6
16	2.0	28.904	129 ⁰	221	7.7
17	2.5	22.904	142 ⁰	230	10.0
18	3.0	19.081	146 ⁰	234	12.3
21	2.0	28.636	114 ⁰	166	5.8
22	2.5	22.904	127 ⁰	172	7.5
23	2.0	28.636	130 ⁰	110	3.8
24	3.0	19.081	104 ⁰	101	5.3
25	1.5	38.189	83 ⁰	53	1.4
26	3.5	16.350	96 ⁰	67	4.1
27	5.0	11.430	65 ⁰	63	5.5
28	2.0	28.636	195 ⁰	125	4.4
29	2.0	28.636	150 ⁰	120	4.2
30	3.5	16.350	66 ⁰	76	4.6
31	2.0	28.636	120 ⁰	64	2.2
32	2.5	22.904	135 ⁰	181	7.9
33	2.5	22.904	150 ⁰	190	8.3
34	3.0	19.081	135 ⁰	124	6.5
35	2.5	22.904	113 ⁰	126	5.5
36	5.0	11.438	148 ⁰	119	10.4
37	6.5	8.777	170 ⁰	122	13.8
38	10.0	5.671	94 ⁰	68	11.8

39	10.0	5.671	90°	72	12.5
40	10.5	5.396	100°	88	16.0
41	10.0	5.671	46°	85	14.8
42	11.0	5.145	49°	41	7.8
43	12.0	4.705	46°	49	10.2
44	13.0	4.332	87°	59	13.3
48	7.5	7.596	130°	67	8.8
49	9.5	5.975	81°	76	12.5
50	6.0	9.514	122°	87	9.1
51	3.5	16.350	73°	63	3.9
52	7.0	8.144	11°	21	2.6
53	6.5	8.777	360°	92	10.4
54	6.0	9.514	18°	96	10.0
55	4.0	14.301	16°	91	6.4
60	5.5	10.385	106°	40	3.8
61	5.0	11.438	120°	52	4.5
62	7.0	8.144	115°	38	4.6
63	6.5	8.777	120°	41	4.6
64	7.0	8.144	112°	36	4.4
65	10.5	5.396	110°	35	6.4
66	7.5	7.596	101°	33	4.3
67	6.5	8.777	93°	30	3.4
70	3.5	16.350	125°	110	6.7
71	4.0	14.301	108°	124	8.7
72	3.5	16.350	92°	52	3.2
73	2.0	28.636	105°	55	1.9
75	2.0	28.636	107°	121	4.2

larger and deeper pools near the lower littoral may be regarded as infra-littoral habitats. From the crest landward extends a platform of 80-200m width; the seaward portion of it is covered by a reefal organism community of corals and algae, which gradually becomes sparser towards land.

The Silversands beach (Plate 1) is bordered on the seaward and landward sides by a fringing reef and beach ridge respectively. The slopes of beaches are commonly 7-10° (Table 4) and the width range from 36 upto 50m (figs. 4,5). Narrow sandy beaches occur to the north and south behind the coral reef at the base of wave-cut cliffs and stacks (Plates 2,3, and 4; fig.6).

4.1.2 Gilani Beach

A rocky platform of about 200m width, with small and large rock pools (Plate 5), extends landward adjacent to the Malindi Reef Light.

The perimeter of outer reef-flat is topped by a ridge of coralline algae which has grown up to about 0.5m above the low-tide level. This ridge provides a partial shelter for the reef-flat creating a situation suitable for development of sand-bars which migrate up and down the upper sandy beach. There is also a 40m wide channel adjacent to this ridge which is partly filled with water even at low-tide.

The Gilani beach is bordered on the seaward and landward sides by a shelf and beach ridge respectively, except the southern portion which is bordered seaward by a fringing reef.



Plate 1. Shore features at Silversands Beach. Note steeply sloping shore and boulders derived from the fringing reef.



Plate 2. Beach, upper sandy platform, cliffs and stacks at Silversands Beach. Note parallel bedding of Pleistocene eolian deposits towards the top of cliffs.



Plate 3. Coastal erosion at the Silversands Beach; showing a house precariously built with no sea walls at the edge of a rapidly retreating eolian cliff.



Plate 4. Concrete slabs placed in front of the monumental Vasco da Gama Pillar for protection against wave erosion.



Plate 5. Uneven surface of a gently sloping coral platform, with parts completely uncovered, parts with shallow water, large and small pools and channels. This is during low tide.



Plate 6. Inter-distributary tidal flat exposed during low-tide showing bifurcating symmetrical wave ripples, characteristic mottling and bioturbation .

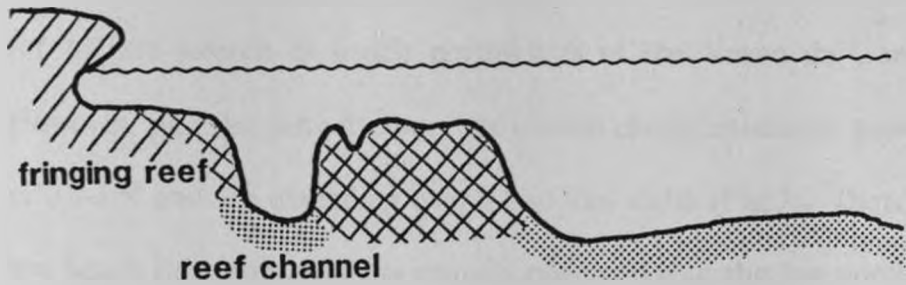


Fig.4. Coastal features of Silversands area at Leopard Point.

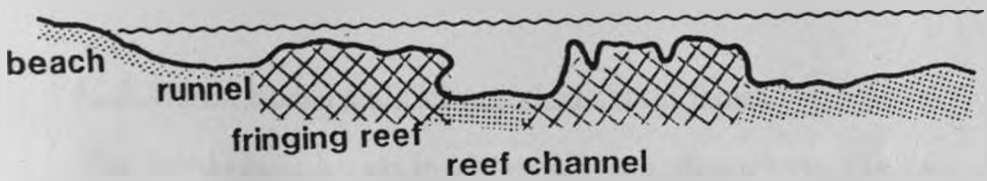


Fig.5. Coastal features of the Silversands area at Driftwood club.

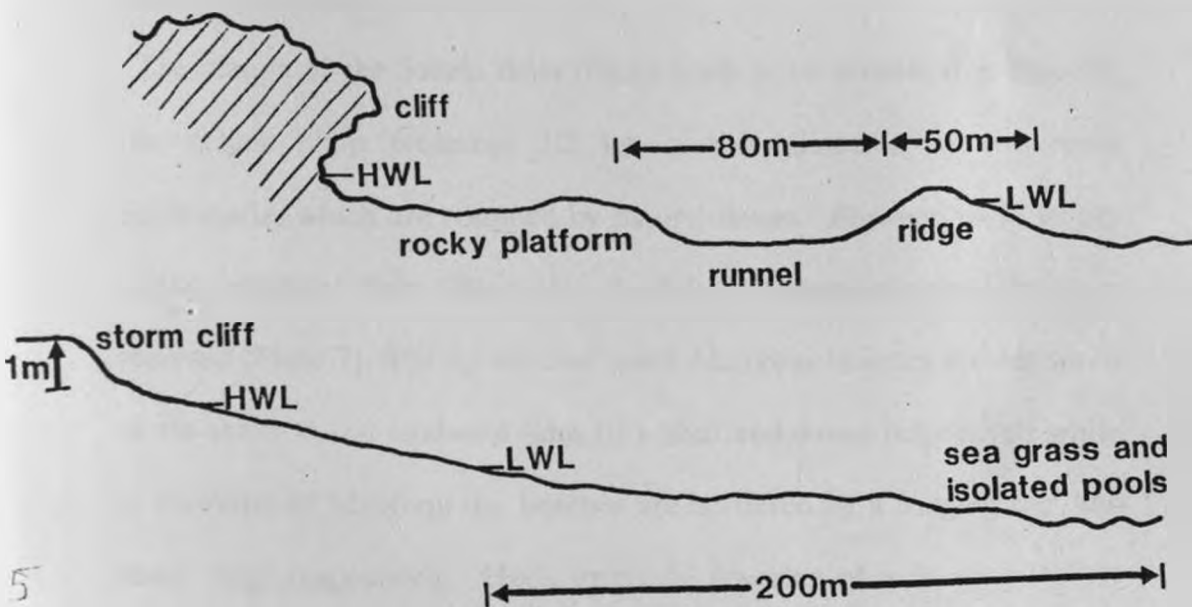


Fig.6. Shore profiles of Silversands Beach.

The beach gradient and width are generally 3° and 40-60m respectively for 1/2 km stretch of beach northwards of the Vasco da Gama Pillar. However, past the jetty the beaches exhibit characteristically gentle slopes of $2.0-2.5^\circ$ and are extending over 110-130m width (Fig.7). There are very low beach ridges and shallow runnels observed near the low tide level.

The backshore is about 60m in width, horizontal and partly covered by vegetation. Morphologically, this area comprises a broad berm zone and low frontal dunes of about 1/2 -1m high.

4.1.3. Sabaki Beach and Delta, and Mambrui Beach

The Sabaki river breaks in a narrow valley, through the Pleistocene coral reef before reaching the sea. Comparison of old and new aerial photographs show that there has been a southward channel migration close to the mouth of the river.

The margin of the Sabaki delta (fig.8) tends to be arcuate (fan-shaped). The deltaic plain measures 1/2 km and is dissected by two main distributaries which are bounded by natural levees. Between these levees extend intertidal flats (Plate 6). A shifting rivermouth sand bar was observed (Plate 7). The Sabaki and south Mambrui beaches are bordered on the seaward and landward sides by a shelf and dunes respectively while to the north of Mambrui the beaches are bordered by a fringing reef and beach ridge respectively. Here, intertidal covering of a fringing reef by

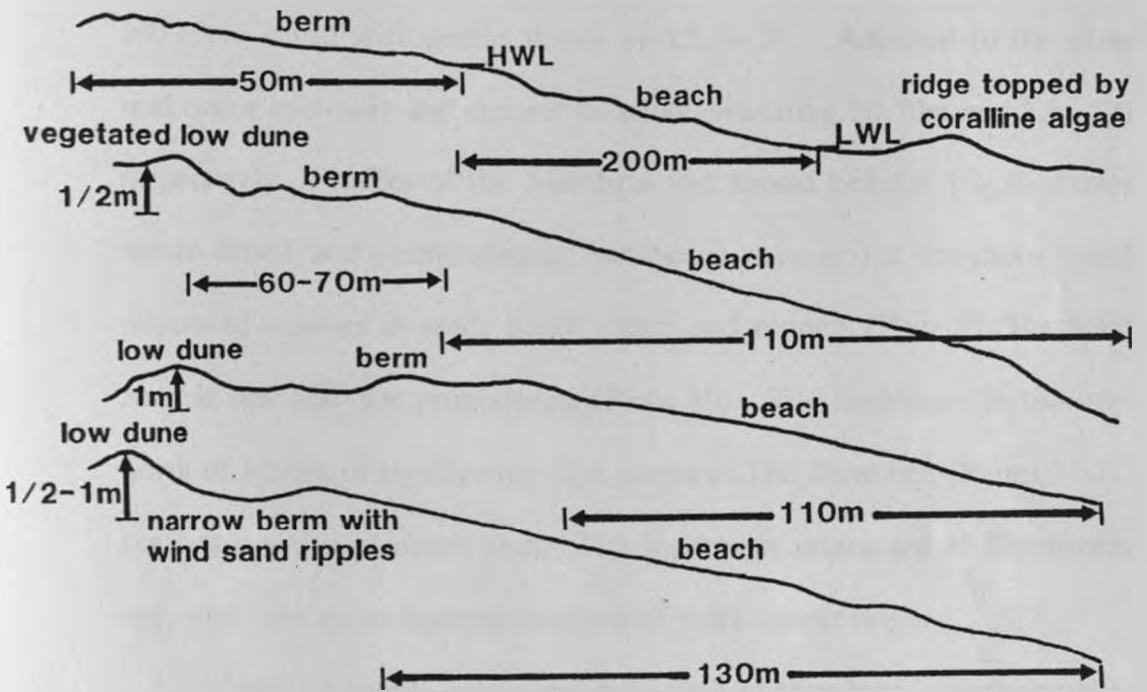


Fig.7. Shore profiles of Gilani Beach.

beach sand (reef siltation) can be observed (Plate 8). The sudden influx of clastic material has covered and presumably killed the reef.

Southward of Mambrui township there are wide beaches extending over 100-250m width with gentle slopes of 1.5. to 3°. Adjacent to the silted reef occur narrower and steeper beaches measuring 50-70m and 3.5.- 5.0° respectively. Profiles of the Mambrui and Sabaki beaches (fig.9) show a rather broad and gently sloping backbeach area and a foreshore which terminate seaward at sandy beach ridges and runnels (Plate 9). The berm zone is low and not pronounced (Plate 10). The backslope in the area north of Mambrui significantly dips seawards. The dune belt (Plates 11-17) reaches a width of about 4km. The innermost ridges are of Pleistocene age, while the more seaward ones are of more recent origin.

A generalized profile across the dune field of Mambrui is given in figure 9. The dominant features are three dune ridges running subparallel to the coast in NNE direction. The seaward dune ridge (1) is somewhat discontinuous, mobile, and has least vegetation. In contrast, the landward ridge (3) is almost completely stabilized by vegetation and exhibits only few bare spots at the upper portion. Along the middle dune ridge, although it is partly covered by vegetation, considerable movement of sand is taking place, and some of its vegetation is burried by moving sand. Estimates of the height of the ridges are 10,15, and 20-25m respectively for the first, second and third dune ridge, counted from sea to land. The ridges react like longitudinal dunes; they exhibit slip faces at their flanks.

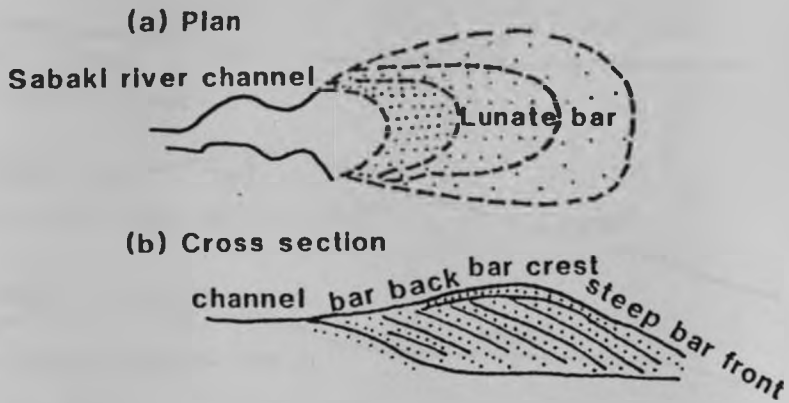
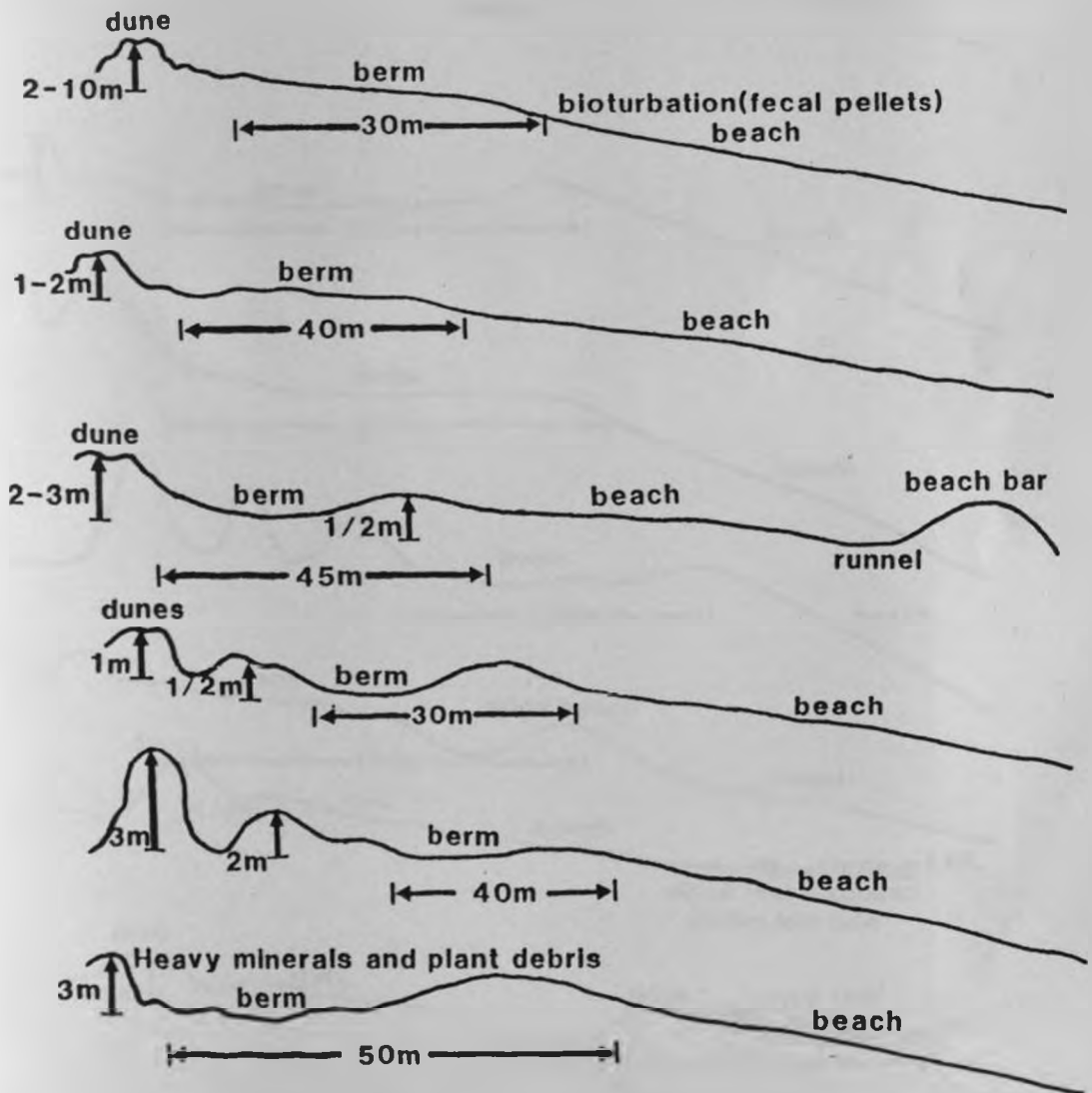


Fig.8. Plan and section views of the Sabaki Delta and its distributary mouth bars.



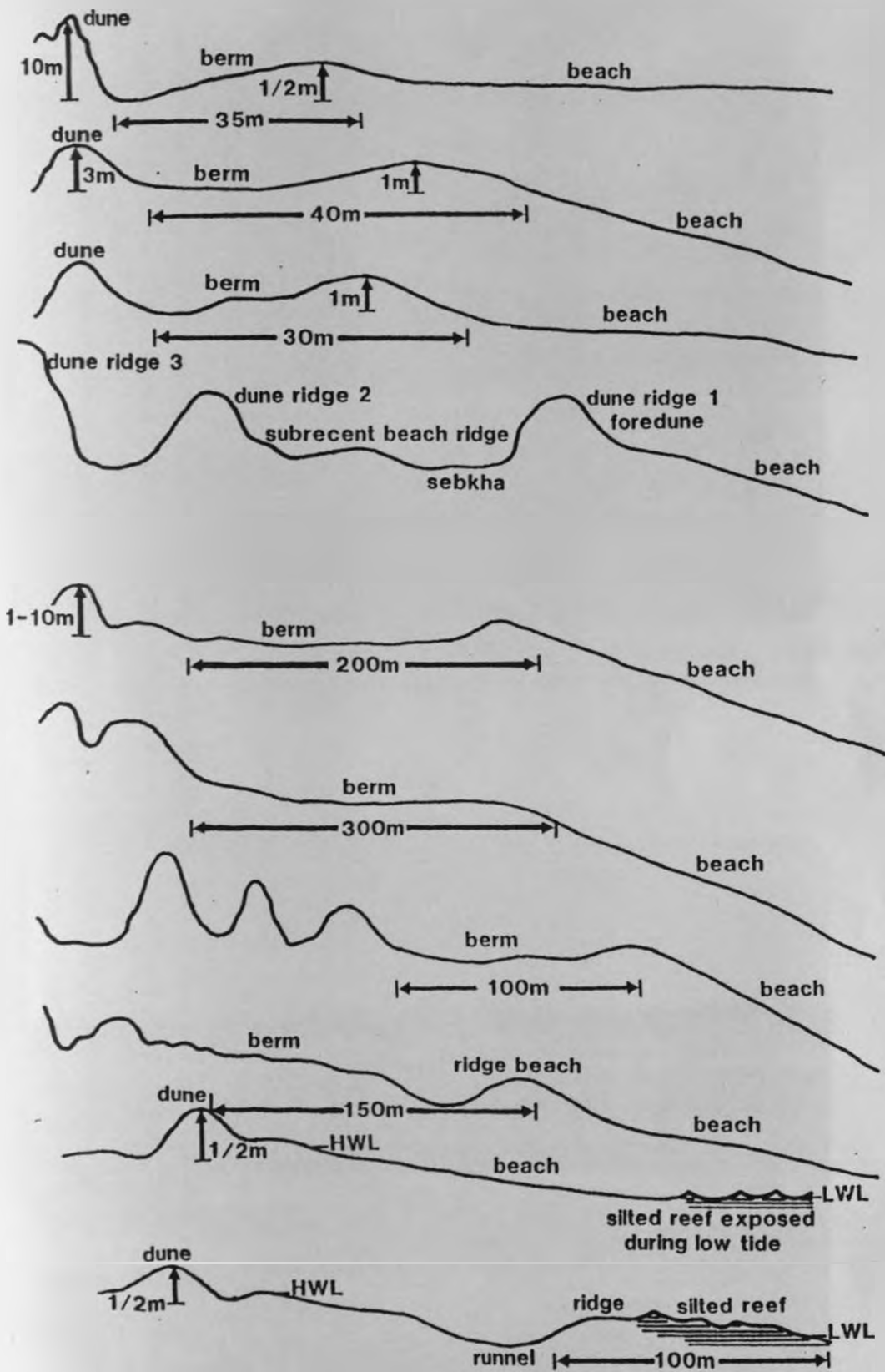


Fig.9. Shore profiles of Sabaki and Mambrui Beaches at dune development.



Plate 7. Sabaki Delta. A shifting rivermouth sand bar and the two main distributaries on either side.



Plate 8. Reef siltation. Covering of fringing reef by beach sand at the Mambrui beach.



Plate 9. Beach runnel with erosional megaripples. To the left is a beach ridge (longshore bar). The view is parallel to the shoreline.



Plate 10. A broad berm with many plant debris leading to vegetated frontal dunes (note stabilizing effect of vegetation). The tree is cyperus.



Plate 11. Barchan dunes. Vegetation is *Ipomea pes carpres*. Note wind sand ripples on a wind blown sandy surface.



Plate 12. A gently sloping beach showing foredune ridge and deflation of upper beach surface.



Plate 13. Seaward view from the innermost dune ridge. Vegetation is present on all ridges, but does not prevent migration of dunes.



Plate 14. Longitudinal dune ridge. Vegetation is present on the adjacent dune ridge landwards.



Plate 15. Transverse second dune ridge showing wind sand ripple marks on the surface and vegetated third dune ridge.



Plate 16. Landward view from second dune ridge across sebkha. Note dark level bottom of sebkha.



Plate 17. Seaward view of the third dune ridge from the first dune ridge across second dune ridge. Vegetation is present on both the second and third dune ridges.



Plate 18. View of crescent-shaped beach located in a bight at Sheshale Bay. Note gentle slope of the foreshore.

At the time of observation (October, 1987) these were dipping to the NNW due to the prevailing SE monsoon. The windward slopes frequently consisted of truncation surfaces.

In front of the seaward ridge, a field of foredunes of about 100m width was found; the dunes have gentle windward slopes, which frequently exhibit deflation surfaces. The slip faces are concave characteristic of barchan dunes. These slip faces are 1-1.5m high with slopes of 32-34°; avalanche were frequently observed.

In the interdune valleys, either sebkhas or obstacle dunes were found. The obstacles at which these dunes formed were either vegetation or remnants of old dunes with vegetation. Some of them coalesce and then give rise to complex structures with convex as well as concave slip faces, on which avalanches were observed. The sebkhas within the dune field south of Mambrui are continental; they are located in interdune valleys (Plate 12) and lack connections to the sea; thus marine inundations and sedimentation is excluded. Moreover, the water table is close to the surface, and the groundwater is not saline but freshwater as determined by taste.

Several sebkhas are found in the Mambrui dune field, all of them are more or less elongate planes. The northermost sebkha was visited in October 1987: it extends 300m in NS direction and 100m in EW extension. The groundwater table was 40cm below the sebkha surface, as determined in several holes dug by local inhabitants, who apparently use the water.

4.1.4. Sheshale Bay, Maridadi Bay and Casuarina Bay

Morphologically, the bays comprise of a series of bights and capes between which are crescent shaped beaches (Map 2). The foreshore slope is about 2-3°, the higher values were observed for the beaches facing the dead patchy reefs. The general shape of the coast is characteristic of a cusped shoreline. Behind the bays, small wind shadow dunes are common on the backbeach (Plates 18-21). The foredunes are typically less than 2m in height and may be discontinuous besides showing varying degrees of stabilization. Changes in the backbeach portion of the profile are minor and are nearly totally wind generated. The foreshore and inner nearshore zones exhibited at least moderate changes of both erosional and accretional nature which occur during the southwest and northeast monsoons respectively. In the convergence zone the berm/s typically rises 2m above mean sea-level, but often subtle in the divergent zones (Fig.10) and divided from the 60-90m wide shoreface by a beach ridge.

Schroeder (1974) has considered the barrier extending southward from Ras Ngomeni a barrier bar composed of beach sands (Plate 21). His interpretation is based on observed sedimentary structures especially cross bedding, the presence of gravel layers and the mineralogy. The South Ngomeni beaches are significantly steeper 5-10° and narrow measuring upto 70m in width. They are bordered landward by a sharp cliff and low foredunes which are already stabilized by vegetation (Plate 21).



Plate 19. General view of Sheshale Bay.





Plate 20. The tombolo at Ras Ngomeni.



Plate 21. Geomorphic forms of beach surface. Wave-cut cliff on foredune at Casuarina Bay.

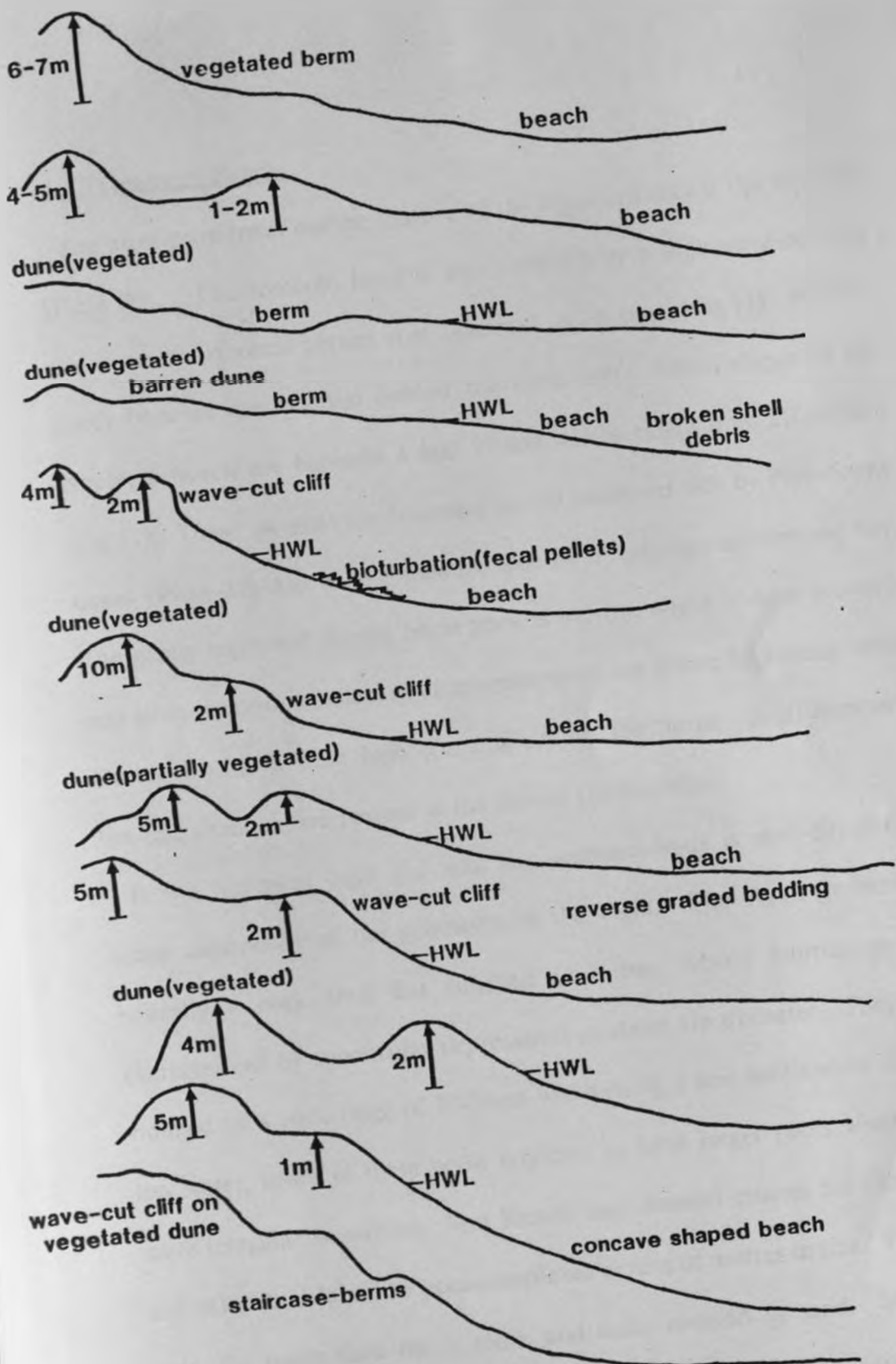


Fig.10. Shore profiles of sheshale Bay Maridadadi Bay and Casuarina Bay.

4.1.5 Ngomeni Beach

The most prominent marine feature of the Ngomeni area is the tombolo (Plate 20). The tombolo head is characterized by a high wave-cut cliff and a near horizontal barrier reef platform at its base (Fig.11). Narrow sandy beaches are isolated behind the coral reef. Mean slopes in the Ngomeni beach are between 4 and 7° and widths range from 20 to 90m (Fig.11). These beaches are bounded on the landward side by Pleistocene dunes (Plate 22) and on the seaward side by a fringing reef rimmed bay. The gently landward sloping berm zone is narrow, about 50-60m in width and fairly prominent, situated at approximately 1m above high-water level. During storms a 1/2m high scarp is cut on the berm. Sand bars and low-tide channels are present at the foot of the shoreface.

In the Ngomeni bight the tidal flat sediment-body is semi-circular, a shape dependent of the geometry of the bight. The Ras Ngomeni is basically a rock tidal flat situated in a bay, whose morphology is characterized by subcircular depressions of about 1m diameter. They are rimmed by a rock ridge of 10-20cm width rising a few centimetres above low water, some of these pools coalesce to form larger pools which are more irregular in outline. Mto Rasini tidal channel crosses the tidal flat and delineate island-like pool-complexes of tens of metres in size. Toward land, the rocky tidal flat is more and more covered by sand. In some places the relief described is just draped by sand, in others sandy bars

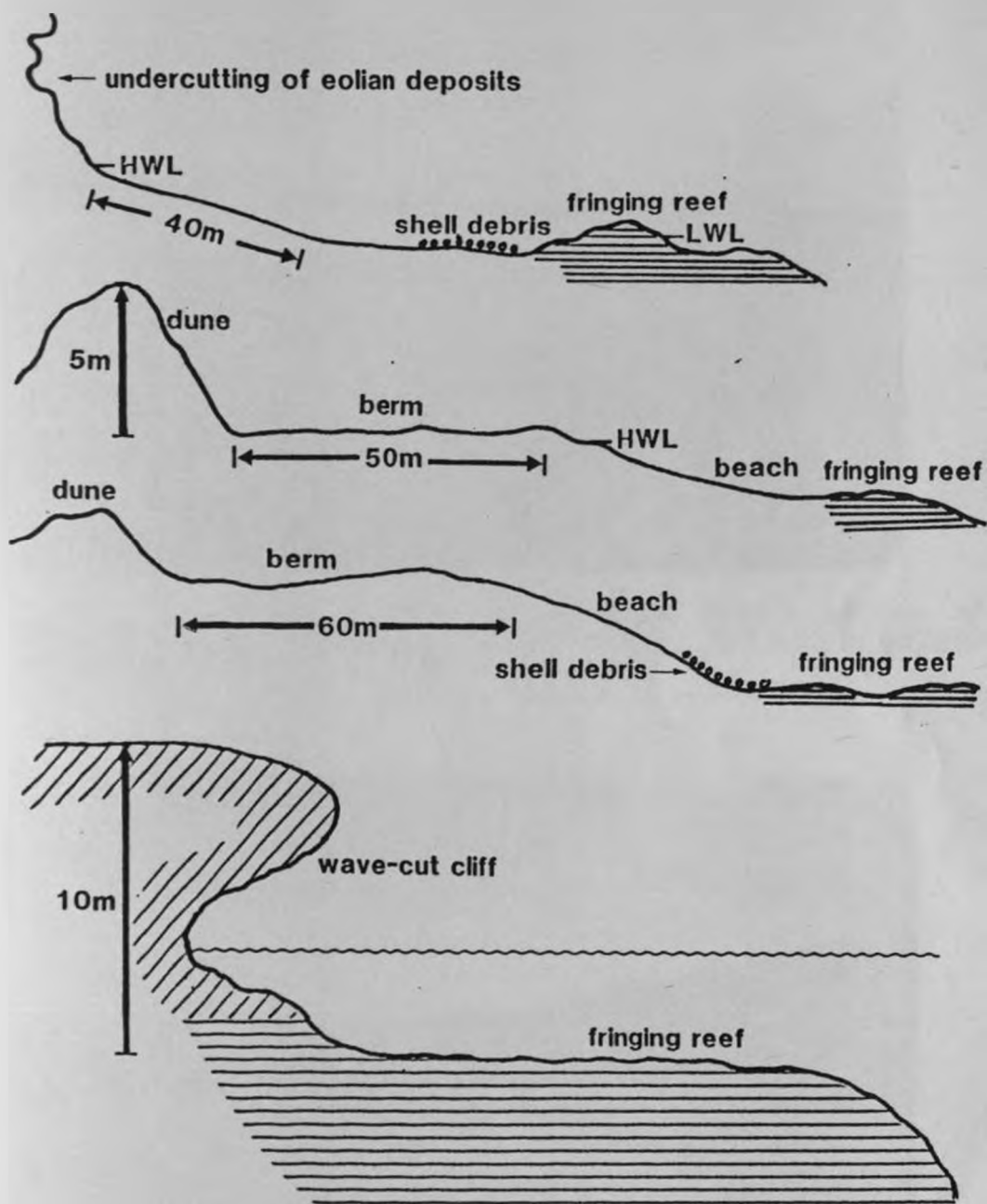


Fig.11. Shore features at Ngomeni Beach.



Plate 22. Landward view of Ngomeni Beach across the Pleistocene rocky reef platform. Note vegetated Pleistocene dunes in the background.



Plate 23. General view of the Simiti Island foreshore showing how marine transgression has caused recession of mangrove zone and leaving behind peat.

exist, the rocky substrate of which is not noticeable. Sandy bars appear to be shaped by the tidal currents.

4.1.6 Simiti Island

Simiti Island is approximately 4km long and about 100m wide. It is more or less straight and segmented by frequent tidal inlets where large flood tidal deltas form on the seaward side of the barrier island. The NW tip is lobate whereas the SE tip is curved and bordered by a bay barrier. Landward of the island is a broad tidal flat on which are meandering tidal channel networks. Seaward of the mangrove zone are tree stumps and peat formation (Plate 23) or algal mats (Plate 24) followed by a steeply sloping foreshore, 10-13° whose width range from 60 to 80m (Table 4). The foreshore berm where present, is seldom more than 2m above the mean high water level and the inshore width of the berm on average less than 100m. Longshore bars and troughs usually mark the seaward termination of the foreshore (Plate 25).

4.1.7 Robinson Island and Giryama Village Island

Robinson island is about 8km long and ranges from 100 to 300m wide. The general shape of Robinson Island is shown in Map 2. In plan view this barrier island is continuous, with a generally smooth, gently curved,



Plate 24. General view of Simiti Island foreslope showing sandy surface protected by thin algal mats, and shallow erosional depressions with ripples.



Plate 25. Seaward view of typical, longshore trough and longshore bar at the northern lobate end of Simiti Island.



Plate 26. View of shore features looking northward along Robinson Island beach. Note heavy mineral concentrations and many shells on active berm zone.



Plate 27. Northern Robinson Island beach showing small wave-cut cliff on foredune ridge. Note the Ghost Crab, a crustacea Ocypode.



Plate 28. View of tidal channel across tidal delta. Note lingoid-shaped small-current ripples, current marks, many shells and heavy mineral concentrations on the surface. The direction of flow is from right to left. Southern Robinson Island.



Plate 29. A lagoon behind Robinson Island. In the left margin of the photograph are sluice gates leading to salat extraction ponds.



Plate 30. A lagoon behind the Giriyama Village Island. Note lagoonward sandy beach surface protected by thin algal mats.



Plate 31. Southern Kisiwakini Island beach showing foredune ridge with vegetation, heavy minerals and seaweed flotsam near base.

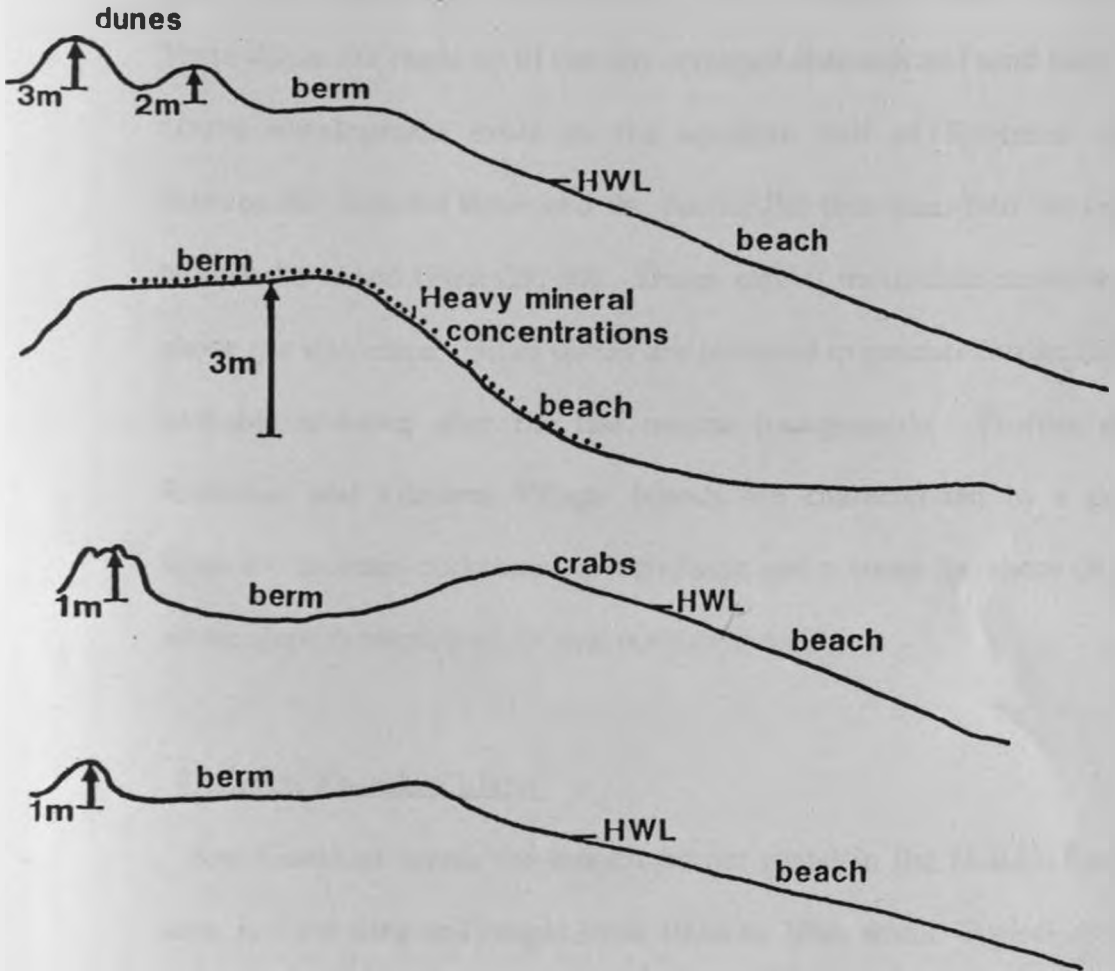


Fig.12. Shore profiles of Robinson Island and Giriyama village Island Beaches.

ocean-facing shore and has an irregular lagoon-facing shore (Plates 26, 27). The connection of lagoons with the open sea is represented by tidal inlets which show the development of underwater deltas (Plate 28). These deltas are made up of radially arranged channels and sand bars.

Dune development exists in the southern half of Robinson island between the seaward shore and the barrier flat that leads into the lagoon behind the island (Plates 29, 30). Dunes exhibit moundlike characteristic above the shoreface. Other dunes are scattered in patches further inland, probably stranded after the last marine transgression. Profiles along Robinson and Giryama Village Islands are characterized by a gentle landward inclined backbeach, a high berm and a steep foreshore (fig.12) whose slope is about 6 to 10° and 60-90m in width.

4.1.8. Ras Kiswakini Island

Ras Kiswakini island, the longest barrier island in the Malindi-Fundisa area, is 7 km long and ranges from 100m to 300m wide. Typical of most barrier islands in the study area, it is elongate parallel to the shoreline, smoothly curved and lobate on both northern and southern ends.

Where truncation of barrier beaches has taken place, fanlike projections (overwash fans) have developed on the tidal flats. The fans measure about 50 by 20m.

It is bounded on the landward side by tidal flats with only limited connection to the open sea by tidal channels on either end. Dunes form a

foredune ridge along the front of the barrier island immediately inland from the back side of the beach (Plates 31, 32, 33, 34). The foreshore berm is seldom more than 2m above the mean high water level and the inshore width of the berm on average less than 50m. Mean beach slopes and widths on Ras Kiswakini Island are between 5-7° and 30-50m respectively (Fig.13). Seaward growth of the barrier island is represented by the numerous ridges on the seaward side (Plates 35, 36). That the shoreline has moved landward is evidenced here by dead tree stumps along the shoreface, which represent a destroyed mangrove zone (Plates 37, 38).

Southward of Ras Kiswakini Island, a rocky Pleistocene reef platform is exposed during low tide water level. It probably belonged to a more extensive reef system that perished as a result of the last marine transgression and increased sedimentation rate. In the immediate offshore area, elongate bodies of sand with crests that are barely visible during low water were observed (Plate 39). They could either represent submerged old dune systems or former positions of barrier islands. However, more underwater surveys need to be carried out to confirm this.

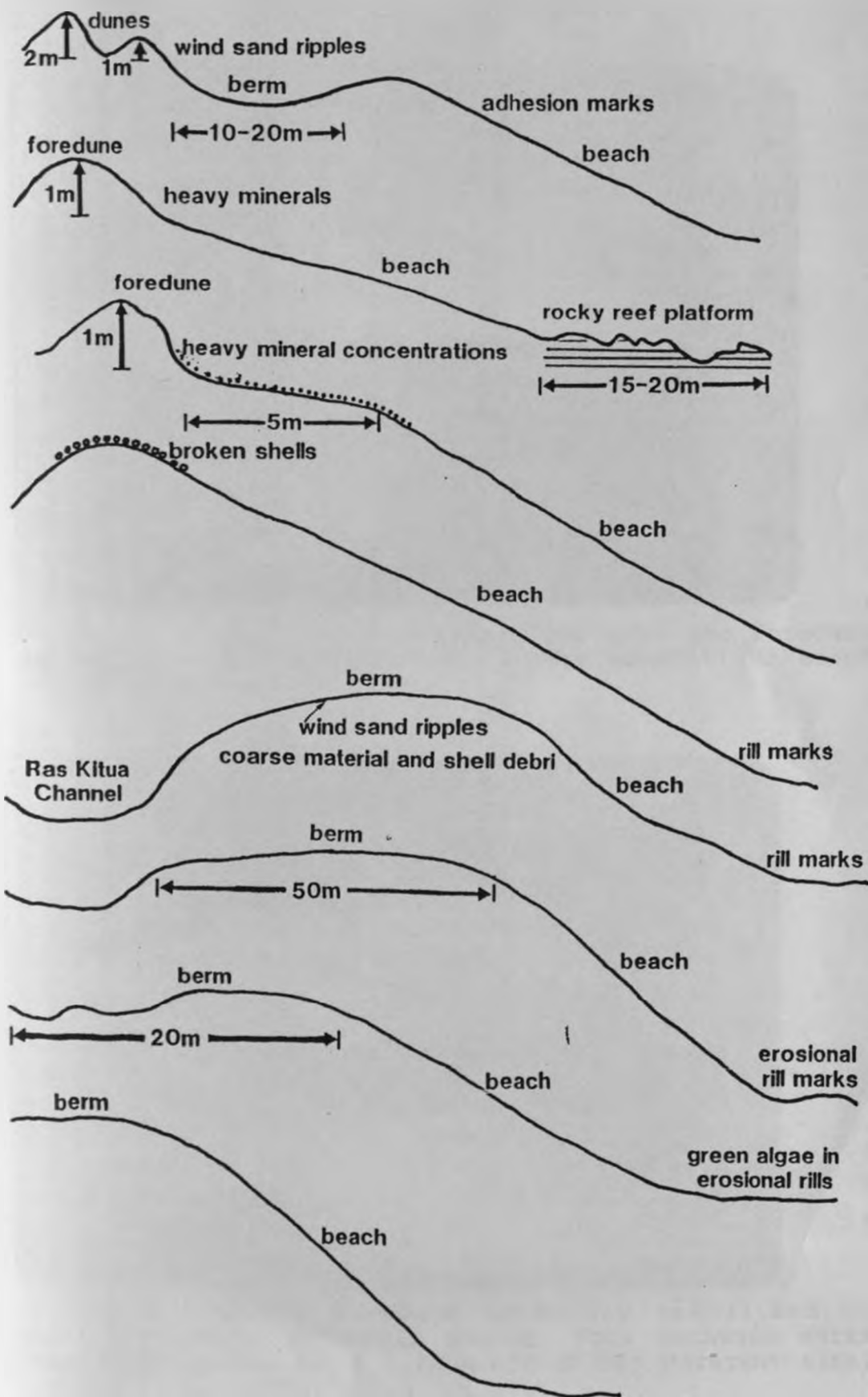


Fig.13. Shore features of Ras Kiswakini Island.



Plate 32. A near vertical scarp, cut into the foredune by large waves, contribution of dune material to beach and heavy minerals.



Plate 33. Relict foredune partially stabilized by mangrove roots: Avicennia marina. Note backwash marks and swash marks. About 1 km north of Mto Marereni tidal inlet.



Plate 34. Foredune ridge showing vegetation and heavy mineral pavement at base. Note erosional rill marks on beach close to the Kiskwini reef flat.



Plate 35. A sandy ridge exposed during low water level. Material is derived from foredune ridge via beach showing shallow erosional depressions. This indicates barrier growth seaward. Southern Kiskwini Island.



Plate 36. Sand ridge indicative of seaward growth of barrier island. About 1 km north of Mto Marereni tidal inlet.



Plate 37. General view of shore features found at about 2km North of Mto Marereni tidal inlet - a typical coast of recent submergence. Rocky Pleistocene reef platform exposed during low-tide water level.



Plate 38. A typical coast of recent submergence shown by destruction of seaward facing mangrove zone. About 2km north of Mto Marereni tidal flat.



Plate 39. Crest of submerged dune barely visible during low tide, a typical coast of recent submergence. Southern Kiswakini Island.

4.1.9. Tamamba Island and Kanagoni Island

The Tamamba and Kanagoni barrier islands stretch northwards for about 5 km and range in width from 100m to 1km. In this area several depositional units can be distinguished: Barrier beaches and foredunes (Plate 40), tidal inlets, tidal deltas, tidal channels (plate 41), ponds (channel bottom), tidal gullies, lower intertidal zone (barren zone) and mangrove zones.

The backbeach slopes seaward or is occasionally horizontal. There is commonly no berm or only a subtle one. Beaches near tidal inlets are broad, ranging from 110-120m in width and narrow elsewhere along the islands, approximately 50m. Mean slopes of barrier beaches are 2-4° (fig.14).

Because of the configuration of these profiles the backbeach zone was commonly encroached by wave activity. Storm washover effects are more evident and in combination with wind deposition has covered most of the tidal flat side of the barrier islands. This growth of the barriers in both directions has resulted in wider islands compared to those present southwards. A system of beach ridges and runnels was observed.

The tidal flat sediment-body is elongate parallel to the shoreline over several kilometres and is intersected by tidal channels.



Plate 40. Tamamba Island beach showing foredune ridge in the background and beach runnel with lingoid-shaped small-current ripples in the lower portion of the photograph. The flow is from left to right. About 1km south of Mto Tamamba tidal inlet.



Plate 41. Seaward view across the Mto Tamamba tidal delta and channel. Note that barrier bar sediments are clean sands and is muddier toward the subtidal ponds.

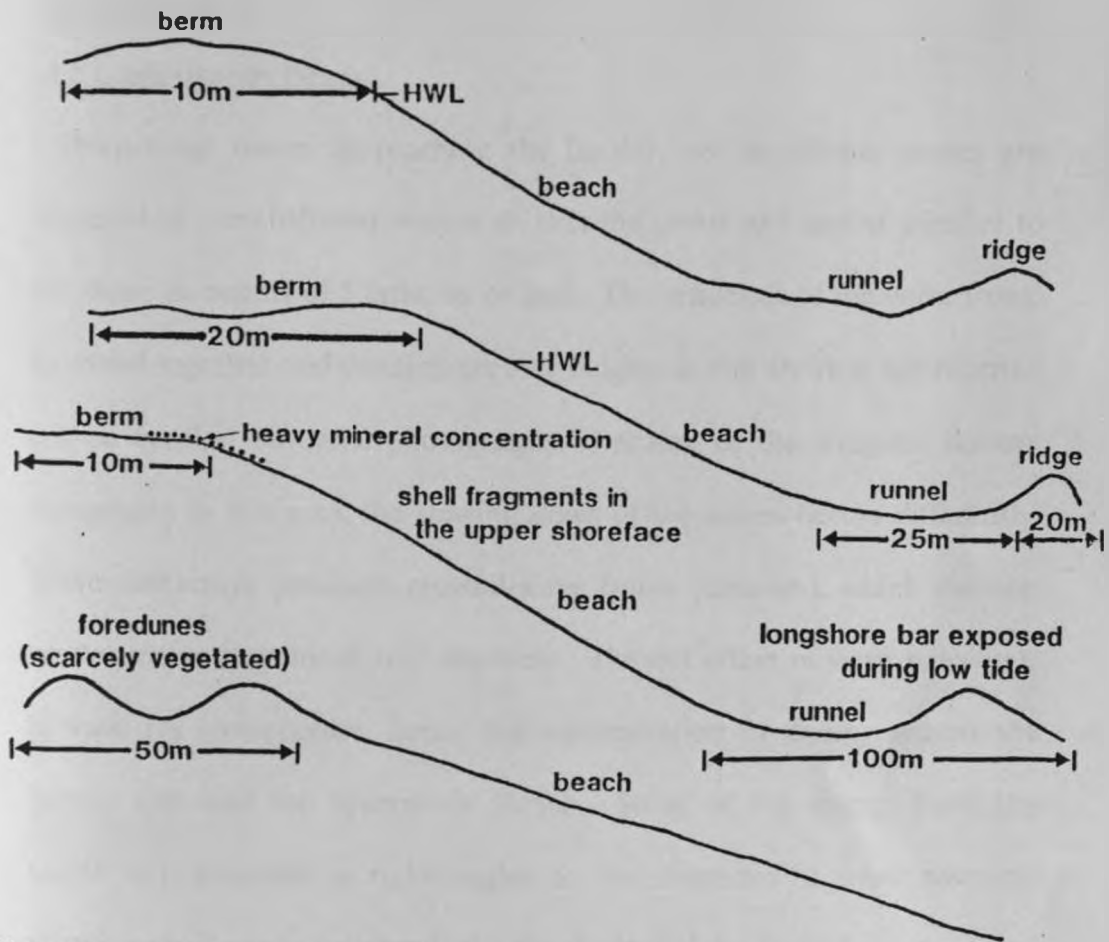


Fig.14. Shore features of Tamamba and Kanagoni Island.

4.2 Processes

4.2.1 Silversands Beach

Deep-water waves approaching the barrier reef at oblique angles are refracted in the shallower waters so that the crests are almost parallel to the shore in depths of 5 fathoms or less. The tendency of the wave fronts to crowd together and develop greater heights as the shore is approached can be verified on aerial photographs. Because of the irregular bottom topography in this area, the slowing down of the waves occurs differently. Wave diffraction produces crossed-wave fronts (caustics), which develop on downwave margins of reef channels. The net effect of wave behaviour is wave ray convergence, hence the concentration of energy against the barrier reef and the Silversands Beach. Some of the energy from the waves is transmitted at right angles to the direction of wave advance, allowing small waves to extend into the shadow of the barrier.

The reef-flats are subject to vigorous wave action, and this combined with the shallow water, means that only sand-sized and gravel-sized sediments can be found here. However, the action of waves favours reef-building corals, as long as it is not too destructive, because waves aerate water, circulate food, and winnow away fine sediment. It was noted that during stormy conditions, large waves destroy corals and throw up banks of coral rubble on the reef and beach, and a near vertical scarp is cut into the beach berm. Beach erosion is taking place at an alarming rate.

Table 5. Wave Conditions Averaged Over All Traverses Along the Malindi-Fundisa Coast: $L=1.56T^2$; $S=H/L$.

Location	Wave direction	Wave period	Wave height	Wave length	Wave steepness
1	240	5.3	0.20	43.8	0.00685
2	298	11.5	0.25	206.3	0.00121
3	325	7.5	0.35	87.8	0.00357
4	325	9.0	0.18	126.4	0.00142
5	320	8.0	0.21	99.8	0.00210
6	325	8.5	0.23	112.7	0.00204
7	298	3.8	2.50	22.5	0.11110
8	267	5.0	2.67	39.9	0.06744
9	244	3.8	1.03	22.5	0.04578
10	115	7.5	0.30	87.8	0.00342
11	157	10.4	0.28	168.7	0.00165
12	176	12.7	0.55	259.6	0.00212
13	190.5	11.2	0.58	195.7	0.00296
14	321	7.2	0.78	80.9	0.00764
15	317.5	5.5	0.45	47.2	0.00953
16	315	3.0	0.96	14.0	0.07060
17	268	5.3	0.60	43.8	0.01370
18	270	3.6	0.37	20.2	0.01832
21	303	8.5	0.87	112.7	0.00772
22	309	9.5	0.75	140.8	0.00533
23	319	9.5	0.66	140.8	0.00468
24	322	6.8	0.65	72.1	0.00902
25	295	6.8	0.95	72.1	0.01318
26	277	11.2	1.00	195.7	0.00511
27	282	6.3	0.65	61.9	0.01050
28	272	19.4	0.87	168.7	0.00516
29	345	17.8	0.70	255.6	0.00274
30	290	6.0	0.57	56.2	0.01011

31	275	11.1	0.60	192.2	0.00312
32	205	12.4	0.52	239.9	0.00217
33	330	7.7	0.45	92.5	0.00487
34	280	20.0	1.00	624.0	0.00160
35	310	10.0	0.55	156.0	0.00353
36	326	9.9	0.90	152.9	0.00589
37	360	9.0	0.20	126.4	0.00158
38	310	4.0	1.50	25.0	0.06000
39	275	8.5	0.55	112.7	0.00489
40	194	4.9	0.62	37.5	0.01653
41	270	9.5	0.15	140.8	0.00107
49	310	9.0	1.20	126.4	0.00347
54	170	6.5	0.25	65.9	0.00379
55	225	3.0	0.20	14.0	0.01429
60	300	3.5	0.55	19.1	0.02880
61	275	10.1	0.33	159.1	0.00207
62	315	7.0	0.35	76.4	0.00458
63	276.5	5.0	0.50	39.0	0.01282
64	303	8.0	0.38	99.8	0.00381
65	295	8.5	0.53	112.7	0.00470
66	282	8.2	0.40	104.9	0.00381
70	310	14.5	0.45	328.0	0.00137
74	265	4.0	0.20	25.0	0.00800
75	300	8.0	0.30	99.8	0.00301

Extending from the Vasco da Gama Pillar to Leopard Point, there was a line of low vertical sea cliff cut into Pleistocene reef. Wave erosion has resulted into retreat of this cliff such that today only a few stacks and caves remain.

During low tide, infragravity flows in the reef channels generate currents ranging in speed from 0.1 to 0.4m/sec.

4.2.2 Gilani Beach

Larger wave measurements occurred around the Malindi Reef Light at a region of wave ray convergences, whereas northward from the jetty represents a shoreline of wave divergence. As a result, erosional and accretional processes take place south and north of the jetty respectively. The types of breaking characteristics of waves in the shore zone change northward from spilling to surging breakers. Wave-generated longshore currents flow northward, and hence the net littoral drift, at speeds ranging between 0.1. and 0.2m/sec. The current movement is mainly confined to the longshore trough (runnel).

There is an undertow (rip current) seaward from the jetty area (Aerial photograph). This localized stream of return flow through the breaker zone has speeds of upto 1m/sec, until it reaches a distance of about 4km from the coast. It is recognizable on aerial photographs as a swirling mass of sediment. Seaward of the breaker zone, the current becomes more diffuse and spreads out. The water is caught up at this point in the general

flow toward the beach. Tidal currents do not affect the Gilani Beach region.

4.2.3. Sabaki Beach and Delta, and Mamburui Beach

The Sabaki is the second largest river discharging into the Indian ocean at the Kenyan coast. Especially during the high-water periods enormous quantities of sediment is discharged into the ocean, which influence the development of the coast considerably. The bulk of this sediment is eventually resuspended by waves in the surfzone and moved along the coast by both longshore and tidal currents, to be carried onto nearby beaches and also deposited on the continental shelf. The longshore current direction is northward at speeds ranging from 0.2 to 0.4m/sec, whereas the tidal range varies between 2 and 3m. The Sabaki delta model illustrates expectations based on the complex balance between erosion and sediment transport dominated by coastal processes. No attempt is made to predict actual annual river-discharge: wave-power ratio (Leeder, 1985) since data on deepwater waves, nearshore waves and river- discharge collected over long term observations was not available.

The relative capacity of the coastal ocean to transport sediment is limited by the low tidal range and associated strength of tidal currents, hence the high wave energy dissipated on the coast does not hinder delta formation. The margin of the Sabaki delta tends to be rounded because coastal processes predominate. Wave reworking due to the high wave power

relative to river discharge has partially disrupted the effluent jets. Further, the effect of wave reworking include shoreward transport of sand to form swash bars around a broad crescentic mouth bar.

The delta formation is accompanied by the river buildup of distributary channels, through which the water flows on its way to the ocean. They extend across the delta as long, radiating and branching fingers. Evidence from photographic studies indicate that active distributaries continuously built their mouths further seaward until the distance to the sea was so great that the river could no longer maintain flow through the old channels. Over the past years, the Sabaki river has gradually shifted its course southwards as successive channels searched for gradient advantages over their precursors. The flow thus presently proceeds through a different set of distributaries to reach the ocean, and increased wave attack on abandoned deltaic sediments.

The restricted tidal range has resulted into the development of several longshore bars and troughs. These bars can be identified even when submerged, by the fact that waves break on them and can be spotted from the lines of breakers offshore.

A secondary phenomenon is the return of water down the foreshore (backwash) at an angle to the uprush (swash), this being the result of the slight angular incidence of waves on the shore (Plates 42-44). This contributes a further velocity component to the water near the shore, in northward direction.



Plate 42. Small breakers of the spilling type, beach 1km south of Sabaki river mouth. Note sea-weeds transported onto the beach.



Plate 43. Spilling breakers; Even though waves are refracted upon entering shallow water so that the crests are more nearly parallel to the coast, the process is rarely complete, and most waves approach the shore obliquely. Beach 1km south of Mambrui.



Plate 44. Surging breakers. Note well-rounded pebbles on the lower foreshore—transported northward from Sabaki river mouth by longshore currents and then pushed toward the shore by waves. About 1km north of Sabaki delta.



Plate 45. Plunging breakers against the beach of Robinson Island. Heights reach upto 1.5m.

The berm sands are usually not moved often, as indicated by the tree growth, accumulation of plastic bottles and other human artifacts.

At Sabaki Beach and Mambrui Beach, shifting sand forms dunes of considerable height. The close proximity of the Sabaki river which supplies the coastal zone with large quantities of sand, and favourable wind systems are conducive to dune formation. The coastal dunes represent subtractions from the beach sand supply. They are built from beach sand carried inshore but occasional offshore winds returns small amounts of dune sand to the beaches. The process of dune stabilization has occurred where they are not actively gaining or losing sediment, through colonization by various salt-tolerant plants or trees.

4.2.4. Sheshale Bay, Maridadi Bay and Casuarina Bay

The waves that do strike the beach are generally of very low amplitude and have short periods. These waves are usually large wind ripples which accompany the fluctuating tide. This constitutes the essence of the nearshore processes on the Sheshale Bay, Maridadi Bay and Casuarina Bay beaches: the breaking of waves, ebb- tide, swash and backwash, wind and sediment transport are also important but however seem to be subservient processes.

The effects of wave retardation off this indented coast are illustrated by aerial photographs. The waves advance more rapidly through the deeper water opposite the bays than through the shallow water opposite the

headlands. Each wave crest in turn begins to approximate to the curves of the shoreline. Consequently there are wave ray convergences and divergences at the headlands and bays respectively. The effect of the two wave phenomena on the region shoreward of the breakers is northward and southward flowing longshore currents simultaneously. Longshore current speeds range from 0.3 to 0.5m/sec. Furthermore, while the headlands experience high wave energy, the embayments are characterized by low energy wave conditions. Besides low wave power, sediment deposition in the bays is also facilitated by tidal-current-wave interaction.

Wave parameter transformations are influenced by bottom friction, crossed-wave patterns (caustic regions), and wave behaviour beyond the zone of breaking waves. Relict barrier reefs cause modifications to the basic nearshore circulation, resulting into certain local processes controlled by their geomorphology. The consequences include shoaling waves travelling in various directions and strong currents produced in the narrow reef channels. Waves reaching the barrier beach area, south of Ngomeni are diffracted, such that energy moves along the crest of waves in the lagoon waters toward the tombolo head. Thus active undercutting of cliff takes place.

Counter currents developed along the sides of the monsoon wind currents forms an integral part of the coastal processes in this area, influencing the coastal configuration.

4.2.5. Ngomeni Beach

Wave rays converge on the tombolo head and diverge in the bay; hence there is concentration of energy released against the headland while energy released in the bay is spread more thinly. This condition produces erosion on the headland shown by undermining of cliff, while deposition of spit (bayment bar) and beach occur in the bay. Another effect of wave refraction in this region is deflection of northward drifting sediments at the tombolo head, which is swept into the bay. The combination of sediment drift and longshore currents deposit a spit at the Ngomeni Bay entrance. The seaward growth of this spit is limited by wave-current action. Refraction of oblique waves north of Ngomeni is due to rapidly sloping sea-floor (Fig. 24) into deep water- hence the spit is curved landward as it tends to migrate. The geometry of the spit is further modified by tidal-wave cross currents.

The backbeach area is characterized by a prominent berm built by the constructive action of waves. The dominant process in the Ngomeni tidal flat is the daily spring and neap tide flooding.

4.2.6. Fundisa Barrier Islands

The barrier system serve as a prototype mesotidal coast with moderate wave energy characterized by development of barriers, tidal inlets and ebb-tidal deltas. The topographic low situation of this area facilitates

effective action of tidal currents. The barrier bars result from a dynamic balance between longshore currents, wave attack, sediment supply, and bottom topography. The islands are broken at intervals by inlets which water is borne in and out of the lagoon or tidal flat by tidal currents. The force of these currents tends to keep the inlets open; thus they act in opposition to the longshore currents, which tend to deposit sediment across the channel. The formation of the inlet shoals (tidal-delta) is therefore related to the tidal-current-wave interaction. These sediment bodies have an important effect on the nearshore wave refraction patterns. This pattern is also modified by the presence of submerged Pleistocene dunes, barrier reefs, fringing reefs and patchy reefs.

Though highly bisected and cut by tidal channels, the distinct convex-seaward arcuate shape of intermittent tidal-delta sediments, encompassing tidal inlets, can be delineated from aerial photographs. The sand bodies, suggestive of ebb-tidal deltas, may also be directly related to the origin of the linear offshore ridges, especially those attached to the shore, as well as many of the arcuate shoals, may owe their origin, in part, to the formation of now relict ebb-tidal deltas.

The barrier beach, like the beaches in Malindi formed on the coastal plain, is normally in a state of being washed away and replaced at a fairly constant rate. It is extremely sensitive to changes in the force with which waves break on it, or changes in the amount of sand carried toward it by



Plate 46. Eolian sand from barrier island migrating into lagoon. Northern Giriyama Village Island.



Plate 47. Waves breaking on the crest of submerged dunes, which is also partly exposed during low-tide. About 1 km south of Mto Tamamba tidal inlet.

those waves (Plates 45 - 47). Leeder (1985) attributes the genesis of new inlets and/or closure of old ones to sudden major storms.

That sufficient amount of sediment of various grain sizes is available, a low gradient coarsening - offshore tidal flat prism builds out by coastal progradation. Thus the incoming wave power is greatly reduced by the low-gradient flat and also waves cannot break on any one part of the tidal flat for any length of time. The effectiveness of waves in this area is thus greatly reduced.

The tidal flats are characterized by the absence of heavy surf as they occur in the shelter of barrier islands. The dominant process is the periodic tidal flooding of the flats. Because the incoming tide has higher velocities than the outgoing tide, sediment deposition is controlled by the scour lag and settling lag processes. Fining onshore indicates an energy gradient across the tidal flats: the highest energy is at the low tide level, the lowest at the high tide level.

4.3. Materials

4.3.1. Silversands Beach

In this area, dispersal of carbonate sediment, and, to a lesser extent, their production are considered. Evidence of the role played by reefs as

excellent examples of biogenic construction and sediment production is clear.

Sediments of the reef platform show a wide spectrum of grain sizes, ranging from clean sand, through coarse sand to gravel and even boulders. In the sandy fraction abundant forams and ostracods are found. Ostracods are more common in the tidal pools.

The upper rocky platform is generally sandy. There is little sand on the lower rocky platform except in the pools. Most of the lower rocky platform is covered by pebble-/gravel-sized sediments.

Coral fragments generally make up only about 15-30% of the reef-flat sediments, probably because coral easily disintegrates into fine sediments, which is winnowed away by the waves. Most of the reef-flat sediment (upto 90%) usually consists of coralline algae. Green algae *Halimeda* is relatively less abundant. Benthic foraminifera, molluscs, pelecypods etc are also important contributors to sediment on the reef-flats.

The Silversands beach is composed mainly of skeletal carbonates (78.4%) with some quartz and heavy minerals admixed (Table 6) especially in the medium to fine grained sand fraction. The bioclastic component of beach sand consists mainly of microfauna and oolites. The gravel is mostly shell gravel composed of gastropods and pelecypods.

Beach material grade from very fine (4.0 ϕ) to very coarse (-1.0 ϕ) sand, and generally moderately-to poorly- sorted. Skewness ranges from 0.16 ϕ to -0.49 ϕ . The shape of carbonate sand grains correspond with the

Code	Carbonates	Mica	Quartz	Ilmenite	Haematite	Magnetite	Rutile	Zircon	Garnet	Monazite	Hornblende	Tourm	Augite
JOZ/2	17.316	27.899	51.299	1.220	1.270	-	0.498	0.498	-	-	-	-	-
JOZ/3-1	88.297	-	10.644	0.211	0.479	-	-	-	-	0.193	-	0.176	-
JOZ/3-2	93.517	-	6.483	0.004	-	-	-	-	-	-	-	-	-
JOZ/4-1	90.224	+	9.548	0.228	-	-	-	-	-	-	-	-	-
JOZ/4-2	85.594	-	13.173	0.539	0.617	-	0.077	-	-	-	-	-	-
JOZ/5	92.364	-	5.701	0.749	0.962	0.220	0.004	-	-	-	-	-	-
JOZ/10	1.033	-	74.732	6.663	13.193	0.293	0.555	0.050	-	2.354	0.952	0.675	-
JOZ/11	3.472	17.439	76.608	0.377	0.224	-	-	-	-	0.715	0.828	0.337	-
JOZ/12	1.440	3.979	87.492	1.158	1.585	0.769	-	-	0.077	3.500	-	-	-
JOZ/13	2.442	18.358	78.105	0.280	0.361	0.093	-	-	-	0.361	-	-	-
JOZ/14-1	0.275	0.813	91.770	1.863	2.213	1.017	0.256	0.330	-	1.089	0.374	-	-
JOZ/14-2	1.172	4.904	92.458	0.394	0.892	0.090	0.018	0.018	-	0.054	-	-	-
JOZ/14-3	0.277	0.425	86.061	2.640	3.855	1.754	0.313	0.215	0.405	2.329	0.373	0.778	0.575
JOZ/15-1	0.285	0.987	91.683	1.830	2.802	0.116	0.030	0.019	-	0.380	1.290	0.578	-
JOZ/15-2	1.086	1.137	95.661	1.067	0.014	0.039	0.001	0.001	0.976	0.018	-	-	-
JOZ/16-1	0.662	+	53.586	14.527	16.078	7.253	2.212	2.036	1.362	2.284	-	1.362	-
JOZ/16-2	0.940	0.384	57.227	12.058	17.278	5.272	1.103	1.045	0.384	2.443	0.547	0.931	0.388
JOZ/16-3	1.191	+	94.092	1.511	2.313	0.094	0.012	0.012	0.455	0.239	0.168	0.023	-
JOZ/17-1	0.269	+	61.517	4.364	11.097	13.606	0.786	0.720	5.565	1.169	0.907	0.261	-
JOZ/17-2	0.364	-	66.484	7.924	12.067	6.394	1.217	0.830	2.398	0.362	1.36	-	0.600

100

Code	Carbonates	Mica	Quartz	limonite	hematite
JOZ/18-1	0.903	0.560	79.104	6.304	6.895
JOZ/18-2	0.491	0.539	87.812	3.505	4.208
JOZ/18-3	2.112	0.140	10.280	10.540	26.015
JOZ/18-4	0.986	0.954	70.495	7.511	7.723
JOZ/19-1	0.464	-	36.744	11.892	19.323
JOZ/19-2	0.866	-	59.992	7.793	14.862
JOZ/19-3	1.429	2.000	-	1.000	2.000
JOZ/20	1.365	1.913	82.830	4.780	6.909
JOZ/21-1	0.561	-	50.352	10.457	14.169
JOZ/21-2	1.105	-	81.636	5.672	7.528
JOZ/22-1	0.763	0.137	70.497	9.706	12.925
JOZ/22-2	0.899	0.344	80.299	5.475	7.552
JOZ/23-1	0.789	-	86.625	2.866	3.954
JOZ/23-2	0.151	0.077	81.577	4.438	9.005
JOZ/23-3	0.367	0.010	68.440	8.919	8.989
JOZ/23-4	0.445	0.424	66.219	6.105	10.606
JOZ/24	1.367	0.952	87.504	3.063	5.091
JOZ/25-1	0.229	1.404	82.986	4.398	5.260
JOZ/25-2	0.921	0.416	92.022	1.740	3.879
JOZ/26	1.350	0.940	92.647	0.575	0.931
JOZ/27-2	1.599	0.731	90.530	2.778	2.475
JOZ/28-1	0.499	5.389	92.910	0.224	-
JOZ/28-2	1.072	1.822	80.226	5.000	5.329
JOZ/29	1.585	1.055	95.176	0.390	0.593

PERIOD	ADJ	ADJ	ADJ	ADJ	ADJ	ADJ	ADJ
2.142	0.113	0.083	1.883	0.748	0.913	0.353	-
0.779	0.078	0.078	0.539	0.694	0.425	0.427	0.425
31.540	6.521	5.627	-	0.634	6.969	-	-
7.644	1.058	0.868	0.239	1.431	0.286	-	-
11.005	8.565	6.702	2.657	1.699	0.949	-	-
7.651	1.036	1.586	0.947	0.922	3.701	0.644	-
2.000	-	-	-	1.000	1.000	-	-
0.973	0.664	0.510	-	0.628	0.628	0.164	-
6.187	4.381	3.982	2.736	2.364	3.786	1.095	-
0.895	0.658	0.615	0.918	0.428	0.616	0.490	-
2.642	1.378	0.616	0.036	0.137	1.16	0.100	0.003
1.708	0.084	0.068	1.951	0.382	0.647	0.591	+
0.483	0.210	0.210	0.645	0.210	0.654	0.635	0.0635
2.319	0.773	0.965	-	-	0.386	-	0.30 ₁
9.413	1.128	0.996	0.224	0.842	0.548	-	-
11.119	1.160	0.954	0.162	2.413	0.293	0.100	-
0.935	0.265	0.299	0.021	0.404	0.120	-	-
1.796	-	-	-	3.252	0.073	0.602	-
0.126	0.033	-	-	0.729	0.066	0.068	-
0.954	-	-	-	0.947	0.947	0.709	-
0.619	0.062	0.062	-	1.045	0.099	-	-
-	-	-	-	0.978	-	-	-
2.590	0.423	0.338	0.085	1.897	0.609	0.609	-
0.032	-	-	0.229	0.550	0.390	-	-

JOZ/30-1	1.982	5.058	92.714	0.123	-
JOZ/30-2	4.717	10.078	83.927	0.094	0.422
JOZ/31-1	3.492	6.700	87.436	0.615	0.614
JOZ/31-2	5.520	3.669	89.655	0.223	0.235
JOZ/32	7.416	11.489	80.470	0.063	0.235
JOZ/33	8.228	29.667	60.794	0.431	0.452
JOZ/34	41.268	20.190	37.975	9.161	11.029
JOZ/35-1	15.634	-	79.460	0.877	1.611
JOZ/35-2	21.994	6.203	71.755	-	0.048
JOZ/36	40.751	1.186	56.635	-	-
JOZ/37	10.510	2.235	84.606	0.938	0.703
JOZ/39-1	1.401	-	87.119	8.484	0.587
JOZ/39-2	0.765	-	95.417	1.769	1.131
JOZ/40-1	0.796	-	51.507	11.515	13.302
JOZ/40-2	0.528	-	4.144	24.399	33.598
JOZ/41-1	1.182	-	8.110	22.469	46.658
JOZ/41-2	0.184	-	84.356	8.547	4.231
JOZ/41-3	3.100	-	94.796	1.017	0.687
JOZ/42	1.240	-	91.641	1.637	4.839
JOZ/43-1	4.658	-	91.270	1.246	1.447
JOZ/43-2	4.821	-	86.131	2.422	2.749
JOZ/44	0.794	-	67.256	7.621	13.052

Diopside	Kaefite	Zircon	Garnet	Monazite	Hornblende	Tourmaline	Augite
-	-	-	-	0.123	-	-	-
-	-	-	-	0.670	0.092	-	-
-	-	-	0.938	0.205	-	-	-
-	-	-	-	0.319	-	-	-
-	-	-	-	0.317	-	-	-
-	-	-	-	0.428	-	-	-
0.456	0.056	-	-	0.055	-	-	-
1.396	0.019	0.161	0.832	-	0.010	-	-
-	-	-	-	-	-	-	-
-	-	0.092	-	0.025	-	-	-
0.681	-	0.045	-	0.182	-	-	-
0.339	0.716	0.684	0.670	-	-	-	102
0.756	0.164	0.158	0.605	-	-	-	-
3.837	6.553	5.935	5.521	0.654	0.344	-	0.036
4.779	12.451	8.584	4.283	3.867	2.454	0.457	0.387
10.414	1.828	1.241	6.472	0.620	0.697	0.587	0.310
1.865	0.988	0.868	0.467	-	0.488	-	-
-	-	-	-	0.116	0.236	-	-
0.008	0.568	0.067	-	-	-	-	-
0.794	0.040	-	-	0.525	0.020	-	-
0.261	1.480	0.944	0.207	0.010	0.985	-	-
3.919	1.658	1.201	2.384	0.779	0.475	0.416	0.445

JOZ	Calcite	Mica	Quartz	Ilmenite	Haematite
JOZ/46-1	1.060	-	74.681	5.881	3.549
JOZ/46-2	0.272	-	66.278	8.356	12.607
JOZ/47	1.329	0.002	55.549	7.542	20.169
JOZ/48	1.200	-	86.111	6.219	3.405
JOZ/49	3.035	-	89.947	1.557	2.330
JOZ/50	2.275	-	91.551	2.461	2.567
JOZ/51-2	3.993	-	85.347	3.507	-
JOZ/52	0.351	-	-	.320	.649
JOZ/53	1.153	-	88.008	3.155	4.647
JOZ/54-1	4.875	-	73.580	3.709	10.136
JOZ/54-2	1.894	-	72.721	7.885	8.716
JOZ/55-1	20.004	-	78.507	0.711	0.504
JOZ/55-2	18.738	0.471	78.911	0.265	0.720
JOZ/55-3	7.863	-	81.592	2.425	3.722
JOZ/56-1	55.660	-	39.539	1.788	2.172
JOZ/56-2	5.767	-	89.949	2.560	3.838
JOZ/56-3	11.674	0.174	81.440	2.560	3.166
JOZ/57-2	9.154	1.00	-	1.000	1.000
JOZ/58	1.298	-	83.603	4.458	6.082
JOZ/59	3.032	-	48.930	15.536	21.117
JOZ/60-1	1.066	-	94.044	0.876	2.940
JOZ/60-2	3.618	-	92.419	1.314	1.141

Magnetite	Rutile	Zircon	Garnet	Monazite	Hornblede	Tourm	Augite
7.039	1.957	1.640	3.827	-	0.212	-	0.211
0.155	2.642	1.436	7.298	0.038	0.918	-	-
3.478	1.478	1.073	7.108	0.426	1.183	0.237	-
1.573	0.435	0.173	0.227	0.029	0.347	-	0.454
0.241	0.539	0.520	0.336	0.503	0.661	0.331	-
0.384	0.266	0.257	0.122	0.177	-	-	-
0.921	0.536	0.144	0.025	0.500	-	-	-
1.890	0.735	0.501	2.744	-	-	-	-
2.030	0.126	0.071	0.450	0.360	-	-	-
6.740	0.014	0.009	-	0.557	0.380	-	-
6.246	0.135	0.022	1.945	0.011	0.427	-	-
0.043	-	-	-	0.213	-	-	-
-	-	-	-	0.391	-	-	0.504
0.827	0.015	0.007	0.568	0.803	-	0.298	-
0.275	-	-	-	0.566	-	-	-
0.010	0.626	0.043	0.582	0.043	0.582	-	-
0.128	0.084	-	-	0.174	0.472	-	0.128
1.000	-	-	-	1.000	-	-	-
0.400	0.624	0.836	0.307	-	2.356	-	-
0.453	1.037	1.008	2.491	1.952	3.298	1.346	-
0.002	0.037	0.077	0.252	0.034	0.343	-	0.329
0.488	0.018	0.017	0.575	0.205	0.205	-	-

JOZ/61-1	0.645	-	22.597	18.696	27.254	4.353
JOZ/61-2	1.100	-	94.431	1.286	2.352	0.037
JOZ/61-3	2.933	-	93.255	1.199	1.430	0.056
JOZ/62-1	0.816	-	45.543	13.255	15.844	3.391
JOZ/62-2	0.144	-	3.866	24.275	38.407	6.433
JOZ/62-3	1.131	-	57.471	9.001	14.130	1.775
JOZ/63	1.456	-	94.637	1.004	1.176	0.312
JOZ/64-1	0.609	-	82.022	5.608	8.263	0.386
JOZ/64-2	2.526	-	96.610	0.016	0.817	0.010
JOZ/65-1	1.269	-	94.699	1.433	1.237	0.758
JOZ/65-2	1.597	-	94.375	1.678	1.166	0.089
JOZ/66-1	3.954	-	83.818	3.622	5.651	0.089
JOZ/66-2	4.950	-	93.282	0.615	0.471	0.063
JOZ/67	2.327	0.022	90.436	2.067	4.123	0.621
JOZ/68	1.243	1.000	79.757	2.000	3.000	2.000
JOZ/69	3.868	-	88.492	1.447	4.196	0.481
JOZ/70-1	2.432	-	88.101	2.247	2.533	1.214
JOZ/70-2	6.124	-	88.687	1.754	1.817	0.065
JOZ/71-1	1.420	-	3.403	32.155	47.730	6.054
JOZ/71-2	4.594	-	94.154	0.877	0.253	0.043
JOZ/72	2.028	-	96.307	0.762	0.863	0.025
JOZ/73	1.702	0.020	97.315	0.640	0.313	0.002
JOZ/74-1	1.013	-	53.348	15.164	20.652	2.087
JOZ/74-2	3.440	-	91.811	1.738	2.288	0.074
JOZ/75	5.542	-	92.663	0.949	0.653	0.126

Lu	KU811a	ZrCon	Garnet	Monazite	Hornblende	Tourm.	Augite
12.255	4.008	5.734	2.718	1.467	0.267	0.006	
0.126	0.125	0.151	0.126	0.142	-	0.124	
0.098	0.066	0.321	-	0.642	-	-	
0.366	0.314	18.248	0.328	1.895	-	-	
2.177	3.651	10.634	0.951	9.034	0.428	-	
0.896	0.870	12.709	0.042	1.544	0.433	-	
0.190	0.032	0.786	0.401	0.006	-	-	
0.151	0.592	1.337	0.574	0.458	-	-	
0.011	0.007	-	0.001	0.002	-	-	
0.439	0.079	-	0.077	0.009	-	-	
0.481	0.147	-	0.467	-	-	-	
0.453	0.169	0.534	0.358	0.267	-	0.285	
0.003	0.003	-	0.300	0.297	-	-	
0.184	0.116	-	-	0.104	-	-	104
-	-	-	1.000	-	-	-	
0.218	0.149	0.560	0.022	0.217	-	0.350	
0.999	1.000	0.433	0.015	0.893	0.133	-	
0.031	0.267	-	0.944	0.311	-	-	
2.330	3.650	-	-	3.620	0.611	-	
0.015	0.010	-	0.054	-	-	-	
0.005	0.005	-	0.005	-	-	-	
0.002	0.002	-	0.002	0.002	-	-	
0.774	1.156	1.412	0.474	1.659	1.809	0.452	
0.056	0.024	-	0.421	0.148	-	-	
0.032	0.029	0.003	-	0.003	-	-	

Code	HM (%)	Phi Median	Phi mean	Mean mm
JOZ/2	3.486	3.0000	2.6026	0.1646
JOZ/3-1	1.059	2.4501	2.092	0.2362
JOZ/3-2	0.004	0.7131	0.7107	0.6110
JOZ/4-1	0.228	1.4150	1.6126	0.3270
JOZ/4-2	1.233	2.7859	2.2361	0.5000
JOZ/5	1.935	1.0515	1.3526	0.1229
JOZ/10	24.235	2.4344	2.4351	0.1849
JOZ/11	2.481	2.7851	2.7729	0.1463
JOZ/12	7.089	2.7661	2.7521	0.1484
JOZ/13	1.095	2.9434	2.9047	0.1335
JOZ/14-1	7.142	2.6897	2.6881	0.1552
JOZ/14-2	1.528	2.4982	2.4691	0.1806
JOZ/14-3	13.237	2.4112	2.4090	0.1883
JOZ/15-1	6.945	2.1203	2.1152	0.2308
JOZ/15-2	2.077	1.9105	1.9065	0.2667
JOZ/16-1	45.752	2.7179	2.7315	0.1506
JOZ/16-2	41.449	2.4035	2.4084	0.1884
JOZ/16-3	4.349	1.9105	1.9192	0.2644
JOZ/17-1	38.214	2.4035	2.4010	0.1893
JOZ/17-2	38.152	2.5564	2.5656	0.1689
JOZ/18-1	19.433	2.0893	2.0905	0.2348
JOZ/18-2	11.158	2.3437	2.3467	0.1962

Phi sorting	Phi Skewness	Phi Kurtosis	Roundness	Sphericity
0.0784	-0.5288	0.7517	0.32	0.68
1.0042	-0.4868	0.7556	0.36	0.70
0.5690	-0.0432	1.2040	0.47	0.74
1.3273	0.1158	0.6566	0.40	0.72
1.7020	-0.6740	1.2157	0.55	0.70
0.8465	0.1571	1.0392	0.42	0.73
0.3821	-0.0800	0.9681	0.33	0.69
0.6186	-0.0716	0.9486	0.30	0.61
0.5121	-0.0651	1.0023	0.30	0.67
0.5216	-0.2058	1.4243	0.30	0.67
0.3947	-0.0230	0.8383	0.37	0.67
0.4978	-0.1400	0.9793	0.31	0.69
0.4806	-0.0133	0.8858	0.30	0.69
0.3732	0.0259	0.9845	0.36	0.70
0.3981	0.0154	0.9956	0.37	0.71
0.4026	0.1322	1.0167	0.38	0.67
0.4362	0.0164	0.7745	0.32	0.69
0.4536	0.0556	0.9904	0.33	0.71
0.4780	0.0031	0.8852	0.34	0.69
0.4287	0.0449	0.9315	0.32	0.68
0.4456	0.0634	0.8561	0.36	0.70
0.4002	0.0062	0.7751	0.34	0.69

Code	HM (%)	Phi Median	Phi mean	Mean mm
JOZ/18-3	87.468	2.8365	2.8214	0.1415
JOZ/18-4	27.565	2.5564	2.5408	0.1718
JOZ/19-1	62.792	2.5735	2.6655	0.1576
JOZ/19-2	39.001	2.4422	2.4271	0.1854
JOZ/20	15.257	2.5649	2.5609	0.1695
JOZ/21-1	49.087	2.3884	2.3924	0.1905
JOZ/21-2	17.820	2.2311	2.2350	0.2124
JOZ/22-1	28.603	2.6082	2.6117	0.1636
JOZ/22-2	18.458	2.0893	2.0955	0.2340
JOZ/23-1	10.502	1.9105	1.9184	0.2645
JOZ/23-2	18.195	2.4580	2.4587	0.1819
JOZ/23-3	31.059	2.6171	2.6192	0.1628
JOZ/23-4	32.912	2.6804	2.6871	0.1553
JOZ/24	10.198	2.0954	2.0927	0.2344
JOZ/25-1	15.381	2.8059	2.8127	0.1423
JOZ/25-2	6.641	2.4501	2.4308	0.1855
JOZ/26	5.063	2.3733	2.3752	0.1927
JOZ/27-	7.140	2.5649	2.5236	0.1739
JOZ/28-1	1.202	2.582	2.5669	0.1688
JOZ/28-2	16.880	2.8573	2.8497	0.1387
JOZ/29	2.184	2.8468	2.7506	0.1486
JOZ/30-1	0.246	1.8110	2.0038	0.2493
JOZ/30-2	1.278	1.9434	1.9842	0.2519

0.4293	-0.1299	1.5510	0.30	0.67
0.5800	-0.0216	1.2648	0.32	0.68
0.4273	0.3413	0.7864	0.31	0.67
0.4519	-0.0741	0.9687	0.33	0.69
0.4295	0.0095	1.0643	0.32	0.68
0.5469	0.0840	1.3470	0.33	0.69
0.5025	-0.0396	0.9402	0.35	0.70
0.3794	0.0254	1.1497	0.32	0.68
2.2768	0.0683	1.1644	0.36	0.70
0.4192	0.0089	1.0502	0.30	0.71
0.4325	-0.0106	0.9483	0.37	0.69
0.5125	0.0557	1.0240	0.36	0.67
0.3798	0.0797	0.9736	0.35	0.67
0.5336	0.0001	0.8966	0.36	0.70
0.3843	0.0012	0.1672	0.30	0.67
0.4293	-0.0767	1.0361	0.33	0.69
0.4587	-0.0658	0.9183	0.34	0.69
0.6561	0.2920	1.0642	0.32	0.68
0.4756	-0.0996	1.0389	0.32	0.68
0.4227	0.0877	0.9505	0.30	0.67
0.4267	-0.3663	1.4415	0.30	0.67
0.0909	0.4632	1.2741	0.37	0.71
0.6125	0.1106	1.2461	0.37	0.71

Code	HM (%)	Phi Median	Phi mean	Mean mm
JOZ/31-1	2.372	2.8365	2.8331	0.1403
JOZ/31-2	0.797	2.6349	2.6341	0.1611
JOZ/32	0.615	2.5228	2.5065	0.1760
JOZ/33	1.311	2.5735	2.5560	0.1700
JOZ/34	20.757	2.1324	2.0124	0.2479
JOZ/35-1	4.906	2.5998	2.6042	0.1645
JOZ/35-2	0.048	2.4982	2.5176	0.1746
JOZ/36	0.117	2.1140	2.1035	0.2327
JOZ/37	2.544	2.8054	2.8081	0.1428
JOZ/39-1	11.480	1.2447	1.2051	0.4337
JOZ/39-2	4.583	1.6215	1.6245	0.3243
JOZ/40-1	47.697	1.6575	1.6604	0.6164
JOZ/40-2	95.259	2.2515	2.2205	0.2146
JOZ/41-1	91.296	2.4501	2.4390	0.1844
JOZ/41-2	17.453	1.8365	1.8109	0.2850
JOZ/41-3	2.056	0.6439	0.6628	0.6317
JOZ/42	7.119	1.5995	1.5968	0.3306
JOZ/43-1	4.072	2.2934	2.2932	0.2040
JOZ/43-2	9.058	2.4659	2.4583	0.1820
JOZ/44	31.950	2.2515	2.2798	0.2059
JOZ/46-1	24.316	1.1976	1.1795	0.4415
JOZ/46-2	33.450	1.6897	1.6902	0.3099
JOZ/47	43.120	2.0116	2.0171	0.2471

Phi sorting	Phi Skewness	Phi Kurtosis	Roundness	Sphericity
0.3850	0.0051	0.7754	0.30	0.67
0.4545	0.8816	1.0040	0.31	0.67
0.5802	-0.0398	0.8550	0.32	0.68
0.5874	-0.0653	0.9451	0.32	0.68
1.0215	-0.2293	0.4220	0.37	0.71
0.3524	-0.0474	0.9203	0.32	0.68
0.5327	0.0509	0.3047	0.32	0.68
0.7261	-0.0255	0.4113	0.36	0.70
0.2740	-0.0534	1.4979	0.30	0.67
0.5910	-0.0896	1.0619	0.43	0.74
0.4098	0.0573	0.9045	0.40	0.72
0.4346	0.0185	0.7682	0.40	0.72
0.5420	-0.3558	0.9077	0.35	0.70
0.4442	-0.1029	0.9570	0.33	0.69
0.7272	-0.0658	0.9288	0.38	0.71
0.9356	0.1148	1.3295	0.48	0.74
0.4951	-0.0380	0.8827	0.40	0.72
0.5808	0.2578	0.8086	0.34	0.69
0.3327	0.0240	1.4101	0.33	0.69
0.4694	0.0456	1.4552	0.34	0.69
0.6678	-0.0416	1.0134	0.44	0.74
0.3913	0.0177	1.0380	0.39	0.72
0.3101	0.0268	0.9816	0.38	0.71

CODE					
JOZ/48	12.689	2.6620	2.2132	0.2157	0.4790
JOZ/49	7.018	1.4739	1.0885	0.4703	1.0988
JOZ/50	6.174	1.3771	1.3607	0.3894	0.7881
JOZ/51	10.660	2.2584	2.2535	0.2097	0.5517
JOZ/52	5.839	1.8997	1.8909	0.2696	0.7192
JOZ/53	10.839	1.9942	1.9888	0.2519	0.5299
JOZ/54-1	21.545	2.3364	2.2798	0.2054	0.5373
JOZ/55-1	1.489	2.7661	2.7293	0.1508	0.5525
JOZ/55-2	1.880	2.4982	2.4493	0.1831	0.6286
JOZ/55-3	10.545	2.4901	2.4915	0.1778	0.4352
JOZ/56-1	4.801	2.5564	2.5463	0.1712	0.4345
JOZ/56-2	8.284	1.6529	1.6249	0.3242	0.4769
JOZ/56-3	6.712	2.0649	1.1932	0.4383	0.9063
JOZ/58	15.063	1.7466	1.7251	0.3025	0.7201
JOZ/59	48.238	2.3954	2.3351	0.1982	0.7470
JOZ/60-1	5.253	1.1746	1.1436	0.4526	0.4959
JOZ/60-2	3.963	1.6897	1.6230	0.3247	0.7890
JOZ/61-1	76.758	1.9051	1.9324	0.2620	0.6685
JOZ/61-2	4.469	1.3659	1.3752	0.3855	0.7762
JOZ/61-3	3.812	1.1016	1.1308	0.4567	1.1671
JOZ/62-1	53.641	2.1329	2.1354	0.2276	0.5445
JOZ/62-3	41.400	1.8417	1.8541	0.2766	0.5290
JOZ/63	3.907	1.6215	1.6217	0.3250	0.6343

-1.1060	1.0857	0.35	0.70
-0.2862	0.9047	0.44	0.74
-0.0285	0.8814	0.42	0.73
-0.0743	0.8719	0.35	0.70
-0.0771	0.9620	0.38	0.71
0.0811	1.1905	0.37	0.71
-0.1546	0.8895	0.34	0.69
-0.2155	0.7858	0.30	0.67
-0.1573	0.9848	0.33	0.69
-0.0421	0.8658	0.33	0.69
-0.1111	1.1055	0.32	0.68
-0.1497	0.8479	0.40	0.72
0.3985	0.7581	0.43	0.74
-0.0661	0.6036	0.39	0.72
-0.1546	0.9681	0.34	0.69
-0.0449	1.1859	0.44	0.74
-0.1286	1.0087	0.40	0.72
0.0707	0.8882	0.37	0.71
-0.0367	1.1286	0.42	0.73
0.2117	0.8468	0.44	0.74
0.0114	0.8341	0.36	0.70
0.0829	1.0001	0.38	0.71
-0.0414	0.8602	0.40	0.72

<u>Code</u>	<u>HM (%)</u>	<u>Phi Median</u>	<u>Phi mean</u>	<u>Mean mm</u>
JOZ/64-1	17.369	1.6304	1.6582	0.3168
JOZ/64-2	0.864	0.9490	0.9539	0.5162
JOZ/65-1	4.032	1.3959	1.4898	0.3561
JOZ/65-2	4.028	1.2176	1.2245	0.4280
JOZ/66-1	11.257	0.8110	0.9404	0.5211
JOZ/66-2	1.768	1.8211	1.7550	0.2963
JOZ/67	7.215	2.0584	1.6373	0.3215
JOZ/69	7.000	1.3005	1.3394	0.3952
JOZ/70-1	9.467	2.1910	2.1818	0.2204
JOZ/70-2	5.189	1.8365	1.7431	0.2987
JOZ/71-2	1.252	0.5564	0.6031	0.6583
JOZ/72	1.665	1.6990	1.7025	0.3073
JOZ/73	0.963	1.6712	1.6752	0.3131
JOZ/74-1	45.639	2.3219	2.3124	0.2013
JOZ/74-2	4.749	2.0710	2.0648	0.2390
JOZ/75	1.795	1.7591	1.7591	0.2954

Phi sorting	Phi Skewness	Phi Kurtosis	Roundness	Sphericity
0.5341	-0.1052	0.8953	0.39	0.71
0.8890	0.0194	0.6210	0.45	0.74
0.6120	0.1345	1.0791	0.41	0.72
0.6569	0.0206	1.0134	0.43	0.73
1.0140	0.1179	0.8546	0.46	0.75
0.8510	-0.1702	0.8012	0.39	0.72
0.9938	-0.4520	0.8776	0.40	0.72
0.6108	0.1259	1.1802	0.42	0.73
0.4095	-0.0981	1.0718	0.35	0.70
0.7512	-0.0999	0.8325	0.39	0.70
0.9712	0.0723	1.1496	0.48	0.76
0.4677	0.05281	0.7894	0.59	0.72
0.4196	-0.0040	0.8050	0.39	0.72
0.5410	-0.244	0.8423	0.34	0.69
0.6273	-0.05812	0.8324	0.36	0.70
0.7643	-0.0424	0.8240	0.29	0.72

generic morphology of shells. Rounded pumice rock fragments ranging in size from 1-5cm are stewn on the berm area. During storms, sea-grass debris are piled up along the beach.

4.3.2. Gilani Beach

Materials of the upper rocky reef platform in southern Gilani beach vary in size from pebble through gravel to cobble, whereas sand occurs in the isolated pools and channels. Sea-grass and broken shell fragments have been transported to the backshore zone where they mix up with land-plant debris.

The beaches mainly consist of medium-to fine- grained sand which are composed predominantly of quartz (Tables 6 and 7). Considerable amounts of carbonates, mica and heavy minerals are also present. The mean, sorting, skewness and kurtosis measurements of 4 samples of the Gilani beach average 2.72 ϕ , 0.51,-0.11 ϕ and 1.09 ϕ respectively. The mean grain size shows fining in the northward direction of the longshore drift. Mean roundness values for Gilani beach sands range from 0.30 to 0.33 and their mean sphericity values range from 0.67 to 0.69.

4.3.3 Sabaki Beach and Mambrui Beach

Most of the sand is derived from the Sabaki river and is quartzitic in composition. Near the rivermouth the beach sediment is characterized by abundant heavy minerals and organic matter besides quartz. The Sabaki

delta interdistributary tidal flat consists of fine sand with a small amount of mud and organic matter. The distributary channel sediments range in size from fine to medium sand, grading into silt or clayey sand. The levees have medium to fine grained sand, with high heavy mineral concentrations.

The Sabaki - Mambrui beach sands are quartzitic and somewhat fine - to medium - grained. They are relatively well sorted and are positively to slightly negatively skewed (averaging $+0.01\phi$, ranging from -0.04 to $+0.07$, Table 7).

Data from the present study indicate that among the richest heavy mineral concentrations are found along the Sabaki beaches and delta and south Mambrui beaches. The heavy mineral content can be as high as 87.5 weight percent and averages 24.8 weight percent. They are composed principally to titaniferous-iron sands (ilmenite, haematite, magnetite) with subordinate zircon, rutile, monazite, garnet and other minerals of economic value.

As illustrated in Table 7, the dunes are composed of fine and very fine sand. Evaluating Tables 6 and 7 further, it is apparent that the most likely source material. i.e. the sediment of the Sabaki river is distributed as follows; the coarser fractions are enriched on the beaches and the finer ones in the dunes. The dune material is also better sorted and are strongly positively skewed, and generally show a better rounding as compared with beach sands. The dune sand is composed mainly of quartz,

but contains some skeletal carbonate particles and heavy minerals. The last are noticeable in the field as they are enriched in ripple troughs.

The sediment of the sebkha consists of very fine to fine sand and is composed mainly of quartz. Comparison with dune sands show that the sebkha sediment is finer than that of the surrounding dunes. This difference is due to the trapping of fine materials by adhesion on the sebkha floor. Subordinate crystals of gypsum and halite were noted.

Table (8). Orientation of long axes of 100 pebbles at South Mambrui Beach.

198	220	212	222	133	240	250	194	235	297
260	205	193	200	100	182	240	253	230	232
210	090	208	232	320	250	210	280	225	344
170	091	222	235	354	263	224	255	244	333
182	140	220	160	313	202	228	181	226	310
205	103	218	150	302	180	229	233	240	304
202	123	206	130	170	213	226	222	238	360
202	106	200	105	324	203	212	221	196	280
182	102	128	125	280	047	209	223	244	297
211	115	223	150	204	210	235	253	222	320

The pebbles which are 0.5-3cm in size are found on the beaches, approximately 4km and 2km to the north and south respectively of the Sabaki river mouth. They are well rounded and generally show a preferred orientation parallel to the beach and longshore drift but are perpendicular to the direction of shallow-water wave approach (Fig.15).

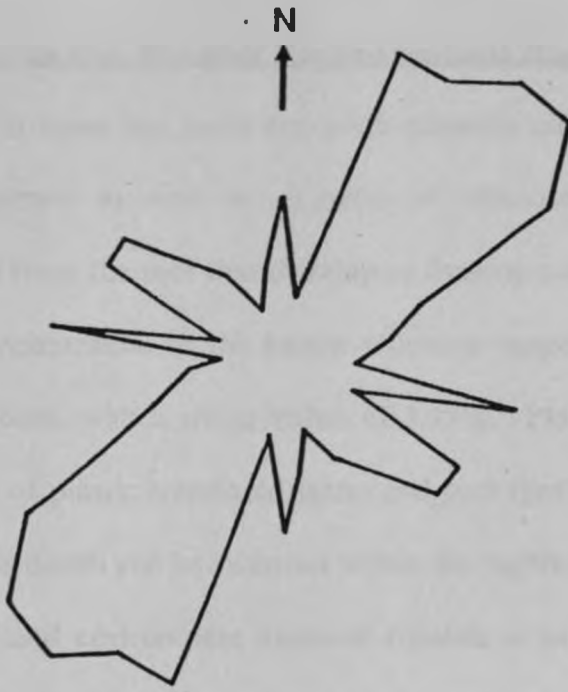


Fig.15. A rose diagram for orientation of long axes of 100 pebbles at South Mambrui.

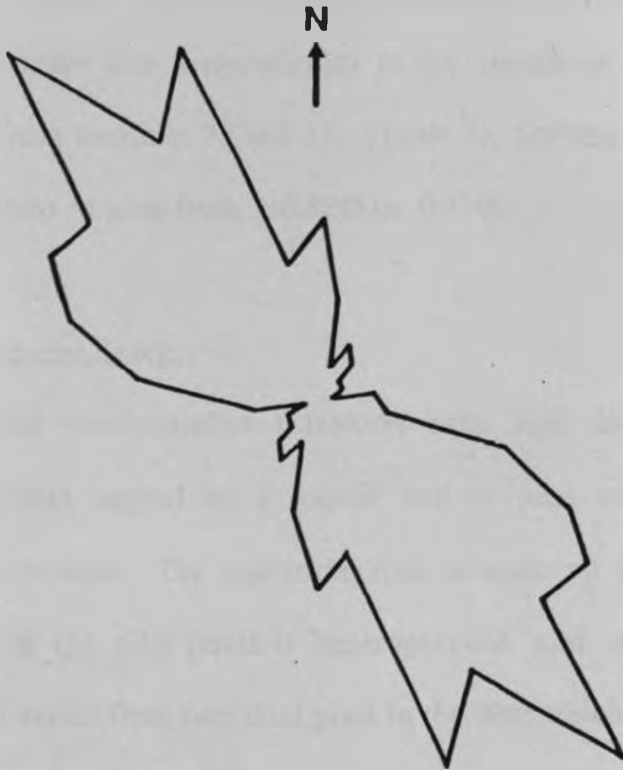


Fig.16. A rose diagram for orientation of long axes of 225 gastropod shells at Ngomeni Beach.

4.3.4. Sheshale Bay, Maridadi Bay and Casurina Bay

Beaches in these bay areas are predominantly composed of quartz and shell fragments as well as remains of microorganisms, particularly foraminifera from the reef that develop as fringing patchy reefs. The heavy mineral concentration in the beach sediment ranged from 0.05. to 20.76 weight percent, with a mean value of 3.95%. Plant debris and various assortment of plastic household items and packages were observed locally piled on the beach and berm zones within the bights (Plate 18).

The headland environment material consists of sand which has a mean grain size of $\sim 0.25\text{mm}$, but sands in the inner bay areas have a mean grain size of $\sim 0.16\text{mm}$. Mineralogic sorting due to size and density is displayed in these sands as shown by an inland increase in heavy minerals and mean grain size perpendicular to the stretch of beach for samples collected from localities 30 and 35. (Table 7). Sorting improves landward with skewness ranging from $+0.88\sigma$ to -0.23σ .

4.3.5 Ngomeni Beach

The mixed sand-/mudflat transition zone lead landward to muddy intertidal flats capped by a rootlet bed or peat accumulation of the mangrove swamps. The supratidal zone is made up of sandy bars. The sediment of the tidal pools is heterogeneous, and, consequently poorly sorted. It varies from one tidal pool to the next which indicates that each pool has its own micro- environment.

On the lower shoreface there is a dearth of mollusc and pelecypod shells. The coarsest material in the sands is represented by samples JOZ/56-2 and JOZ/56-3 from the base of wave-cut cliff, corresponding to that size fraction absent in samples from the beach (Table 7). Representative cumulative grain-size distributions for the Ngomeni beaches are given in Appendix I. Sands in these beaches typically have the composition: quartz, 72-88%; heavy minerals, 2-25%; carbonates, 1-20% with minor amounts of mica. Although relative abundance of the heavy mineral component show general spatial variation along the beach it is also evident that the highest concentration is found in the upper shoreface and berm zone.

The beach sand generally show negative skewness because the fine grains are selectively winnowed out by constant wave action and are moderately to well-sorted (ranging 0.43 to 0.71). Conversely the carbonate content of beach sands is low despite the presence of a nearby rim of fringing reef. Quartz sand grains show greater dissolution owing to the high energy of this environment.

Table 9: Positions of pelecypod valves on the sediment surface at Ngomeni Beach. Counting was done on 1m square at 200m interval from locality 53 to locality 55.

Area	Number of Specimens	Percentage	
		Concave up	Concave down
1	277	4.3	95.7
2	388	12.4	87.6
3	393	10.2	89.8
4	479	11.1	88.9
5	383	12.3	87.7

The data in table 9 indicate that in the swash zone, a large number of pelecypod valves show convexity downward, this being the most stable orientation in a wave hydrodynamic regime. However, when a small surface irregularity is present on the beach, then the valves are kept in a near vertical position.

Table (10). Orientation of long axes of gastropod shell at Ngomeni Beach

352	020	340	337	263	304	332	350	282
310	310	320	298	280	303	028	326	350
307	347	262	340	042	319	337	324	342
315	010	285	338	006	313	312	326	335
041	330	322	315	005	309	290	318	200
008	310	285	290	040	302	014	297	303
282	320	290	004	350	323	360	292	340

Table 10 continued....

358	357	270	020	274	298	324	292	337
307	293	342	027	284	328	324	315	300
320	302	322	343	305	330	338	350	226
317	344	320	057	355	315	300	283	355
337	317	329	040	341	322	008	320	331
350	318	340	010	034	338	354	321	337
277	305	298	338	287	298	334	270	338
310	293	340	333	355	278	307	004	335
347	276	275	360	337	278	310	003	290
327	326	314	304	046	334	323	007	298
306	311	264	304	355	312	330	352	344
316	292	310	325	325	290	283	324	356
322	330	300	356	343	258	272	271	302
330	287	312	310	033	295	302	294	330
328	275	360	364	045	360	292	295	335
290	320	004	065	336	336	343	324	299
325	276	314	360	292	026	290	293	283
316	240	315	352	302	331	323	310	324

On the Ngomeni beach, the long axes of gastropod shells are oriented parallel to the coastline and perpendicular to the direction of breaker wave line (Fig. 16).

4.3.6 Simiti Island

Sediments in the intertidal zone are located between the high and low water lines over a vertical range of approximately 3m. Intertidal flat sediments are mostly fine-grained usually mud (silt and clay) and fine sand. Gravels are rare, mainly rounded pumice, mollusc shells and fragments thereof. The sediments are non-laminated, but generally show

gray mottling that results from the decay of plant roots. These result in extensive peat bed formations (Plate 23) near organic-rich sands. Inlet sediments include lag broken shell debris near the center of the channel and decreases in grain size toward the lagoon. Mud pebbles and shells are abundant in tidal channels and are occasionally dispersed onto the tidal flat surface.

Shoreface sediments are deposited along the front of the barrier island seaward from the low tidal level to a water depth of about 9 to 12m; for most places, quantitative data do not exist for accurately fixing the seaward limit of the toe of the island. However, from aerial photographs we can deduce a qualitative estimation of approximately 2km from the barrier beach - extent of the swirling mass of sediment.

7 samples of beach sediments averaged 23.3 weight percent, mostly shell and shell detritus. Quartz is usually the major component (ranging from 67.3 to 94.8%) although heavy mineral content may be as high as 91.3% in the upper foreshore. Berms contain abundant heavy minerals where mollusc shells are often concentrated and upto 80% of the shells were found convexity-up oriented (Plate 48).

Mean size values for Simiti barrier beach sands range from 0.66 ϕ to 2.44 ϕ , and their median values are from 0.64 ϕ to 2.45 ϕ . Sorting shows little difference perpendicular to the beach, and average sorting is about 0.57. Hence the vast majority of sands in the Simiti barrier beach are

moderately-to well-sorted. Further, sorting improves from low-to high-water line.

4.3.7 Robinson Island and Girvama Village Island

The tidal delta is made up of clean sand, many gastropod and mollusc shells, and some drift wood. The tidal channels coming from the inlet leading into the lagoon are made up of clean sand somewhat coarser-grained than sand in the sand flats. Some mud pebbles and shells are associated with sand. Sediments of the subtidal ponds are muddy in nature and black in colour. The mud near the surface contains upto 9% water.

The barrier beach is composed of fine-to medium sand, mainly laminated bedding with low-angled discordances. Individual laminae may differ in grain size and in mineral content: Sometimes small shelly laminae are present. The beach sands in 10 samples from Robinson - Girvama Village Island beaches are 1.09 ϕ to 2.46 ϕ in mean grain size. These graded sands display a mineralogic sorting landward of the foreshore which demonstrates the efficiency of the wave-current mechanism to hydrodynamically segregate particles according to size and density. Shelly lag-gravel deposits were frequently encountered on the lower foreshore. These samples contained 51.5-91.6% quartz. The average mineral composition of beach sand heavy minerals in weight percent is 7.43% ilmenite, 8.93% haematite, 2.14% magnetite, 2.52%

rutile, 1.87% zircon, 2.73% garnet, and trace amounts of monazite, hornblende, tourmaline and augite. Calcareous fragments form as much as 3.99% of the beach composition.

On the sandy surfaces located above the high-water line (Plate 26), where mollusc shells are often concentrated, the orientation is normally convexity upward. Here, the sediment is generally coarse, may contain upto 95.3% heavy minerals, is positively skewed (ranging from +0.40 to +0.58 ϕ).

4.3.8. Ras Kiswakini Island

The sediments in the Kiswakini tidal flats are predominantly sand and clayey sand that may or may not be laminated. Tidal flat sediments immediately on the back side of the island are fine sand to silty-clay. The tidal channel constituents consist of a sand-silt mixture with plant fragments that may make up as much as 2% of the deposit. The washover fan deposits consist mainly of heavy minerals thinly spread inland in a semicircular area. Sediments of the supratidal zone are fine sand interfused by plant roots.

The 16 sieve-size analyses of the Ras Kiswakini Island beach sands from various sample locations indicate a wide range of textural parameters. Sands landward from high-water line containing 75% heavy minerals is generally better sorted (sorting is ~ 0.50) than mid-tide and lower foreshore sands containing less than <5% heavy minerals (sorting is ~ 0.70). The data also indicate that the beach sands are typically

negatively skewed, but samples of the berm zone and dune foot are slightly positively skewed (Table 7).

Characteristically, cumulative grain-size distribution data of beach sands display a consistent truncation at $\sim 2.5\phi$. Finer sediment ($<2.5\phi$) is apparently transported as longshore drift. Grains finer than 4.0ϕ is absent, having been winnowed out by longshore current and waves. The coarsest material in the beach sands has a mean grain size just finer than 1.0ϕ . Materials coarser than 2.0ϕ constitutes 50-80% of the total weight percent for the sands.

These sands are dominantly carbonate free ($<2\%$) except near the patchy barrier reef at the northern tip of the island where upto 4.95 weight percent is carbonate. Along the Ras Kiswakini barrier beaches, the heavy mineral content averages 20.98%, ranging from 0.86 to 95.99 weight percent and the quartz component range from 3.87 to 96.61 weight percent. The highest heavy mineral concentrations are almost entirely confined above the high-water level, particularly in the active berm zone (Plates 48, 49, 50).

4.3.9. Tamamba Island and Kanagoni Island

Tidal flats that form directly behind shelly beaches contain shell detritus from the open-sea beach.

The channel bottoms of the larger tidal channels are mostly sandy, enriched in shells and mud pebbles. The bottom sediments of smaller channels of the intertidal zone are mainly muddy in nature with a few



Plate 48. Heavy minerals and many shell confined to the active berm zone, shore of northern Simiti Island.



Plate 49. Trench showing laminated beach ridge sediments. Dark portions are rich in heavy minerals. Note various levels of erosional truncation. About 1 km north of Mto Marereni tidal inlet.



Plate 50. Beach sediments showing transitional forms between current marks and rill marks, and heavy mineral concentrations on surface. About 1km north of the reef platform.



Plate 51. Barrier bar sediments at Mto Tamamba tidal delta. Current marks and heavy mineral concentrations on the surface. Note a tidal channel connecting the sea (right) to the lagoon.

sandy intercalations (coarsely interlayered sand/mud bedding). Often lenticular bedding is developed. Nevertheless, shell layers and mud pebbles are always present. Shells and mud pebbles may be present as channel lag deposit. Such channel lag deposits sometimes develop over wider distances than the width of the channel, as a result of channel migration.

The barrier bar sediments are made up of clean sand, mainly quartz with minor amounts of heavy minerals, many mollusc shells and some drift wood (Plate 51). Further, barrier beach sediments are generally composed of clean, well-sorted, bedded sand. Scattered unbroken shells and shell fragments are locally prominent on the lower foreshore.

The beach sand quartz content average 78.42%, 18.54% heavy minerals, and carbonate is only about 3.03%. Mica is present in trace quantities. The average heavy mineral composition of the beach sands in weight percentages is : 6.25% ilmenite, 8.57% haematite, 1.08% magnetite, 0.47% rutile, 0.68% zircon, 0.21% garnet, 0.21% monazite, 0.74% hornblende, 0.28% tourmaline and traces of augite, They are concentrated mainly in the storm berm (Plate 52).

The sand samples examined indicate an average size of about 1.80ϕ (0.29mm) whereas the median diameter is 1.81ϕ (0.29mm). Thus the typical beach sand of the Tamamba-Kanagoni islands is medium-grained and well-to moderately-sorted. They are negatively skewed (averaging -0.20ϕ , ranging from +0.08 to -0.10, Table 7).



Plate 52. Trench showing laminated storm berm sediments: dark layers are heavy mineral concentrations. Note various levels of erosional truncation. Tamamba Island.



Plate 53. Straight, partly bifurcating symmetrical wave ripples in coarse to very coarse sand. Also flat-topped and rilled to the right. Wave propagation was from bottom. Silversands Beach.

4.4 Structures

4.4.1. Silversands Beach

The Silversands beach is characterized at low tide by features associated with falling water level and intermittent subaerial emergence of the sedimentation surface: swash marks, foam marks, bubble sand imprints, rill marks, flat-topped wave ripples, deformed wave ripples and current ripples during the last phase of emergence by flowing water:

Field data shows that the length of symmetrical and asymmetrical wave ripples varies from 70 to 100cm, and height from 10 to 12 cm (Plate 53). The crests are flat-topped in shape, usually straight and partly bifurcating. Megacurrent ripples (Plate 54) are present in the lowest part of the shoreface. Transitional forms between straight to undulatory crested are represented. Localized trains of straight-crested to linguoid small-current ripples (average length and height are 7cm and 1.5cm respectively) occur adjacent to these megaripples. Both wave ripples and megaripples are generally found in coarse to very coarse sand and are cut through by small channels. On the lee face of the ripples water is present.

Swash marks (Plate 55) are characterized by debris left at the highest point reached by waves along the beach. They are usually 40-50cm apart.

Beach lamination show reverse grading. Each lamina is coarser-grained near the base and grades upward into a finer-grained part.



Plate 54. Asymmetrical undulatory current-related ripples in coarse to very coarse sand. Current travelled from right. Silversands Beach.



Plate 55. Swash marks, debris let at the highest point reached by waves. The sand shows bubble sand structure which was produced from the entrapment of air bubbles in the beach sand.

4.4.2 Gilani Beach

Many sedimentary structures are found on this beach. Beach structures and imprints include depositional (lamination, ripple marks, swash marks and erosional (channels, scours) ones. Among the biogenic structures are dwelling and feeding traces of the crustacean *Dotilla fenestrata* and the gastropod *Polinices*.

The backshore is subjected to constant wind activity and so wind sand ripples are commonly generated. They generally have straight long, parallel crests, and are asymmetrical. Ripple wavelengths commonly range between 12 and 14 cm and heights are mostly between 0.5 and 1.0cm.

On the foreshore, backwash ripples develop as a result of the backwash of the waves setting up as turbulent motion. These ripples usually are 40-60cm apart and extend parallel to the contours of the beach. They are low in amplitude and have concentrations of mica in the troughs. Swash marks were also observed, superimposed on backwash ripples. Backwash marks (Plate 56) are made on the beach by projecting plant debris, which deflect the backwash of the waves.

Small-current ripples and/or megaripples, are produced in the beach runnel in which water flows during high water condition, and are exposed at low tide. The small-current ripples (Plate 57) range in length between 20 and 50cm, and height varies from 4 to 6cm. They are asymmetrical, straight- to undulatory-crested and often contain coarse sand in their troughs. Rhomboid forms are also present.

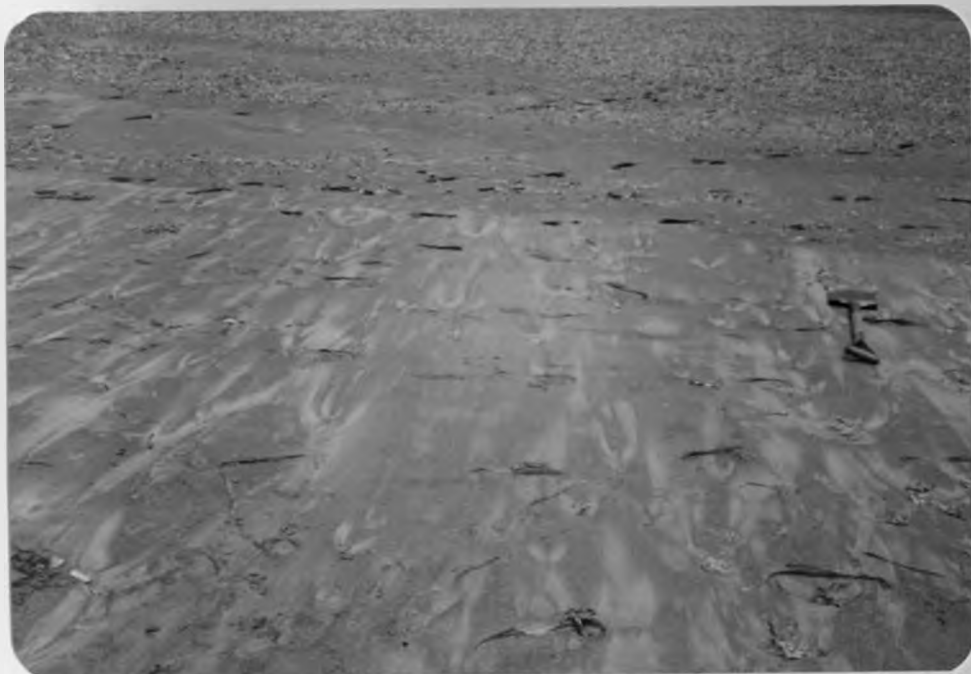


Plate 56. Backwash marks on a fine-sand beach at Gilani Beach made by projecting plant debris, which deflect the backwash of the waves.



Plate 57. Typical current ripples produced in beach runnel along the lower foreshore by longshore currents. Wavelength approximately 20cm. Gilani Beach.

Obstacle marks are produced in association with shells giving rise to current crescent features comprising ridges of 10-60cm length which taper down- beach. There are also surface markings produced by foam blown across the beach sediment surface resulting in the formation of elongated bubble impressions (Plate 58).

A zonation of structures across the beach is apparent and is presented in Fig.17 as observed during the course of this study.

4.4.3. Sabaki Beach and Delta, and Mambrui Beach

The Sabaki delta exhibit various sedimentary structures, both small-and large-scale. There is characteristic mottling of the interdistributary tidal flat sediments (Plate 6). A combination of various ripple forms and cross-bedding produces irregularly bedded sediments in the interdistributary channel fine sediments. Among the large-scale structures topset, bottomset and foreset beds (Fig. 8) are distinguished, the first two being subhorizontal, the foresets dipping seaward, Another large scale feature are the barfinger sands, which are deposited by the channels and attain thicknesses upto 2cm; they are elongate and, in cross- section, lense-shaped. Water level marks are engraved on the surface of barfinger sediment, marking a series of water levels during the falling water level (Plate 59). During this process rill marks are also formed (Plates 60, 61). Also found in the Sabaki delta are mudlumps, diapirs of mud rising into overlying coarser material, thus forming mounds.



Plate 58. Surface markings produced by foam blown across a beach sediment surface. Elongated bubble impressions arranged in rows are formed. Gilani Beach.



Plate 59. Water-level marks on a shifting sand bar (left). They are produced as a result of a discontinuously falling water level. The distributary (right) running seaward. Sabaki Delta.

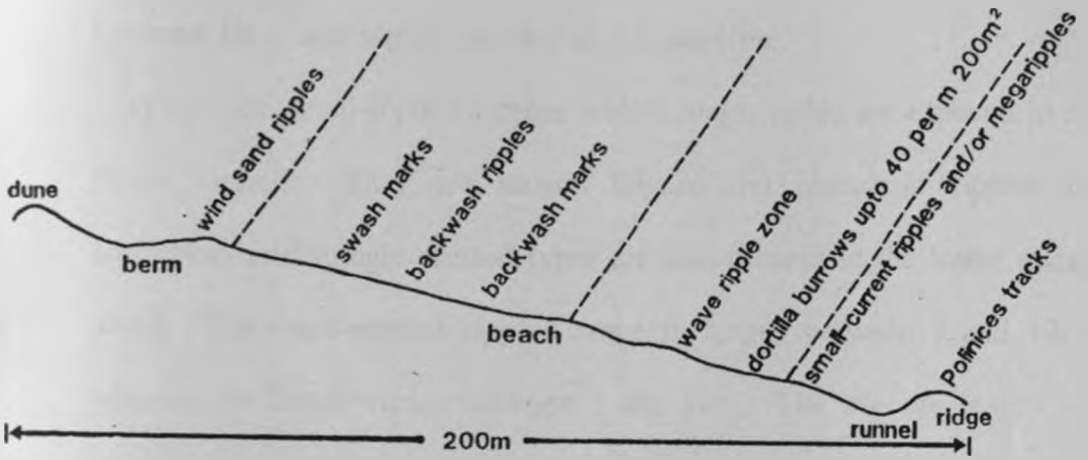


Fig.17. Zonation of structure across Gilani Beach.

Backwash ripples (Plate 62) are found on the Sabaki and Mambrui fine-sand beaches, due to runoff of retreating waves. They are separated by about 50cm and extend parallel to the shoreline.

At low tide small-current ripples and/or megaripples are exposed in the beach runnels. They are mostly lingoid and rhomboid ripples but undulatory and straight-crested types are also present in the lower energy areas. The small-current ripples range in length between 7 and 12cm, whereas the height varies between 1 and 6cm. The average length and height for the megacurrent ripples is about 1.5 and 0.1m respectively, and are generally oriented at right angles to the shoreline.

Moreover, both symmetrical and asymmetrical wave ripples, and transitions thereof, are frequently developed on the foreshore. During this study, they ranged in length between 8 and 30cm, and height varied from 1 to 5cm. The orientation of the wave ripples is either parallel or perpendicular to the runnel axis. They are essentially straight-crested, partly showing bifurcation. At locality 14 antidunes were observed developed on the emerged surface of the foreshore. Their length varies from 30 to 50cm and heights range from 1 to 2mm. They are more or less symmetrical in form.

Beach stratification was visible in trenches cut through the beach (Plate 63) exhibiting alternating dark and light coloured layers with low-angled discordances. The dark layers are rich in heavy minerals whereas the light ones are mainly quartz. Biological structures mainly resulting from *Dotilla*



Plate 60. Comb-shaped rill marks on a sharp, steep edge of shifting rivermouth sand bar. The flow is toward northern distributary (left). Sabaki Delta.



Plate 61. Rill mark with accumulation tongues. Sediment eroded during rill formation is deposited at the end of the rill system in the form of tongues a few centimetres thick. The flow is toward the lower left. Sabaki Delta.



Plate 62. Backwash ripples with a typical 40-cm wavelength on a fine sandy beach due to runoff of retreating waves. Sabaki Beach.



Plate 63. Trench showing laminated beach sediments; dark layers are heavy mineral concentrations and light layers are mainly quartz. Mambrui Beach.

fenestrata bioperturbations (Plate 64) occasionally tend to obliterate these even sediment laminations.

Foam marks, bubble sand imprints and rill marks are other surface structures noted on the present beaches. Elongated adhesion marks measuring between 0.5 and 3cm are commonly found in the upper part of the foreshore as a result of deflation by wind on a wet sediment surface.

Wind sand ripples on the berms and stoss-side of dune surfaces have their crests oriented at right angles to the wind direction. They range in length from 7 to 15cm, in height from 0.5 to 1.0cm, with long, parallel, straight crests which are asymmetrical and partly bifurcating. Sand tails of upto 10cm in length are produced by the deposition of wind blown sand behind small obstacles mostly represented by plant debris and broken household materials. In the regions between sand tails, deflation is active.

Steep slip faces of dunes (Plate 65) give rise to the characteristic high angle cross-bedding; that these are preserved is amply evident on various truncation surfaces (Plate 66). The windward slopes either exhibit truncation surfaces or wind sand ripples. As obstacle dune ripples swing around, and where obstacle dunes are coalescing a remarkable diversity of ripple directions can be observed (discouraging anyone from determining paleo-wind direction by measuring orientation of wind sand ripples).

Most portions of the sebkha were found to be covered by finely laminated sediment, however, in marginal portions truncation of high angle



Plate 64. Sedimentary biostructures are abundant on these beaches, among them the radial feeding tracks and the vertical burrows of the Dotilla fenestrata, a crab. Scale is 1m long.



Plate 65. Slip or avalanche face on leeward side of dune. Avalanches are set in motion when the slope of the slip face exceeds 34° . With each avalanche the dune advances a few centimetres. Mambrui Beach.



Plate 66. Truncation of dunes by deflation. Level of truncation is determined by the position of the groundwater table. Note shell pavement at the base of leeward slope of dune. Mambrui Beach.



Plate 67. Flat topped asymmetrical wave-formed ripples in medium to coarse sand (spade 1m long). They are formed in runnel in the landward side of fringing reef. Sheshale Bay.

olian crossbeds (Plate 66) indicate a change in level and/or location of deflation and sedimentation.

4.4.4 Sheshale Bay, Maridadi Bay and Casuarina Bay

Beach cusps formed by the waves at the shoreline of these bays are usually rather evenly spaced, separated by distances from about 5 to 8cm. Shepard (1978) and Johnson (1919) have clearly shown that the spacing of cusps is related to the height of the waves when they were produced. Their genesis can be attributed to piling of water on the upper beach and depositing some of the sand as the water sinks into the beach at the end of a swash, and the subsequent backwash causes small embayments.

Swash marks occur in a pattern of tiny imbricating sand ridges, curved with their convexity landward- marking the line of farthest encroachment of the waves. Such ridges of swash marks are invariably less than 2mm in height and are composed of coarser but hydrodynamically light materials such as mica, broken shells and sea-weeds. The swash mark spacing usually is between 0.5 and 3m, and have comma-shaped forms seaward of the ridges.

Backwash ripples typically range in spacing from 35 to 45cm. Other minor features include backwash marks due to obstacles that deflect the downbeach flow, leaving a chevron-shaped feature, often with a concentration of dark-coloured sand.

Diverse forms of rill marks are also shown on the lower beach at low tide. These are the results of water running out of saturated sand when the tide is low and water collecting in small rivulet channels. Their morphology is controlled mainly by the local geomorphology, slope of the sediment surface and grain size (Reineck and Singh, 1973).

Flat-topped asymmetrical wave ripples (Plate 67) were observed at the northern limit of the silted barrier reef at Sheshale Bay. They are bifurcated, with lengths ranging from 6 to 40cm and heights from 1 to 5cm. The orientation of the wave ripples is commonly parallel to the runnel axis. Toward the landward fringe of the runnel, lingoid and rhomboid small-current ripples are present.

Between Localities 37 and 38 isolated small-current ripples were encountered, in cases where sand is heaped up in the form of isolated crests on a rocky bottom and where the underlying sand is much coarser. Their heights are usually less than 2cm.

Deflation marks are formed on the upper beach and sand tails as well as obstacle dunes further inland from the berm crest. The beach sands are usually stratified, often showing reverse graded bedding. Biogenic structures are mainly trails of echinoid and bioperturbation from activities of *Donax* spp. and *Dotilla fenestrata*.

4.4.5 Ngomeni Beach

On the sandy bars, ripples occur, also small channels and rills. Biostratification by algae, worms, and pelecypods are common where sand drapes the rocky relief of tidal flats. Rhomboid and lingoid small- current ripples are commonly produced in the tidal channel, whereas various transitions of undulatory ripples are rare. They generally range between 8 and 9cm in length, and height vary from 1 to 2cm.

The Ngomeni beach sand is characterized by irregular laminations, erosional unconformities and bioperturbations. Individual layers are slightly inclined seaward and show alternating dark coloured, heavy mineral-rich laminae and light-coloured, quartz- rich laminae. Further, different sets of evenly laminated sand are separated from each other by very low-angled erosional unconformities. Vertical trench cuts on beach sediments also show burrows of the crustacean, *Dotilla fenestrata*. Erosional current structures such as rills and small channels are observed, but are not abundant.

All transitions from straight-crested to undulatory, and undulatory to lunate megaripples are present in the landward channel. They range in length from 60 to 75cm, and in height from 10 to 15cm. These megaripples are frequently cut through by rills and small erosional channels on the leeside. In the lower part of the foreshore wave ripples with their current transformations are formed. The landward fringe of the channel show development of lingoid and rhomboid small- current ripples.

Other minor markings noted on the beach sediment surface are swash marks, backwash marks, backwash ripples and foam marks.

Wind sand ripples are produced in the backbeach area. The wavelengths vary from 10 to 11 cm.

4.4.6 Simiti Island

The structures present in shoreface and foreshore sediments along the Simiti barrier island vary greatly - they are ripple marks, laminations, rill marks, foam marks and backwash marks.

Various types of ripple systems (Plates 68, 69, 70, 71) of varied directions are present which are produced at the same time or one after the other. Modified ripples also characterize the falling water level and ultimate emergence of sediments. Normal wave ripples are modified by the falling water level and the resultant current action. During the final emergence, ripple crests are sometimes broken through, producing rill marks. Rill marks also develop on unrippled inclined foreshore surface during emergence (Plate 44). Other important features suggesting intermittent subaerial exposure of such sedimentation surface are backwash marks and foam marks. The foreshore sediments seem to consist largely of poorly laminated sand (Plate 72).

Current marks (Plate 73), and ripple marks, including megaripples (Plates 74, 75), and cross-bedding are present in the inlet sediments. Beds generally dip toward the center of the inlet perpendicular to the inlet



Plate 68. Lunate megaripples observed on sediments of the northern part of Ngomeni bay barrier. Heavy mineral concentrations are found on crests.



Plate 69. Asymmetrical wave-related ripples in medium to coarse sand (spade 1m long). Waves propagated from left. Simiti Island.



Plate 70. Pattern of wave ripples produced by two equally strong wave directions. Simiti Island.



Plate 71. Pattern of wave ripples produced by two simultaneously working wave directions of unequal strength. In the lower margin of the photograph are lingoid-shaped small current related ripples. The direction of flow is from left to right. Ngomeni Bay barrier.



Plate 70. Pattern of wave ripples produced by two equally strong wave directions. Simiti Island.



Plate 71. Pattern of wave ripples produced by two simultaneously working wave directions of unequal strength. In the lower margin of the photograph are lingoid-shaped small current related ripples. The direction of flow is from left to right. Ngomeni Bay barrier.



Plate 72. Trench in small wave-cut cliff on berm showing irregular alternating light and dark layers; the dark ones are rich in heavy minerals and light ones are indicative of disconformity. Simiti Island.



Plate 73. Current marks and heavy mineral concentrations on surface sediments. Tidal inlet, Simiti Island.



Plate 74. Transverse ripples, crests are slightly undulatory, partly bifurcating. They originate under the combined action of waves and currents. Ripple crests run perpendicular to the current. Tidal inlet, Simiti Island.



Plate 75. Longitudinal ripples, crests are straight, showing no bifurcation. They originate under the combined action of waves and currents. Ripple crests run parallel to the current. The direction of wave propagation is at right angles to it. Tidal inlet, Simiti Island.

margin, some as much as 20°. Ripple marks and bedding are very common on parts of the tidal delta covered by shallow water.

On sand flats small-scale cross bedding of current ripple origin is most common. Sometimes this is developed in the form of herringbone cross-bedding in sections cut normal to the ripple crest axis and festoon-shaped units in sections parallel to the ripple crest axis. Laminated sand if found, in only small amounts. Climbing-ripple lamination is very rare, occurring only near the mouth of tidal channels. Megaripple bedding is common in the tidal channels.

Mud cracks are noted on the outer rim sediments of tidal flats. Where algal mats are present, the sides of cracked plates are curled up. Occasionally, these plates are eroded into thin sheet sediment and brought together by blowing wind.

4.4.7 Robinson Island and Giryama Village Island.

Shallow erosional depressions are often found on intertidal flats. Such depressions are often sculptured by wave ripples, whereas the surrounding sediment is covered by algal mats. In many cases the sandy layers are horizontally laminated and often developed as wave ripples and wave-ripple cross-bedding.



Plate 76. Straight crested wave-generated ripples in medium to coarse sand (spade 1m long). Wave propagation was from top. Ripple marks are crossed by small erosional channels. View from Robinson Island beach facing southern tidal inlet.



Plate 77. Ripple train showing transitional forms between lingoid and rhomboid megaripples. Flow is from left to right. Tidal delta, southern Robinson Island.

In the inlet channels and partly on the sand flats megaripples and small ripples are formed (Plates 76, 77), mainly in the current direction. In the high parts of inlet laminated sand is also present. Tidal channel sediments show ripple bedding and lamination as the major bedding types.

Sand washed into the lagoon forms steep foreset beds on the backside of the barrier bar, whereas the lagoonal bottom mud is finely laminated and thinly bedded.

Biogenic structures are made by pelecypods, molluscs and crabs (Ocyrode). Tracks of insects and birds are common. As a result, the inorganic primary sedimentary structures, i.e. bedding are destroyed by bioperturbation, which can be locally rather extensive.

Current marks and rill marks are commonly developed on the foreshore. Along the Robinson Island beach swash marks spaced approximately 1m are represented by plant debris aligned in lobate forms.

Wind sand ripples, small dunes and deflation surfaces are produced on the gentle backslope of the barrier.

4.4.8 Ras Kiswakini Island

Lamination in beach deposits (Plate 49) is caused by variation in heavy mineral content. The main bedding type is 1-10cm thick bedsets of evenly laminated sand with low-angled discordances. Sand laminae have been deposited from suspension clouds, brought by incoming waves. In the swash zone, swash and backwash produces a characteristic sorting in individual laminae according to size and density of sediment grains.



Plate 78. Cut in foredune showing nearly parallel bedding in the upper left portion of the photograph and large-scale cross-bedding in the upper-right of photograph. Note heavy minerals, swash marks and root horizons. About 1 km north of Mto Marereni tidal inlet.



Plate 79. Swash marks showing linear arrangement of shell material. Spacing is about 40-50cm. Ras Kiswakini Island beach.



Plate 80. Swash zone showing approximately 90% of the bivalves arranged with convexity downward. Note branching, bifurcating and meandering rill marks. The flow is toward the right. About 1/2 km south of the Mto Tamamba tidal delta.



Plate 81. Straight-crested megaripples. Ripple troughs are still partly filled with water. On the lee face of the megaripples water-level marks are present. Megaripples are covered with small ripples, which were generated after megaripples ceased to migrate. Flow is toward the observer. Note current marks and heavy mineral concentrations on surface. Tamamba tidal delta.



Plate 82. Lunate megaripples. Flow is from left to right. Foreshore, about 1km south of Tamamba tidal delta.



Plate 83. Eolian sand from Kanagoni barrier Island migrating into lagoon. Small rill marks towards the lagoon are formed during emergence of the surface.

Interbedding between eolian and beach sands is common in the backbeach areas. In the foredune ridge, nearly parallel bedding (Plate 78) is noted near the base and large-scale cross-bedding in the upper part.

On the shoreward side of the longshore bars there is a gentle shoreward dip of low-angled laminated sand bedsets (3 to 5°). Undulatory small-current ripples are present in the runnel, oriented at right angles to the axis of the trough. Swash marks (Plate 79), erosional rill marks (Plate 80) and bubble sand structures are formed on the foreshore. Straight-crested megaripples are developed on tidal delta sediments (Plate 81). On the leeside of the megaripples water-level marks and erosional rills are present. Megaripples are covered with small ripples, which were generated after megaripples ceased to migrate. Current marks are also present on the sediment surface. Lunate megaripples (Plate 82) are less abundant.

The tidal flat sediments commonly contain algal mats, slump structures, ripple marks, megaripple marks, and mud cracks. Megacurrent ripples and megaripple bedding is sometimes developed in the intertidal zone of sand bars and shoals.

Large-scale structures included channels and sand bar deposits. These channels are cut into older underlying sediments. Large-scale erosional unconformities separate older channel deposits from newer channel deposits.

The major part of the intertidal zone is made up of longitudinal cross-bedding of small dimensions. Erosional discordances are common. Bedsets of differing bedding types alternate with each other. Alternating bedding developed in the form of flaser and lenticular bedding, and finely interlayered sand/mud bedding is abundant. Bedding surfaces are uneven and wavy in nature.

4.4.9 Tamamba island and Kanagoni island

Bedding in the beach sands is even but variable in thickness. Stratification is usually visible in trenches cut through the beach (Plate 52). Alternating dark and light coloured layers commonly underly the foreshore, indicating changes in wave intensity. The dark layers have an abundance of heavy minerals, whereas the light ones consist mainly of quartz and a small amount of carbonate. Banding is also commonly imparted by layers of coarse shell fragments. Beach stratification usually shows various levels of erosional truncations.

Rill marks are formed when water entrapped in sediments returns to sea at low tide, cutting miniature channels (Plates 83, 84). Other features that characterize the beach surfaces are swash marks and backwash marks. Wind sand ripples, obstacle dunes and various truncation surfaces (Plate 52) are sometimes present in the backshore area.

On subaerial vegetated parts of the inlet delta, the sand is generally structureless and scour channels and algal mats are common on the



Plate 84. Branching rill marks. Small rills meet together to form a broad main channel. Bifurcation is in an up-current direction. The flow is toward the sea. Kanagoni Island.



Plate 85. Current marks and heavy mineral concentrations on surface in the lower portion of the photograph and line of breakers in the background indicating seaward extension of the barrier island. About 100m north of Mto Tamamba tidal inlet.



Plate 86. Symmetrical wave-related ripples in fine sand (spade 1m long). They are straight crested and partly bifurcating. Waves propagated from bottom. Intertidal zone, Mto Tamamba inlet.



Plate 87. Lingoid-shaped small-current ripples. The flow is from bottom to top. Metre rule as scale. Mto Tamamba tidal inlet.



Plate 88. Current crescent- obstacle mark produced in association with a treestump 1m in height. The flow is away from the observer. Kanagoni Island intertidal zone.



Plate 89. Isolated wave ripples originated on a sandy bottom covered with a thin layer of sand differing in grain size characteristics. Tamamba intertidal flat.

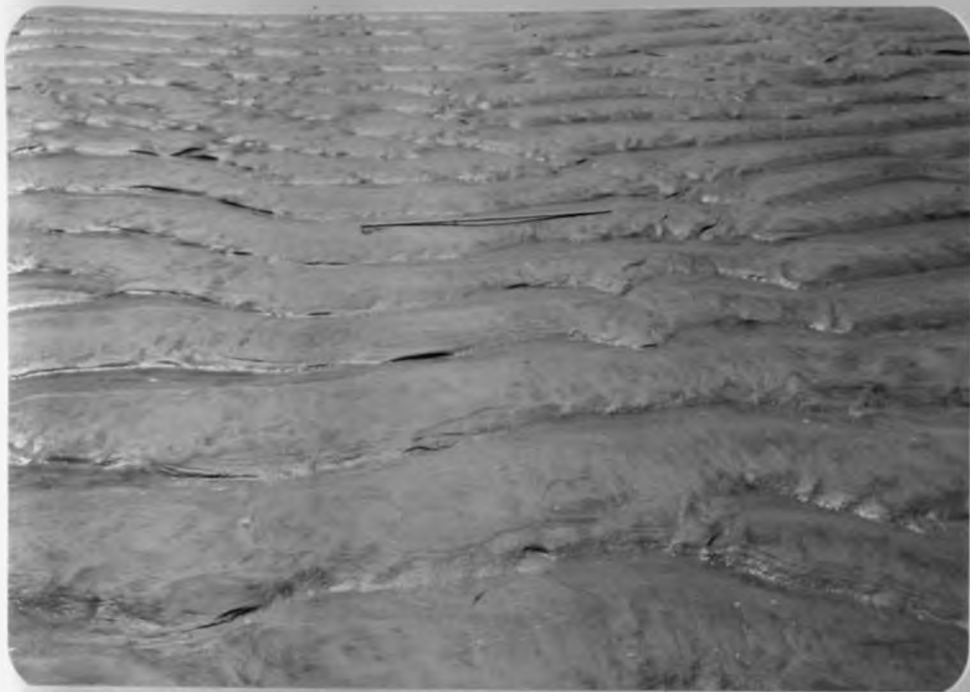


Plate 90. Undulatory megaripple ripples. Crests are continuous but projected forward into tongue-like extensions. On the lee face of the megaripples easter-level marks are present. Flow is toward the observer (Metre rule as scale). Mto Tamamba tidal channel.



Plate 91. Straight-crested megaripples. They are partly made up of dark heavy minerals. Megaripples are covered with small ripples, which were generated after megaripples ceased to migrate. Flow is from right to left. Tamamba intertidal flat.



Plate 92. Flat-topped, straight-crested wave-related ripples in coarse sand (spade 1m long). They are symmetrical and partly bifurcating. Barren zone, Kanagoni Island.



Plate 93. Trail left by echinoid crawling along the beach.

surface. Sponge-cake structure, apparently formed by emission of gas from underlying algal mats are also noted on the tidal delta at the Tamamba and Kanagoni tidal inlets. Current marks, wave-related ripples, small-current ripples and obstacle marks shown on Plates 85, 86, 87 and 88 respectively are developed on the tidal delta sediments.

In the intertidal zone sand flats and mixed flats small-current ripples, megaripples and wave ripples (Plates 89, 90, 91, 92) -mainly asymmetrical wave ripples are most abundant. The mixed flats are characterized by flaser bedding, wavy bedding, lenticular bedding, and finely interlayered sand/mud bedding. These bedding types are especially well- developed in the layers of longitudinal cross-bedding of point bar deposits of tidal channels. Megaripples are often produced in the tidal channels.

4.5. Fauna and Flora

4.5.1 Silversands Beach

The present knowledge of the local reef fauna and flora is rather limited; a detailed taxonomic list is not available. However, an attempt toward this end is presented in the following sections.

The dominant component of the reef frame are scleractinian corals, the genera *Acropora*, *Porites*, *Goniastrea*, *Favia*, *Montipora*, and *Galaxea* are

some of the common ones, the last, commonly form steep slopes. The coral growth form largely determines shape and internal structure of the reef. Octocorals are another dominant component of the reef surface, since the skeletons of most of them consists of microscopically small needles, they do not contribute to the frame, but to the sediments. Another important sediment contributor is the green alga *Halimeda*.

Among the destructive organisms is the asteroid *Acanthaster plancii*, the crown of thorns, which has devastated large portions of the reef by feeding on the soft parts of scleractinian corals. By stopping coral growth, it seriously affects reef formation without leaving any destructive trace.

The living corals are colonies of polyps which secrete a calcareous sheath around themselves. A host of marine fauna exist on the coral reef. Representatives of the following phyla are common: Porifera, Hydrozoa, Echinodermata, Mollusca, Annelida, and Crustacea.

Encrusting calcareous algae, mainly *Lithothamnion*, *Lithophyllum* and *Porolithon* are a feature of the seaward edge of the reef. On the reef platform there is a great wealth of green algae (Plate 4), especially of siphonales and siphonoclares. Brown algae are generally more predominant.

Most of the reef-flat has been colonized and stabilized by a sea-grass *Thalassia*.

Various benthonic animals inhabit the tidal platform in great numbers, producing highly bioperturbated sediments. The degree of

bioperturbation is 30-60%. During low water certain benthonic populations produce fecal pellets of diameter 4-5mm on the beach surface. The beach area also consist of beds made up mainly of pelecypod tests.

4.5.2 Gilani Beach

When the sandy beach is exposed at low tide, it first appears to be barren and with no form of life. However, after some time the surface becomes broken with worm casts and depressions of various kinds indicating the presence of animal life below the surface.

A bivalve *Mytilus edulis* makes fecal pellets. The degree of bioperturbation ranges between 30-60% which is medium bioperturbation. Among the fauna also present here are *Dotilla fenestrata*, the gastropod *Polinices* and the bivalve *Donax* spp. These bivalves of 1-2cm size are exposed and moved up the beach by uprushing water, and immediately after the water recedes dig into the sediments and disappear from the surface. A small plant, *Ipomea pes-capres* has settled on the berm area.

4.5.3. Sabaki Beach and Mambrui Beach

Extensive bioperturbation activity of the bivalve *Donax* spp. and a crab *Dotilla fenestrata* was observed in the middle zone of the beach. Crawling traces (Plate 93) are made by echinoid moving on beach sediment surface. A large number of organisms inhabit the delta region; They excrete fecal pellets which measure 2-5mm and also produce characteristic mottling

(Plate 6). The fauna is attracted to this area due to high amount of nutrients present in the sediments. Therefore the residents of this area come here to catch fish, shrimps and crabs for food.

An attempt has been made to identify the flora present by virtue of the role played by vegetation as obstacle trapping sand and as stabilizing element in dune formation. The lower part of the beach is free of vegetation because of flooding of storm wave. At the foot of the dunes above the normal storm-wave line *Ipomea pes-capres* settles as pioneer plant(Plate 11), partly accompanied by *Sesuvium*, *Lepturus* and *Tridax*. Further inland the grasses *Sporobolus* and *Cyperus* occur, as well as trees like *Hyphaene*, *Pandanus* and *Casuarina*. At the seaward positions of the foredunes, crustacean burrows occur. In the top laminae of the sebkha, the presence of microscopic green algae was suggested by a green stain. In marginal portions sebkha grass was growing.

4.5.4 Sheshale Bay Maridadi Bay and Casuarina Bay

Concentration of coarse hard skeletal parts of epibionts are encountered on beaches and are particularly locally abundant near mollusc colonies mainly comprised of gastropods and pelecypods. They thrive on the adjoining dead patchy reefs. The shell concentrations have been strongly reworked and are exposed to wave and current action. Thus, broken shells are rather abundant. Endobiont parts are mainly derived from *Donax* spp. and echinoids which die of exposure when erosion is strong and much

sediment is removed such that they are unable to dig in downward from the sediment surface to survive.

As a result of the activity of benthonic animals, the beach sediment is bioperturbated: These are crawling traces of echinoid and biogenic structures produced by *Dotilla fenestrata*. The dunes show varying degrees of stabilization by vegetation (Plates 18-21). The plants *Ipomea pes capres* and *Sesuvium* grow on the berm zone (Plate 19).

4.5.5. Ngomeni Beach

On the rocky reef platform and tidal pools, a variety of organisms were encountered including corals, echinoids, asteroids, holothurians, sponges, and epiphytic foraminifera, also brown and green algae as well as grass. On the rocky rims of the tidal pools barnacles and/or oysters are common.

Mangroves occupy a large portion of Ras Ngomeni tidal flat. Between Ras and Maweni, mangroves cover a narrow strip of the intertidal zone and extend beyond to the supratidal barren zone. A zonation of mangroves is apparent: *Rhizophora mucronata* starts on the lowest level and is followed by *Ceriops tagal* and *Avicennia marina*. Stems and stilt roots of *Rhizophora* provide a substrate for invertebrates: 40-80cm above the bottom barnacles settle, above to 120cm gastropods and pelecypods are found.

4.5.6. Simiti Island

Evidence from taxonomic consideration of mangrove species within the Simiti tidal flats exhibit a close relation to geomorphological distribution, and hence the zonation. The woody species mangroves, the families Avicenniaceae, Rhizophoraceae and Sonneratiaceae are well-differentiated and taxonomic position is almost certain; zonation on geomorphological subdivision characteristically stand out.

Sonneratia alba with intercalations of *Xylocarpus granatum* have colonized the immediate area landward of the shoreface where the accretion processes are also markedly dominant. The mangrove *Rhizophora mucronata* grows in deeper mud and *Ceriops tagal* occupy the central areas of the swamps. *Bruguiera gymnorhiza* seems to be confined to the *Rhizophora spp.* and *Ceriops spp.* habitats. *Avicennia marina* and sporadic presence of *Lumnitzera racemosa* are usually restricted to the more inland zones.

The animal life of mangrove swamps is varied and sometimes abundant. Molluscs, crustaceans and fishes are common. They attach themselves to the mangroves or just exist on the bottom of tidal flat.

A thin surface algal mat usually marks the position of the transition zone

4.5.7. Robinson Island and Giriyama Village Island

The intertidal and supratidal zones of the lagoon environment are covered with mangrove vegetation. The mangroves on the margin of the lagoon show zonation according to tidal level. *Ceriops tagal* grow in the upper parts of the intertidal zones while *Avicennia marina* flourish within the inner rim of the supratidal zones. Large areas of lagoonal bottom are covered by eelgrass.

Algal mats (Plate 30) are sporadically distributed, and during dessication, surfaces covered with algal mats develop mud cracks with curled margins.

The degree of bioperturbation by *Callianasa* burrows in the tidal channels and lagoon bottom is rather high. Besides, many benthonic lamellibranchs, tube-dwelling polychaetes, echinoids, gastropods, arthropods, rays, flat fishes and plant roots also cause destruction to primary bedding.

It was noted that although a high number of individuals are present, there are only a few species of animals with preservable hard skeletal parts. In addition, there is almost no post-mortem transport of hard parts from one depositional unit into the other, and the distribution of dead fauna corresponds well with the living fauna.

The vertical zonation of organisms in the intertidal zone shows some relationship with the water level of the tides. In the subtidal zone of the lagoonal bottom vertical zonation is rather indistinct. However, here,

there is a lateral zonation depending on distance from inlet, current velocity and grain size. The activity of organisms is very low on tidal delta reflecting the stronger influence of sedimentation.

Along the Robinson Island beaches the Ghost crab, a crustacean *Ocypode* was noted (Plate 48) Minor skeletal debris on the lower shoreface and berm zone usually comprises echninoids and molluscs. (Plate 26).

4.5.8. Ras Kiswakini Island

The tidal flat deposit show high population density and strong bioperturbation. Horizons of mollusc shells in living position, are common, often with escape traces. The fauna within the tidal flat area also include crabs, an abundance of polychaete worms, algae and sometimes small fish in localized ponds.

The mangrove species *Avicennia marina* thrive in the supratidal zone including foredunes (Plates 32,33) where their roots have protected the dunes against denudation by storm waves. Along the beaches of Kiswakini barrier island, a 10-15m zone of dead *Sonneratia alba* seem to suggest discontinuous depositional marine transgression (Plate 38).

4.5.9. Tamamba Island and Kanagoni Island

Rolled algal mats are commonly found forming extensive beds on the tidal flat surface exclusive of the sandy bars. Localized pools which

generally contain brackish water, support luxuriant green algae that later form matlike layers in the sediment. This phenomenon was also observed on beaches close to the tidal delta where rill marks are present. Black-coloured beds in the pool-bottom sand are the apparent result of reducing conditions and organic decay. The following mangrove species were found to exhibit a taxonomic distribution according to the local geomorphological position in the tidal flat sub-environments: *Sonneratia alba*, *Rhizophora mucronata* *Ceriops tagal* and *Avicennia marina*.

Occasionally, fecal pellets excreted by crabs, polychaete worms and cerithid gastropods are found concentrated in definite layers. Living horizons of benthonic molluscs are found with escape-traces under them, especially in larger channels, escape-traces are rather common.

5. DISCUSSION AND CONCLUSIONS

5.1 MALINDI -FUNDISA NEAR-SHORE ENVIRONMENTS

The major environments of coastal deposition comprise (a) beach and intertidal flats, (b) dunes, (c) barrier, spit and lagoon complexes, (d) shallow-water carbonates. Within these major environments, there are subenvironments such as berm zones, tidal pools and channels, tidal deltas and inlets, and sebkhas.

The present study provides a more comprehensive picture of the nature of beach sedimentation along the Malindi-Fundisa area. The area of study offers a large variety of beaches varying in lithology, degree of protection, and adjacent environments, which would warrant a comparative study with repeated observations over a long period of time. Additional data are necessary to completely characterize the sedimentology of this area and the present study provides a significant step toward that goal.

5.1.1. Coastal processes on the Malindi-Fundisa Coast

The Malindi - Fundisa coast is subjected to relatively simple coastal processes insofar as marine coasts are concerned. Tides are in the mesotidal range, 2-3m, and the presence of significant inlets throughout the Fundisa area indicates a greater effect of tidal currents on the shallow sea floor and coastal configuration. Because of the difference of times of tides in the bays from those on the open coast, the water flows with considerable velocity through the bay entrances. It is evident from aerial

photographs that the water in Ungama Bay is subject to whirlpools due to the tidal-current-wave interaction. Unlike the ocean currents mentioned hereunder, where the velocity decreases rapidly with depths, the velocity of tidal currents is essentially the same from top to bottom in a water column, although near the floor the bottom friction reduces the flow considerably. Hence we can safely assert that tidal currents have been important in contributing to sedimentological characteristics of the Fundisa area.

Physical processes along this coast are wind induced. These include the size and orientation of waves, and to a lesser extent the direct effect of wind on the backbeach zone. Rip currents are typically present but are not considered to have a significant effect on beach morphology or sediments.

An oceanographic study focussed on the transient monsoon current regime of the northwestern Indian ocean (Johnson, et al., 1982) has improved our understanding of interactive monsoonal wind and currents in this region. Moreover, the monsoon wind system over the western Indian Ocean has been well charted by Findlater (1977). The present coastal region experiences seasonally reversing monsoon wind. This reversing part of the current system is generally referred to as the Somali Current. Further, the two types of weather systems exert much influence on the Malindi-Fundisa coast. The southwest monsoon wind current originates in the southern hemisphere generally in March or April, and

penetrates progressively further north while increasing in strength until it reaches its maximum development in July. It reinforces the speed of the East African Coastal Current (E.A.C.C.) and speeds of upto 3-5 knots can occur (Johnson et al., 1981). From May to October the core of the wind current has the appearance of a western boundary current, locked to the topography of eastern Africa (Anderson, 1976; Findlater, 1977). The northeast monsoon wind current generally begins in November or December along the east African coast. It is less intense than the southwest monsoon, with a less well-defined core hence the low and high energy conditions respectively. The northeast winds not only work against the E.A.C.C. direction but also reinforce the southerly flowing Somali Current coming from the north. Depending on the strength of the winds, the Somali Current may push the E.A.C.C. back as far as off Malindi.

According to Shepard (1978), the ocean currents are maintained primarily by the prevailing wind. However, evidence from data on current movements indicate that the current direction, although variable throughout the year, has a dominating southerly flow tendency (Johnson et al., 1982). Its speed varies from 0.5-5 knots. The monsoon wind do not seem to effect the current direction which is probably strongly influenced by the flow of the escaping water out of the Ungama Bay and also by the tides and the flow of the Sabaki river.

The annually reversing monsoon wind currents develop counter currents along the sides which have an important influence on the coastal

configuration of the northern Malindi area, where there is a series of capes and concave bights. From the area where the Somali Current and the E.A.C.C. meet, originates a seaward flowing current called the Equatorial Countercurrents (E.C.C.). These countercurrents could probably be the reason for low heavy mineral concentrations at the bays. During the moderate to low velocity northeast monsoon winds of beaufort force ranging 0.5-2, small waves are generated which approach the coast so as to trigger off northward flowing longshore currents in most of the study area. This occurs during a falling barometer. Abrupt change in wind direction occurs during the southwest monsoon accompanied by a very rapid increase in wind speed ranging from 3-4 beaufort force. Large waves are generated which approach from the southeast and cause rapid longshore currents moving to the north in the study area. These conditions occur during rapidly rising barometric pressure.

Longshore currents and the accompanying sediment transport along the Malindi-Fundisa coast show both temporal and geographical variations. Studies of the sediment transport using a variety of criteria indicates that sediment on Malindi-Fundisa beaches is moving to the north. This conclusion is based on the mineralogy, especially the distribution of heavy mineral concentrations, grain size, and shell composition of the beach sediments. It may appear that the distribution of these parameters is irregular due to the presence of reefs which interfere with sediment transport. However, examination of consecutive and closely spaced

mid-tide level points makes the theory of northward longshore drift more valid. This is also inferred from observation of drift bottle, milk packets and other plastic items found to the north of Malindi town.

Observations made in the field by the author confirm that there is a convergence of longshore currents in the vicinity of Maridadi and Casuarina bays. Examination of available monthly wind data in comparison with coastal orientation provide a tentative support of the presence of littoral drift convergence.

5.1.2 Malindi-Fundisa Beaches

5.1.2.1 Beach Sediments

Beaches along Malindi-Fundisa shores consist predominantly of terrigenous minerals, the residue of disintegration of the Mozambique Belt metamorphic rocks. Because quartz is the most stable of the common rock forming minerals it is the most abundant in the sands, and in some areas where there has been extensive chemical weathering, beach sediments are almost entirely composed of quartz. Notable examples are the beach sediments of Sheshale Bay, Maridadi Bay and Casuarina Bay. Mica is abundant in the Gilani beach, and layers of mica are quite common in beach sands. The heavy minerals, ilmenite, haematite, magnetite, zircon, rutile, garnet, monazite and traces of hornblende, tourmaline and augite are interbedded in many beach sands or concentrated on the berm zones.

Biogenous constituents, mainly calcareous materials are abundant in certain beaches and is predominant in the Silversands beach. In areas where there are fringing reefs, barrier reefs and offlying patchy reefs from which the sand is derived, the beaches have an abundance of foraminifera, and mollusc, echinoid and coral fragments. Calcareous secreting algae are also common. Tentatively, the order of abundance in calcareous beach sands is: foraminifera, mollusc, algae, echinoids and then corals. The Malindi-Fundisa coast shows an alternation of terrigenous beaches and shell beaches, the former are mainly fine-grained with low foreslope and the latter are coarse-grained and steep.

The grain sizes vary across individual beaches: the coarser material occurs at the higher portions of the beaches. Plots of grain-size distribution curves for the beaches (Appendix I) show subpopulations which can be related to the three modes of transport namely suspension, saltation and rolling. Further, the mean grain size of clastic sediment is a measure of the energy of the depositing medium and the energy of the basin of deposition. It provides a comparative indication of the weight force that must be balanced by an applied fluid stress before transport by water or wind is possible. Since sediments occur in a range of grain sizes, the mean grain size of the deposit reflect the energy of the environment in terms of transport and deposition. Beach grade bedding is a record of time-varying flow at a point. Sediment of the berm crest is generally

coarser, for it consists of material thrown up during storms and are essentially rich in organic matter.

Samples collected at mid-tide level for consecutive locations often indicate variation in sediment size in a longshore direction. There is a tendency for mean particle size to decrease in a down-coast direction due to selective winnowing and subsequent deposition of finer material in the direction of longshore drift. However, local variations in the coastline morphology, such as the presence of low-energy bays and relatively high-energy headland environments complicate this pattern. Finer materials are deposited in the low-energy areas while coarse materials accumulate in the high-energy areas. This pattern is further complicated in details by the presence of beach surface markings and structures, runnels and ridges, each characterized by a change in sediment type. At the Gilani beach platy mica particles tend to be concentrated in distinct zones as a result of the sorting action of wave movements. Owing to their lower settling velocity, they are transported further inland, and once deposited are not readily reworked. Finer-grained spheres and rods, conversely, are caught up in the backwash and rolled down the beach. In this way mica accumulate as coarse lag deposits.

Beaches bordered by cliffs and fringing reefs contain the coarsest sand because it has been locally derived from the cliffs and reefs, whereas the long beaches are commonly fine-grained because here the sand has come from the Sabaki River (coarse materials do not reach the coast). There

are indications that the barrier island beaches have received some of their sand from erosion of submerged Pleistocene dunes on the adjacent continental shelf which are barely exposed during neap tides. First, these islands keep growing northwards and seawards even during dry-weather periods when there is less sand supply from the Sabaki river. Secondly, the content of heavy minerals concentrated on barrier beaches seem to contrast with the Malindi mainland beach deposits. Underwater investigations off the Fundisa coast might prove this point.

Sneed and Folk (1958) found that shape was more closely related to particle size than the distance of transport, apparently because larger particles wear more rapidly than smaller ones. With increasing wear and tear during transport, sand grains increasingly become more and more spherical. The sphericity of sand grains therefore increases with grain size. Furthermore, the roundness of sand grains also show a strong relationship to grain size. Coarser sand grains possess better roundness than finer ones. Contrary to the general belief inherent in the definitions of roundness and sphericity, the shape of clastic grains seem to be predetermined by the initial crystal properties in substantial and recognizable degree even after more than one cycle of transport.

Bioclastic grains exhibit a large variety of shapes. Besides, the skeletal particles contain internal cavities and/or are perforated ; or else they may have large protrusions such as spines. Because of internal cavities, pores

and external protrusions, the behavior of bioclastic grains during transport depends much less on their sizes than those of clastic mineral grains.

Sorting values display a pattern that is quite comparable to that of the mean grain size. The result of a regression analysis for a series of observations, shown in figure 18, from beaches in Malindi and Fundisa gave a negative correlation of -0.51 for these variables, thus accounting for 26% of the variability. Both of these values are significant, and the sorting gets worse as the diameter increases, but as ϕ units are used this is shown as a negative correlation. It is not however easy to tell whether the sand size affects the sorting or the other way round. In fact the most likely reason for the relationship is that both variables are affected in the same way by the process of transport and deposition. The finer particles are selectively moved and deposited together, thus giving rise to the fine grade and the good sorting. The fine grained sediments occur in an environment that is in equilibrium with the forces acting upon it, while the coarser, less well sorted sediments are characteristic of an environment that was undergoing active change and movement. It can also be seen that beach sand, by way of contrast, generally show negative skewness because the fine grains are selectively winnowed by constant wave action, leaving a tail of coarser grains. It is noteworthy that wind-blown sands (section 5.1.3) generally show positive skewness because of the low efficiency of the wind in moving coarse particles which are usually left behind to form a lag deposit. A simple plot of skewness

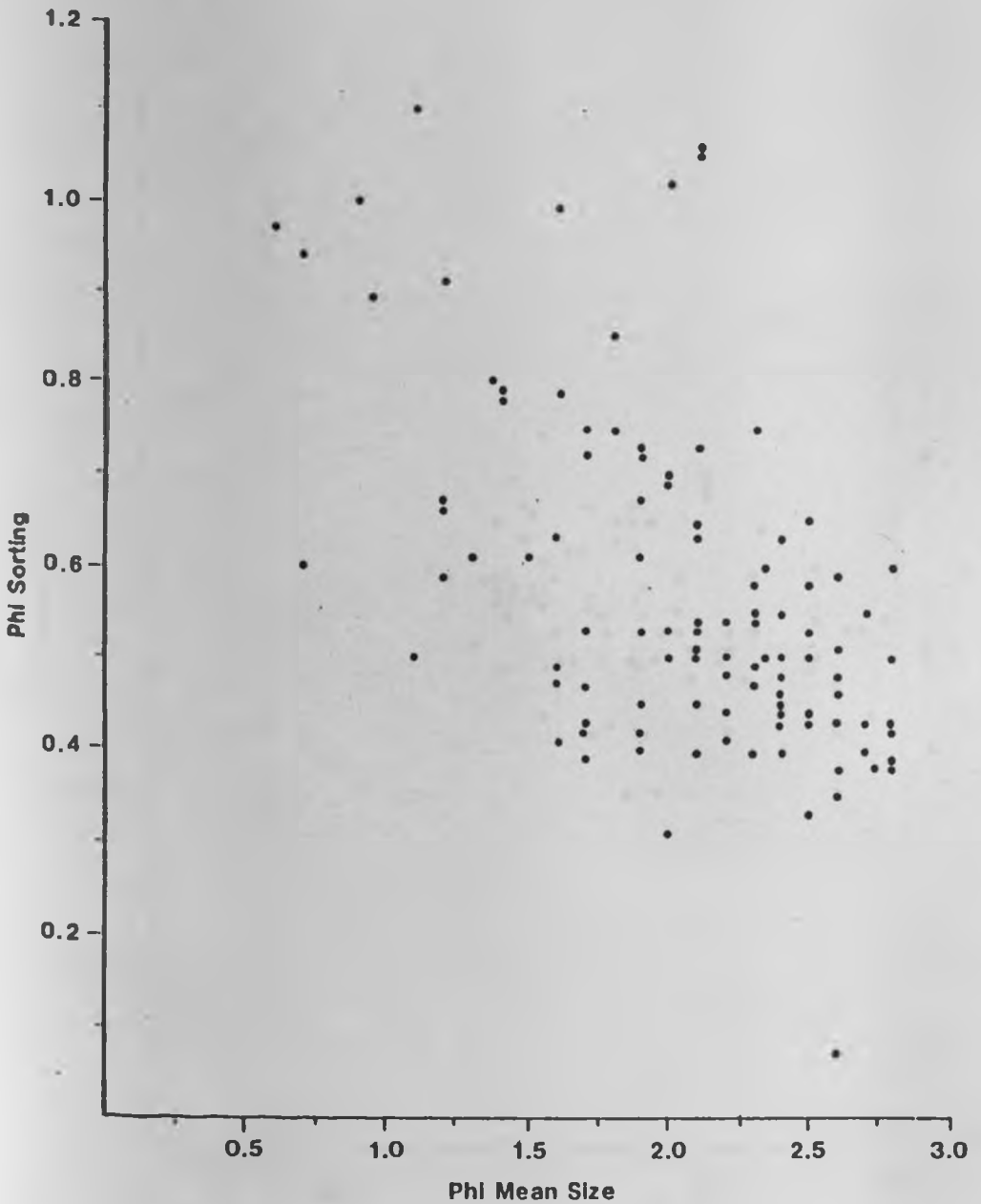


Fig.18. Correlation of sorting and mean diameter, for the beach samples from Malindi-Fundisa area.

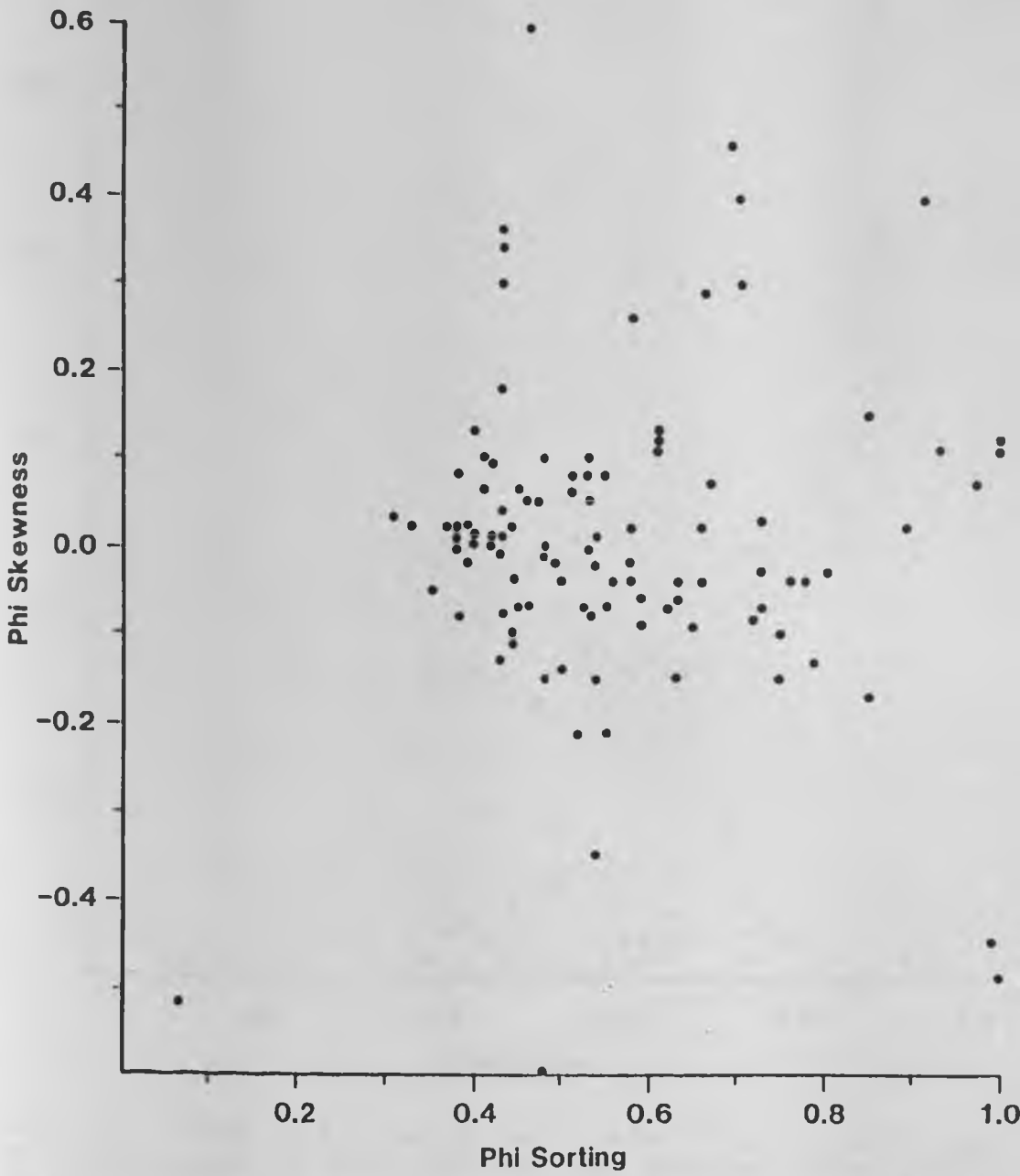


Fig.19. Plot of skewness Vs. sorting of sand samples from Malindi-Fundisa area.

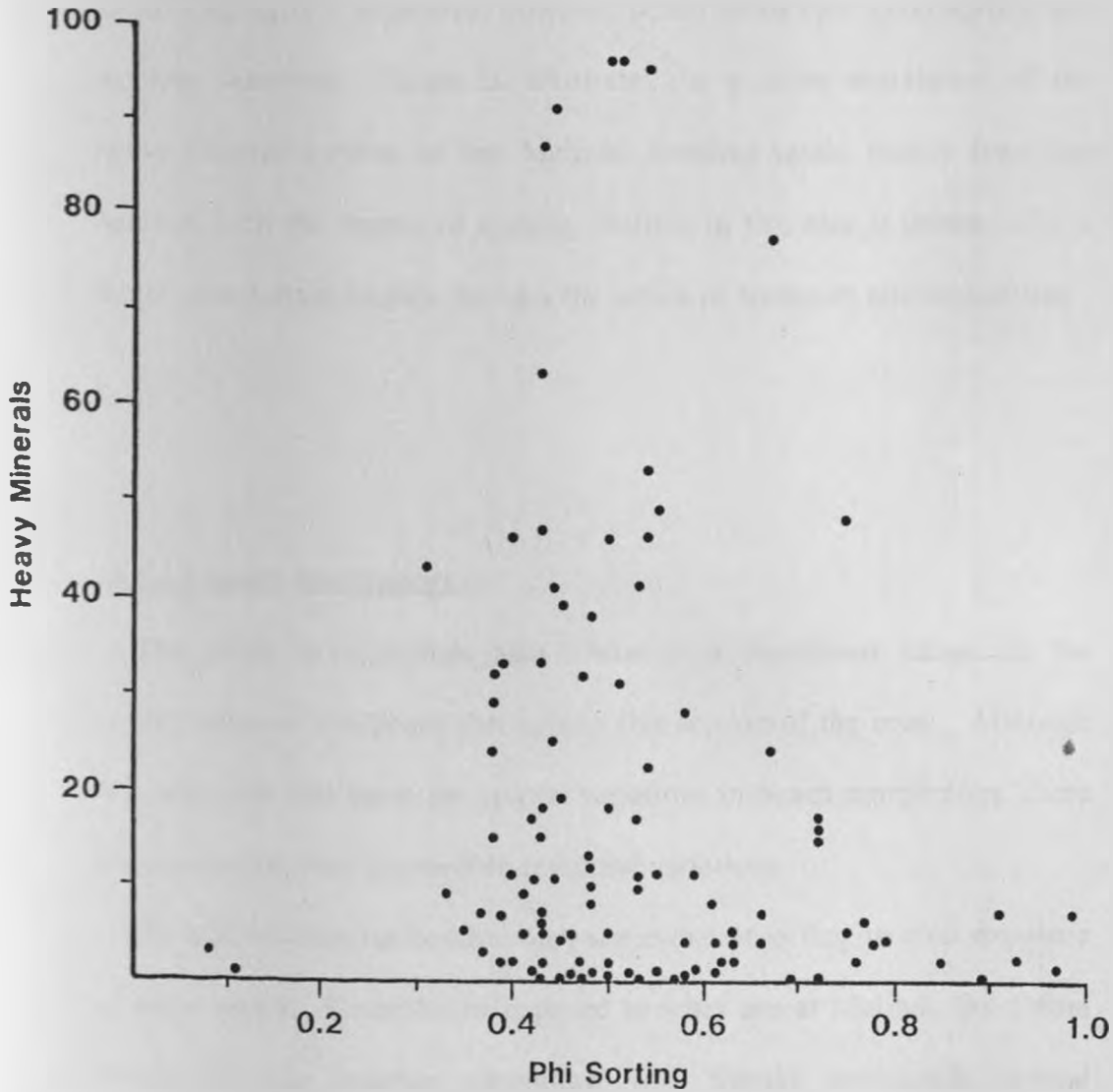


Fig.20. Plot of heavy minerals Vs. Sorting determinations of sand samples from Beaches in Malindi-Fundisa area.

against sorting for beach sands illustrates some of the above features although results of the present study cast doubt on the generality of this approach (Fig.19). In general however, beach sands have good sorting and negative skewness. Figure 20 illustrates the positive correlation of the heavy mineral content of the Malindi- Fundisa sands, mostly from the beaches, with the degree of sorting. Sorting in this case is shown to be a factor of sediment density, besides the action of transport and deposition.

5.1.2.2 Beach Morphology

The study area reveals that there is a significant range in the configuration of the beach throughout this section of the coast. Although it is apparent that there are spatial variations in beach morphology, there are no existing data on possible temporal variations.

The Malindi-Fundisa beaches vary somewhat according to their exposure to wave attack. Examples of exposed beaches are at Malindi, the Gilani beach and the beaches extending from Sabaki northwards beyond Mambui. The overall shape of these beaches is characterized by wide, gently landward sloping backbeach areas, and a gentle, broad foreshore. Examples of protected beaches are the Silversands beach and the Ngomeni beach. The beaches here are narrow, have more steeply sloping backbeach areas with prominent berms and steep foreshores. The berms

are usually built up from the constructive action of waves. A series of berms could sometimes be observed on beach profiles. This is a manifestation of shifting positions of the berm crest and therefore the position of the foreshore.

Mean values for the slope of the foreshore in exposed beaches are between $1.5-3^\circ$ while in protected beaches the foreshore slopes are significantly steeper. These steeper slopes however, could also indicate the areas of convergence (Davis, 1978). Therefore steep foreshore gradient along Robinson Island can be construed as resulting from the presence of a convergence zone.

In areas where the tidal influence is minimal, beaches are often bordered by a series of longshore bars and troughs, and conversely, broad terraces are developed, each with at most one large bar exposed at low tide level. Another fundamental difference in beaches is related to their ground plans. Thus the long continuous and relatively straight beaches of the barrier types and exposed mainland coasts are in marked contrast to the short beaches bordered by fringing reefs.

Higher wave energy zones apparently have steeper beach gradient; the swash slope depends on the length of the waves. For this reason, the volume of the swash relative to the backwash increases as the waves become longer. In model wave tank experiments, where the other factors on which the gradient of the beach depends can be held constant while the wavelength is varied, the two variables show a very close correlation

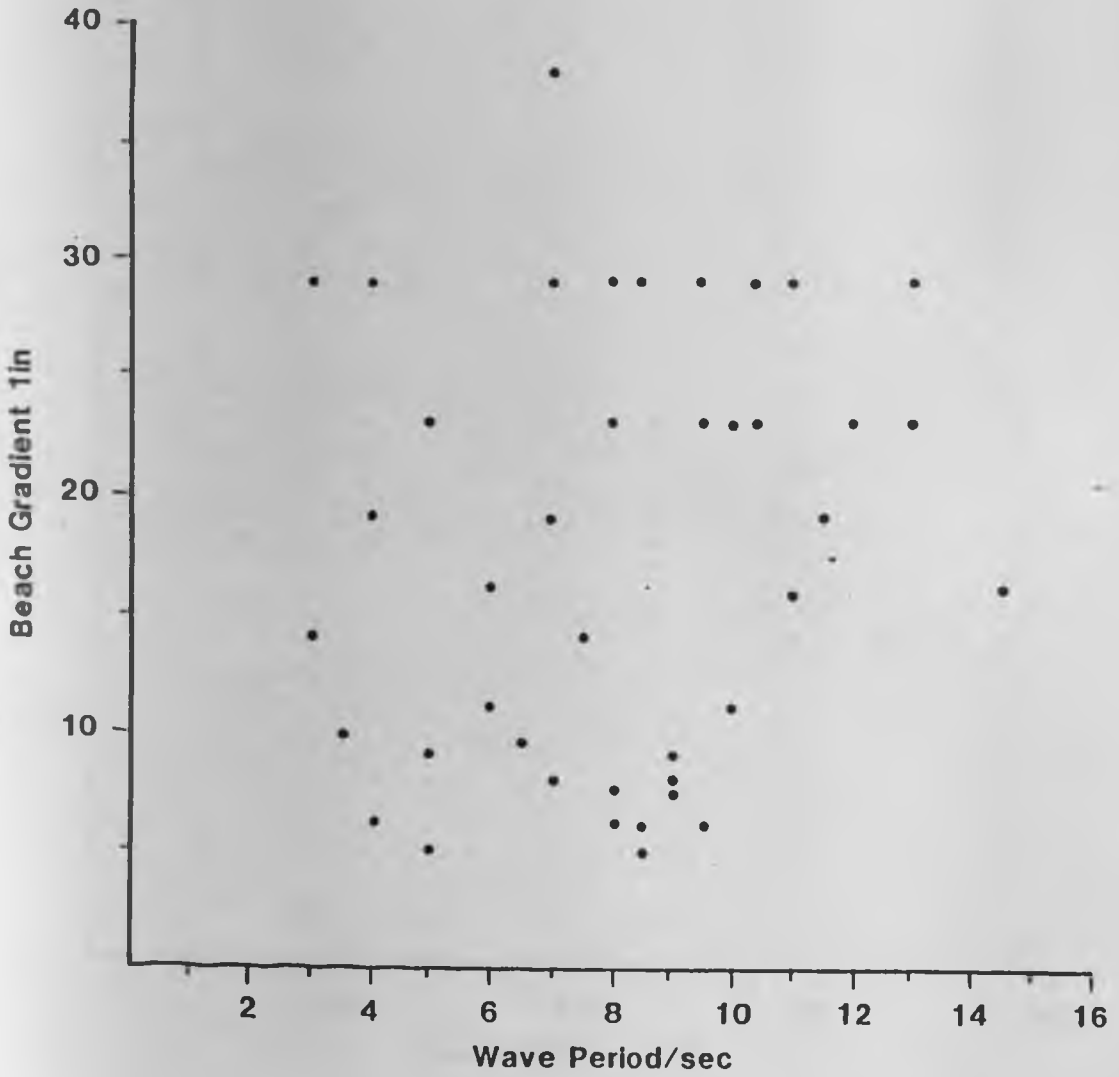


Fig.21. Correlation of beach gradient and wave period for observations made in Malindi-Fundisa area.

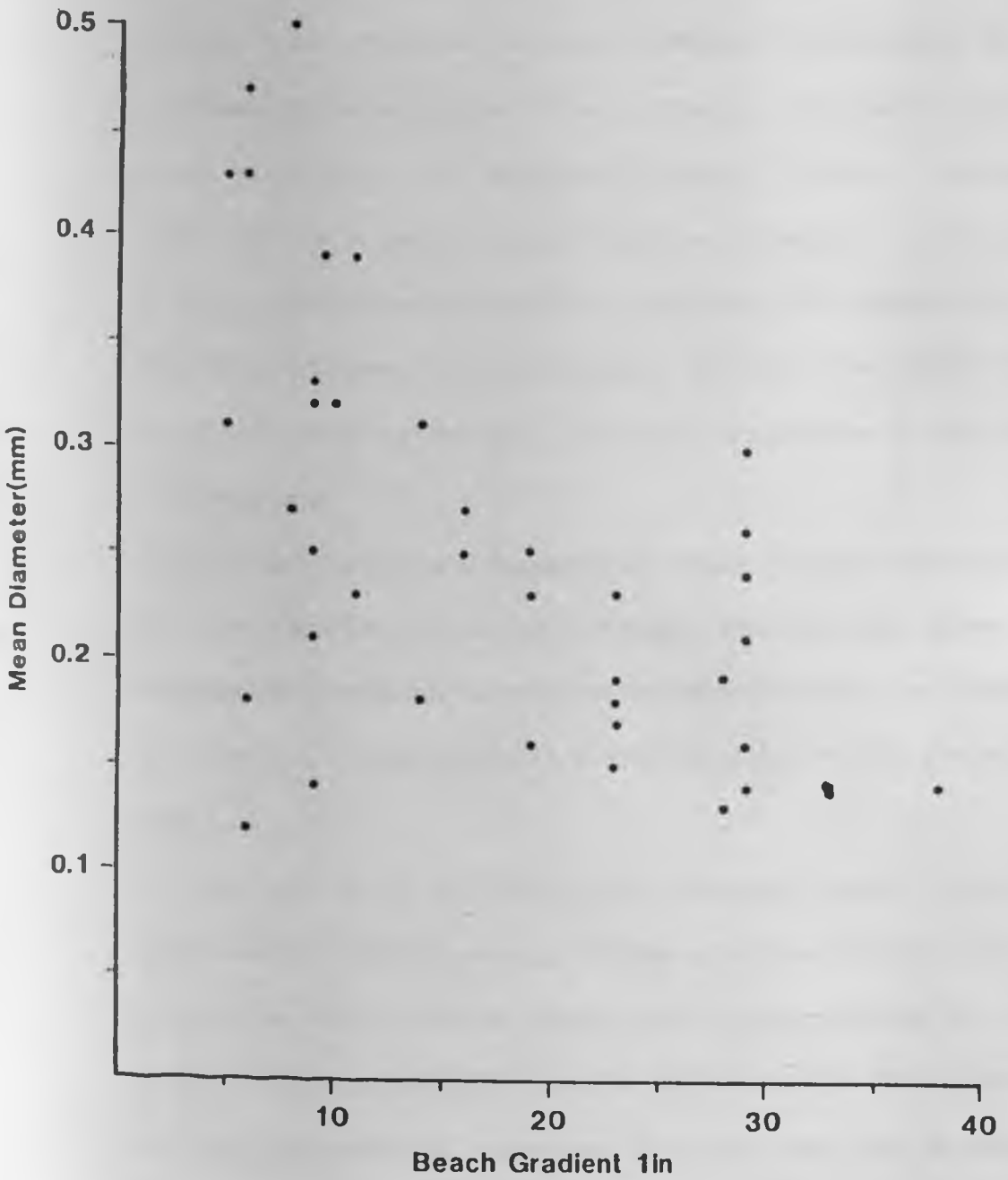


Fig.22. Correlation of the mean diameter of beach sand and beach gradient for beaches in Malindi-Fundisa area.

(Kings, 1967). The correlation is almost 1 in this case. When full-scale prototype values are plotted, as shown for Malindi-Fundisa data in figure 21, the scatter is much greater. In fact it appears so great that the validity of the correlation is not immediately apparent. However, statistical analysis shows that there is in fact a significant correlation. In this case study, the coefficient of correlation was found to be -0.52; this value for 46 pairs of observations gives a probability of less than 1 in 100 that this result could occur by chance, or the result is significant at the 99% confidence level.

The reason for the greater spread of the results in natural conditions is that other variables, such as wave steepness, which has been shown to influence the beach gradient, could not be controlled as they can in model experiments. Thus the correlation, although shown to be valid, was not so close.

Another point to be considered is the relationship between sediment parameters and beach morphology. Notable is the close correlation shown between the size of sand at mid-tide level on the foreshore and the gradient of the beach (Fig.22); clearly in this instance it is the size of the sand that determined the beach slope, the coarser sand being associated with the steeper slope because as the sand size increases so its permeability increases and the backwash loses volume relative to the swash and in order to compensate for this the gradient must be increased.

5.1.3 The Coastal Sand Dunes of Sabaki-Mambrui Area

In this area the active dune fields have a maximum width of 100m. Due to the seasonal climatic changes, especially those in wind direction, these dunes are complex in morphology and internal structure. They provide an interesting subject for continuous observation over an extended period of time. The active dune fields are backed by ancient dunes that were formed under different climatic conditions, particularly those associated with the final retreat of Pleistocene ice-sheets.

Dune sediments are piled up by onshore winds transporting sand in the 100-500 μ m size range, which has been supplied to the beaches by waves. In general sand accumulations in low dunes begins usually around some plants and other obstacles (Gripp, 1968). However, Cooper (1967) contended that development of sand dunes does not require any plants. Sand dunes can be thought of as migrating bedforms resulting from wind action, and they can be stabilized by vegetation, which traps the moving sand and tends to bind it. They will, of course, develop only where the wind system is favourable, and large reserves of sand in the coastal zone and the beach sediments fall into the appropriate size range. As with bed-load transport by currents, the rate of transport of wind-blown sand is proportional to the cube of the shear velocity.

The wind activity on beach sediments produces the following effects: Median size is increased, sorting is improved, skewness changes from negative or zero to positive values, relative enrichment of heavy minerals,

localized abundance of broken shells and tests of smaller organisms e.g. foraminifera, and improvement of roundness of mineral grains. All these changes are only relative, and they are not always well-marked.

A detailed study of grain characteristics in this coastal area has shown that sand grains of coastal dunes have a better roundness than sand grains from the beach (Table 7). This difference has generally been assumed to result from abrasion during wind transport. Given the short distance of transport involved in moving materials from a beach to the neighbouring dunes this interpretation seems unsatisfactory and instead it is suggested that the increased roundness of the sands is a result of selective transport. In order to test this hypothesis, an investigation was carried out to measure the roundness of sands in adjacent beach and dune deposits on the south coast of Mambui area. The coastline in the Sabaki and south Mambui which was selected for detailed study consists of a sandy beach ridge and shallow backslope region, inland of which are a series of almost parallel dunes.

The results (Fig.23) show a consistent difference between the beach and dune materials. Mean roundness tends to remain constant across the beach, but increase markedly at the junction with the dune sands. A slight decline in roundness occurred inland across the dunes. In all the areas studied a similar relative change in roundness was found, but no absolute difference could be distinguished between the beach and dune materials: Thus in some areas the beach sands were as rounded as dune sands in

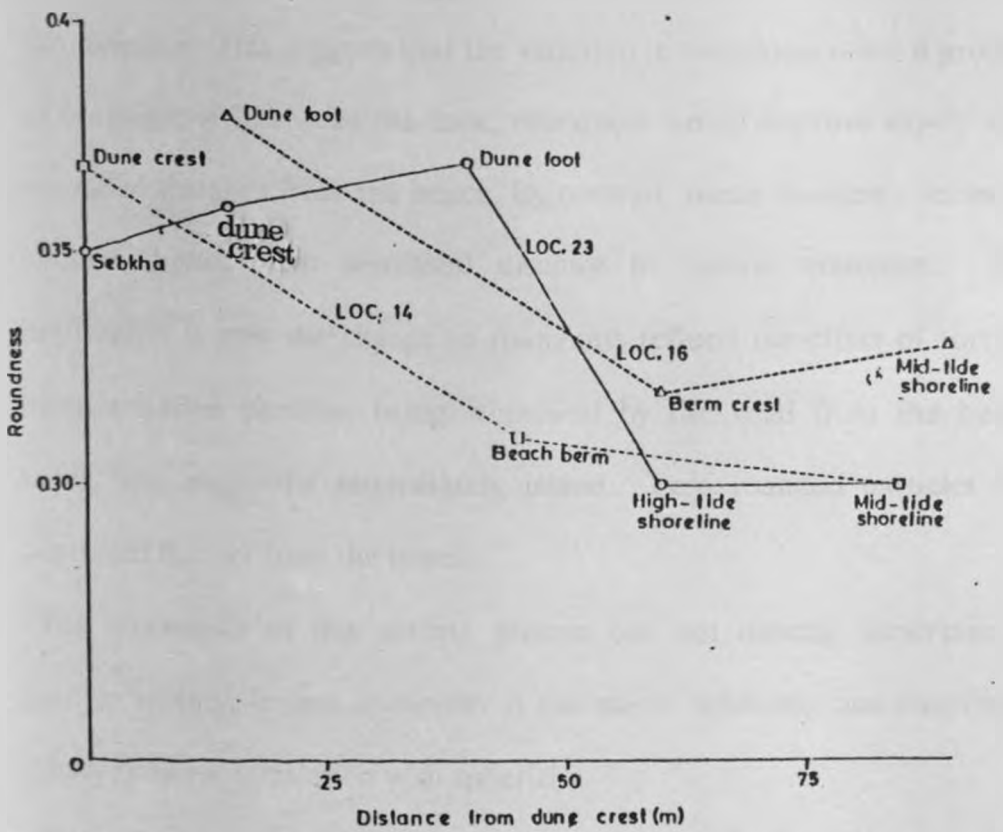


Fig.23. Changes in particle roundness in beach and dune environments.

other areas. Consequently it is not possible to identify a threshold roundness value characteristic of dune sands; instead it is the relative change in roundness away from the coast which locates the passage from beach to dune environment.

An important feature of the results is the very sharp junction between the two environments. Roundness increased within a distance of 1-2m at this junction. This suggests that the variation in roundness is not a product of abrasion; if this were the case, roundness would improve slowly with increased distance from the beach. By contrast, mean roundness seems to decline slightly with increased distance of aeolian transport. The implication is that the change in roundness reflects the effect of sorting, more rounded particles being winnowed by the wind from the beach sands, and deposited immediately inland. Less rounded particles are deposited further from the beach.

The mechanics of this sorting process are not directly important in particle sorting, instead sphericity is the major influence, and roundness simply shows a correlation with sphericity.

It is also unclear whether the wind selectively entrains only the more rounded or spherical material, or whether it entrains all shapes but deposits the more rounded materials first. This latter explanation seems more feasible, since spherical particles tend to be concentrated in the traction load and thus move shorter distances than the more angular material which dominates the suspension load.

5.1.4. Barrier Systems

In the Fundisa area these systems comprise barrier islands, spit developments and lagoon complexes.

The spit at Ngomeni bay mouth has developed as a linear ridge of sediment attached at one end to the southern tip of Simiti Island. The other end of the deposit points in the direction of longshore drift and terminates in the open water. The open water end of the spit is curved into the bay as a result of current action. An important feature noted here is that tidal currents are strong enough to keep the mouth of the bay open, thus preventing further extension of the spit which would otherwise develop into a bay barrier. The tombolo feature at Ngomeni probably resulted from the growth of a spit, as a sand ridge that connected the mainland to an island.

Barrier islands are found along most of the lowland coasts of the study area. Approximately 50% of the Malindi-Fundisa coast is bordered by some type of barrier. They are almost continuous from Ngomeni to Kanagoni.

The barrier islands are typically elongate and lie parallel to the shore, separated by a lagoon or tidal flat. They attain lengths of 4-7km and widths of several hundred metres. The seaward side of the barrier islands is a beach structure typical of the continental shore observed in the Malindi area. A dune development usually exists between the seaward

shore and the barrier flat that leads into the lagoon or tidal flat behind the island. The genesis of barrier systems is rather complex and still controversial despite over a hundred years of research. There are several explanations for their existence besides knowing that many such structures developed during the rise in sea level that was initiated with the last melting of the glaciers some 18000 years ago.

The early idea of de Beaumont (1845) was that barrier islands were formed simply by upward growth of a sand-bar or bank. However if this were so, then open marine beach sediments would be expected to occur on mainland beaches behind barrier islands. The emergence theory is contradicted by information obtained from virtually all of the drillings into barriers, which suggest that there has been submergence and that the barriers have grown upward with the late Holocene rise of sea-level (Shepard, 1978). Lagoons and tidal flats that develop behind spits and barrier islands are common and act as very efficient sediment traps.

A second theory, originally proposed by Gilbert (1885), suggests that barriers result from the breaching and isolation of former spits. A third theory maintains that barriers result from the partial drowning of normal coast-attached beaches during periods of transgression (Hoyt, 1967). Therefore, Hoyt (1967) believed that the barriers were originally beaches or dune ridges that were separated from the shore by regional submergence. This appears to be supported by most of the evidence.

In the present area of study, it was observed that there were no mainland beaches present immediately behind the barrier islands on the landward side of tidal flats or lagoons. Therefore these barrier islands cannot have originated as offshore bars after transgression. To begin with, the barrier islands were mainland beaches, and during the Flandrian transgression, they were separated from the mainland. In the last phase of marine transgression the areas behind the barrier islands were converted into a lagoon and tidal flats, while the barrier islands grew upward with the rising sea level. The question of whether this process is responsible for the genesis of all the barrier islands is still open. For example there are indications elsewhere in the world that certain barriers have formed according to the de Beaumont and Gilbert hypotheses (Shepard, 1978).

Having formed by these methods, the barriers were subjected to seaward and lagoonward growth. Many barriers in Fundisa have grown seaward, as shown by the numerous ridges on their seaward side. Comparison of old and new aerial photographs and satellite data also confirm some of the seaward growth.

The inheritance model proposed by Halsey (1979) is widely applicable in the study of barrier evolution. This model, although not tackling barrier origin, recognizes the role played by inherited coastal topography generated during the low sea-level stand before the Flandrian transgression. The regressive phase during the last glacial period left a palaeochannel network separated by higher interfluvial areas. As the

Flandrian transgression began, beaches formed against the interfluves and estuaries formed along the river channel outlets. Depending upon the height of the interfluves and the density of palaeochannels, a variety of barrier, spit and lagoon- tidal flat environments evolved as transgression continued.

It is evident that the genesis of the barriers is intimately connected with transgressions but it is less evident how barrier-lagoon-tidal flat systems maintain an equilibrium morphology.

The Simiti, Robinson and Giriyama village islands are situated in mesotidal areas and tidal inlets clearly play an important role, providing sediment to infill the back-barrier lagoons, tidal flats and channels and tidal currents to maintain an equilibrium. However, the situation in the northern islands of Kiswakini, Tamamba and Kanagoni is different, in that they seem to be situated along a microtidal coast. The dynamic equilibrium here is so limited such that their landward lagoons and tidal-flats have been infilled by storm washover sediments.

5.1.5. Tidal Flats

The extensive tidal flats and supratidal marshes on the west, leeward, side of Simiti Island, Robinson Island, Kiswakini Island, Tamamba Island and Kanagoni Island serve as the type examples of this environment. The tidal flat sediment body is elongate parallel to the shoreline over tens of kilometres and are intersected by a dense tidal channel network. The

channels are 1-200m wide and 0.1-4m deep. They meander but show little evidence of lateral migration. Comparison of aerial photographs taken in 1954, 1969 and 1977, and even more recent satellite data collected in 1987 support this observation. At Ngomeni bay there is a semi-circular tidal flat sediment-body cut by a single-tidal channel called Mto Rasini.

The tidal flats are protected by barrier islands or sand bars or occur in a sheltered bay for example at Ngomeni. Wave action is not too strong because of the sheltered nature of tidal flats but it is nevertheless an important factor.

The origin and dynamics of shoreward-fining tidal flats depend upon a steady supply of sediment, particularly of sand-, silt-, and mud-grade, and a low degree of wave action. Onshore-fining is controlled by two related processes, termed scour lag and settling lag which encourage silt- and mud-grade sediment to accumulate on the upper tidal flats and sand near the low-water line. Sediments in the intertidal zone lie between high and low water line over a vertical range of 2-3m which corresponds to the tidal range. Limited percolation of tidal waters because of sediment cohesion encourages surface runoff and hence meandering tidal channel networks are established. These channels then act as arteries and veins, funneling the rising tide onto the tidal flat and transferring the residue back during the ebb seaward transport of rain water that falls onto the tidal flat during ebb or low tide also occurs.

Salinities of the tidal waters fall in the range 34-35‰, but may fall as low as 10‰, after heavy rainfall (Schroeder, 1974). This periodic freshwater flushing creates a high stress environment and fauna found in the study area tidal flats although noted to be abundant, only a limited number of species is represented. Most parts of the tidal flat surface layers are highly bioperturbated by bottom living animals. The semi-diurnal tides have a mean maximum range of 3m, but the tidal range is much affected by periodic storm surges. Currents on the tidal flats range from 20-30cm/sec and form small-scale current ripple marks on sandy bottoms. The current velocity in channels is 0.5 upto 2.0m/sec., so that underwater small-current ripples, megacurrent ripples and dunes are formed in increasing order of current velocity.

The facies of tidal flats are dominated by the nearshore to-offshore coarsening trend and characteristic zonation of fauna and flora mainly according to height above low-water level. The supratidal salt-marsh zone with hydrophilous/halophytic plants passes gradationally outward at a very low slope into a mudflat with a rich infauna. The mangrove *Rhizophora mucronata* flourishes in deeper mud with *Bruquiera gymnorhiza* commonly interspersed behind it and *Cerriops tagal* usually in the central areas of the swamps. *Avicennia marina* and sporadic presence of *Lumnitzera racemosa* characterizes the sandy landward fringe of the tidal flats.

Seaward coarsening gives rise to a mixed sand - /mudflat with a variety of laminations including flasers. Again, bioperturbation by the abundant

infauna is intense. This transition zone comprise a high marsh with continuous algal mats of the genera *Avrainvillea*, *Caulerpa*, *Halimeda*, *Udotea*, *Padina* and *Glacilaria*. This area also consist of muddy pelleted sands that are loosely bound by a surface scum of algae which sometimes destroy the thin laminations.

Sandflats down toward the mean low water mark show a great variety of wave-and current-formed ripple bedforms with complex interference forms caused by infragravity runoff effects. Local dunes may result if tidal flows are strong enough. On the sandy areas in and around mangrove swamps a creeping succulent *Sesuvius portulacastrum* and *Salicornia herbacea* are frequently found. The mangrove species *Sonneratia alba* usually forms the outermost zone near the low-tide level. *Xylocarpus granatum* does not form a separate zone, but grows within the zone of *S.alba*. The intertidal flat ecosystem also comprise animals that are adapted to withstand the changing environmental conditions. The following invertebrates were recorded both on the ground and on the mangroves: Mollusca, *Littorina*, *Cerithium*, *Terebralia* and ostrea; Crustacea, *Uca*; Pisces, *Periothalmus* and barnacles.

The channels contain lag gravels of skeletal debris, intraclasts and a few fragments of pumice rock. The channel banks and stationary point bars are heavily bioturbated by the crab, *Uca* and overgrown by the mangrove *Avicennia marina* and covered by complex hemispherical stromatolite heads. Rapid deposition on the bars discourages infaunas and hence

deposits here are relatively free of bioturbation. The channel levees are only rarely covered by tidal waters and are coated by a thin algal mat which on dessication give rise to characteristic polygon heads as the algae attempt to heal over the upturned polygonal rims.

The most common feature on the tidal flats is current ripple marks, but symmetrical and asymmetrical oscillation ripples are also present. Subaerial marks are also important, small to minor runnels and erosional depressions are often sculptured by algal mats. Tracks of birds and other land animals, foam marks and dessication cracks occur on the surface. Groove casts and flattened ripples are also common.

There is ample field evidence that the zonation of the mangrove community, invertebrates and surface structures show some degree of correlation to the hydrodynamic regime, distance from low-tide level and stability of the substratum. The latter three are in turn controlled by the current and wave systems, morphological situation and grain-size distribution.

5.2 SUBTIDAL ENVIRONMENTS

5.2.1 Malindi-Fundisa shallow-water Carbonates

The total area of the Malindi-Fundisa shelf covered by reefs is not known, there are many reefs seaward of the patch reefs which do not reach the surface and are not marked on any map. The shallow-water

carbonates are mainly of biogenic origin, however their accumulation is largely constrained by the freshwater influx and the clastic sedimentation attributed to materials brought in through the Sabaki and Tana rivers.

5.2.1.1. Reefs

Most present-day carbonate sedimentation in shallow water (less than 5 fathoms) occurs on coral reefs. The living corals are colonies of polyps which secrete a calcareous sheath around themselves. A host of marine fauna exists on the coral reef, notably Porifera, Echinodermata, Mollusca, Annelida, Crustacea, Coelenterata.

Salinities within the range of 30-40‰ and the mean annual water temperature of approximately 23-25°C would otherwise favour luxuriant coral growth but high evaporation rates and influx of freshwater through the major rivers inhibit this. In addition, increased sediment transport into the reef area has smothered corals in part or wholly as exemplified north of Mambui.

Off Leopard Point, reefs are growing at present and exhibit a well developed coral fauna. These reef-building corals are favoured by the action of waves which aerate the water, circulate food, and winnow away fine sediment without being too destructive. Off Silversands Beach however, large waves have destroyed corals and thrown up banks of coral rubble on the reef. There appears to be greater development of the reef on the windward side than on the leeward side. This suggests that the reef

grows most rapidly where wave activity due to wind is greatest - effect of wave promoting the growth of corals.

Scleractinian corals, the genera *Acropora*, *Porites*, *Goniastrea*, *Favia*, *Montipora*, and *Galaxea* provide the main framework of reefs but they are not the only organism contributing to reef development. There are also coralline algae (carbonate-secreting benthic plants), mainly *Lithothamnion*, *Lithophyllum*, and *Porolithon*, which add encrustations of calcareous material to the reef and provide essential cement for the basic framework. Here, they are an important feature of the seaward edge of the reef. Biological activity by certain organisms have led to considerable changes in the Malindi reefs. These boring animals have attacked parts of the reef and destroyed the initial structure. Of note is the asteroid *Acanthaster planci* has, in part, devastated reefs by feeding on the soft portions of Scleractinian corals. The resulting voids have since been filled in by encrustations of carbonate-secreting organisms and by carbonate mud.

5.2.1.2 The reef-flats

On the Malindi-Fundisa coast the rocky shores are generally old reef platforms which are left exposed at low tide. Much of the platform probably is an erosional terrace, in the Pleistocene substrate. As yet, the observations made do not suffice to assess relative proportions of reef and

erosional terrace respectively. The reef-flats are generally bounded on the landward side by shelving and there may or may not be a narrow sandy upper beach. In any case the upper rocky platform is generally sandy. There is little sand on the lower rocky platform except in the pools.

On the reef-flats most of the original reef material has been broken down into loose sediment by the action of waves and through biological degradation, and this sediment is subject to the physical processes and controls that have been mentioned in connection with clastic sediments. Reef-flats are subject to vigorous wave action, and this, combined with the shallow water, generally less than 1m, means that only sand-sized and gravel-sized sediments are found here. Coral fragments generally make up only about 15-30% of the reef-flat sediments, which will be winnowed away by the waves.

The rocky platform provides a stable and permanent substratum for the attachment of marine plants and animals, and therefore usually rich in the variety of both flora and fauna. The biota, however, must be able to withstand the exposure and dessication when the tide is out. The biota on the outer rocky platform must also be able to withstand the mechanical force of the breaking waves. The varying extent to which different plants and animals are adapted for life on the rocky shore leads to their zonation (Leeder, 1985). The zonation is not very distinct in the study area. The many rock pools on the reef-flat create distinctive habitats and make it

difficult to recognize zones since each pool has its own microenvironment.

Most of the reef-flat sediment (upto 90%) consists of coralline algae. Green algae *Halimeda* is relatively less abundant. Red algae are present everywhere in unobstrusive form. Benthic foraminifera and molluscs are also important contributors to sediments on the reef-flats.

The perimeter of the outer reef-flat is often topped by a ridge of coralline algae, particularly brown algae, which grow upto about 1m above the low-tide level if it is moistened by constant vigorous surf. This is verified at Ras Ngomeni. This ridge provides partial shelter for the reef flat, so that sediment is not continuously removed by the action of waves. The barrier bar extending southward from Ras Ngomeni probably formed in this manner.

5.2.1.3. The reef front

Seaward of the reef-flats, both corals and coralline algae grow on the reef front, where loose sediment from the reef-flats also accumulate. The reef front is usually not a continuous slope, but generally includes at least one terrace formed during a time of low sea-level. It is also characterized by a spur-and-groove structure developed perpendicular to the reef. The spurs develop by biogenic growth, and the grooves act as channels for water and sediment. The origin of these features is problematic, but they are thought to be vital to the dissipation of the wave energy incident on

the reef, the grooves acting as channels for the offshore movement of water and sediment. The current in the grooves are therefore analogous to rip-currents in the beach environment.

5.2.1.4. Lagoon

Both the reef itself and the patch reefs (isolated bodies within the lagoon) supply sediment to the lagoon. The karst lagoon southward of Ras Ngomeni, with lagoonal pinnacle reefs derive sediments directly from the reef. However, at the Marine National Reserve both the patch reefs and fringing reef contribute to the lagoon sediments. The transport and sorting of these sediments depend on bottom currents, which are in turn controlled by the size and depth of the lagoon. Depth of lagoon at Ras Ngomeni ranges from 2-5m while at a wider reef of the Marine National Reserve the lagoon attain depths of 10 to 15m.

At the Marine National Reserve, the complex circulation resulting from the presence of a well- developed leeward reef, has made it possible for a wide range of grain sizes to be deposited among the lagoonal sediments. The absence of a leeward reef at Ras Ngomeni results in a rapid flow of water through the lagoon, and here, the sediments are better sorted and mainly rather coarse grained.

The distribution of sediments in lagoons govern the type of benthos present, infauna predominating in fine- grained sediments where currents

the reef, the grooves acting as channels for the offshore movement of water and sediment. The current in the grooves are therefore analogous to rip-currents in the beach environment.

5.2.14. Lagoon

Both the reef itself and the patch reefs (isolated bodies within the lagoon) supply sediment to the lagoon. The karst lagoon southward of Ras Ngomeni, with lagoonal pinnacle reefs derive sediments directly from the reef. However, at the Marine National Reserve both the patch reefs and fringing reef contribute to the lagoon sediments. The transport and sorting of these sediments depend on bottom currents, which are in turn controlled by the size and depth of the lagoon. Depth of lagoon at Ras Ngomeni ranges from 2-5m while at a wider reef of the Marine National Reserve the lagoon attain depths of 10 to 15m.

At the Marine National Reserve, the complex circulation resulting from the presence of a well- developed leeward reef, has made it possible for a wide range of grain sizes to be deposited among the lagoonal sediments. The absence of a leeward reef at Ras Ngomeni results in a rapid flow of water through the lagoon, and here, the sediments are better sorted and mainly rather coarse grained.

The distribution of sediments in lagoons govern the type of benthos present, infauna predominating in fine- grained sediments where currents

are slow, and epifauna on the coarse sediment where currents are fast. The benthos not only contributes skeletal carbonate to the sediment, but also reworks them, forming fecal pellets of carbonate. Non-skeletal carbonate make a small contribution to the sediment.

5.2.1.5. The role of plants in the formation of shallow- water carbonates.

Field observation showed that sea-grasses, along with algae and mangroves stabilize sediment. They do this by binding the sediment, or by reducing bottom currents so that there is no erosion of sediment. The sea-grass *Thalassia*, which often almost covers the bottom, acts as a baffle to currents, stabilizing the sediments with its roots, which grow upto a thickness of 75cm. The attachment holdfasts of *Halimeda* and *Penicillus* similarly bind sediment down to a depth of about 10cm.

5.2.2. The shelf Environment of Malindi-Fundisa area.

The shelf width varies between 3-25 km; depth of the shelf edge is about 30-40m. The shelf profiles off Malindi and Sabaki areas (Fig.24) show two benches on the sea-floor at -35m and -44m respectively marked A and B. The platforms represent bevels cut during Middle Pleistocene and upper Pleistocene times respectively. Of note are the offshore bars that developed on the edge of the continental shelf. The relief of the shelf is determined by Recent reefs (section 5.2.1) and grassbeds evident in the Malindi area, and by ridges paralleling the coast and thought to be

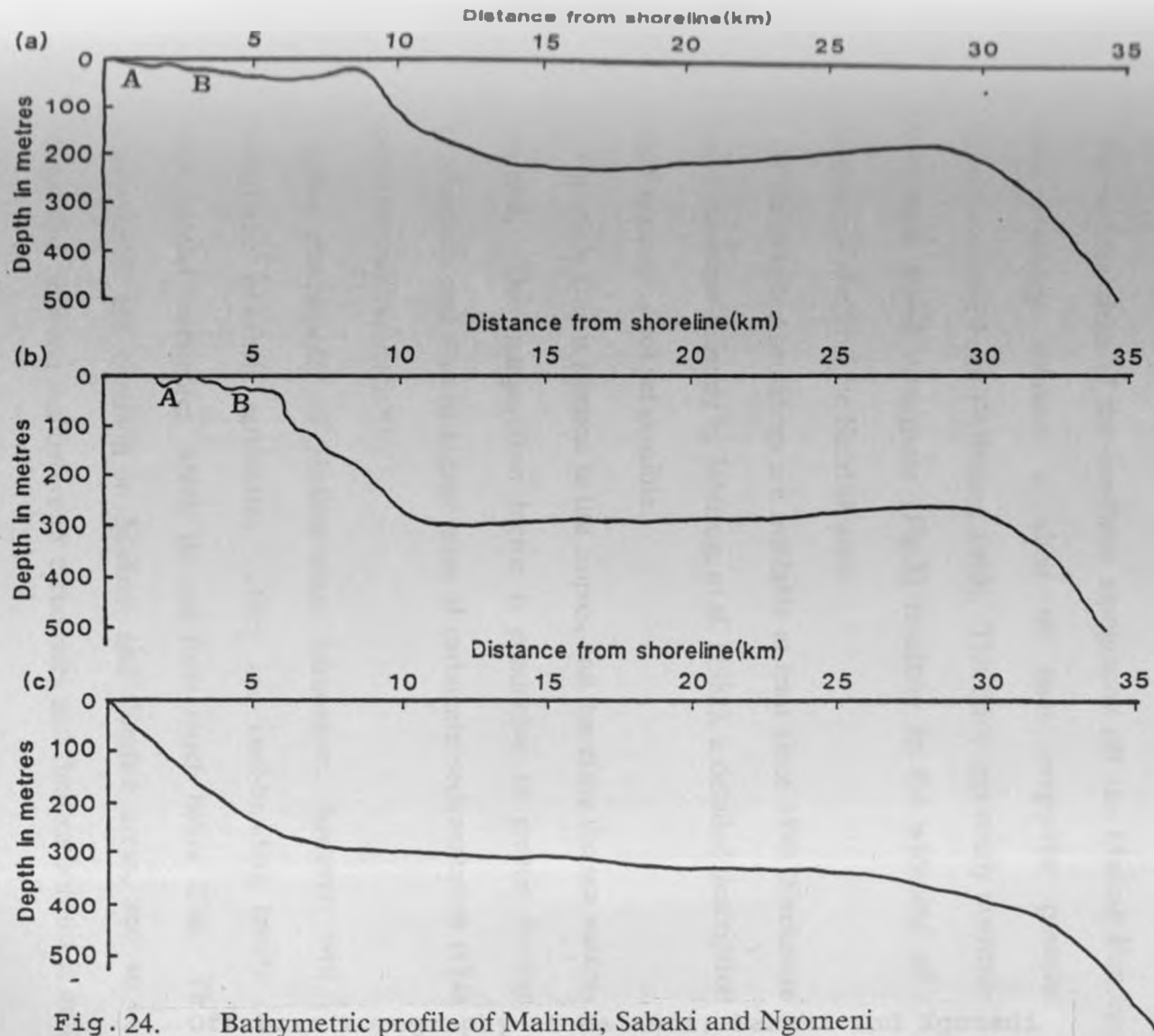


Fig. 24. Bathymetric profile of Malindi, Sabaki and Ngomeni

continental shelf areas.

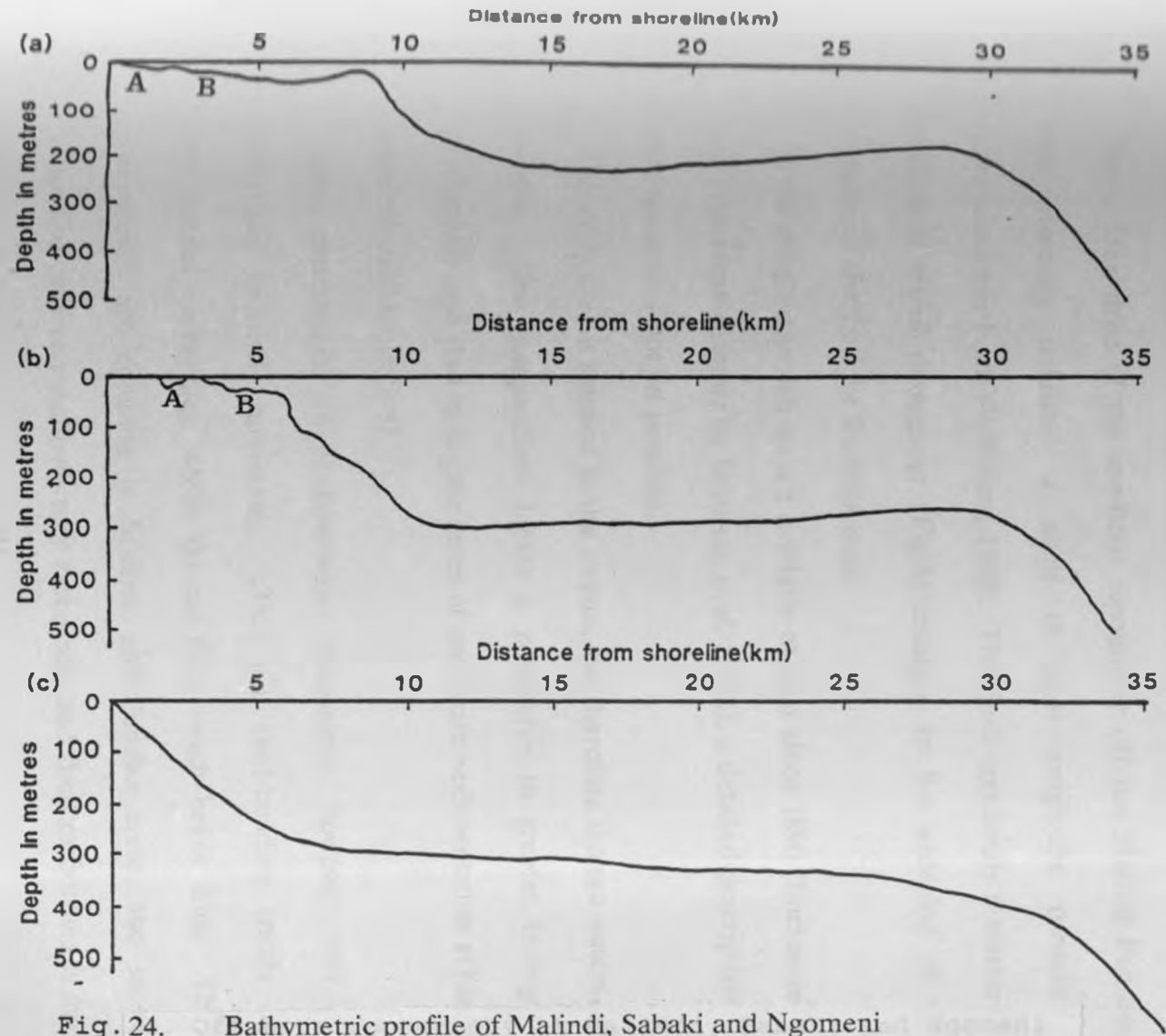


Fig. 24. Bathymetric profile of Malindi, Sabaki and Ngomeni

continental shelf areas.

Pleistocene eolinites or coquinas represented in the Fundisa area. Ocean currents are also partly responsible for the bottom topography.

The sudden drop of the sea-floor topography off the Malindi-Fundisa area probably indicates a shelf of fault origin—the postulated Ruvu-Mombasa Fault (Williams, 1963). This fault apparently maintains a NNE-SSW trend throughout (Fig.3) resulting in the widening of the continental shelf off the Fundisa area.

While detailed soundings are available at least since 1890 (Enclosure 3) and even more recently by Johnson, et al. (1982), a detailed description of shelf features is not yet possible.

The study area is situated in the tropics, and therefore the sea waters are warmer. This temperature factor is conducive to greater biological productivity and thus to higher rates of carbonate sedimentation (Odada, personal communication).

Some components of shallow-water carbonates, however, will not contribute to shelf carbonates. They are reef-building corals and non-skeletal carbonates, which do not form much below 25m. These components are common in Malindi and Fundisa areas, and so the distinction between shallow-water carbonates and shelf carbonates is most easily made here.

Biogenic carbonates, derived from shells of molluscs, echinoids, barnacles, brachiopods, ahermatypic (non reef building) corals, Bryozoa, and planktonic and benthic Foraminifera dominate. Local conditions

determine which of these are present. Generally only 4- 6 types of organism contribute 90% or more of the carbonate at any one locality. However, inorganically precipitated CaCO_3 is also important locally (International Indian Ocean Expedition, 1975).

Most shelf carbonate deposits are sand-sized, but some deposits consist of gravel-sized material particularly where molluscan shells have accumulated. Finer grained sediment is contributed by the abrasion and biodegradation of shells and by micro-organisms such as coccolithophores, but is often winnowed away by the waves and current that prevent clastic sedimentation and enable carbonates to accumulate.

Besides bioclastic and authigenic carbonate sedimentation, the Sabaki and Tana rivers also supply terrigenous material to the continental shelf. Thus the Malindi-Fundisa shelf with its well defined two major sources could provide a model of sediment mixing on a narrow continental shelf.. Extending between the outer reefs are grassbeds whose importance in the process of sedimentation can be envisaged as that of exerting drag on bottom currents.

A vorticity model presented by Johnson, et al. (1982) suggests that the rapid switching action of the Somali Current and the East African Coastal Current is topographically controlled. The regions where the switching action occurs are the Malindi Banks and the North Kenya Banks.

5.3. Heavy Mineral Beach Sand Deposits

The Sabaki River transports weathered country rocks in the form of clastic material from the highlands to the coast where sedimentation occurs. Here the heavy mineral ores are found as stringer deposits. The surf and currents of the ocean serve as natural beneficiation of these mineral, separating and concentrating the light from the heavy on the basis of their different relative densities. The main concentration of heavy minerals takes place in wide beach areas which dry out at low tide. Winds blowing inland tend to effect a further concentration of these minerals in the coastal sand dunes.

Concentrations of heavy mineral placers which contain economically valuable minerals have been found at several sites along the East African Coast (Fay, personal communication). These placer deposits are located north of Malindi, in the estuary of the Sabaki river, in the neighbourhood of the Ras Ngomeni Peninsula and the beaches of Fundisa barrier islands (Fig.25).

Beinge (1957), Schroeder (1974) and Halse (1980) have already reported on these placers in past years. They have reported the presence of ilmenite, magnetite, rutile, zircon, monazite, apatite and kyanite, and have brought attention to the high Ti-Fe contents of sands in the present area. The detrital heavy minerals of Malindi and Fundisa are composed principally of titaniferous iron sands with subordinate zircon and rutile. Garnet is an easily obtainable by-product, whereas only a negligible

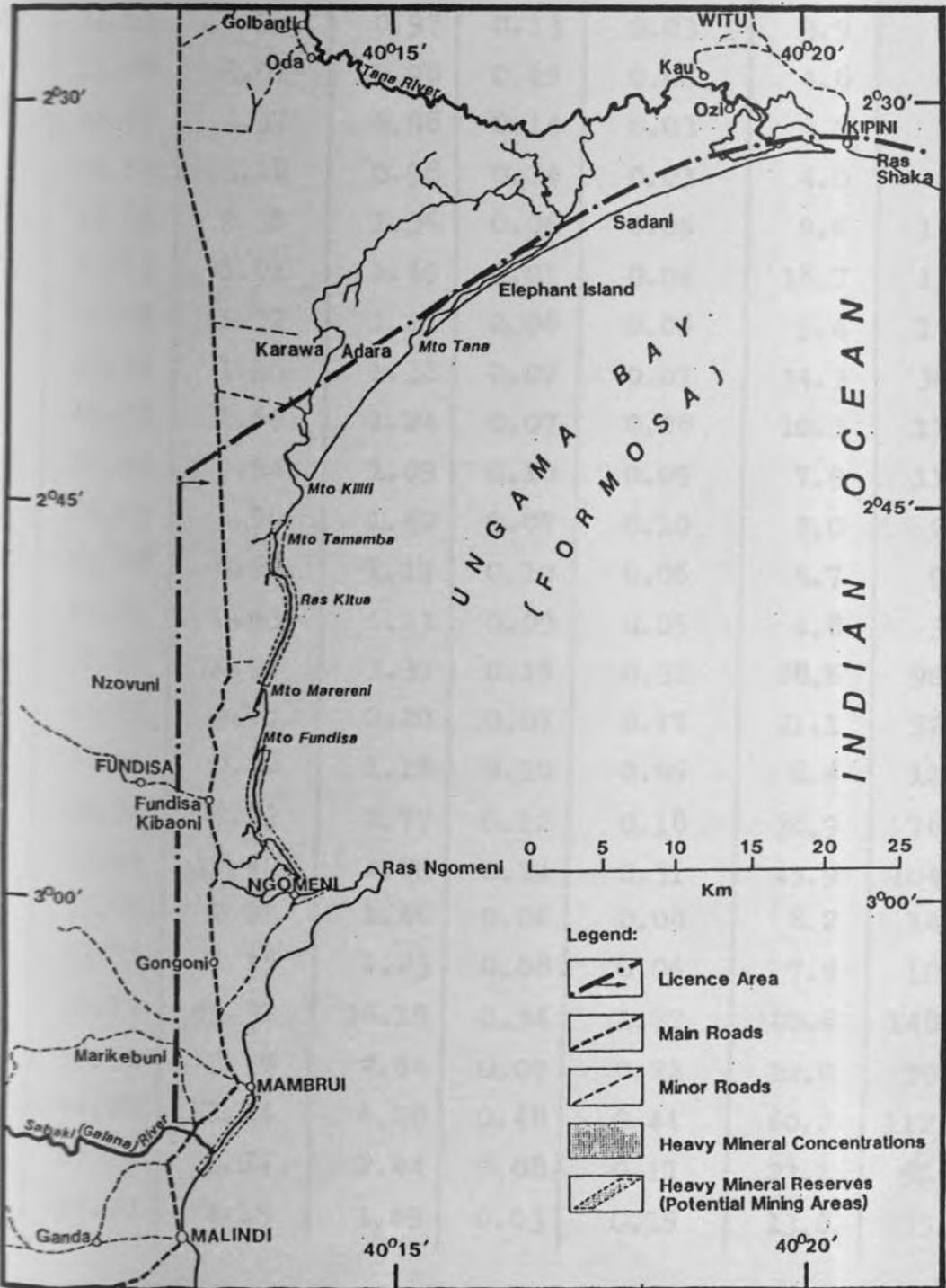


Fig.25. Location of heavy mineral deposits north of Malindi

Table 11 : Chemical composition of Coastal Sediments
from Malindi-Fundisa area.

	SiO ₂ %	Fe ₂ O ₃ %	TiO ₂ %	MnO %	ZrSiO ₄ %	Cr ppm	V ppm
12/2	41.56	6.49	0.97	0.05	0.05	29.0	42.3
12/3-1	13.71	3.88	0.98	0.14	0.03	5.1	0.1
12/3-2	11.54	2.99	0.97	0.13	0.03	3.9	0.1
12/4-1	11.78	3.01	0.98	0.15	0.04	4.8	0.9
12/4-2	12.67	3.37	0.98	0.14	0.03	3.6	1.0
12/5	14.53	3.18	0.98	0.14	0.03	4.0	0.5
12/10	53.36	2.35	1.36	0.06	0.06	9.6	13.9
12/11	43.63	5.01	1.49	0.01	0.04	18.7	18.7
12/12	55.22	1.72	1.21	0.08	0.06	9.4	15.1
12/13	60.34	1.15	1.38	0.07	0.07	14.3	30.9
12/14-1	65.72	1.69	1.24	0.07	0.08	10.3	11.1
12/14-2	56.50	0.94	1.09	0.10	0.05	7.9	11.1
12/14-3	66.64	1.96	1.40	0.07	0.10	5.0	2.1
12/15-1	63.88	0.67	1.17	0.10	0.06	5.7	9.1
12/15-2	67.85	0.63	1.11	0.09	0.05	4.8	3.5
12/16-1	52.52	10.94	3.37	0.15	0.32	28.6	90.4
12/16-2	63.63	6.75	2.20	0.07	0.17	21.1	52.9
12/16-3	58.51	0.72	1.18	0.10	0.06	6.4	10.9
12/17-1	60.84	9.72	2.77	0.12	0.18	38.9	78.9
12/17-2	47.97	17.42	4.80	0.24	0.31	45.9	104.0
12/18-1	55.27	2.58	1.46	0.06	0.08	8.2	14.2
12/18-2	63.31	1.45	1.23	0.08	0.06	7.5	10.8
12/18-3	19.17	45.31	16.15	0.54	1.72	100.6	148.1
12/18-4	58.30	7.75	2.54	0.07	0.22	22.0	59.7
12/19-1	44.80	22.24	6.28	0.48	0.44	60.2	112.0
12/19-2	61.29	7.54	2.44	0.08	0.17	23.1	56.2
12/19-3	52.70	4.13	1.69	0.03	0.15	13.6	35.2

	SiO ₂ %	Fe ₂ O ₃ %	TiO ₂ %	MnO %	ZrSiO ₄ %	Cr ppm	V ppm
20	59.22	2.40	1.37	0.07	0.08	16.4	21.2
21-1	52.80	14.18	4.11	0.22	0.33	29.3	77.1
21-2	53.87	3.59	1.63	0.03	0.09	10.3	23.7
22-1	56.07	7.49	3.05	0.18	0.22	31.5	82.0
22-2	59.21	3.06	1.51	0.04	0.08	10.4	18.2
23-1	62.19	3.40	1.47	0.02	0.07	13.2	20.4
23-2	64.57	1.94	1.32	0.05	0.08	7.5	6.0
23-3	60.79	8.25	2.70	0.08	0.28	34.8	55.2
23-4	59.93	9.32	3.37	0.10	0.21	20.5	26.7
24	52.72	2.69	1.48	0.05	0.08	8.7	12.2
25-1	54.66	2.54	1.43	0.06	0.10	14.3	24.6
25-2	66.50	0.79	1.14	0.10	0.06	7.1	6.3
26	63.89	0.49	1.13	0.11	0.05	5.4	5.1
27	61.51	2.58	2.51	0.05	0.08	9.7	22.3
28-1	54.48	3.04	1.52	0.04	0.08	11.2	19.1
28-2	58.00	1.06	1.09	0.10	0.04	7.4	5.1
29	48.19	1.45	1.21	0.09	0.05	8.1	8.6
30-1	49.95	2.10	1.25	0.08	0.04	10.5	10.4
30-2	50.75	2.40	1.20	0.04	0.05	10.5	14.8
31-1	60.81	1.15	1.11	0.11	0.05	8.6	11.5
31-2	45.88	1.31	1.12	0.10	0.04	6.1	6.8
32	49.71	2.43	1.15	0.08	0.04	13.4	17.8
33	13.71	7.93	1.77	0.04	0.04	37.2	44.0
34	27.94	5.12	0.34	0.01	0.04	29.9	30.3
35-1	49.82	2.95	1.25	0.07	0.05	13.6	17.4
35-2	41.19	1.91	1.05	0.10	0.04	7.9	8.3
36	31.14	2.52	1.03	0.11	0.04	7.5	7.0
37	33.70	2.44	1.07	0.10	0.04	6.4	5.0
38-1	73.69	0.55	1.06	0.13	0.05	7.1	9.5
38-2	80.48	0.89	1.34	0.09	0.06	3.5	3.6
39-1	61.90	9.78	3.59	0.34	0.12	34.2	25.5

Code	SiO ₂ %	Fe ₂ O ₃ %	TiO ₂ %	MnO %	ZrSiO ₄ %	Cr ppm	V ppm
Joz/40-2	20.51	38.11	23.94	1.30	1.04	97.8	32.4
Joz/41-1	18.44	41.72	27.46	0.85	1.17	94.4	11.8
Joz/41-2	56.30	11.90	6.57	0.19	0.38	6.5	11.3
Joz/41-3	73.21	0.77	1.11	0.13	0.06	3.0	3.0
Joz/42	72.14	1.05	1.24	0.07	0.05	9.6	6.7
Joz/43-1	55.37	1.12	1.28	0.10	0.06	7.0	7.9
Joz/43-2	52.86	1.53	1.39	0.12	0.07	7.0	9.6
Joz/44	60.33	12.18	54.01	0.28	0.37	49.6	98.2
Joz/46-1	68.77	10.27	5.01	0.25	0.19	26.9	92.6
Joz/46-2	63.96	6.04	1.71	0.17	0.06	19.6	48.4
Joz/47	44.70	13.18	6.58	0.19	0.20	35.1	41.7
Joz/48	66.17	5.32	2.57	0.04	0.16	25.1	32.2
Joz/49	54.71	1.13	1.50	0.08	0.08	9.2	22.7
Joz/50	74.53	1.42	1.54	0.08	0.10	12.5	24.4
Joz/51	45.63	1.42	1.32	0.08	0.06	7.7	15.4
Joz/52	62.88	11.36	5.54	0.16	0.38	35.6	15.3
Joz/53	67.17	2.12	1.63	0.07	0.11	9.6	21.7
Joz/54-1	59.60	1.61	1.41	0.08	0.07	9.7	19.1
Joz/54-2	57.34	7.04	3.42	0.10	0.18	22.6	41.3
Joz/55-1	42.29	1.22	1.07	0.11	0.04	6.8	6.1
Joz/55-2	42.68	0.95	1.05	0.12	0.04	6.8	6.1
Joz/55-3	58.09	0.79	1.05	0.12	0.04	6.2	7.5
Joz/56-1	19.99	3.35	1.22	0.07	0.06	8.4	19.4
Joz/56-2	63.17	0.41	1.06	0.11	0.05	7.0	10.4
Joz/56-3	45.24	2.08	1.49	0.08	0.08	7.5	20.8
Joz/57	38.40	2.56	1.52	0.07	0.12	16.0	16.4
Joz/58	60.25	7.95	2.92	0.15	0.15	25.7	38.0
Joz/59	47.51	26.44	14.03	0.43	1.41	60.8	2.9
Joz/60-1	69.61	0.04	1.09	0.11	0.05	6.4	6.3
Joz/60-2	70.04	0.03	1.08	0.12	0.05	6.5	8.1
Joz/62-1	42.28	20.87	8.42	1.01	0.45	48.8	116.5

Code	SiO ₂ %	Fe ₂ O ₃ %	TiO ₂ %	²¹³ MnO %	ZrSiO ₄ %	Cr ppm	V ppm
Joz/61-2	78.08	0.44	1.30	0.09	0.07	5.5	14.1
Joz/61-3	72.64	0.25	1.33	0.10	0.08	5.8	9.8
Joz/62-1	49.83	17.58	9.66	0.46	0.63	47.8	131.1
Joz/62-2	16.24	43.93	31.31	0.89	1.20	99.5	4.8
Joz/62-3	60.08	9.39	4.78	0.24	0.25	26.6	65.1
Joz/63	75.85	0.06	1.15	0.11	0.06	5.4	10.2
Joz/64-1	66.26	5.41	2.56	0.06	0.12	20.9	49.2
Joz/64-2	75.31	0.01	1.07	0.12	0.05	6.2	8.3
Joz/65-1	72.94	0.27	1.12	0.12	0.05	3.7	7.5
Joz/65-2	63.07	0.20	1.09	0.12	0.05	3.8	6.0
Joz/66-1	60.07	0.44	1.22	0.11	0.06	5.7	10.5
Joz/66-2	61.54	0.03	1.06	0.12	0.05	4.3	10.9
Joz/67	71.39	0.96	1.37	0.09	0.07	7.4	14.1
Joz/68	41.24	4.27	1.52	0.06	0.07	18.1	26.9
Joz/69	69.52	0.67	1.37	0.07	0.06	6.2	10.9
Joz/70-1	57.16	2.07	1.15	0.11	0.05	10.3	21.2
Joz/70-2	58.23	1.96	1.08	0.10	0.05	5.4	10.2
Joz/71-1	23.95	32.95	23.09	0.94	1.00	64.5	60.1
Joz/71-2	70.96	1.15	1.51	0.08	0.09	4.9	7.1
Joz/72	65.70	0.11	1.08	0.12	0.05	5.0	7.4
Joz/73	72.57	0.46	0.98	0.13	0.04	13.0	21.6
Joz/74-1	47.11	10.81	5.25	0.21	0.35	28.3	52.5
Joz/74-2	58.02	1.04	1.46	0.09	0.10	8.0	13.0
Joz/75	57.47	0.30	1.16	0.11	0.06	5.1	7.6

amount of heavy minerals of economic interest (hornblende, tourmaline and augite) could be ascertained in raw sands. The deposits are generally described as non-economical by the previous investigators. For this reason, no attempts to obtain marketable mineral concentrates have been undertaken until now. However, due to the fact that technologies and market capacities do change, which in turn affects the classification of reserves, the value of a mineral deposit will change as well. Thus a re-assessment of known deposit must be made from time to time. In the opinion of the author, these detrital heavy minerals may be present in the beaches and dunes of Malindi and Ungama Bay areas in greater quantities than previously estimated.

The grain-size distribution of the examined sediments show that the mean size range from 150-170 μm . These dimensions are considered to be characteristic of marine heavy mineral placers. The heavy mineral contents of a specific density greater than 2.8 vary greatly within the sands examined. Known reserves (Fig. 25) in these beaches amount to about 3 million tonnes of heavy minerals, the main constituent being titaniferous haematite, ilmenite, and magnetite containing between 1.2 and 54.0 % of TiO_2 and from 6.75 to 43.9 % Fe_2O_3 . The average grade of the sands is of the order of 14.5 % but the heavy mineral content ranges between 5 and 40 % with local enrichments on the berm zones reaching as high as 40-90 %.

Ilmenite and haematite were established as the most abundant valuable minerals in the samples from the Malindi-Fundisa placers. About 80 % of the ilmenite grains are more or less highly interstratified with haematite. Results (table 6) show that haematite is often in excess of ilmenite by weight. In as much as there is no market for haematite-rich ilmenite concentrates at present, an economic evaluation of these raw sands is very difficult. Altered ilmenite consisting of amorphous Ti-Fe oxides and leucoxenised ilmenite are present.

A promising zirconium deposit occurs between the mouth of the Sabaki River and Mambui township in a beach-dune complex. The raw sand contains between 0.2 and 0.4 % zircon, but rutile and monazite can also be exploited. Sands from Ungama Bay show a distinctly higher content of heavy minerals, although the deposits are smaller, than those from Sabaki, Mambui and Ngomeni. Relatively high contents of garnet which on average comprise 5 % of the raw sands, were determined. Furthermore, the raw sand fractions of 125 μ m have rutile and ilmenite which increases the value of raw sands.

Petrographic studies show that the heavy mineral concentrates in this region appear to have an average content of about 6.6 % haematite, 4.5 % ilmenite 2.1 % magnetite, rutile, zircon and monazite amounting only to about 0.9 % , 0.7 % , and 0.6 % respectively of the raw sands. Under existing conditions, an average grade of at least 5%, but probably higher, would be needed for economic operation.

The processing of sands from the study area is encumbered with particular difficulties due to crystal intergrowth of ilmenite and haematite, hence the ilmenite cannot be enriched in a monomineralic concentrate. However, through the successive application of density, electrostatic and magnetic separation, it is possible to obtain both $ZrSiO_4$ concentrate and a titanium ore concentrate of 42 % TiO_2 (Gock and Jacob, 1978). This concentrate then is suitable raw material for production of titanium-slugs, from which in turn TiO_2 pigment can be derived by means of the wet-chemical sulphate process. At the Technical University of Berlin a wet chemical processing of polymineral concentrates has been developed involving vibration milling, which allows the production of TiO_2 - pigment (by sulphate extraction) from such a titanium ore concentrate (Gock, 1977).

The results of petrographical and geochemical investigations of the heavy mineral sands from the Sabaki delta to Kanagoni (Fig.25) give cause to reconsider the previous studies of these deposits. While the potential of these deposits is clearly indicated by this and while methods of processing are suggested, further studies are required to establish the economic feasibility of exploiting these deposits. The present infrastructure of roads, shipping facilities, bulk loading and bagging, electrical supply, water supply, local product demand, and local fabrication facilities and personnel is suitable for beach mining.

These findings and estimations justify an extensive exploration programme to locate old berm deposits below considerable depths of low grade windblown sand. It will be necessary to use mechanical excavation or more sophisticated deep drilling techniques in the course of a mining development programme. The high mineral concentrations often evident in the swamp areas immediately behind the active beach are economically viable despite high silt content. In conjunction with the exploitation of adjacent berm deposits, consideration could be given to the recovery of this material by wet concentration and washing. Exploitation in this environment could best be achieved by light mobile mining equipment or manual excavation.

Grain-size distribution analysis and mineralogy of beach samples from Ungwana Bay indicate offshore source for the heavy minerals. It would therefore be necessary to extend the exploration programme seaward to locate fossil placer deposits in the offshore bars.

REFERENCES

Anderson, D.L.T. (1976): The low level jets as a western boundary current. *Monthly Weather Review*, 104, pp. 907-921.

Andrew, N.R. (1981): Sedimentology and Lithification of Quaternary reef-rock on the coast near Mombasa, Kenya. Ph.D Thesis. University of Leeds.

Ase, L.E. (1978): Preliminary report on studies of shore displacement of the southern coast of Kenya. *Geogr. Ann. Ser.*, A60(3-4) pp. 209-221.

Ase, L. E. (1981): Studies of shores and shore displacement on the southern coast of Kenya-especially in Kilifi District. *Geogr. Ann. Ser.* A63 (3-4), pp. 303-310.

Beinge, F.W. (1957): Report on Kenya Coastal Sand-Sabaki River Area, Unpublished Study, Mines and Geological Department, Nairobi. 11p.

Bloom, A. L. (1965): The explanatory description of coasts (with German and French abs.), *Zeitschr. Geomorphologie*, V.9, no.4, pp.422-436.

Bright, R. and Anderson, J.B. (1982): The importance of sediment gravity flow to sediment transport and sorting in glacial marine environment. E. Weddel Sea, Antarctica. Geol. Soc. America Bull., Vol.92, pp.951-963.

Caswell, P.V. (1953): The geology of the Mombasa-Kwale Area. Geol. Surv. Kenya, Report No.24, 69p.

Cooper, W.S. (1967): Coastal dunes of California. Geol. Soc. American. Mem. 104, pp.1-131.

Cousminer, H.L. and Puffer, J.H. (1982): Factors Controlling the accumulation of titanium-iron oxide-rich sand in the Cohansey Formation, Lakehurst area, New Jersey. Econ. Geol Vol.77, pp.379-391.

Davis, R.A. (Jr). (1978): Beach Sedimentology of Mustang and Padre Islands: A time series approach. Journ. Geol. Vol.86, pp.35-46.

De Beaumont, E. (1845): Leçons de géologie pratique. Paris, pp. 22-252.

Fairbridge, R.W. (1961): Eustatic changes in sea level. In Physics and Chemistry of the Earth. Vol.4, Pergamon, New York, pp.99-185.

Findlater, J. (1977): Mean monthly airflow at low levels over the western Indian Ocean. Geophysical Memoirs, London, 16, pp. 1-53.

Folk, R.L. and Ward, W. (1957): Brazos River bar: A study in the significance of grain size parameters. J. Sediment. Petrol. 27, pp. 3-26.

Gilbert, G.K. (1885): The topographic features of lake shores. U.S. Geol. Survey 5th Ann. Report., pp. 75- 123.

Gock, E. and Jacob, K.-H. (1978): Method of Processing used to Obtain Synthetic Titanium dioxide through the Direct Dissolution of Rutile using Sulphuric Acid -German Patent Application. Deutsche Patentanmeldung, pp. 2855- 4678, 19-12.

Gock, E. (1977): Influencing the Dissolution Behavior of Sulphide Raw Materials through solid State Reactions Caused by Comminution with a Vibrating Ball Mill. Habilitationsschrift, Technische Universität Berlin, Fachbereich Bergbau und Geowissenschaften, Hardenbergstraße 42, D-1000 Berlin 12.

Gripp, K. (1968): The encyclopedia of oceanography. New York (Reinhold). pp. 1021.

Halse, J.E.P. (1980): Formosa Bay Heavy Mineral Beach Sand Deposits. Initial Exploration Report. Ministry of Environment and Natural Resources. 12p.

Halsey, S.D. (1979): Nexus: new model of barrier island development. In Leatherman (1979), pp.185-210.

Hori, N. (1970): Raised coral reef along the southern coast of Kenya, East Africa. Geogr. Repts. Tokyo Metropol. Univ., 5, pp. 25-47.

Hoyt, J.H. (1967): Barrier Island formation. Geol.Soc. Amer Bull., V.78, pp.1125-1136.

Inman, D.L. and Bagnold, R.A. (1963): Littoral processes. In The Sea, M.N. Hill (ed) 3, pp. 529-583. New York: Wiley.

Inman, D.L. and Norstrom, C.E. (1971): On the tectonic and morphologic classification of coasts. Journ. Geol., V.79, No.1, pp.1-21.

International Indian Ocean Expedition (1975): Geological-Geophysical Atlas of the Indian Ocean. Moscow; Academy of Sciences of the USSR Main Administration of Geodesy and Cartography Under the Council of the Ministers of the USSR (IOC/UNESCO Project). pp. 118 - 144.

Johnson, D.R., Nguli M.M. and Kimani, E.J. (1982): Response to annually reversing monsoon winds at the southern boundary of the Somali Current. *Deep-sea Research*, Vol.29, No.10A, Pergamon press Ltd. pp.1217- 1227.

Johnson, D.W. (1919): *Shore Processes and Shoreline Development*. John Wiley and Sons, New York, 584pp.

Kenya Meteorological Department (1984): *Climatological Statistics for Kenya*. Dagoretti Corner, Ngong Road, Nairobi.

Kenya Ports Authority (1987): *Tide Tables for Kenya Ports and Tanzania Harbours*. The Rodwell Press Ltd., Mombasa. 50pp.

Kings, C.A.M. (1967): *Techniques in geomorphology*. Robert Cunningham and Sons Ltd., Alva. 342pp.

Krumbein, W.C. (1961): The analysis of observational data from natural beaches. Beach Erosion Board, Tech. Memo. 130, Corps of Engineers, Washington, D.C.

Krumbein, W.C. and Pettijohn, F.J. (1938): *Manual of Sedimentary Petrology*. New York (Appleton-Century Crofts), 549pp.

Leader, M.R. (1982): *Sedimentology: Process and product*. London (Allen and Unwin). 479pp.

Morner, N.A. (1976): Eustatic changes during the last 8000 years. *Paleogeography, Paleoclimatology, Paleoecology* 19 (1).pp.63-85

Muller, G. (1966): Grain size, carbonate content, and carbonate mineralogy of Recent sediments of the Indian Ocean off the eastern coast of Somalia. *Die Naturwissensch.*, V.53, no.21, pp. 547-550.

Nzioka, R.M. (1981): The general water movement off the Kenya coast. The Kenya Marine and Fisheries Research Institute. Unpublished manuscript, Mombasa.

Ojany, F.F. (1984): Some aspects of the Geomorphic evolution of the Kenya coast with special reference to the Kambe Limestone rocks of the Kilifi Area. In *Natural and Man-Induced environmental changes in tropical Africa*. Kadomura, H. (ed). Kosoku Printing Center, Sapporo, Japan.

Ottman, F. (1962): Sur la classification des côtes. *Bull. Soc. Géol. France*, 7 sér., V.4, pp.620-624. 40.

Powers, M.C. (1953): A new roundness and sphericity scale for sedimentary particles. *Journ. Sediment. Petrol.*, Vol.23, pp.117-119.

Pulfrey, W. (1942): Report on the Alleged Gedi Silver- Lead Deposits. Mines and Geological Dept., Nairobi. Unpublished manuscript.

Reineck, H.E. and Singh, I.B. (1973): *Depositional Sedimentary Environments*. New York (Springer-Verlag Berlin Heidelberg).

Ryan, W.A. (1953): Report on an Investigation of the Silversands Beach Sands, near Malindi, Unpublished Study, Mines and Geological Department, Nairobi.

Sakalowsky, P.P.(Jr).(1975): Beach morphology and nearshore processes on a sheltered beach - A case study of Napatre Beach, Rhode Island. *Mar. Geol.* Vol. 18. pp. 35-43.

Sasaki, T. and Horikawa, K. (1975): Nearshore current system on a gently sloping bottom: *Coastal Engineering in Japan*, V.18, pp. 123-142.

Schott, W. and von Stackelberg, U. (1965): Über rezente sedimentation in Indischen Ozean, ihre Bedeutung für die Entstehung Kohlenwasserstoffhaltiger sedimente. Erdöl und kohle, Erdgas, Petrochemie, V. 18, pp.945-950.

Schroeder, J.H. (1974): Sedimentology of coast and shelf environments. Notes for Regional Training Course, Malindi, Kenya. TU Berlin, 39pp.

Schroeder, J.H. and Jacob, K.-H.(1976): In-situ Resin Impregnation of Cores and Profiles in Coastal Sediments. Senckenbergiana marit. 8, pp.81-85 Frankfurt/Main.

Service Hydrographique de la marine (1980): Admiralty chart no.6271,1980 and 6272, 1970.

Shepard, F.B. (1978): Geological Oceanography. Heinemann, London, 225pp.

Short, A.D. (1979): Three Dimensional Beach-Stage Model. Journ. of Geol. Vol.87, pp.553-571.

Sneed, E.D. and Folk, R.L. (1958): Pebbles in the lower Colorado River, Texas, a study in particle morphogenesis. J. Ged. 66, pp. 114-150.

Smirnov, V.I. (1976): *Geology of Mineral Deposits*. MIR Publishers, Moscow. 315pp.

Sutherland D.G. (1982): *The Transport and Sorting of Diamonds by Fluvial and Marine Processes*. *Econ. Geol.* Vol.77, pp.1613-1620.

Thompson, A.O. (1956): *The Geology of the Malindi Area*. *Geol. Surv., Kenya Report No.36*, pp.56-57.

Toya, H., Kadomura, H., Tamura, T. and Hori, N. (1973): *Geomorphological studies in south - east Kenya*. *Geog. Repts. Tokyo Metrop. Univ.*, No 8, pp. 51-137.

Valentin, H. (1954): *Die Küsten der Erde (2nd ed.)* - Gotha (VEB Geographisch - Kartographische Anstalt) pp.118.

Walther, J. (1884): *Lithogenesis der Genenovart. Beobachtungen ber die Bildung der Gesteine an der heutigen Erdoberfläche; Dritter Teil einer Einleitung in die Geologie als historische Wissenschaft*. Jena: Verlag Gustav Fisher. pp.535-1055.

Wentworth, C. (1922): *A method of measuring and plotting shapes of pebbles*. *Bull. Geol. Surv. US.* vol. 730, pp.91-96.

Werth, E. (1952): Die eustatischen bewegungen des meeresspiegels. Abhandl.

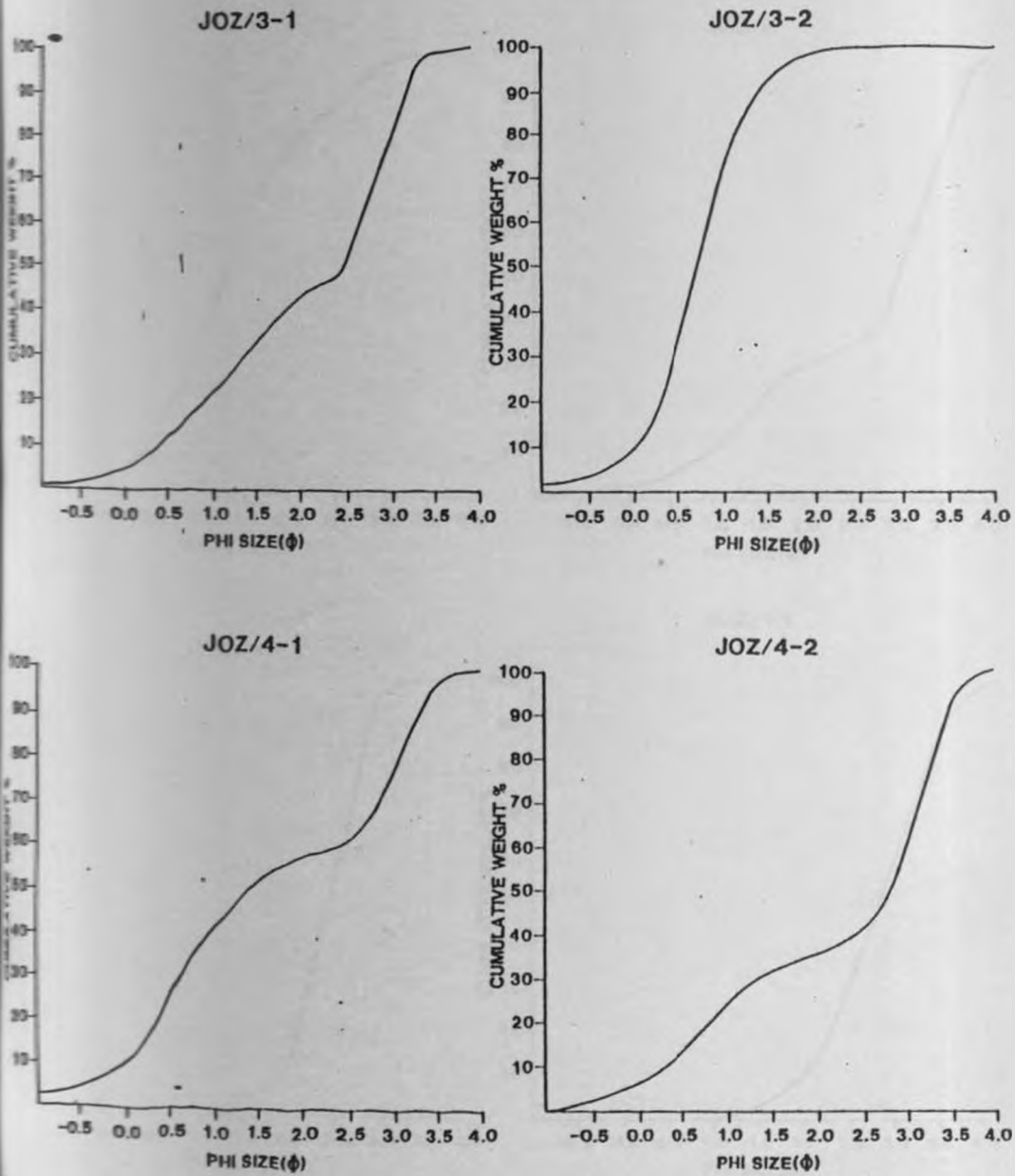
Mat - Naturwissenschaftl. Klasse 8: pp. 1-142.

Williams, L.A.J. (1962): The Geology of the Hadu- Fundisa Area, North of

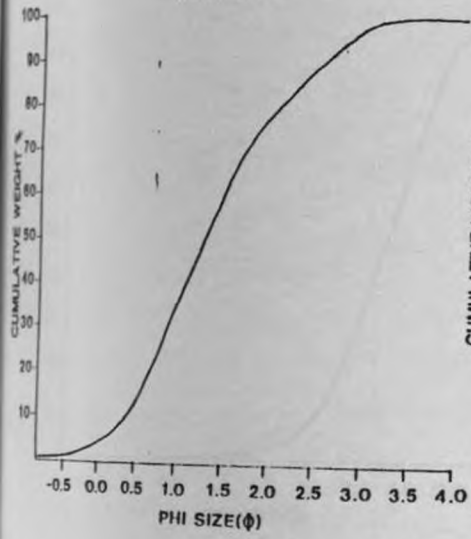
Malindi, Geol. Surv., Kenya., Report No.52, pp. 56-59.

APPENDIX I

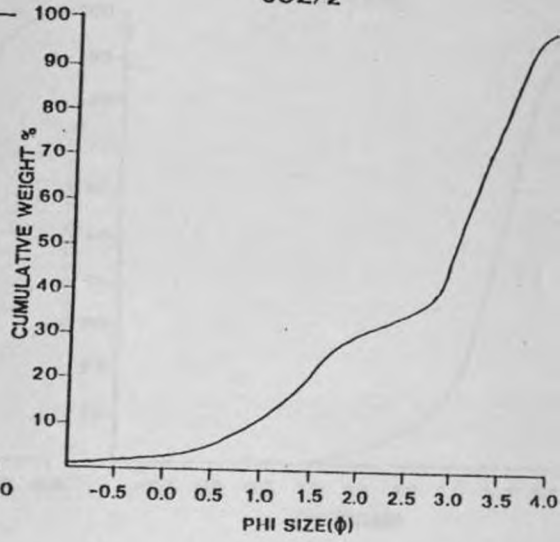
Cumulative grain-size distribution curves for coastal sediments in the Malindi-Fundisa area.



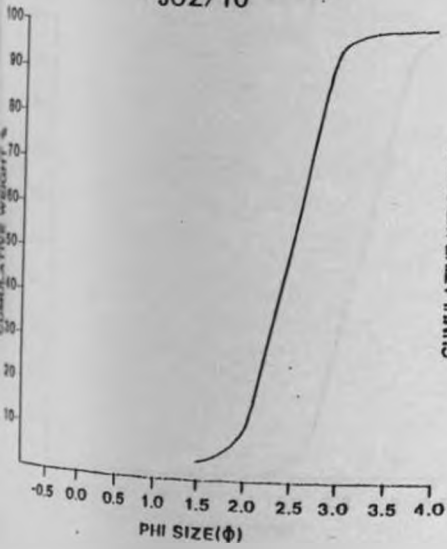
JOZ/5



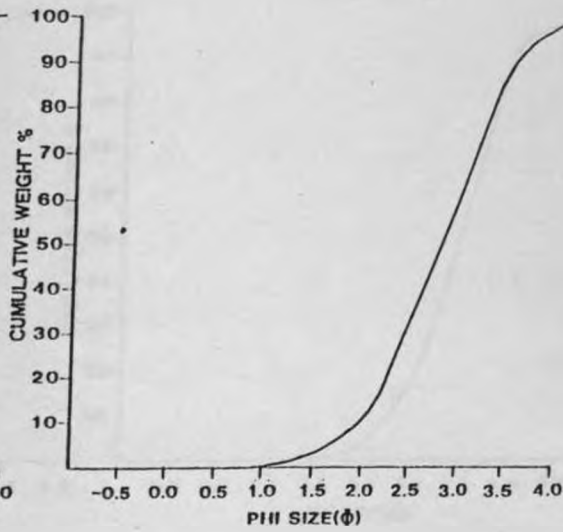
JOZ/2

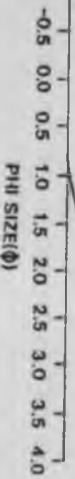
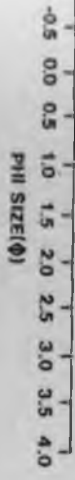


JOZ/10

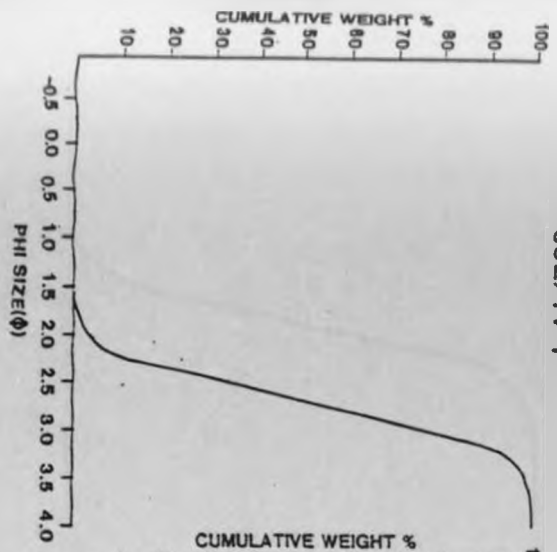


JOZ/11

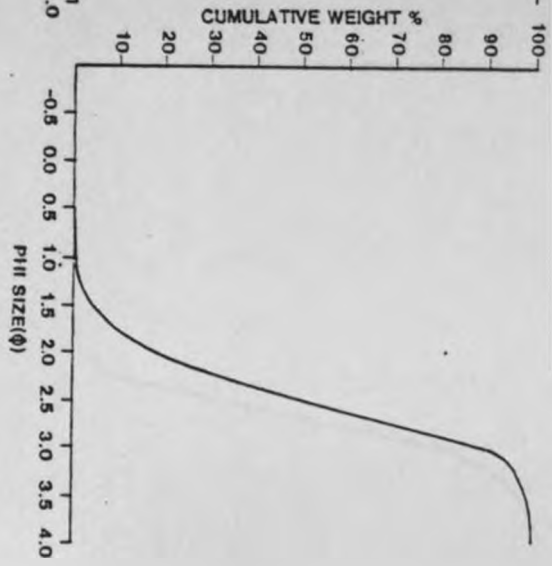




JOZ/14-1



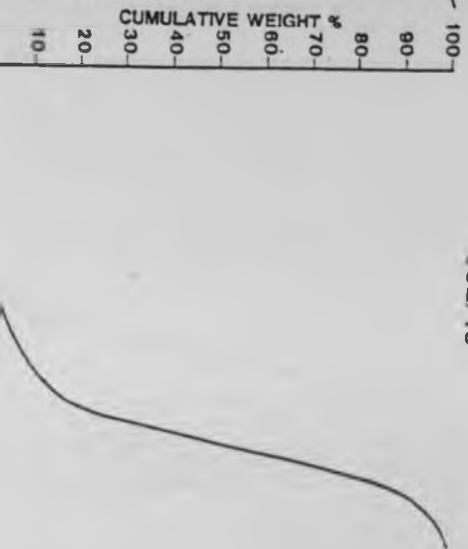
JOZ/14-2

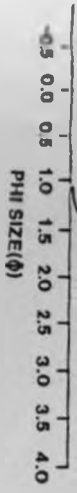


J02/12

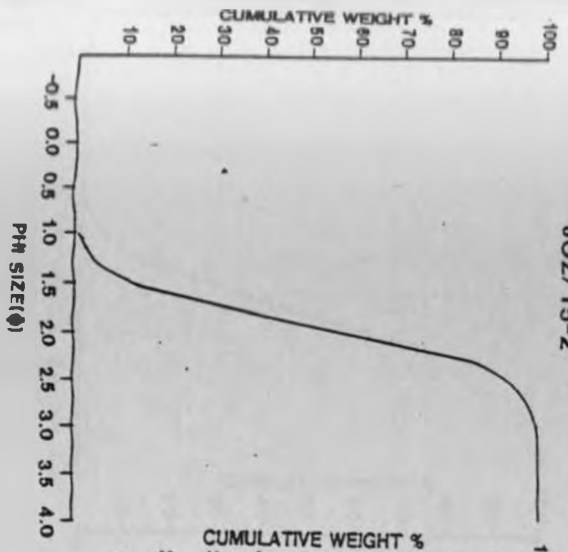


J02/13

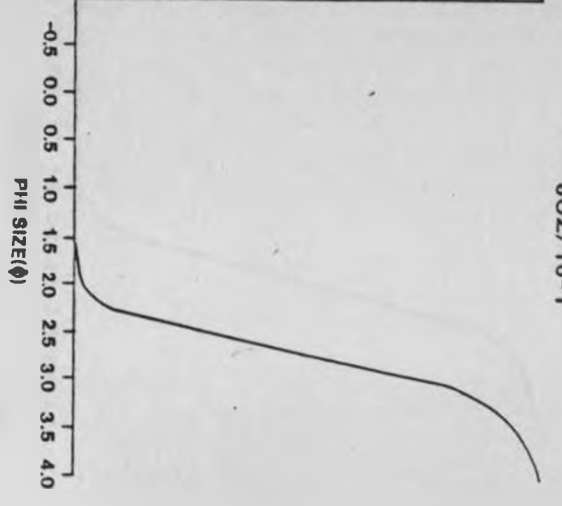
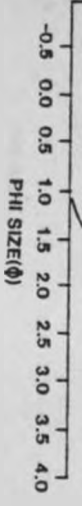




JOZ/15-2



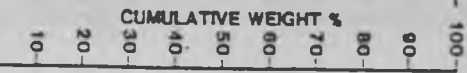
JOZ/16-1

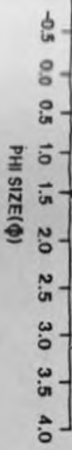


JOZ/14-3

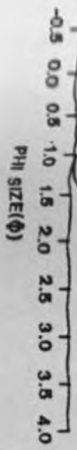


JOZ/15-1

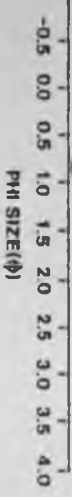




JOZ/17-1

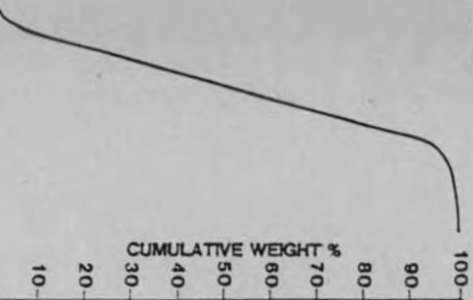


JOZ/17-2



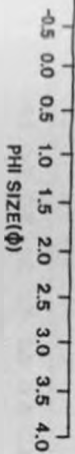
JOZ/17-2

J0Z/16-2

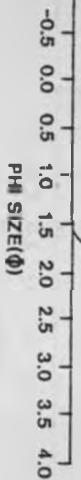
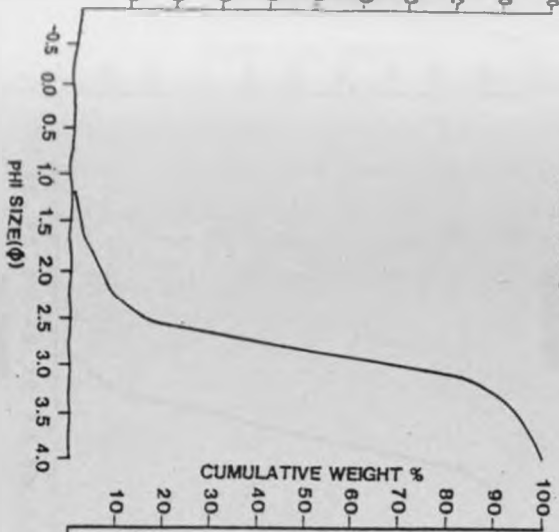


J0Z/16-3

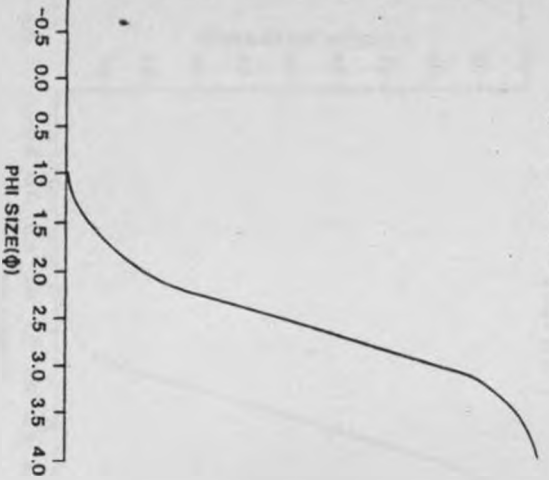




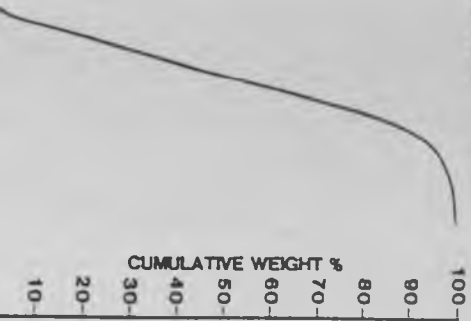
JOZ/18-3



JOZ/18-4

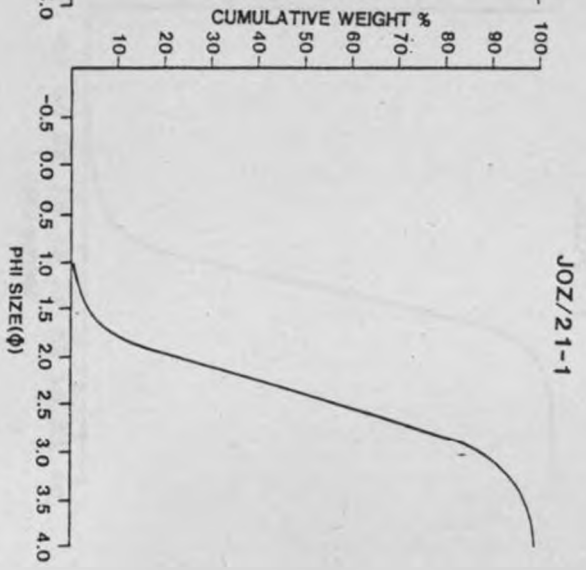
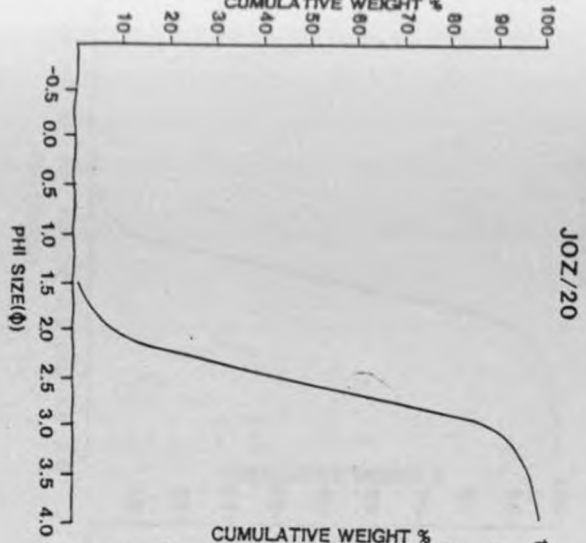
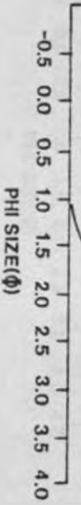
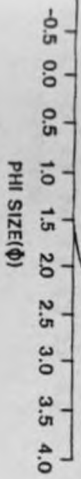


JOZ/18-1

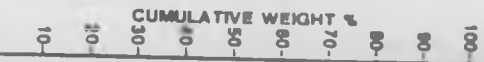


JOZ/18-2

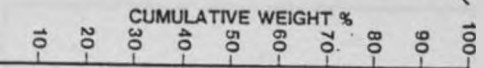




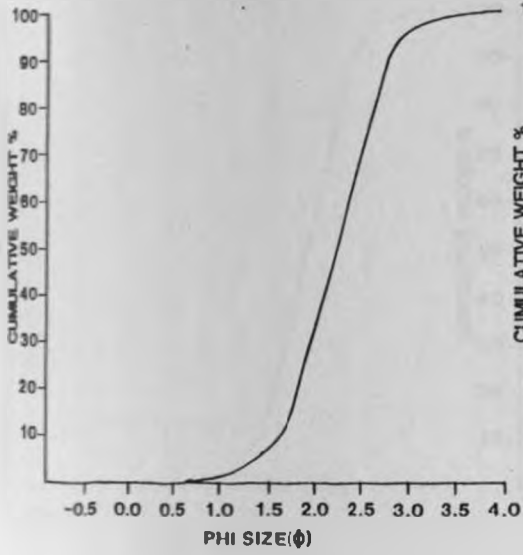
JOZ/19-1



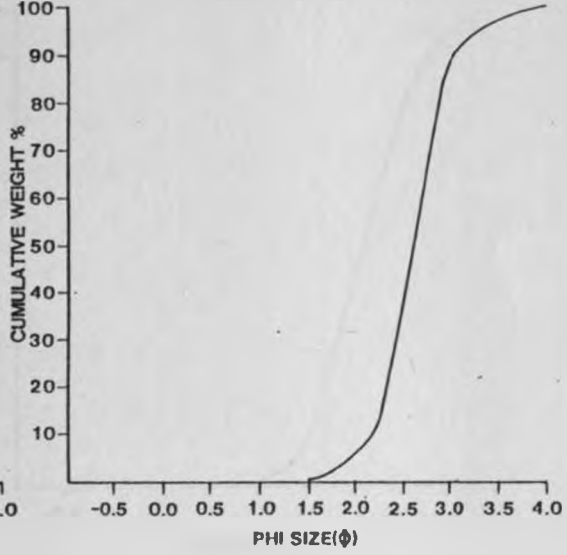
JOZ/19-2



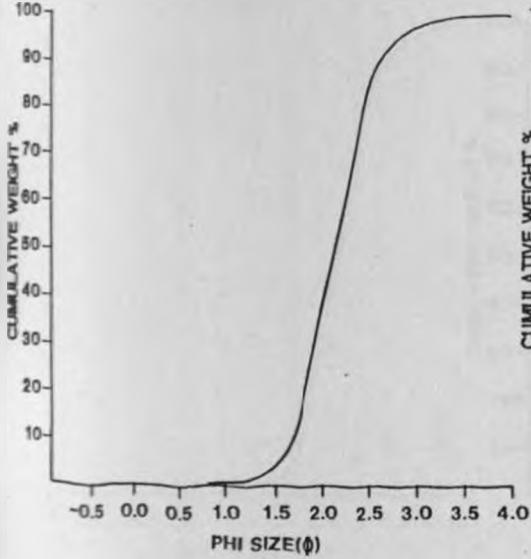
JOZ/21-2



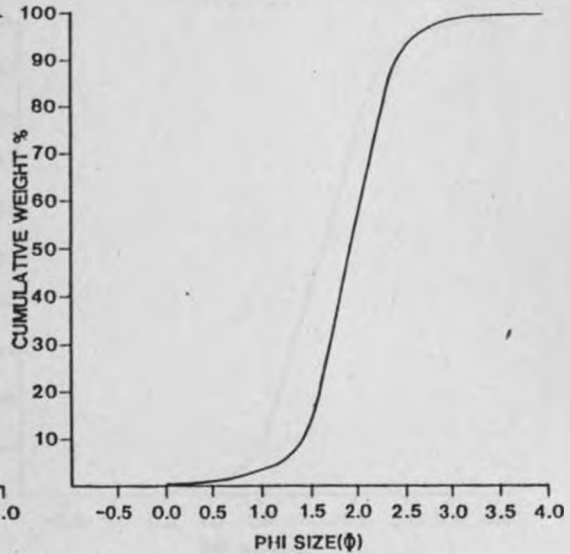
JOZ/22-1

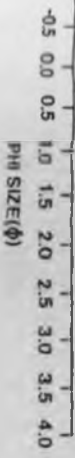


JOZ/22-2

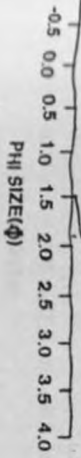


JOZ/23-1

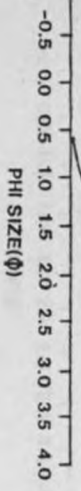




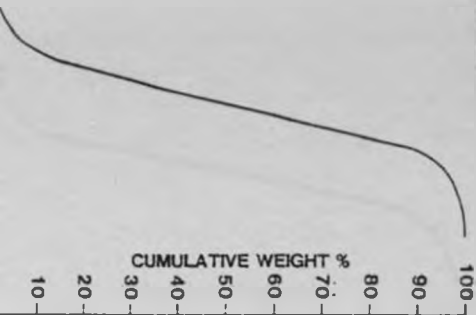
JOZ/23-4



JOZ/24

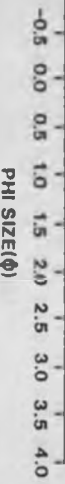
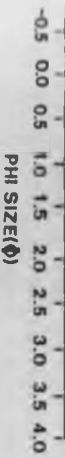


J0Z/23-2



J0Z/23-3





JOZ/26

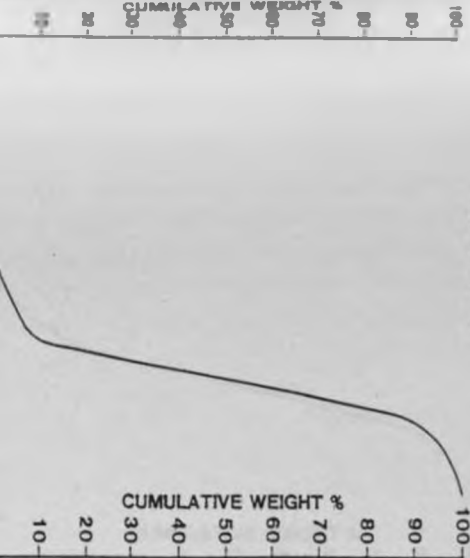
JOZ/27

PHI SIZE(φ)

PHI SIZE(φ)

CUMULATIVE WEIGHT %

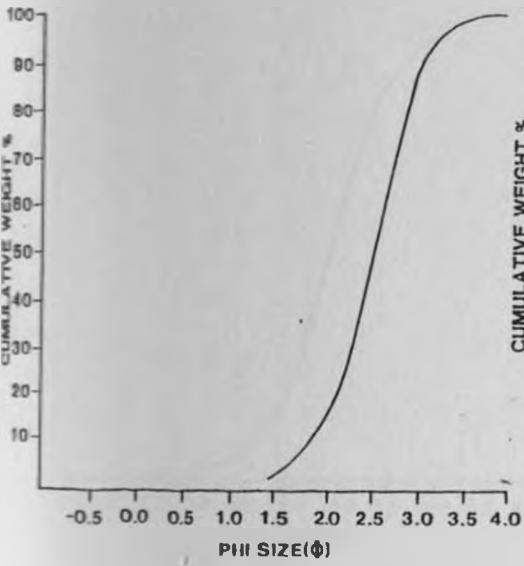
JOZ/25-1



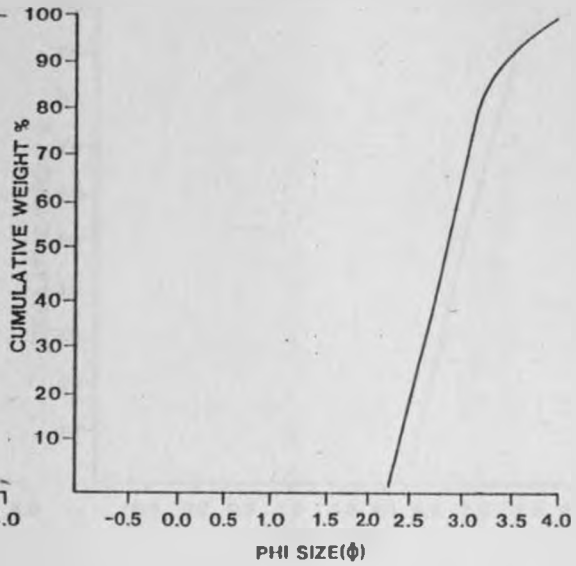
JOZ/25-2



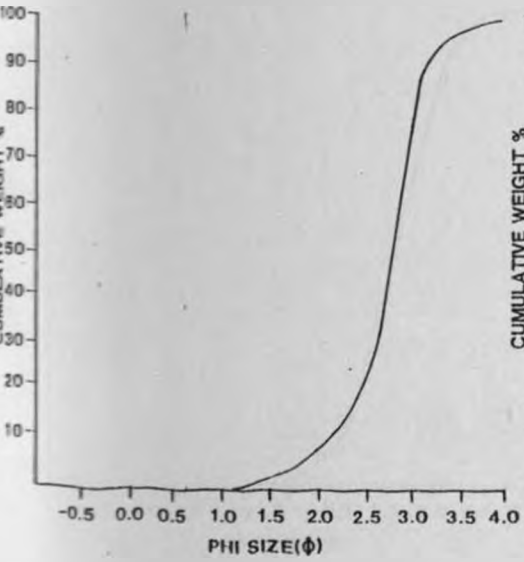
JOZ/28-1



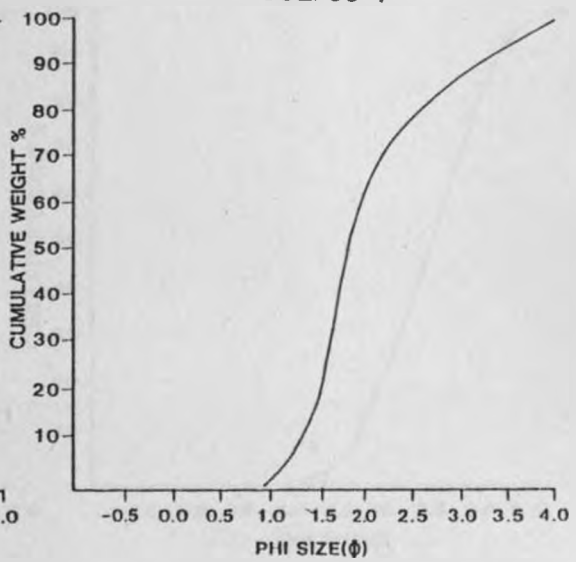
JOZ/28-2

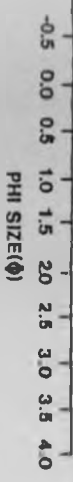


JOZ/29

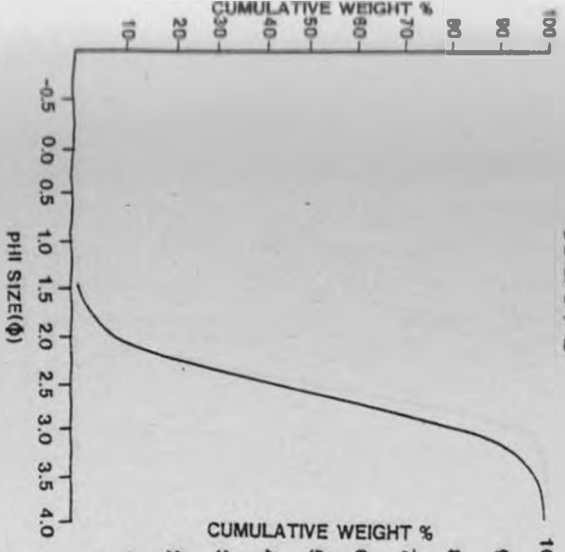


JOZ/30-1

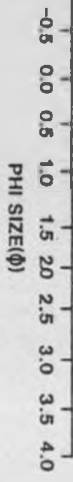




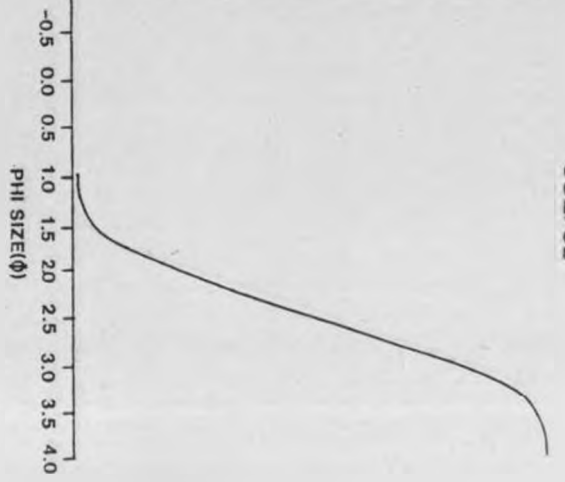
JOZ/31-2



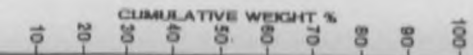
JOZ/32



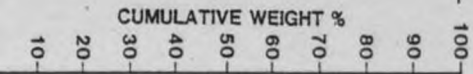
JOZ/32



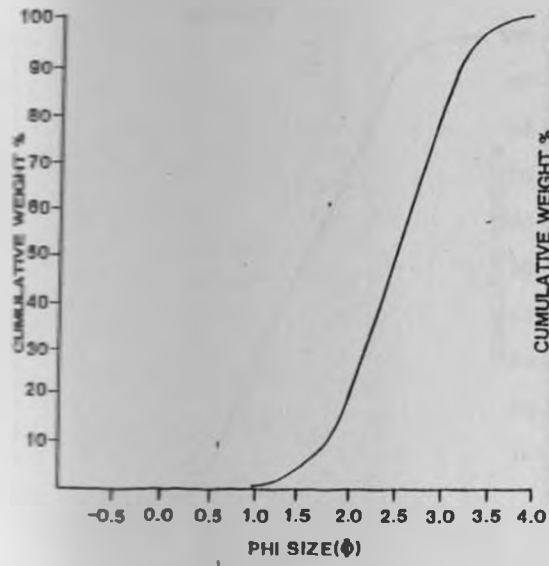
JOZ/30-2



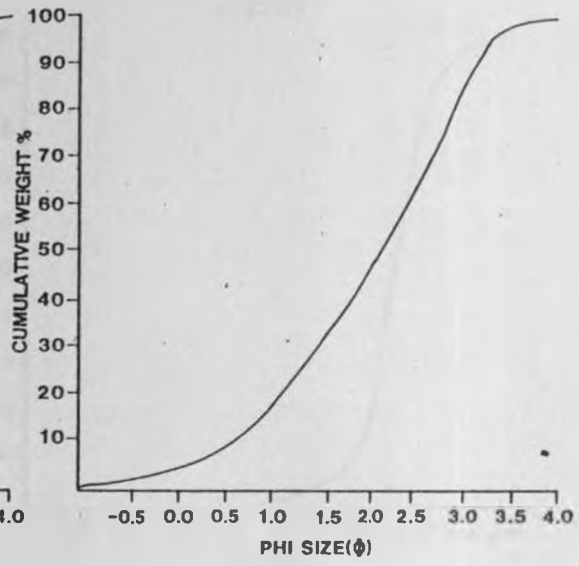
JOZ/31-1



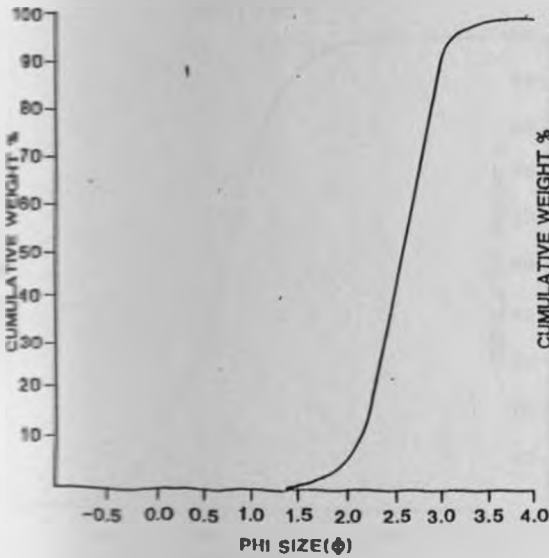
JOZ/33



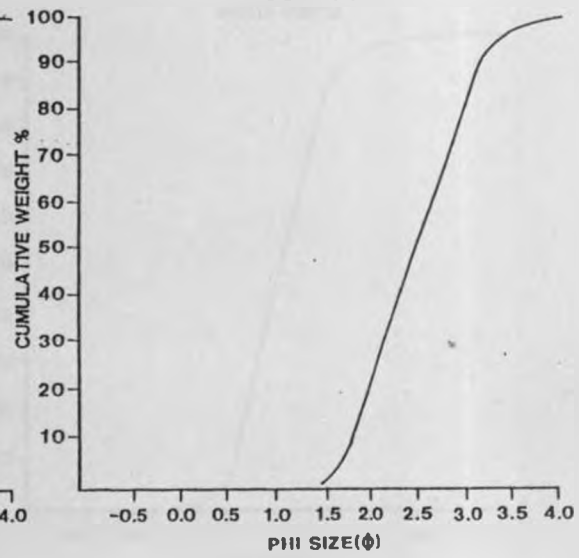
JOZ/34

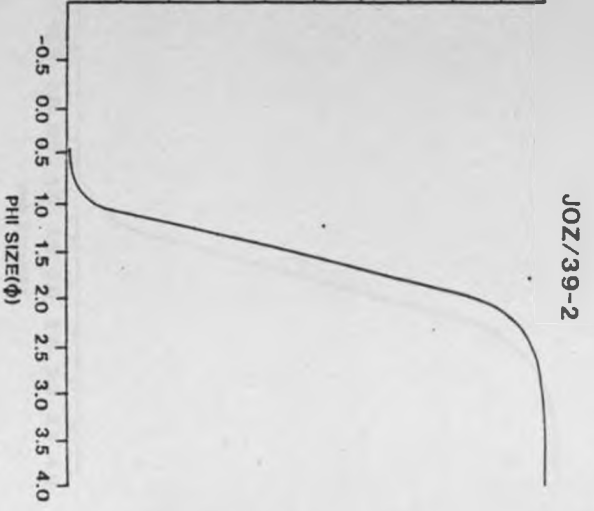
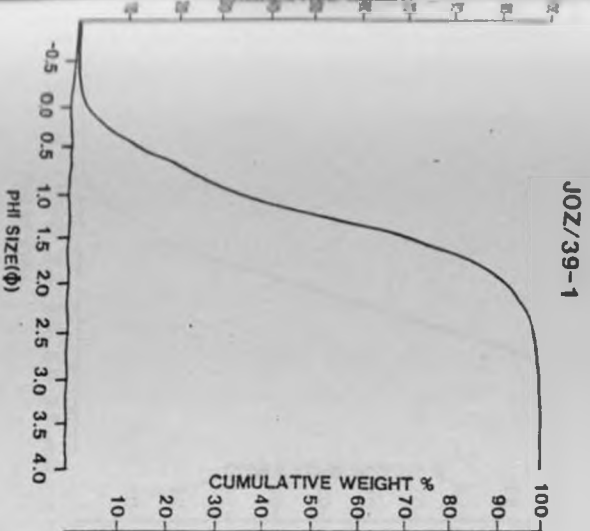


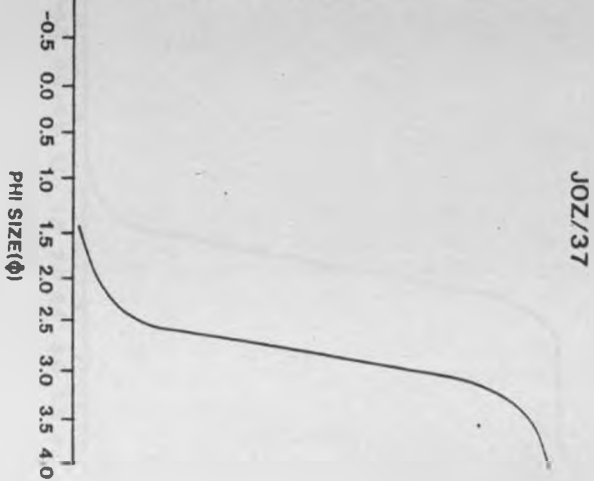
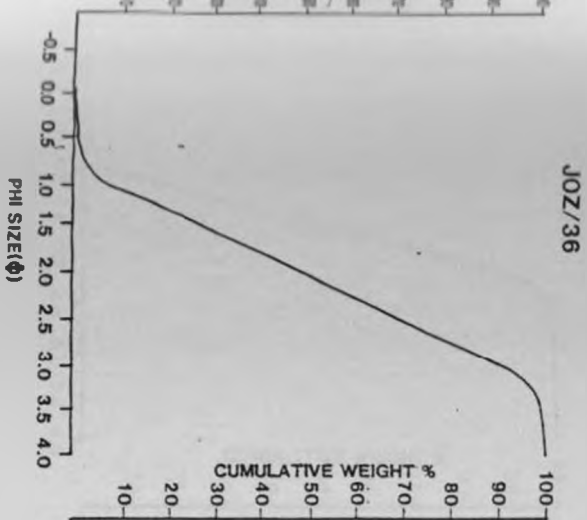
JOZ/35-1



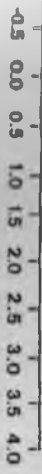
JOZ/35-2





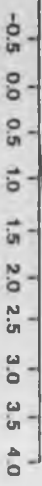


PHI SIZE(ϕ)



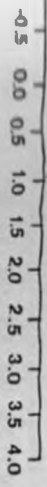
JOZ/40-2

PHI SIZE(ϕ)



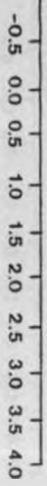
JOZ/48

PHI SIZE(ϕ)

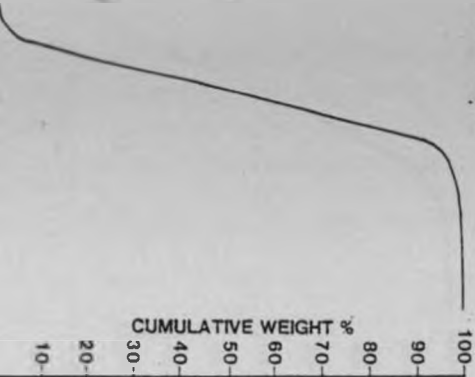


CUMULATIVE WEIGHT %

PHI SIZE(ϕ)

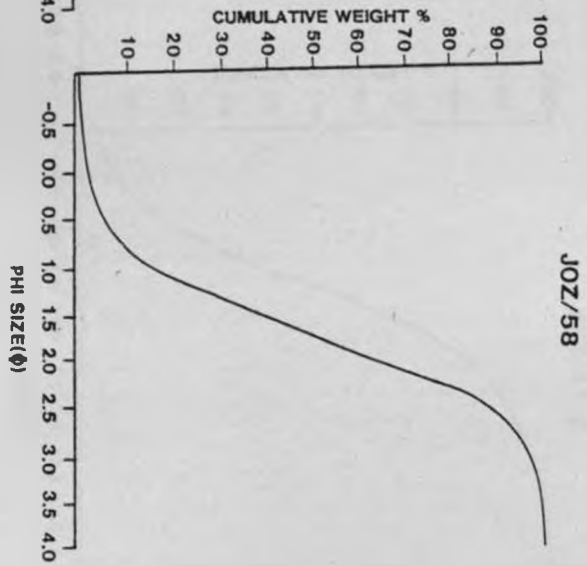
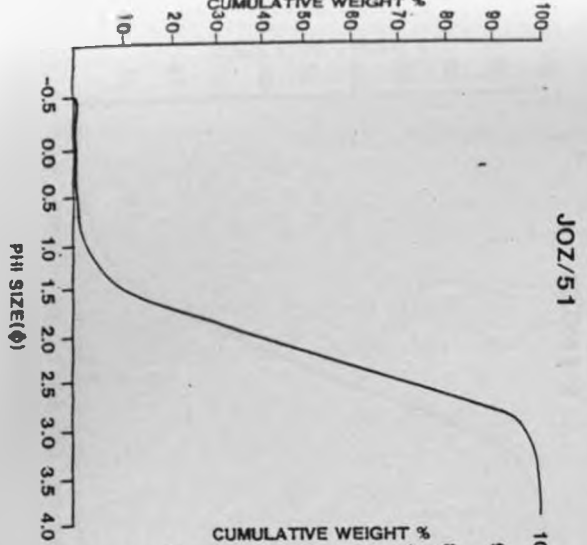
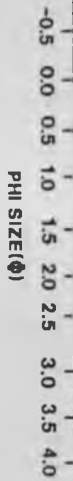
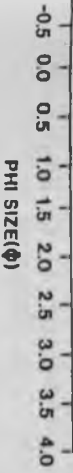


JOZ/40-1



JOZ/47



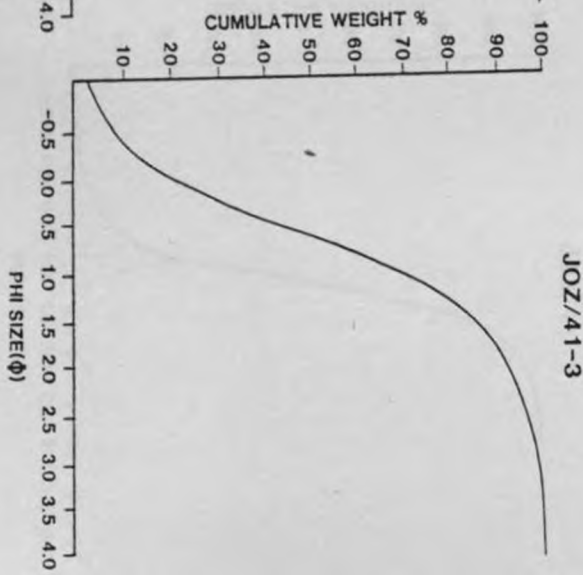
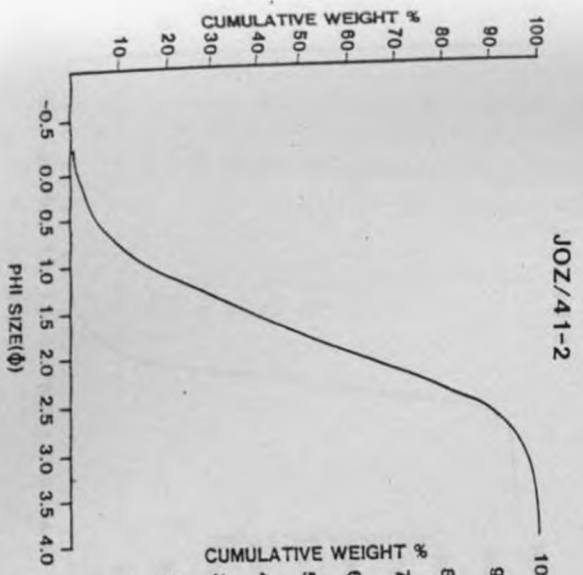
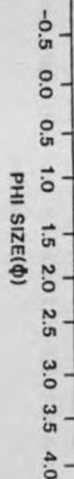
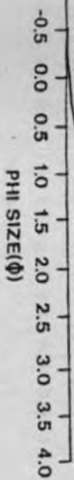


JOZ/49

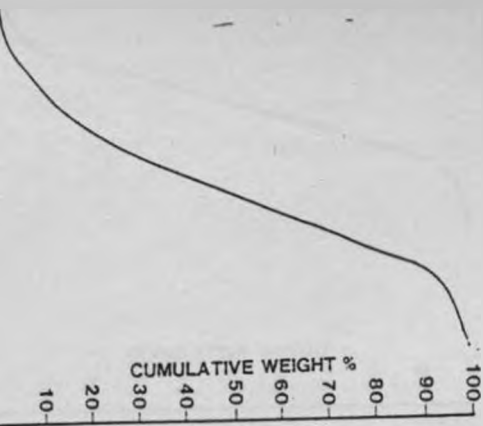
100-
90-
80-
70-
60-
50-
40-
30-
20-
10-

JOZ/50

100-
90-
80-
70-
60-
50-
40-
30-
20-
10-
CUMULATIVE WEIGHT %

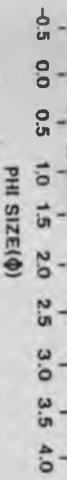


JOZ/59

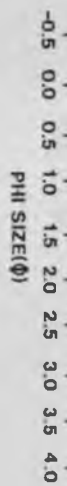
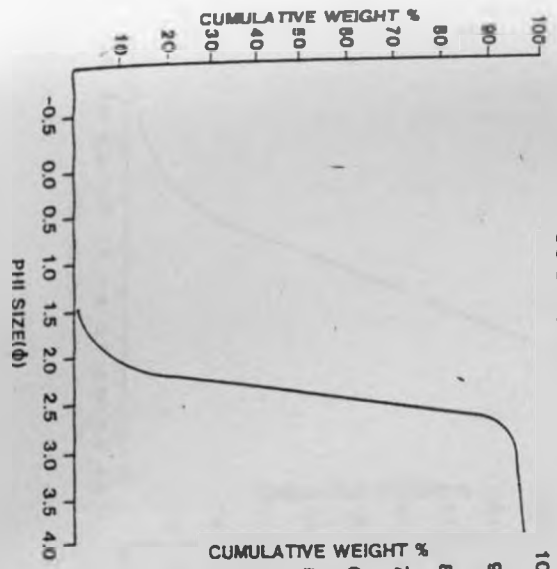


JOZ/41-1

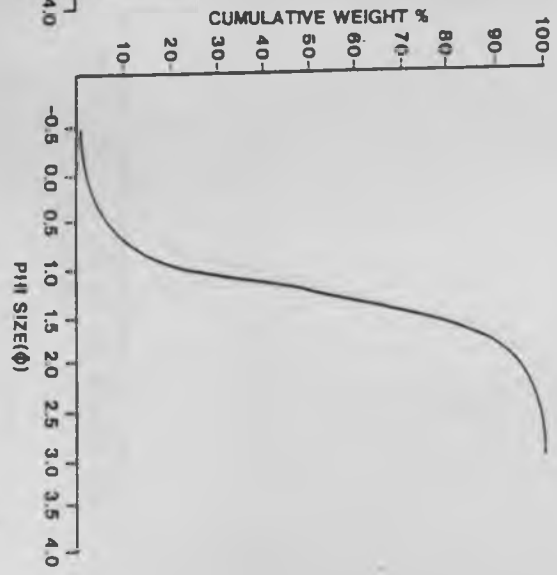




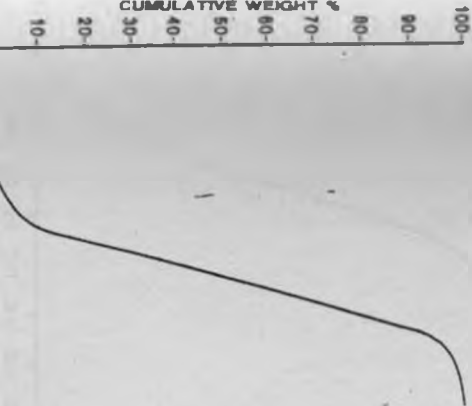
JOZ/43-2



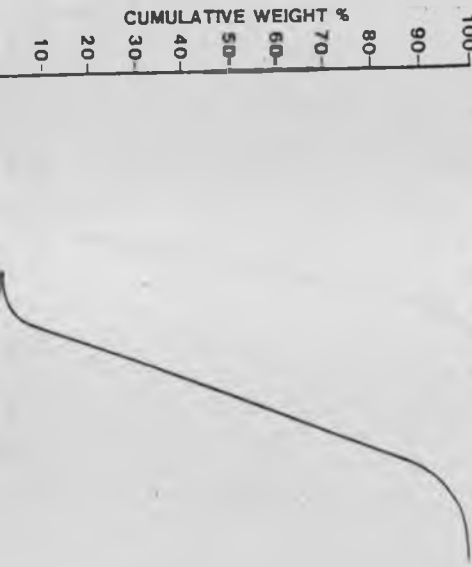
JOZ/44



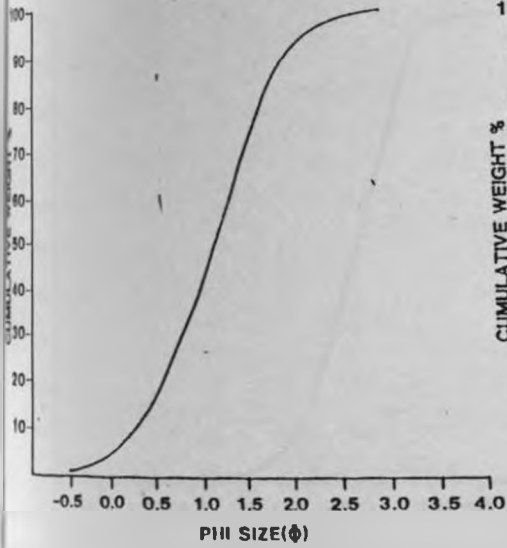
J0Z/42



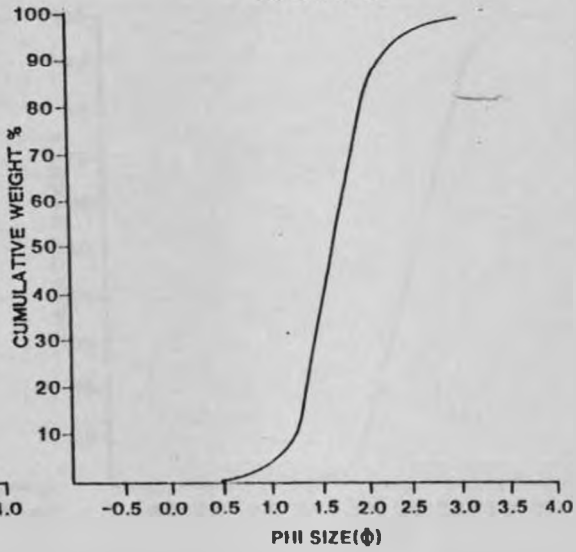
J0Z/43-1



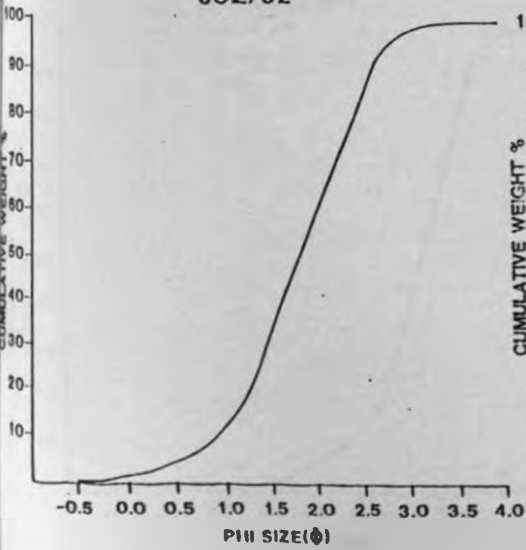
JOZ/46-1



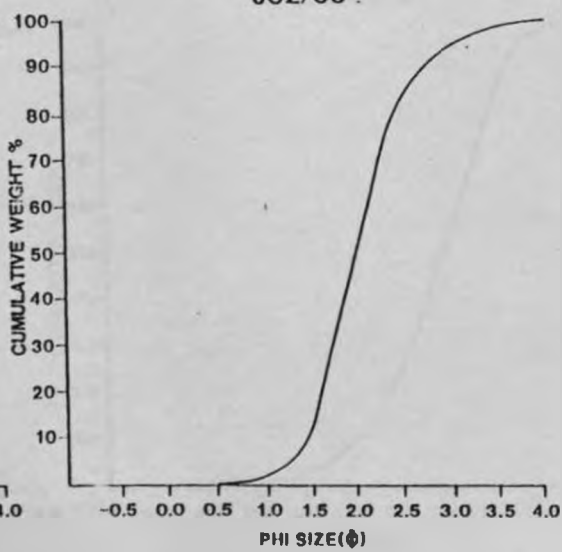
JOZ/46-2

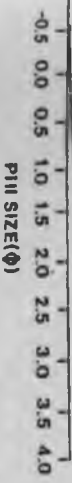


JOZ/52

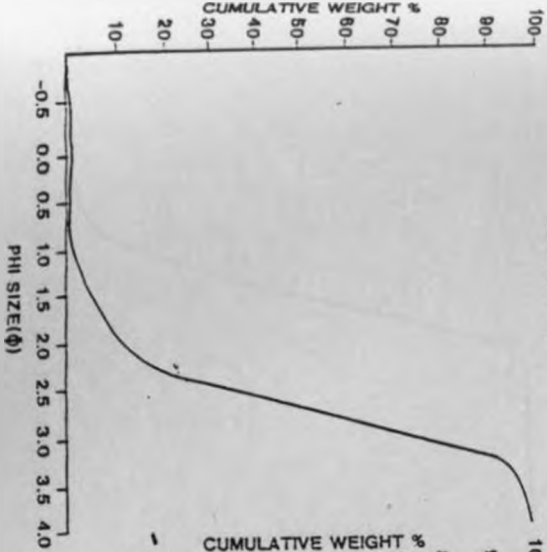


JOZ/53

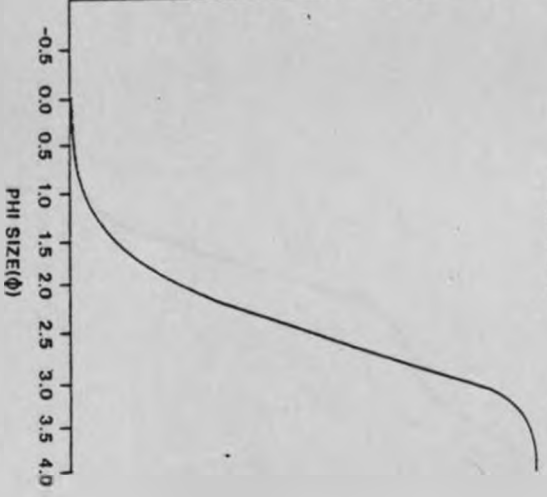
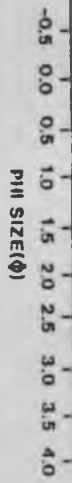




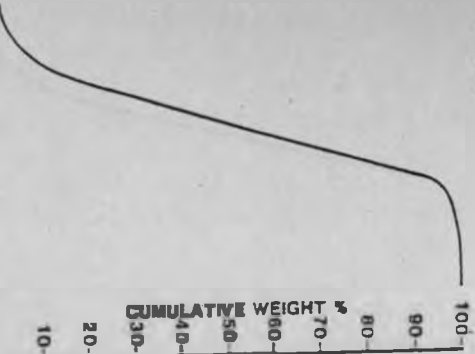
JOZ/55-1



JOZ/55-2



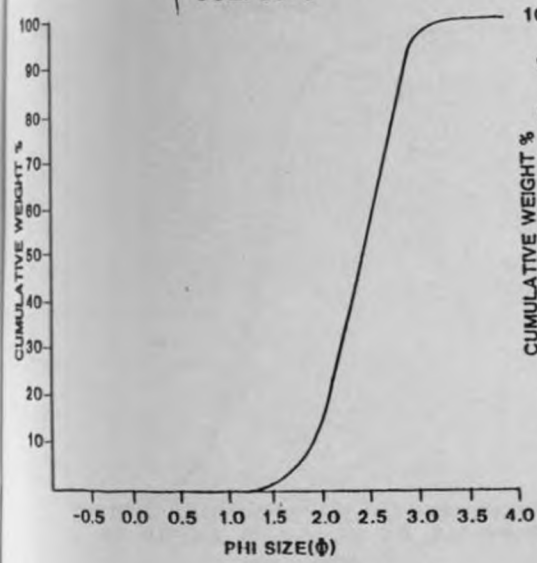
JOZ/54-1



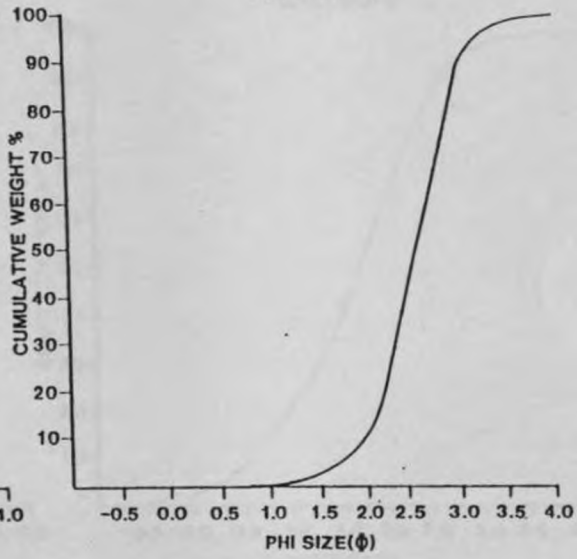
JOZ/54-2



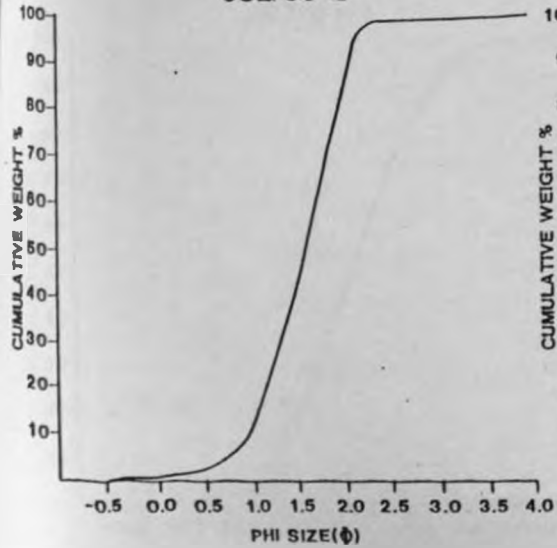
JOZ/55-3



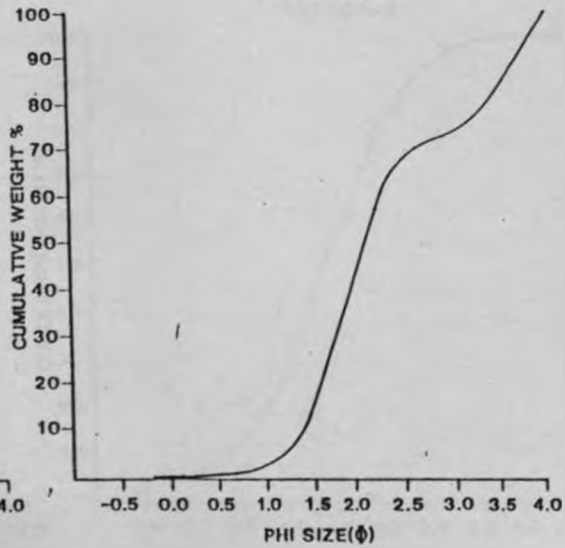
JOZ/56-1



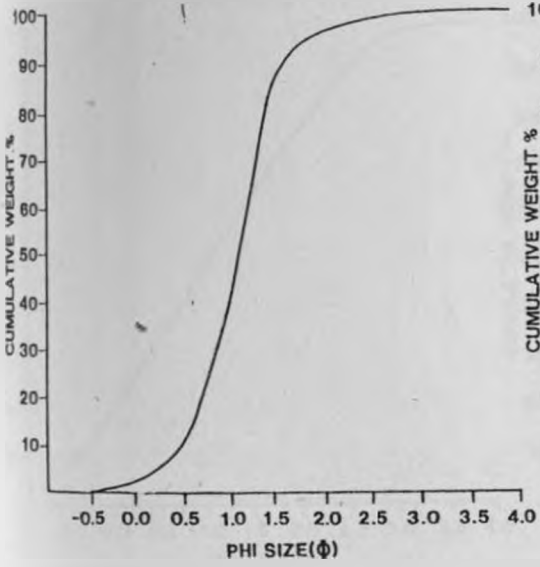
JOZ/56-2



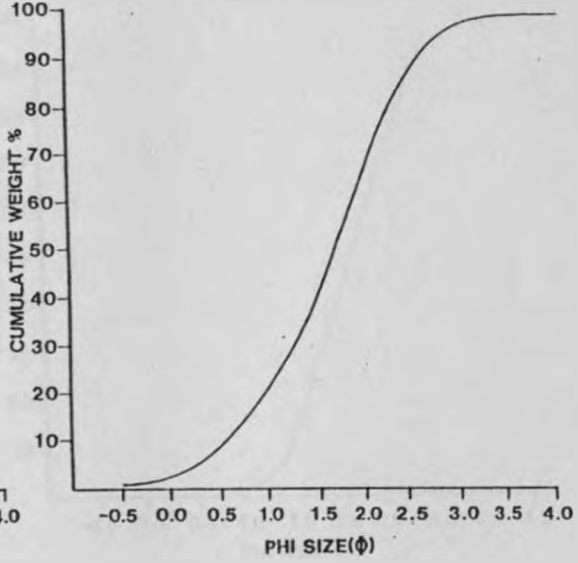
JOZ/56-3



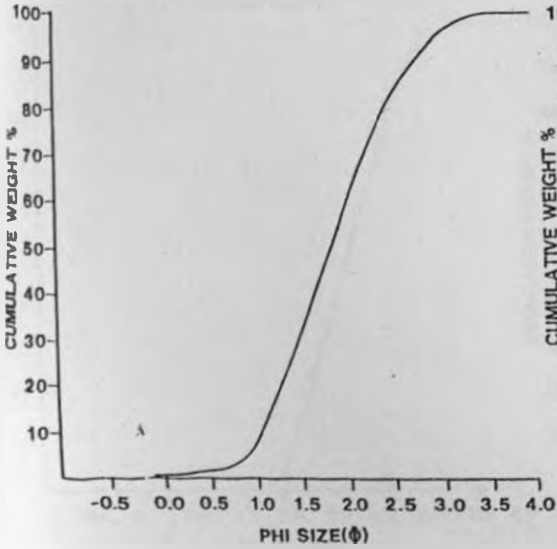
JOZ/60-1



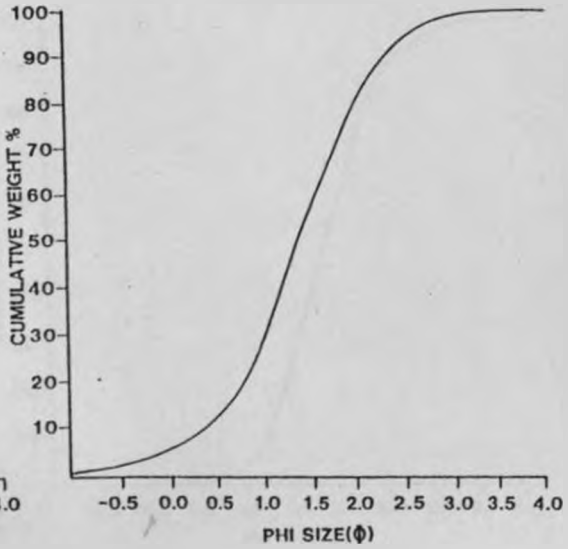
JOZ/60-2

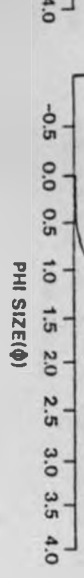
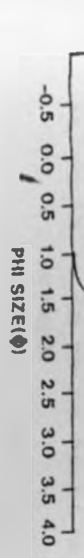
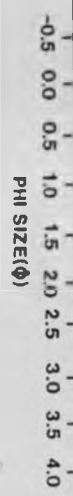
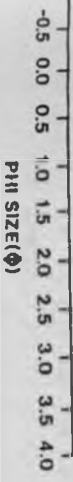


JOZ/61-1

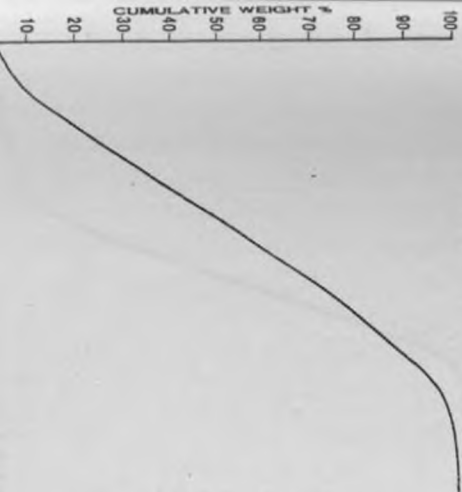


JOZ/61-2

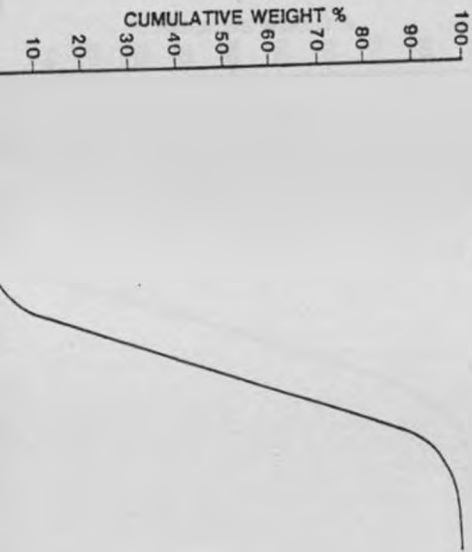


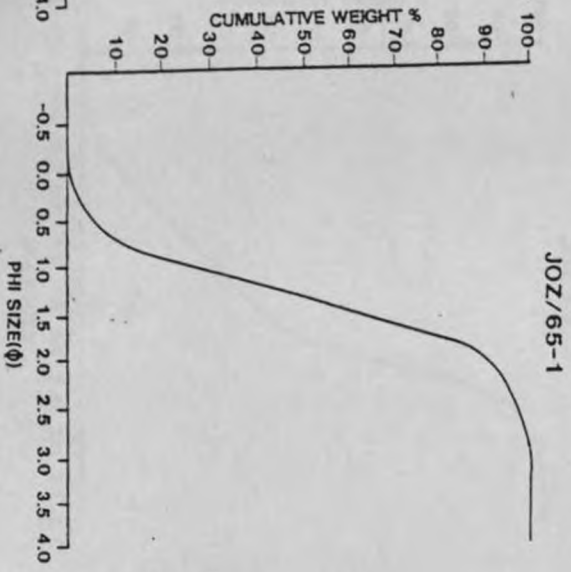
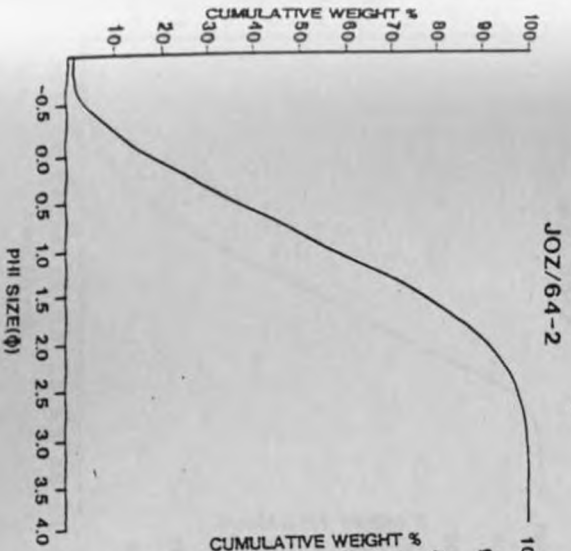
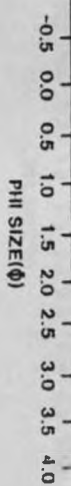
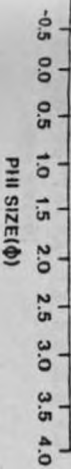


J0Z/61-3

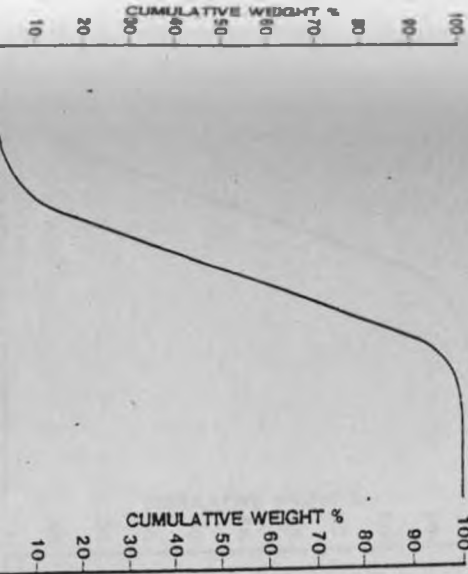


J0Z/62-1

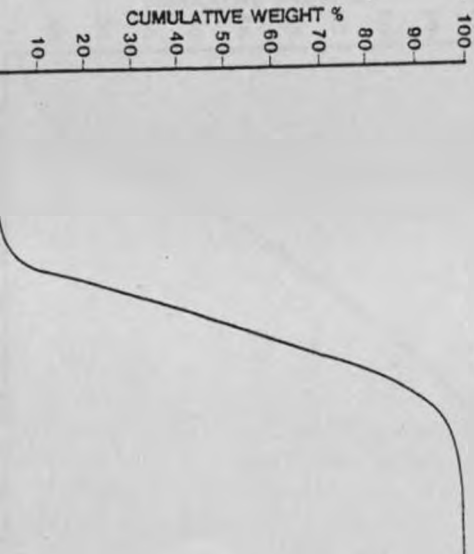




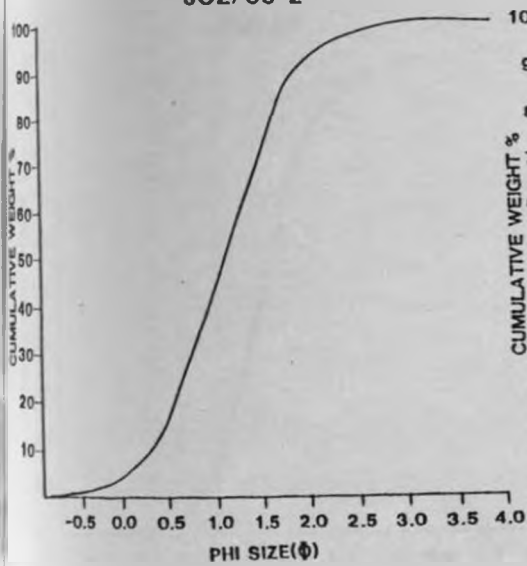
JOZ/63



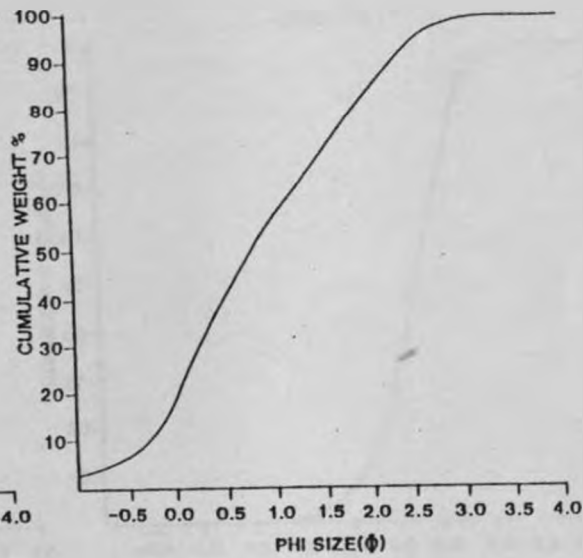
JOZ/64-1



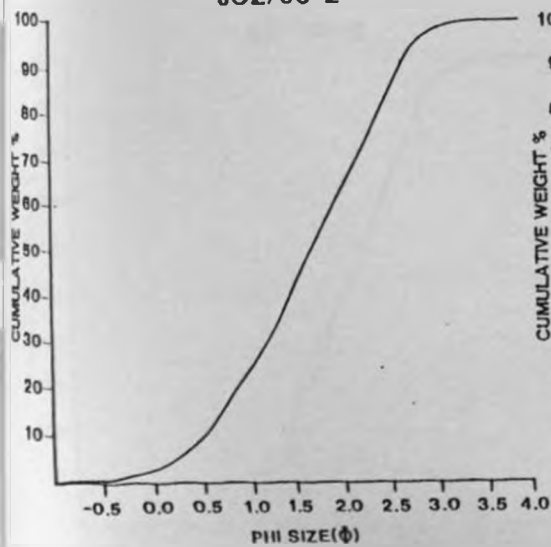
JOZ/65-2



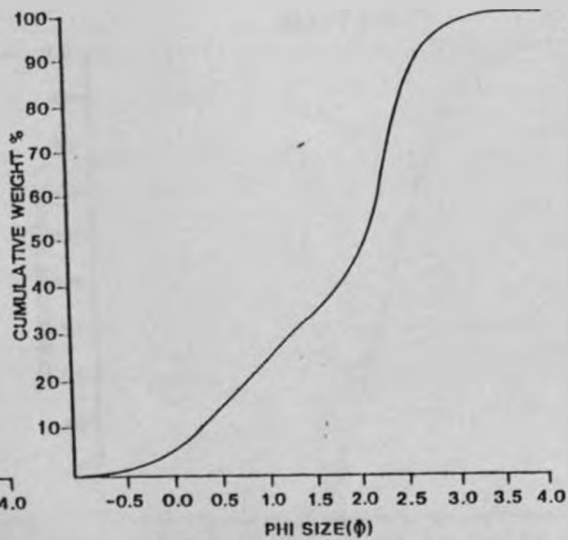
JOZ/66-1

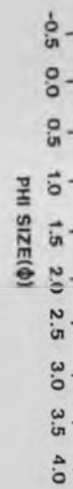
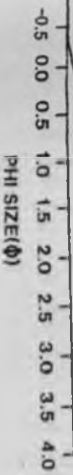


JOZ/66-2



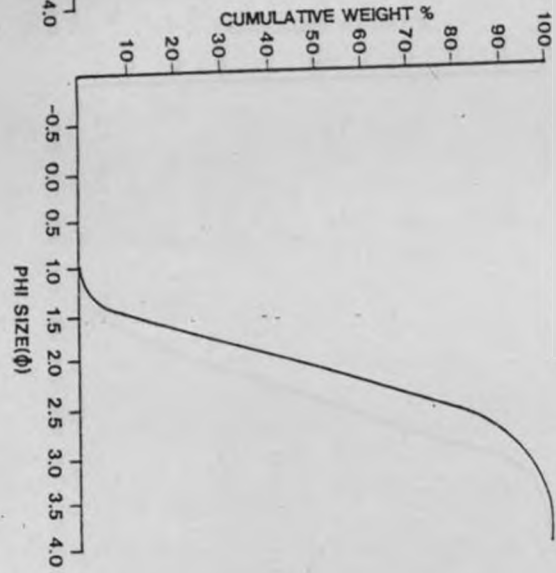
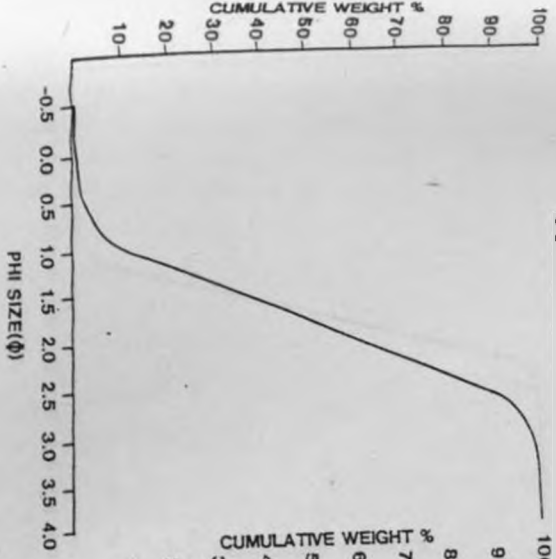
JOZ/67





JOZ/70-2

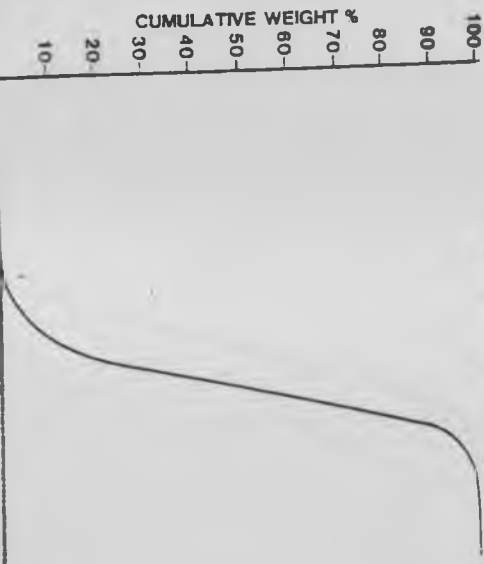
JOZ/71-1

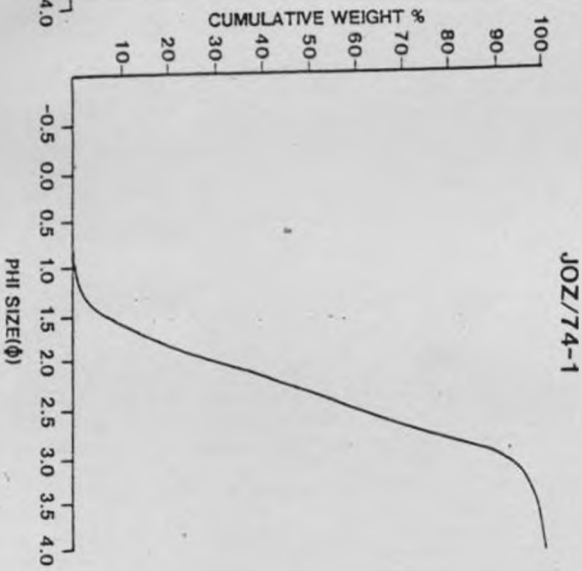
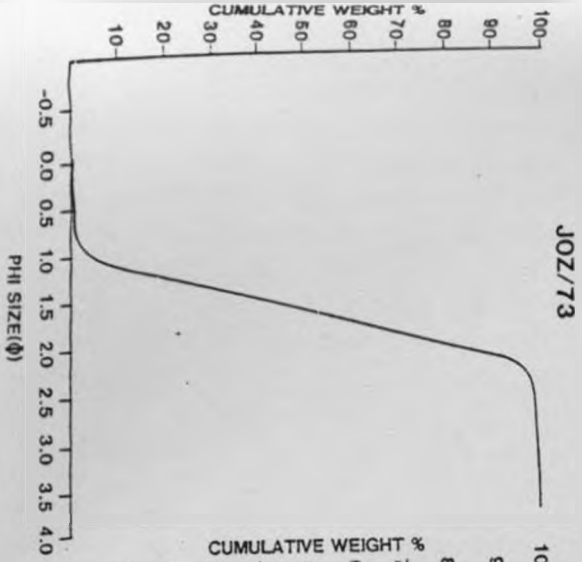
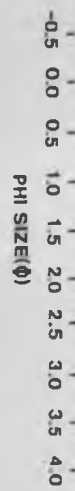
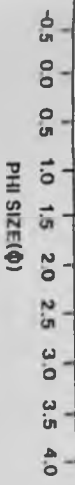


JOZ/69



JOZ/70-1





JOZ/71-2

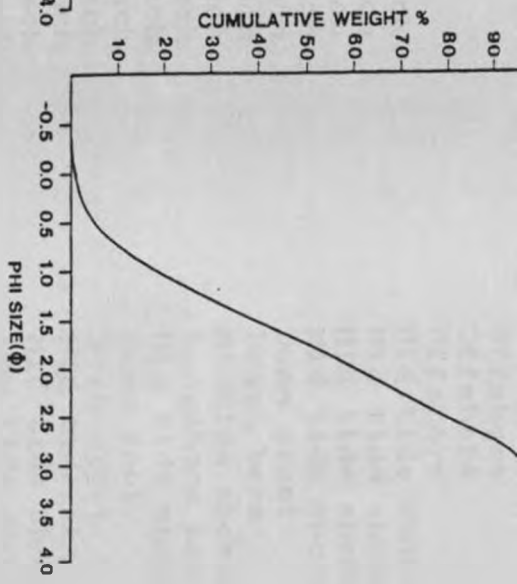
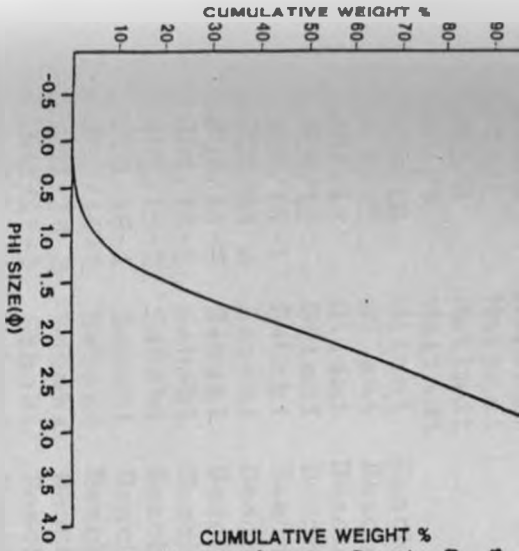
100-
90-
80-
70-
60-
50-
40-
30-
20-
10-

CUMULATIVE WEIGHT %

100-
90-
80-
70-
60-
50-
40-
30-
20-
10-

JOZ/72

100-
90-
80-
70-
60-
50-
40-
30-
20-
10-



255

J0Z/74-2

J0Z/75

100

100

Appendix II: Source data for petrology, chemistry, and texture of modern beach sand, Malindi Fundisa area.

Code	Title	Area
JOZ/2	Gilani Beach	Mid tide shoreline
JOZ/3-1	Siversands Beach	Wave-cut cliff base
JOZ/3-2	Siversands Beach	Wave-cut cliff base
JOZ/4-1	Siversands Beach	High tide shoreline
JOZ/4-2	Siversands Beach	Mid tide shoreline
JOZ/5	Siversands Beach	Mid tide shoreline
JOZ/6	Malindi	Offshore
JOZ/7	Malindi	Offshore
JOZ/8	Malindi	Offshore
JOZ/9	Malindi	Offshore
JOZ/10	Gilani Beach	Mid tide shoreline
JOZ/11	Gilani Beach	Mid tide shoreline
JOZ/12	Gilani Beach	Mid tide shoreline
JOZ/13	Gilani Beach	Mid tide shoreline
JOZ/14-1	Sabaki Beach	Dune crest
JOZ/14-2	Sabaki Beach	Beach berm
JOZ/14-3	Sabaki Beach	Midtide shoreline
JOZ/15-1	Sabaki Beach	Longshore bar
JOZ/15-2	Sabaki Beach	Mid tide shoreline
JOZ/16-1	Sabaki Beach	Dune foot
JOZ/16-2	Sabaki Beach	Berm crest
JOZ/16-3	Sabaki Beach	Mid tide shoreline
JOZ/17-1	Sabaki Beach	Mid tide shoreline
JOZ/17/2	Sabaki Beach	Low tide shoreline
JOZ/18-1	Sabaki Beach	Mid tide shoreline
JOZ/18-2	Sabaki Beach	High tide shoreline
JOZ/18-3	Sabaki Beach	Interdistributary levee
JOZ/18-4	Sabaki Beach	Interdistributary bar
JOZ/19-1	Sabaki Beach	Steep south bank
JOZ/19-2	Sabaki Beach	Steep south bank
JOZ/19-3	Sabaki Beach	Steep south bank
JOZ/20	Sabaki Beach	Northern levee
JOZ/21-1	Sabaki Beach	Beach berm
JOZ/21-2	Sabaki Beach	Mid tide shoreline
JOZ/22-1	Sabaki Beach	Beach berm
JOZ/22-2	Sabaki Beach	Mid tide shoreline
JOZ/23-1	South Mambrui Beach	High tide shoreline
JOZ/23-2	South Mambrui Beach	Dune foot
JOZ/23-3	South Mambrui Beach	Sebkha
JOZ/23-4	South Mambrui Beach	Dune crest
JOZ/24	South Mambrui Beach	Mid tide shoreline
JOZ/25-1	South Mambrui Beach	Mid tide shoreline
JOZ/25-1	Mambrui Beach	Mid tide shoreline

JOZ/25-2	Mambrui Beach	Dune
JOZ/26	North Mambrui Beach	Mid tide shoreline
JOZ/27	North Mambrui Beach	Low tide shoreline
JOZ/28-1	Sheshale Bay	Dune foot
JOZ/28-2	Sheshale Bay	Mid tide shoreline
JOZ/30-1	Sheshale Bay	Mid tide shoreline
JOZ/30-2	Sheshale Bay	Low tide shoreline
JOZ/31-1	Maridadi Bay	Beach berm
JOZ/31-2	Maridadi Bay	Mid tide shoreline
JOZ/32	Maridadi Bay	Mid tide shoreline
JOZ/33	Maridadi Bay	Mid tide shoreline
JOZ/34	Maridadi Bay	Mid tide shoreline
JOZ/35-1	Casuarina Bay	High tide shoreline
JOZ/35-2	Casuarina Bay	Mid tide shoreline
JOZ/36	Casuarina Bay	Mid tide shoreline
JOZ/37	Casuarina Bay	Mid tide shoreline
JOZ/38	Casuarina Bay	Near fringing reef
JOZ/39-1	Robinson Island Beach	Dune foot
JOZ/39-2	Robinson Island Beach	Berm crest
JOZ/40-1	Robinson Island Beach	Berm crest
JOZ/40-2	Robinson Island Beach	High tide shoreline
JOZ/41-1	Simiti Island Beach	Mid tide shoreline
JOZ/41-2	Simiti Island Beach	High tide shoreline
JOZ/41-3	Simiti Island Beach	Low tide shoreline
JOZ/42	Simiti Island Beach	Mid tide shoreline
JOZ/43-1	Simiti Island Beach	High tide shoreline
JOZ/43-2	Simiti Island Beach	Low tide shoreline
JOZ/44	Simiti Island Beach	Mid tide shoreline
JOZ/45	Mto Simiti Channel	Tidal inlet
JOZ/46/1	Mto Simiti Channel	Tidal channel
JOZ/46-2	Mto Simiti Channel	Tidal delta
JOZ/47	Robinson Island Flat	Higher part of tidal flat
JOZ/48	Robinson Island Beach	High tide shoreline
JOZ/49	Robinson Island Beach	Mid tide shoreline
JOZ/50	Giryama Village Island Beach	Mid tide shoreline
JOZ/51-1	Giryama Village Island Beach	Low tide shoreline
JOZ/51-2	Giryama Village Island Beach	High tide shoreline
JOZ/52	Ngomeni Beach	Mid tide shoreline
JOZ/53	Ngomeni Beach	Mid tide shoreline
JOZ/54-1	Ngomeni Beach	Mid tide shoreline
JOZ/54-2	Ngomeni Beach	Longshore bar
JOZ/55-1	Ngomeni Beach	Low tide shoreline
JOZ/55-2	Ngomeni Beach	Mid tide shoreline
JOZ/55-3	Ngomeni Beach	High tide shoreline
JOZ/56-1	Ras Ngomeni Flat	Wave-cut cliff base
JOZ/56-2	Ras Ngomeni Flat	Wave-cut cliff base
JOZ/56-3	Ras Ngomeni Flat	Wave-cut cliff base
JOZ/57-1	Fundisa Kijadoni Island	Tidal channel levee
JOZ/57-2	Fundisa Kijadoni Island	Tidal channel bottom
JOZ/58	Mto Marereni Channel	Tidal channel bottom
JOZ/59	Mto Marereni Channel	Tidal channel bank
JOZ/60-1	Ras Kiswakini Island Beach	Beach berm

JOZ/60-2	Ras Kiswakini	Island Beach	Mid tide shoreline
JOZ/61-1	Ras Kiswakini	Island Beach	High tide shoreline
JOZ/61-2	Ras Kiswakini	Island Beach	Mid tide shoreline
JOZ/61-3	Ras Kiswakini	Island Beach	Low tide shoreline
JOZ/62-1	Ras Kiswakini	Island Beach	Dune foot
JOZ/62-2	Ras Kiswakini	Island Beach	Beach berm
JOZ/62-3	Ras Kiswakini	Island Beach	Low tide shoreline
JOZ/63	Ras Kiswakini	Island Beach	High tide shoreline
JOZ/64-1	Ras Kiswakini	Island Beach	Beach berm
JOZ/64-2	Ras Kiswakini	Island Beach	Mid tide shoreline
JOZ/65-1	Ras Kiswakini	Island Beach	Beach berm
JOZ/65-2	Ras Kiswakini	Island Beach	High tide shoreline
JOZ/66-1	Ras Kiswakini	Island Beach	Mid tide shoreline
JOZ/66-2	Ras Kiswakini	Island Beach	Low tide shoreline
JOZ/67	Ras Kiswakini	Island Beach	Mid tide shoreline
JOZ/68	Mto Kiswakini	Channel	Tidal channel bottom
JOZ/69	Mto Kiswakini	Flat	Tidal flat
JOZ/70-1	Tamamba	Island Beach	High tide shoreline
JOZ/70-2	Tamamba	Island Beach	Low tide shoreline
JOZ/71-1	Tamamba	Island Beach	Beach berm
JOZ/71-2	Tamamba	Island Beach	Mid tide shoreline
JOZ/72	Tamamba	Island Beach	High tide shoreline
JOZ/73	Tamamba	Island Beach	Mid tide shoreline
JOZ/74-1	Kanagoni	Island Beach	Beach berm
JOZ/74-2	Kanagoni	Island Beach	Mid tide shoreline
JOZ/75	Kanagoni	Island Beach	Mid tide shoreline